National Library of Canada

Acquisitions and Bibliographic Services Branch

395 Wellington Street
Ottawa, Ontario
K1A 0N4

Bibliothèque nationale du Canada

Direction des acquisitions et des services bibliographiques

395, rue Wellington
Ottawa (Ontario)
K1A 0N4

Your file Votre référence

Our file Notre référence

NOTICE

The quality of this microform is heavily dependent upon the quality of the original thesis submitted for microfilming. Every effort has been made to ensure the highest quality of reproduction possible.

If pages are missing, contact the university which granted the degree.

Some pages may have indistinct print especially if the original pages were typed with a poor typewriter ribbon or if the university sent us an inferior photocopy.

Reproduction in full or in part of this microform is governed by the Canadian Copyright Act, R.S.C. 1970, c. C-30, and subsequent amendments.

AVIS

La qualité de cette microforme dépend grandement de la qualité de la thèse soumise au microfilmage. Nous avons tout fait pour assurer une qualité supérieure de reproduction.

S'il manque des pages, veuillez communiquer avec l'université qui a conféré le grade.

La qualité d'impression de certaines pages peut laisser à désirer, surtout si les pages originales ont été dactylographiées à l'aide d'un ruban usé ou si l'université nous a fait parvenir une photocopie de qualité inférieure.

La reproduction, même partielle, de cette microforme est soumise à la Loi canadienne sur le droit d'auteur, SRC 1970, c. C-30, et ses amendements subséquents.

Canada

UNIVERSITY OF ALBERTA

An Experimental Study of Fracture Propagation and Well Communication by Hydraulic Fracturing

BY ©

Fuchang Guo

A thesis submitted to the Faculty of Graduate Studies and Research in partial fulfillment of the requirements for the degree of **Doctor of Philosophy**.

in
Geotechnical Engineering

DEPARTMENT OF CIVIL ENGINEERING

Edmonton, Alberta

Spring, 1993

National Library
of Canada

Acquisitions and
Bibliographic Services Branch

395 Wellington Street
Ottawa, Ontario
K1A 0N4

Bibliothèque nationale
du Canada

Direction des acquisitions et
des services bibliographiques

395, rue Wellington
Ottawa (Ontario)
K1A 0N4

Your file Votre référence

Our file Notre référence

The author has granted an irrevocable non-exclusive licence allowing the National Library of Canada to reproduce, loan, distribute or sell copies of his/her thesis by any means and in any form or format, making this thesis available to interested persons.

L'auteur a accordé une licence irrévocable et non exclusive permettant à la Bibliothèque nationale du Canada de reproduire, prêter, distribuer ou vendre des copies de sa thèse de quelque manière et sous quelque forme que ce soit pour mettre des exemplaires de cette thèse à la disposition des personnes intéressées.

The author retains ownership of the copyright in his/her thesis. Neither the thesis nor substantial extracts from it may be printed or otherwise reproduced without his/her permission.

L'auteur conserve la propriété du droit d'auteur qui protège sa thèse. Ni la thèse ni des extraits substantiels de celle-ci ne doivent être imprimés ou autrement reproduits sans son autorisation.

ISBN 0-315-82166-3

Canada

UNIVERSITY OF ALBERTA

RELEASE FORM

NAME OF AUTHOR: Fuchang Guo

TITLE OF THESIS: An Experimental Study of Fracture Propagation and Well Communication by Hydraulic Fracturing

DEGREE: Doctor of Philosophy

YEAR THIS DEGREE GRANTED: Spring 1993

Permission is hereby granted to the University of Alberta to reproduce single copies of this thesis and to lend or sell such copies for private, scholarly or scientific research purposes only.

The author reserves all other publication and rights in association with the copyright in the thesis, and except as herein before provided neither the thesis nor any substantial portion thereof may be printed or otherwise reproduced in any material form whatever without the author's prior written permission.

Permanent address:
Xihou
Pinglu County
Shanxi Province
People's Republic of China

Date: Nov. 25. 1992

UNIVERSITY OF ALBERTA

FACULTY OF GRADUATE STUDIES AND RESEARCH

The undersigned certify that they have read, and recommend to the Faculty of Graduate Studies and Research for acceptance, a thesis entitled **An Experimental Study of Fracture Propagation and Well Communication by Hydraulic Fracturing** submitted by **Fuchang Guo** in partial fulfillment of the requirements for the degree of **Doctor of Philosophy**.

Dr. N. R. Morgenstern

J. D. Scott
Dr. J. D. Scott

Dave Chan
Dr. D. H. Chan

Prof. K. O. Anderson

Dr. D. Schmitt

John Curran
Dr. J. H. Curran

Date: Oct. 23, 1992

To my parents, Minghua and Shufeng

and to my wife, Jianjun

and to my children, Malinda and Victor

Abstract

Hydraulic fracturing is a process used in the petroleum and geothermal energy industry to enhance recovery or injectivity, and in rock engineering to determine tectonic stresses. Knowledge of the fracture propagation and interaction of the fractures is usually necessary to evaluate the numerical models used to simulate hydraulic fracturing, to understand breakdown and shut-in pressures, and to establish a path of communication between wells. The objective of this thesis is to produce experimental data on fracture propagation and interaction of the fractures through large-scale hydraulic fracturing experiments.

The experiments were conducted in a large test frame capable of applying true triaxial stresses. Leak-off was incorporated. Boundary displacements, bottomhole pressures, and the three principal stresses were measured. The oil penetration area and the fracture induced were determined after testing. The experiments included two parts: single well and double well hydraulic fracturing. The single well hydraulic fracture tests were conducted on Gypstone blocks of 305 x 305 x 305 mm and 610 x 584 x 305 mm. Considerable data on fracture propagation and the influences of σ_3 and injection rate on fracture propagation have been produced. The double well hydraulic fracture tests were conducted on

Gypstone blocks of 610 x 584 x 305 mm. These tests evaluated the possibility of well communication.

The bottomhole pressure has also been analyzed by various methods. The analyses resulted in the main conclusions below. Build-up of the bottomhole pressure before breakdown is affected by the wellbore storage, the skin effect, and the change in permeability. Fracture mechanics methods are promising to explain the high breakdown pressure and the other phenomena observed on breakdown. The fracture pressure declines after breakdown, and the fracture propagates in the manner prescribed by the GdK and the radial models. The models predict quantitatively only part of the pressure-time curve due to application of the special leak-off model and the mass conservation equation. The methods to identify indistinct shut-in pressure are capable of determining the least principal stress even though large leak-off has been incorporated into the hydraulic fracture tests.

Acknowledgement

I would like to acknowledge my gratitude to all those people and organizations who made this work possible. In particular to:

Dr. N. R. Morgenstern, my supervisor, for his guidance, encouragement, and critical evaluation of this manuscript;

Dr. J. D. Scott for his support, encouragement, and thorough review of this manuscript;

the Natural Sciences and Engineering Research Council of Canada and Shell Canada Ltd. for the financial support for this project;

Mr. Jay Khajuria, Mr. Gerry Cyre, Mr. Steve Gamble, and Mrs. Christine Hereygers for their help and assistance with fabrication of specimens, modification of the test apparatus, and the other experimental work, as well as for their partnership in badminton;

Mr. Shuzhan Xu and Mr. Yungyaw Loo for their warm friendship;

and my family, my parents, Minghua and Shufeng, my wife, Jianjun, and my children, Malinda and Victor, for their love, patience, understanding, and encouragement.

Table of Contents

Chapter 1 **Introduction** 1

Chapter 2 **An Experimental Investigation into Hydraulic Fracture Propagation Part 1: Experimental Facilities** 8

- 2.1 Introduction 8
- 2.2 Experimental Rock, Its Fabrication and Properties 14
  - 2.2.1 Fabrication of Gypstone Specimens 15
  - 2.2.2 Physical and Mechanical Properties of Gypstone 15
- 2.3 Loading System 17
  - 2.3.1 Hydraulic Fracture Test Frame and External Pressure 17
  - 2.3.2 Pump System and Internal Pressure 18
- 2.4 Specimen, Layout of Wells, and Sealing 19
- 2.5 Instrumentation and Data Acquisition System 20
  - 2.5 1 Injection Rate 20
  - 2.5.2 Bottomhole Pressure 20
  - 2.5.3 Boundary Displacements 22
  - 2.5.4 Stresses 23
  - 2.5.5 Data Acquisition 23
- 2.6 Testing Procedures 24
- 2.7 Results and Discussions 25

2.7.1 A Representative Test and Data Presentation 25

2.7.2 Effects of Specimen Size on Breakdown Pressure 29

2.8 Summary 30

2.9 References 32

Chapter 3 **An Experimental Investigation into Hydraulic Fracture Propagation Part 2: Single Well Tests** 48

3.1 Introduction 48

3.2 Summary of Hydraulic Fracture Tests 49

3.3 Hydraulic Fracturing under Various σ_3 51

3.4 Hydraulic Fracturing under Various Injection Rates 58

3.4.1 Hydraulic Fracturing under Various Injection Rates: without Stresses 59

3.4.2 Hydraulic Fracturing under Various Injection Rates: a Step-Rate Test 61

3.4.3 Hydraulic Fracturing under Various Injection Rates: with Similar Stresses 63

3.5 Discussion 66

3.5.1 Intersection of a Fracture with the Surface of Specimens 66

3.5.2 Boundary Displacements and Fractures 68

3.6 Conclusions 70

3.7 References 73

Chapter 4 **An Experimental Study of Well Communication by Hydraulic Fracturing** 94

4.1 Introduction 94

4.2 Research Strategy 98

4.3 Experimental Facilities 101

4.4 Experimental Results and Discussions 105

4.4.1 Summary of Double Well Hydraulic Fracturing 105

4.4.2 Double Well Hydraulic Fracturing Tests under a Low Stress Difference 106

4.4.3 Double Well Hydraulic Fracturing Tests under a High Stress Difference 109

4.4.4 Fracture Initiation 111

4.4.5 A Representative Instrumentation 113

4.5 Conclusions 114

4.6 References 117

Chapter 5 **Interpretation of Bottomhole Pressure** 142

5.1 Introduction 142

5.2 Build-up of Bottomhole Pressure before Breakdown 143

5.2.1 Introduction 143

5.2.2 Theoretical Considerations 143

5.2.3 Application to the Hydraulic Fracture Tests 146

5.3 Breakdown Pressure 151

5.3.1 Introduction 151

5.3.2 Review of Breakdown Models 152

    - 5.3.3 Tensile Strength and Classical Breakdown Model 155
    - 5.3.4 Pore Pressure Effect and Poroelastic Model 161
    - 5.3.5 Shear Failure Model 163
    - 5.3.6 Nonlinear (softening) and Point Stress Model 165
    - 5.3.7 Stable Fracture Propagation and Fracture Mechanics Model 166
    - 5.3.8 Conclusions 172
  - 5.4 Fracture Pressure Analysis 174
    - 5.4.1 Introduction 174
    - 5.4.2 Behavior of Fracture Pressure 179
    - 5.4.3 Discussion 181
    - 5.4.4 Conclusions 187
  - 5.5 Shut-in Pressure and σ_3 189
    - 5.5.1 Introduction 189
    - 5.5.2 Shut-in Pressure Identification Techniques 190
    - 5.5.3 Results and Discussion 193
  - 5.6 Conclusions 196
  - 5.7 References 201

Chapter 6 **Conclusions** 244

  - 6.1 Single Well Hydraulic Fracturing and Fracture Propagation 245
  - 6.2 Double well Hydraulic Fracturing and Well Communication 249

Appendix A: **Measurements of Properties of Gypstone** 251

  - A.1 Measurements of Physical Properties 251

A.2 Measurements of Tensile Strength 251

A.3 Measurements of Deformation and Shear Strength 252

A.4 Measurements of Hydraulic Conductivity 253

A.5 References 254

Appendix B: **Injection Procedures, Bottomhole Pressure, Stresses, and Boundary Displacement Measured in Double Well Hydraulic Fracture Tests** 262

List of Tables

Table 2.1 Properties of Gypstone

Table 3.1 Summary of Hydraulic Fracture Tests

Table 4.1 Properties of Gypstone
Table 4.2 Summary of Double Well Hydraulic Fracture Tests
Table 4.3 Orientation of Fracture Initiation and Breakdown Pressure

Table 5.1 Fracture Reopening Pressure
Table 5.2 Comparison of Observed and Calculated Internal Rupturing Pressure of Cylinders of Rocks
Table 5.3 Statistical Analysis of Breakdown Pressure
Table 5.4 Determination of σ_3

List of Figures

Figure 2.1 Strength and Deformation of Gypstone
Figure 2.2 Hydraulic Fracture Test Frame
Figure 2.3 Pump System
Figure 2.4 Layout of wells, Injection Tubing, and Sealing
Figure 2.5 Deformation Monitoring
Figure 2.6 Schematic Diagram of Set-up and Data Acquisition for Hydraulic Fracture Tests
Figure 2.7 Hydraulic Fracture Test 3
Figure 2.8 Hydraulic Fracture Tests under Different Specimen Size

Figure 3.1 Hydraulic Fracture Test 8
Figure 3.2 Hydraulic Fracture Test 5
Figure 3.3 Bottomhole Pressure under Various σ_3
Figure 3.4 Boundary Displacement under Various σ_3
Figure 3.5 Oil Penetration Area under Various σ_3
Figure 3.6 Breakdown Pressure against Stresses
Figure 3.7 Bottomhole Pressure under Various Injection Rates: without Stresses
Figure 3.8 Oil Penetration Area under Various Injection Rates: without Stresses

Figure 3.9 Breakdown Pressure against Injection Rate

Figure 3.10 Hydraulic Fracture Test 10

Figure 3.11 Oil Penetration Area and Fractures under Various Injection Rates: with Similar Stresses

Figure 3.12 Bottomhole Pressure under Various Injection Rates: with Similar Stresses

Figure 3.13 Boundary Displacement under Various Injection Rates: with Similar Stresses

Figure 3.14 Intersection of a Fracture with the Surface of a Specimen

Figure 3.15 Boundary Displacements for Vertical and Horizontal Fractures

Figure 3.16 Bottomhole Pressure and Boundary Displacement of Hydraulic Fracture Test 3

Figure 4.1 Hydraulic Fracture Test Frame

Figure 4.2 Pump System

Figure 4.3 Layout of Injection Wells

Figure 4.4 Injection Tubing and Sealing

Figure 4.5 Double Well Hydraulic Fracture Test 1 (ß=0°)

Figure 4.6 Double Well Hydraulic Fracture Test 2 (ß=15°)

Figure 4.7 Double Well Hydraulic Fracture Test 3 (ß=30°)

Figure 4.8 Double Well Hydraulic Fracture Test 4 (ß=45°)

Figure 4.9 Double Well Hydraulic Fracture Test 5 (ß=60°)

Figure 4.10 Double Well Hydraulic Fracture Test 8 (ß=30°)

Figure 4.11 Double Well Hydraulic Fracture Test 6 (ß=15°)

Figure 4.12 Double Well Hydraulic Fracture Test 7 (ß=30°)
Figure 4.13 Double Well Hydraulic Fracture Test 9 (ß=45°)
Figure 4.14 Double Well Hydraulic Fracture Test 10 (ß=60°)
Figure 4.15 Double Well Hydraulic Fracture Test 8

Figure 5.1 Build-up of Bottomhole Pressure: Test 7
Figure 5.2 Build-up of Bottomhole Pressure: Test 12
Figure 5.3 Build-up of Bottomhole Pressure: Test 23
Figure 5.4 Build-up of Bottomhole Pressure: Test 21
Figure 5.5 Build-up of Bottomhole Pressure: Test 22
Figure 5.6 Build-up of Bottomhole Pressure: the Second Injection Cycle of Test 20
Figure 5.7 Bottomhole Pressure of Tests 3 and 5
Figure 5.8 Bottomhole Pressure of Tests 16 and 20
Figure 5.9 Leak-off Test 2
Figure 5.10 Breakdown Pressure Measured and Predicted by the Classical Breakdown Model
Figure 5.11 Stress Path during Fracturing for Permeable Case
Figure 5.12 Stress Path during Fracturing for Impermeable Case
Figure 5.13 Development of a True Crack
Figure 5.14 Fracture Pressure Analysis: Test 3
Figure 5.15 Fracture Pressure Analysis: Test 9
Figure 5.16 Fracture Pressure Analysis: Test 16
Figure 5.17 Fracture Pressure Analysis: Test 19
Figure 5.18 Fracture Pressure Analysis: Test 22
Figure 5.19 Inflection Point Method

Figure 5.20 P_w vs log $(t+\Delta t)/\Delta t$ Method
Figure 5.21 P_w vs log Δt Method
Figure 5.22 log $(p_w - p_a)$ vs Δt Method (Muskat Method)
Figure 5.23 log p_w vs log t Method
Figure 5.24 dp_w/dt vs p_w Method
Figure 5.25 p_w vs $\sqrt{\Delta t}$ Method
Figure 5.26 Maximum Curvature Method
Figure 5.27 Hydraulic Fracture Test 16: Shut-in in Cycle-1

List of Symbols

A	area
B	pore pressure coefficient
C	leak-off coefficient
c	cohesion
c_0 to c_3	constant
c_4	relative coefficient
C_t	compressibility of the fracture fluid
d	radius of strain-softening zone
E	Young's modulus
F_r	radial body force
G	shear modulus
h	depth of wells
L	half fracture length
L_0	part of the fracture which is filled with the fracture fluid
n	power-law exponent for the fracture fluid
m	power exponent for decline in fracture pressure
k	permeability or hydraulic conductivity
K_I	stress intensity factor for mode I
K_{Ic}	fracture toughness

p	pore pressure in the formation or pressure in the fracture
p_a	the asymptotic pressure in shut-in curve
p_b	breakdown pressure–the peak bottomhole pressure in an injection cycle
p_{b1}, p_{b2}, p_{b3}	the breakdown pressure or peak bottomhole pressure in the first, second, third injection cycle
p_c	fracture closure pressure
p_s	shut-in pressure
p_w	bottomhole pressure
p_0	initial pore pressure
p_1	pressure recorded by pressure transducer 1
p_2	pressure recorded by pressure transducer 2
Δp	fracture pressure (p_w-p_c)
q	flow rate into the formation from wells
q_f	the flow rate through the fracture
q_i	injection rate
q_l	total leak-off rate
r	radial coordinate
r_w	radius of wellbores
R	oil penetration radius
s	coefficient for the skin effect
t	time
t_0	time correction parameter for the wellbore storage
Δt	time since shut-in
u_r	radial displacement of wellbores under internal pressure

u	pore pressure in triaxial tests
V	volume of oil in pump, injection tubing and wellbore
w	fracture width
x	x coordinate
α	Biot's poroelastic parameter
β	the angle between the well line and the direction of the maximum horizontal stress
μ	viscosity of the fracture fluid
υ	Poisson's ratio
ϕ	friction angle
ε_f	strain at failure
σ_t	tensile strength
σ_1	the maximum principal stress
σ_2	the intermediate principal stress
σ_3	the least principal stress
σ_{ver}	the vertical stress
σ_{hmin}	the minimum horizontal stress
σ_{hmax}	the maximum horizontal stress
σ_r	radial total stress
σ_θ	tangential total stress
σ'_r	radial effective stress
σ'_θ	tangential effective stress

Chapter 1

Introduction

Hydraulic fracturing is a process whereby a fluid is pumped into a well at a rate and pressure high enough to overcome the in situ confining stress and the tensile strength of a formation resulting in the formation of a fracture or parting.

Hydraulic fracturing plays a major role in enhancing petroleum reserves and the rate of production [1-2]. The fracturing process, introduced to the oil and gas industry in 1947, is a standard operating practice. By 1981, more than 800,000 treatments had been performed. As of 1988, this had grown to exceed 1 million. About 35% to 49% of all currently drilled wells are hydraulically fractured, and about 25% to 30% of the total U. S. oil reserves have been made economically producible by the process. Since its inception, hydraulic fracturing has developed from a simple, low-volume, low-rate fracture stimulation method to a very highly engineered, complex procedure that is used for many purposes. It can be used to improve well productivity by overcoming drilling and completion damage near the wellbore; it can also be used to make deeply penetrating, high-conductivity fractures in low-permeability reservoirs. The fracturing of disposal and injection wells to increase injectivity is common. Fracturing has been used in secondary and tertiary recovery processes, such as water- and steam-flood operations, to improve injectivity and sweep efficiency. Fracturing treatments typically have varied in size from the small mini-hydraulic fracturing treatments for short fracture length to the deeply penetrating massive hydraulic fracturing (MHF) treatments which now exceed 3.8 x 10^3 m^3 (1 million gal). The design difficulties and high cost of MHF have made obvious the need to enhance fracture design and treatment capabilities.

Fracture design is usually carried out by theoretical and numerical models such as the two-dimensional PKN and GdK models [2], the pseudo-three-dimensional numerical models [2], and the general three-dimensional numerical models [2].These models are generally run on a trial and error basis until the desired geometry is obtained. An estimate is then made for a treatment based on a given fracture length. An optimal design is selected for maximum return from a well. However, various theoretical and numerical models cannot be verified by theoretical predictions and field tests alone because the critical parameters, such as fracture width and length, cannot be measured with confidence in the field. The verification of hydraulic fracturing models must be done through using laboratory experiments.

Hydraulic fracturing is also one of the techniques used for stress measurements [3-4]. The concept of estimating the in-situ stresses from hydraulic fracturing was introduced by Scheidegger in 1962 [5] although the mechanics of hydraulic fracturing and the influence of tectonic stresses had been analyzed by the Hubbert and Willis in 1957 [6]. The concept that the shut-in pressure is approximately equal to the least principal stress was introduced by Kehle in 1964 [7]. It was after Haimson's study in 1968 [8], in which the pore pressure and the poroelastic effect were incorporated into the equation and a number of small scale laboratory experiments were conducted to evaluate the model, that hydraulic fracturing was treated as a possible method for stress measurement. Since then, wide research has been conducted. These studies mainly concentrated on the following aspects: mechanisms of fracture initiation, fracture orientation, effects of the packer, effects of the perforation, effects of the fracture fluid, effects of the wellbore size, effects of the injection rate, the poroelastic effects, effects of nonlinear properties of the rocks, effects of discontinuities, effects of non-homogeneity and anisotropy, and so on. In the past decades, much in situ experience was accumulated.

Although many efforts have been made, this technique is still challenged in several aspects. The most serious question is on the breakdown pressure. The experiments showed that the breakdown pressure is a rate-dependent, fracture fluid-dependent, rock property-dependent, and wellbore size-dependent variable. No theory can explain the observed phenomena persuasively. The mechanisms of breakdown still are open questions. The other challenge is estimation of the shut-in pressure. An indistinct shut-in pressure is often observed in hydraulic fracturing due to significant fluid leak-off. There is no commonly accepted answer on how to identify the shut-in pressure. The inadequate understanding of the breakdown process and the difficult identification of the shut-in pressure have made obvious the demands to conduct large scale, leak-off incorporated hydraulic fracture tests.

Hydraulic fracturing has also been applied in the exploration of hot dry rock masses [9] and oil sands [10]. A new demand is raised in these applications. Well communication is generally necessary to establish an artificial circulation loop in hot dry rock masses or to obtain a hot communicating path in oil sands. Studies on this aspect are limited. It is logical to conduct laboratory tests before any costly field experiments.

The objective of this thesis is to perform controlled hydraulic fracturing experiments in a large scale laboratory apparatus capable of applying true triaxial stresses. The first purpose of the experimental program is to allow verification of the numerical models and evaluation of hydraulic fracturing theories for stress measurements. This objective is carried out by a single well hydraulic fracturing program. The second purpose of the program is to evaluate the possibility of well communication by hydraulic fracturing. This objective is carried out by a double well hydraulic fracturing program.

Chapter 2 describes the experimental facilities in detail. It begins with choice, fabrication, and properties of the artificial rock–Gypstone. It then continues with a description of the test frame, which applied external pressure (the three principal stresses) on specimens, and the pump system that exerted internal pressure (bottomhole pressure) in wells in specimens. This is followed by specification of specimen size, well size, layout of wells, and sealing of wells. After that, instrumentation of the experiments is discussed and testing procedures are presented. Finally, one representative test and hydraulic fracture tests using different specimen sizes are discussed to illustrate data presentation and repeatability of the tests.

Chapter 3 presents the experimental results from the single well hydraulic fracturing program. First, all the single well hydraulic fracture tests are summarized. Subsequently, effects of the least principal stress and the injection rate on fracture propagation are discussed. Finally, several interesting observations are noted.

Chapter 4 presents the experimental apparatus and results for the double well hydraulic fracturing program. It begins with a discussion of the factors that control well communication by hydraulic fracturing and the choice of these factors in the research program. This is followed by a description of the experimental apparatus. Finally, the experimental results are analyzed and discussed.

Chapter 5 interprets the bottomhole pressure observed in the single well hydraulic fracturing program. The analysis begins with the bottomhole pressure before breakdown. Build-up of the bottomhole pressure and the factors which affect the build-up are studied. Subsequently, the breakdown models are checked by the experimental results. After that, fracture pressure analysis based on 2D hydraulic fracturing models is used to study the bottomhole pressure. Following that, the shut-in curve is analyzed, and the methods to determine the least principal stress are evaluated. Finally, possible reasons for the high breakdown pressures are evaluated.

The last chapter integrates the different aspects of hydraulic fracturing that are discussed in the previous chapters and summarizes the main conclusions.

References

1. Howard G. C. and Fast C. R. *Hydraulic fracturing*, Monograph Series, SPE, New York (1970).

2. Gidley J. L., Holditch S. A., Nierode D. E., and Veatch R. W. *Recent advances in hydraulic fracturing*, Monograph Series, SPE, Richardson, TX **12** (1989).

3. *Hydraulic fracturing stress measurements*, Proceedings of a Workshop, National Academy Press, Washington, D. C. (1983).

4. Haimson B. C., Roegiers J. C., and Zoback M. D. *Hydraulic Fracturing Stress measurements*, Proceedings of the Second International Workshops, Geological Engineering Program, University of Wisconsin-Madison (1988).

5. Scheidegger A. E. Stresses in Earth's crust as determined from hydraulic fracturing data. *Geologie und Bawvasen* **27**, p. 45 (1962).

6. Hubbert K. M. and Willis D. G. Mechanics of hydraulic fracturing. *Petroleum Transactions, AIME* **210**, 153-166 (1957).

7. Kehle R. O. Determination of tectonic stresses through analysis of hydraulic well fracturing. *Journal of Geophysical Research* **69**, 259-273 (1964).

8. Haimson B. C. Hydraulic fracturing in porous and nonporous rock and its potential for determining in-situ stresses at great depth. Ph.D. Thesis, University of Minnesota, U.S.A. (1968).

9. Nemat-Nasser S., Abé H., and Hirakawa S. *Hydraulic fracturing and geothermal energy*, Proceedings of the First Japan-United States Joint Seminar and Symposium on Fracture mechanics Approach to Hydraulic Fracturing and Geothermal Energy, Martinus Nijhoff Publishers, The Hague (1983).

10. Chhina H. S. and Agar J. G. Potential use of fracture technology for recovery of bitumen from oil sands. *Paper presented at the 3rd International Conference on Heavy Crude and Tar Sands*, Long Beach, California, U. S. A. (1985).

Chapter 2

An Experimental Investigation into Hydraulic Fracture Propagation Part 1: Experimental Facilities

2.1 Introduction

Hydraulic fracturing is a process whereby a fluid is pumped into a well at a rate and pressure sufficient to overcome the in situ confining stress and tensile strength of a formation such that a fracture or parting forms. This process is used to determine in situ stresses and to enhance either injectivity or recovery in the petroleum and geothermal energy industries .

To optimize a hydraulic fracture treatment, theoretical and numerical models are used for design. These models are generally run on a trial and error basis until the desired geometry is obtained. An estimate is then made for a treatment based on a given fracture length. An optimal design is selected for maximum return from a well.

Many theoretical and numerical models [1] have been developed to predict fracture geometry, such as the two-dimensional PKN and GdK models, the pseudo-three-dimensional numerical models, and the general three-dimensional numerical models. However, as Rubin [2] stated, various theoretical and numerical models cannot be verified by theoretical predictions and field tests alone because the critical parameters such as fracture width and length, cannot be measured with confidence in the field. The verification of hydraulic fracturing models must be done through using laboratory experiments.

Since the development of hydraulic fracturing to enhance recovery and injectivity and to measure in situ stresses, numerous laboratory experiments have been conducted to understand this process. Hydraulic fracturing experiments may be divided into three types. The first one includes experiments to establish and evaluate hydraulic fracturing theory for stress measurements. These experiments are usually conducted on small specimens and mainly focus on the orientation of the fractures, the breakdown pressure, and the shut-in pressure. These experiments have also paid attention to the factors which influence the breakdown pressure and the orientation of the fractures, such as the injection rate, the fracture fluid, the well orientation, the well dimensions, the leak-off, the packer, the perforation. There is a large database for this type of experiments contained in references, such as Scott et al. [3], Haimson [4], Von Schonfeldt [5], Daneshy [6-7], Komar et al. [8], Lockner et al. [9], Solberg et al. [10], Zoback et al. [11], Medlin et al. [12], Avasthi [13], Boyce et al. [14], Cheung et al. [15], Schmitt et al. [16], Behrmann et al. [17], Haimson et al. [18]. A common feature of the above is that they do not investigate how fractures continue to propagate after breakdown. Obviously, their application is restricted to hydraulic fracturing for stress measurements as an aid to the interpretation of breakdown pressures and the investigation of fracture initiation. They are not capable of producing data for evaluation of numerical models of large scale fractures.

The second type of experiment studies the interaction between a fracture driven hydraulically and a pre-existing fracture or an interface such as Lamont et al. [19], Anderson et al. [20], Daneshy [21], Anderson [22], Avasthi [13], Hanson et al. [23], Warpinski et al. [24], Blanton [25], Hanson et al. [26], Teufel et al. [27], Blanton [28], Warpinski et al. [29], Blair et al. [30]. These experiments are usually conducted on large samples. The experiments focus on whether a fracture is contained by structural planes in rocks or not. Breakdown pressure and other aspects of fracture propagation are not of concern. These experiments are useful to understand fracture containment, but do not help to evaluate hydraulic fracturing numerical models.

The final type of experiment produces data for verification of numerical models and understanding of the whole process of fracture propagation. Unfortunately, only three studies have been found in the abundant hydraulic fracturing literature. One was carried out by Medlin et al. [31-32]. Hydraulic fracture tests were performed in Mesa Verde sandstone, Carthage limestone, and Lueders limestone blocks of 76 x 102 x 305 mm (3" x 4" x 12"). Triaxial stresses were applied to specimens. The injection well was scratched to control the orientation of the fracture. The fracture length was monitored by ultrasonic signals and pressure pulses generated in miniature cavities. The fracture width was determined by a capacitance method. Another study was carried out by Rubin [2]. Hydraulic fracture tests were conducted in impermeable polymethylmethacrylate (PMMA) blocks of 305 x 96 x 142 mm (12" x 3.8" x 5.6"). The fracture length was recorded by pressure pulse technique, and the fracture width was measured by LVDTs. The fluid pressure at some points in the fracture was obtained. The injection well was also scratched to control the orientation of fractures. No stresses were applied on specimens. The third study was reported by Johnson et al. [33]. They stimulated hydraulic fracturing through reopening an interface. All three sets of experiments were conducted under limited conditions. Effects of some important parameters such as the least principal stress, injection rate, and the like on fracture propagation have not be studied. Obviously, this database is not large enough to satisfy demands raised by hydraulic fracturing design.

There are several other interesting experiments which should be mentioned. One was performed by Majer et al. [34] in 1986. They placed 3D arrays of piezoelectric sensors around the immediate hydrofracturing zones in a laboratory experiment (300 x 300 x 450 mm, triaxially confined salt block) and a shallow field experiment (5 x 5 x 5 m, granite mine). During hydrofracturing, acoustic emission (AE) activities were detected. Through AE, the process of fracture propagation and fracture location were identified. Unfortunately, effects of controlled parameters on fracture propagation have not been studied. Another is a large-scale hydraulic fracture test performed by Kosar et al. [35] in 1989 to understand fracture growth in unconsolidated oil sands. Bottomhole pressure was examined and the fracture induced was described in detail in their experiment. Again, only one experimental result was reported. The third was hydraulic fracture tests in jointed rock performed by Blair et al. [30]. The objective of the experiments was to study the interaction between a fracture driven hydraulically and an interface or lens. They also recorded fracture length through detecting electrical continuity of tungsten wires embedded in the block specimens, and they described fractures after testing in three of their experiments.

Leak-off is an important parameter for hydraulic fracturing. It dominates not only fracture geometry, but also breakdown pressure, shut-in behavior and bottomhole pressure during fracture propagation. As a result, leak-off always is controlled by injection rate, fracture fluid, and permeability of reservoir rocks in laboratory experiments. However, the detailed penetration area of the fracture fluid caused by leak-off were rarely reported although effects of leak-off have been recognized. In either field or laboratory hydraulic fracturing, fracture propagation is driven by the pressure exerted on the rock around a fracture by injection of the fracture fluid. The magnitude and direction of this pressure are dominated by flow of the fracture fluid. The mode of flow of the fracture fluid is recorded by the penetration area of the fracture fluid. Therefore, it is believed that observation of the penetration area of the fracture fluid is helpful and necessary to understand transformation of load distribution during fracture propagation and to interpret bottomhole pressure and fracture propagation.

For the above reasons, this hydraulic fracturing program was initiated. The objective of this program is to produce experimental data for verification of hydraulic fracturing numerical models and evaluation of hydraulic fracturing theories for stress measurements. Leak-off was incorporated. Hydraulic fracture tests under various stresses and injection rate were performed. The fracture induced and the oil penetration area were observed and recorded after testing. The properties of the rock used were evaluated comprehensively to supply necessary information for interpretation of the hydraulic fracturing experimental results. Deformations of specimens during fracturing were monitored.

Whether laboratory experiments can simulate field hydraulic fracturing behavior and verify numerical models depends, to a large extent, on the artificial rocks used, capability of equipment, instrumentation, data acquisition, and testing procedures. When the rocks used and the boundary conditions applied by the experimental apparatus are similar to field conditions, and the same testing procedures as the field are adopted, the results under these conditions should be able to simulate field behavior if data acquisition systems do not distort experimental results. To obtain reliable results for verification of numerical models, the following efforts were made in this research project. Gypstone was chosen as the artificial rock. In comparison with natural rocks, its homogeneity and isotropy, which result in improved repeatability of experiments and simplified interpretation of experimental results, are an advantage. Its properties are similar to sedimentary rocks, which ensured that the fracture behavior produced was similar to that in rocks. A test frame capable of applying true triaxial stresses up to 10 MPa (1,450 psi) on 610 x 584 x 305 mm (24" x 23" x 12") block specimens was employed. Consequently, the state of in situ stress was capable of being simulated. Moreover, the test frame was capable of testing block specimens up to 610 x 584 x 305 mm (24" x 23" x 12"), which makes it possible to study fracture propagation by laboratory experiments. In addition, the test frame was equipped with a high speed data acquisition system which successfully acquired data on stresses, deformations, and bottomhole pressure during injection. These efforts have improved the reliability of the experimental results.

This chapter is devoted to describing the experimental facilities. It begins with choice, fabrication, and properties of the artificial rock–Gypstone. It then continues with description of the test frame, which applied external pressure (the three principal stresses) on specimens, and the pump system that exerted internal pressure (bottomhole pressure) on specimens. This is followed by specification of specimen size, well size, layout of wells, and sealing of wells. After that, instrumentation of the experiments is discussed, and testing procedures are presented. Finally, one representative test and hydraulic fracture tests under different specimen sizes are discussed to illustrate data presentation and repeatability.

2.2 Experimental Rock, Its Fabrication and Properties

Gypstone was chosen as the artificial rock to be used in this research program. It consists of 10% gypsum, 14.15% water, 75.8% quartz sand and 0.05% retarder, Na_2HPO_4, by mass. Gypstone has properties similar to soft sedimentary rocks. This has been discussed by Indraratna [36-37] and is not repeated here. Its homogeneity is controllable in contrast with natural rocks, and the cost of its fabrication is low due to the use of quartz sand and gypsum. Furthermore, some mechanical properties had been established, and some experience on fabricating specimens was available. Based on these qualifications, the choice of Gypstone was made.

2.2.1 Fabrication of Gypstone Specimens

The specimens were fabricated according to the procedure described by Indraratna [36]. First the inside wall of the aluminum mould was lined with Vaseline petroleum jelly. Then the mould was fixed on a vibrating table. Subsequently, sand and gypsum were mixed for ten minutes to ensuretf homogeneity of the overall compound. While sand and gypsum were being mixed, retarder was dissolved in water at room temperature. After mixing was completed, the water-retarder solution was added to the sand and gypsum mixture. It was again mixed for 15 minutes. After that, the mould was filled with the thoroughly mixed material in 30 to 40 mm (about 1.5") thin layers. The excess water was removed before the addition of the subsequent layer. Compaction of specimens was achieved by simultaneous vibrating and tamping. Systematic poking with a pointed steel rod was also necessary to accelerate the expulsion of trapped air. After the specimen was cast, the mould was removed from the vibrating table and kept at room temperature for about 12 hours until the initial setting was complete. Finally, the mould was stripped, and the specimen was cured at 46±2°C at 30% relative humidity for four weeks.

2.2.2 Physical and Mechanical Properties of Gypstone

Hydraulic fracturing is a response of rocks under natural state (in-situ stresses and pore pressure) to loads applied artificially (bottomhole pressure). As a result, it depends on the properties of the rock, in-situ stress, initial pore pressure, injection fluid, injection rate, and injection procedure. Hence, it is essential to know the properties of the rock to interpret hydraulic fracturing. For this reason, the physical and mechanical properties of Gypstone were studied comprehensively. Eight Brazilian tests and seven splitting tests were conducted to obtain the tensile strength of Gypstone. Thirteen triaxial tests under natural water content and 14 saturated and drained triaxial tests were carried out to evaluate deformation parameters and shear strength. Seven permeability tests were conducted to estimate hydraulic conductivity of Gypstone. Bulk density, dry density, void ratio, porosity, water content, and degree of saturation of the Gypstone specimens were also measured. The results obtained are summarized in Table 2.1 and Figure 2.1. The detailed description is presented in Appendix A.

As shown in Table 2.1, the tensile strength of Gypstone is variable although the fabrication of specimens has been carefully controlled. The tensile strength from the Brazilian tests ranges from 156 to 343 kPa (23 to 50 psi), while the tensile strength from the splitting tests is from 113 to 154 kPa (16 to 22 psi). Even though they are variable, all the results from both the Brazilian and the splitting tests show that Gypstone has a low tensile strength.

The triaxial tests were conducted first under the saturated and drained condition at a 1×10^{-6} s^{-1} strain rate. To satisfy drained conditions, such a low strain rate was used. However, the loading rate in hydraulic fracturing usually is very high. Although the saturated and drained triaxial tests are able to represent the properties of Gypstone under saturation, they cannot reveal the properties of Gypstone under high loading rates. Hence, three sets of triaxial tests were performed under natural water content and high strain rates. Their strain rates were 8.4 x 10^{-6}, 8.4 x 10^{-5}, and 4.20 x 10^{-4} s^{-1}, respectively.

The results of the shear strength are interesting (Figure 2.1 a). The cohesion increases with an increase in strain rate. It is 29.4 kPa (4 psi) at the strain rate of 1 x 10^{-6} s^{-1}. It increases up to 333.9 kPa (48 psi) when the strain rate arose to 8.4 x 10^{-5} s^{-1}. It is also of interest to note the change of friction angle. The friction angle obtained from the tests under natural water content is about 46°. It changes little with strain rate. The friction angle for the saturated and drained tests is 39.6°. Those seem to reveal that a high strain rate leads to high cohesion, and saturation lowers the friction angle. The obtained tangent modulus also is reasonable (Figure 2.1 b). The tangent modulus rises with increases of confining pressure and strain rate. It ranges from 58 to 229 MPa (8,412 to 33,214 psi) for uniaxial load.

Hydraulic conductivity was measured in the triaxial tests after the B (pore pressure coefficient) test and before the shearing phase. The hydraulic conductivity of Gypstone is variable, and ranges from 4.14 x 10^{-4} to 4.09 x 10^{-5} cm/s (0.43 to 0.04 μm^2).

2.3 Loading System

2.3.1 Hydraulic Fracture Test Frame and External Pressure

Hydraulic fracture tests were carried out in a large test frame (Figure 2.2) developed by Kaiser and Morgenstern [38] at the University of

Alberta. The large test frame can take block specimens up to 610 x 584 x 305 mm (24" x 23" x 12"), and is capable of applying true triaxial tresses up to 10 MPa (1,450 psi) on specimens. The vertical load is developed through pressing a rigid loading head through four hydraulic rams against the upper vertical reaction head and the specimen, which seats on a concrete pedestal (covered with a steel plate) above the lower vertical reaction head. The horizontal loads are applied through a series of load distributing triangular shaped platens and plates. The applied loads are recorded by 12 load cells. Four of them are for the vertical load, and the others for the horizontal loads. The hydraulic loading system can maintain pressure over a period of several days with stress fluctuations of less than one percent. The true triaxial stresses were applied in all hydraulic fracture tests through this frame.

In the oil industry, vertical fractures are the main fracture mode. In hydraulic fracturing stress measurements, vertical fractures are able to provide information for the magnitude and direction of the horizontal principal stresses, so vertical fractures are also the preferred fracture mode. For the above reasons, vertical fractures were studied in this research program. The stresses were designed so that vertical fractures would be produced.

2.3.2 Pump System and Internal Pressure

A pump (Figure 2.3) was designed and fabricated for hydraulic fracture tests. It consists of a compression test machine and a hydraulic jack with a 63.5 mm (2.5") inside diameter, a 127 mm (5") outside diameter, and a 216 mm (8.5") height. The hydraulic jack is controlled by the compression test machine. Various constant injection rates are obtained by changing the displacement rate of the compression test machine. The obtained maximum injection rate is 3.2 cm^3/s. The maximum volume for this pump is 400 cm^3, and the maximum injection pressure is 31 MPa (4,469 psi).

Internal pressures were supplied through the one pump. A constant injection rate was chosen to obtain the controlled fracture propagation.

2.4 Specimen, Layout of Wells, and Sealing

All hydraulic fracture tests except Tests 21 and 22 were conducted on 305 x 305 x 305 mm (12" x 12" x 12") block specimens. Tests 21 and 22 were run on 610 x 584 x 305 mm (24" x 23" x 12") block specimens. The size effect can be estimated by comparison of the two different sized blocks.

The layout of a well is shown in Figure 2.4. The well consists of an upper hole and a lower hole. The upper hole is used to install injection tubing, and the lower hole serves as the injection segment. The upper hole was drilled vertically in the central top of the block. The lower hole was drilled concentrically at the bottom of the upper hole. Consequently, the injection segment was kept in the center of specimens. Two sets of well size were used. Group I has an upper hole of 12.7 mm (0.5") diameter and 101.6 mm (4") depth, and a lower hole of 6.4 mm (0.25") diameter and 101.6 mm (4") depth. The other has an upper hole of 12.7 mm (0.5") diameter and 120.7 mm (4.75") depth, and a lower hole of 3.2 mm (0.125") diameter and 63.5 mm (2.5") depth.

Tubing, with a 381 mm (15") length, a 6.4 mm (0.25") outside diameter and a 3.86 mm (0.152") inside diameter, was cemented to the wall of the upper hole with 3M 2216 Epoxy Adhesive. This tubing serves as injection tubing, and the 3M 2216 Epoxy Adhesive as sealant. At the top of the injection tubing, a pressure transducer, which was called pressure transducer 1, was installed to monitor injection pressure. To obtain bottomhole pressure, another piece of 381 mm (15") tubing and another pressure transducer, which was called pressure transducer 2, was connected to the previous pressure transducer. Injection tubing, sealing, and pressure transducers are shown in Figure 2.4 b.

2.5 Instrumentation and Data Acquisition System

2.5 1 Injection Rate

Injection rate was calculated by the velocity of displacement of the compression test machine times the inside area of the hydraulic jack.

2.5.2 Bottomhole Pressure

Bottomhole pressure is a variable which depends strongly upon fracture propagation and fracture geometry, so its monitoring will produce data to diagnose fractures. In addition, monitoring is inexpensive and immediately available after fracturing. As a result, it is always measured during hydraulic fracturing whether hydraulic fracturing is a massive hydraulic fracture stimulation in an oil field or microfracturing in the laboratory. In the field, bottomhole pressure can be directly measured in the well segment sealed without any difficulties because of the large borehole diameter. In the laboratory, it is usually impractical to directly measure it in a borehole due to the small borehole diameter. If an injection rate is low and the fracture fluid is light, loss of pressure in injection tubing is negligible. Measurements are usually taken in injection tubing just outside the specimen without significant error being introduced. When loss of pressure in injection tubing is large such as under a high injection rate and the viscous fracture fluid, the above method is still applicable, but a correction is necessary. In all hydraulic fracture tests in this project, injection pressure was measured in injection tubing just outside of the specimen and then it was corrected to obtain real bottomhole pressure.

The correction method is as follows. Two pressure transducers were installed, as in Figure 2.4. They were connected by a piece of tubing with the same size and length as that between pressure transducer 1 (close to the specimen) and sealed well segment. The pressure loss caused by the two pieces of tubing is the same because they have the same size and length. Therefore, the pressure loss between pressure transducer 1 and the sealed well segment can be obtained from the pressure difference between the two pressure transducers. The bottomhole pressure is equal to the pressure at pressure transducer 1 minus the loss of pressure in the tubing between pressure transducer 1 and the sealed well segment. If p_1 is used to express the pressure recorded by pressure transducer 1, and p_2 is used to express the pressure recorded by pressure transducer 2, then the pressure difference between pressure transducers 2 and 1 is p_2-p_1. The bottomhole pressure is equal to $2p_1$-p_2.

2.5.3 Boundary Displacements

Although bottomhole pressure is closely related to fracture geometry, it is not enough to characterize fracture geometry only by bottomhole pressure. Other variables should also be monitored during testing to verify numerical models. In this research program, the deformation of rock specimens or boundary displacement was chosen as a variable to characterize fracture propagation.

Displacements on the five moveable faces of a specimen in the direction of the three principal stresses were monitored by 16 LVDTs. Four LVDTs which were installed vertically at the four top corners of the rigid loading head were used to obtain vertical displacements. The average gives the vertical boundary displacement. The other 12 LVDTs which were installed horizontally on four sides of the specimen (three LVDTs each side) were used to monitor horizontal displacement. Three LVDTs on each side were installed at the upper corners and center of the side, respectively. The average of three recorded displacements gives the horizontal displacement on the corresponding side. Summation of displacement on two opposite sides in the direction of each principal stress gives the total displacement along that principal stress, which is called boundary displacement in this thesis. The set-up of LVDTs is presented in Figure 2.5.

2.5.4 Stresses

To check responses of the test frame to hydraulic fracturing and reliability of displacement measurements, stresses were monitored during injection. The monitoring of stresses was achieved through the measurement of loads. The changes of loads were monitored by 12 load cells. After testing, the loads from the 12 load cells were converted into stresses.

2.5.5 Data Acquisition

In hydraulic fracture tests 0 to 16, data acquisition was carried out by a Fluke 2240B Datalogger. All load cells, LVDTs, and pressure transducers (30 instruments) were scanned in an interval of 10 seconds. The readings were then sent to an IBM compatible computer and recorded on a floppy disk. The data from two pressure transducers were also recorded continuously by a SERVOGOR 460 YT-recorder. The experimental results showed that this system did not work properly for hydraulic fracture tests. The rate of scanning was too low, and the extra readings must be added from the YT-recorder to obtain accurate breakdown pressure and bottomhole pressure curves.

A new system was developed to avoid this problem. The new system consists of a Macintosh IIx, NB-MIO-16x board, and a Multiplexer. Signals from load cells, LVDTs, and pressure transducers entered the NB-MIO-16x board through the Multiplexer. After the signals were converted from analogue into digital by the NB-MIO-16x Board, they were sent into the Macintosh microcomputer. The whole process was controlled by the Macintosh microcomputer through LabVIEW software. The new system was able to scan 64 channels at a rate of one sample per second. The data were stored on disk and were accessible by data analysis/graphics application software. Bottomhole pressure and other variables were also shown on the screen of the microcomputer during testing. Data in the rest of the tests and the double well hydraulic fracture tests was obtained by this system.

The schematic diagram of set-up and data acquisition for all hydraulic fracture tests is shown in Figure 2.6.

2.6 Testing Procedures

The hydraulic fracture tests with stresses were conducted in the following steps.

1. Installation of Injection Tubing: After a well was drilled at the designated locations, It was cleaned by compressed air. Then, injection tubing was cemented to the wall of the upper hole with 3M 2216 Epoxy Adhesive. The specimen was left at room temperature overnight or for about 12 hours to allow the adhesive to harden.

2. Set-up of Loading System and Instrumentation: After the adhesive had hardened, the specimen was placed into the test frame, and the load system, load cells, LVDTs, and pressure transducers were set up.

3. Loading: The three principal stresses were applied hydrostatically at an increment of 0.5 MPa (73 psi) until σ_3 was up to the designated value. Subsequently, σ_1 and σ_2 were synchronously increased up to the designed σ_2 at an increment of 0.5 MPa (73 psi). Finally, σ_1 was raised to the required value at an increment of 0.5 MPa (73 psi). To minimize the effect of creep on boundary displacement, the applied stresses were maintained for 24 hours before hydraulic fracturing.

4. Fracturing: Fracture fluid was injected into the injection well at a constant injection rate until a fracture extended to or the fracture fluid leaked out of the surface of a specimen.

5. Description of Fractures: After the specimen was taken out of the test frame, it was cut into slices to describe the fracture. This step was completed on the day after fracturing.

The hydraulic fracture tests without stresses were conducted in the following steps. First, injection tubing was installed in the same manner as the tests with stresses. After that, pressure transducers were connected, and the specimen was fractured. The specimen was not set up into the test frame. Another difference was that boundary displacements and stresses were not monitored during injection. Injection in the tests without stresses was terminated as soon as the specimen was broken. The description of fractures was completed just after fracturing.

2.7 Results and Discussions

2.7.1 A Representative Test and Data Presentation

Figure 2.7 shows a representative test (Test 3). The three principal stresses are 6.40 MPa (928 psi) vertical stress, 4.30 MPa (624 psi) and 1.90 MPa (276 psi) horizontal stresses. Injection well (low hole) is 6.4 mm (0.25") in diameter and 101.6 mm (4") in depth. Fracture fluid was gear oil with 1000 mPa•s viscosity. Injection rate was 3.114 cm^3/s. The experimental results are presented in four types of graphs:

Bottomhole Pressure and Injection History (Figure 2.7 a): All records are plotted and joined in straight lines (solid or dash lines). Bottomhole pressure is the pressure in the injection well. The time is increment time from the beginning of injection. The time intervals among injection cycles are real wait time during testing.

Figure 2.7 a illustrates injection history and bottomhole pressure. From the viewpoint of mechanics, this figure reflects the loading history. When fracture fluid is injected into a well, a body force is exerted on the rock around the injection well through fluid flow. It is this body force that drives a fracture to propagate. Bottomhole pressure is just a measurement for this body force. Therefore, this figure reveals the loading history of hydraulic fracturing. While the fracture fluid is injected at a constant rate, the response in bottomhole pressure differs among different injection cycles. Obviously the different responses result from fracture propagation. Hence the data also characterizes fracture propagation.

Figure 2.7 a is a typical bottomhole pressure curve. In the first injection cycle, bottomhole pressure increases slowly at the beginning of injection due to well storage and compression of fracture fluid. Subsequently, bottomhole pressure rises quickly until breakdown pressure.

After breakdown pressure, the fracture starts to propagate unstably. A series of drops following an instantaneous rise occurs. In the second injection cycle, the fracture extends rapidly so that bottomhole pressure plunges. Afterwards, a large drop following an instantaneous rise develops, which indicates that the fracture propagates unstably again, then stops or closes due to the decline of the pressure in the fracture. In the third injection cycle, bottomhole pressure plunges again, then maintains constant. A possible explanation is that the fracture extends to the surface of the specimen in this plunge, and injection rate is balanced by leak-off rate out of specimen and into the rock so that steady flow is formed. This bottomhole pressure curve indicates that fracture propagation is not a smooth and stable process but a series of discrete events. In fact, similar fracture propagation was observed by Majer and Doe [34] with high frequency seismic monitoring. They found that seismic activity caused by hydraulic fracturing is not a continuous process, but is a series of discrete events. From this, they concluded "......the hydrofracture process is not a smooth stable one but a series of discrete events which seem together to make the "hydrofracture"."

Principal Stresses (Figure 2.7 b): All records are plotted and connected in straight lines (solid or dash lines). The principal stresses are calculated from the load recorded by load cells during testing. The time axis, like Figure 2.7 a, is increment time from the beginning of injection.

Figure 2.7 b is the principal stresses monitored during testing. It examines reaction of the test frame to hydraulic fracturing. σ_{hmax} and σ_3 change little, and σ_{ver} declines slightly. The decline is so small that the constant stress boundary condition is still maintained. This demonstrates that the loading system is suitable for hydraulic fracture tests.

Boundary Displacements (Figure 2.7 c): All records are plotted and connected in straight lines. Boundary displacements are the displacements between two opposite surfaces of a specimen. These displacements result from injection of the fracture fluid and do not include the displacements caused by application of the three principal stresses. They are zero at the beginning of injection. The positive boundary displacements mean the contraction of specimens, the negative displacements mean the expansion of specimens.

Figure 2.7 c shows a typical boundary displacement curve. It is of interest to note the mode of the boundary displacements. The boundary displacement in the direction of σ_3 is negative, i.e. expansive. The boundary displacement in the direction of σ_{hmax} is also negative, but the magnitude is very small. The boundary displacement in the direction of σ_{ver} is positive, i.e. contractive. These boundary displacements are consistent with the observed fracture orientation. When a fracture opens, the expansion in the direction perpendicular to the fracture is expected, the contraction in another direction with higher stress is expected. In the other direction, the boundary displacement should be slight. The fracture induced basically propagates in the direction perpendicular to σ_3, and the vertical stress is more than the horizontal maximum stress. Therefore, the boundary displacements monitored – the expansion in the direction of σ_3, the contraction in the direction of σ_{ver}, and the slight expansion in the direction of σ_{hmax} – are logical. It is also of interest to note the magnitude of the boundary displacements. When a fracture is induced in a specimen, the volume of the specimen should increase. This is clearly illustrated by the boundary displacements in Figure 2.7 c. The specimen is a cubic block so the sum of three boundary displacements represents the change in the volume of the specimen. The positive sum means the contraction of the specimen, the negative sum indicates the expansion of the specimen. The minimum sum is -0.0726 mm (2.9 x 10^{-3} in.). Therefore, the mode and magnitude of the boundary displacements are all reasonable.

Fracture description (Figure 2.7 d): After testing, a specimen was cut. The fracture induced and the oil penetration area are drawn in this figure. The fracture is expressed as a line, and the oil penetration area is a shaded zone. The location of cutting planes is shown in a cavalier oblique projection. The fracture induced hydraulically is initiated vertically, and then propagates in the direction perpendicular to σ_3. It deviates from the vertical when it migrates upward.

2.7.2 Effects of Specimen Size on Breakdown Pressure

The value of laboratory experimental results are often questioned in rock mechanics. One of the main reasons is specimen size and whether specimen size is big enough to avoid size effects. For hydraulic fracture tests, the same question has to be answered. For this reason, Tests 21 and 22 were conducted.

The experimental results of Tests 20 and 22 are plotted in Figure 2.8. Both tests used the same injection rate (3.186 cm^3/s), the same fracture fluid (1000 mPa•s gear oil), and the same borehole diameter (3.2

mm diameter). They also have similar states of stress. The three principal stresses in Test 20 are vertical stress of 4.88 MPa (708 psi) and horizontal stresses of 4.68 MPa (679 psi) and 2.95 MPa (428 psi), respectively. The three principal stresses in Test 22 are vertical stress of 5.35 MPa (776 psi) and horizontal stresses of 5.01 MPa (727 psi) and 2.69 MPa (390 psi), respectively. The only difference between them is specimen size. Test 20 was conducted in a block specimen of 305 x 305 x 305 mm (12" x 12" x 12"); while Test 22 was performed in a block specimen of 610 x 584 x 305 mm (24" x 23" x 12").

The experimental results are interesting. At the beginning of injection, both bottomhole pressures increase rapidly at the same rate. The breakdown pressures produced in both tests are very close. The breakdown pressure of Test 20 is 20.50 MPa (2,973 psi), and that of Test 22 is 19.23 MPa (2,789 psi). This small difference may result from the difference in the stresses applied in the two specimens. After breakdown pressure, the bottomhole pressures in two tests continue to decline at a close rate. The two curves depart at 22 seconds. After the specimens were cut, it was found that the fracture in Test 20 deviates from the direction perpendicular to σ_3 at a distance from the injection well. The high bottomhole pressure in Test 20 may be caused by this deviation. This comparison illustrates clearly that the 305 x 305 x 305 mm (12" x 12" x 12") block specimen is big enough to obtain real breakdown pressure information for the injection rate and borehole size used.

2.8 Summary

The reliability of laboratory experimental results depends on how close the experimental facilities are capable of simulating in situ conditions. To obtain reliable laboratory hydraulic fracturing results, Gypstone, whose properties are similar to sedimentary rocks, is used. The test frame capable of applying true triaxial stresses up to 10 MPa (1,450 psi) on a block specimen of 610 x 584 x 305 mm (24" x 23" x 12") is employed. In addition, the test frame is equipped with a high speed data acquisition system. These efforts have improved the reliability of the experimental results.

One representative experimental result is presented to illustrate data presentation. It also proves that this system is suitable for hydraulic fracture tests. Although the principal stresses recorded change slightly during injection, this change is so small that constant stress conditions are still maintained. The boundary displacements are consistent with the fracture induced hydraulically. Bottomhole pressures are reasonable. Effects of specimen size on breakdown pressure have been examined by comparison of hydraulic fracture tests conducted in 305 x 305 x 305 mm (12" x 12" x 12") with 610 x 584 x 305 mm (24" x 23" x 12") block specimens. No effect of specimen size on breakdown pressure is found. All these facts demonstrate that this system works properly.

2.9 References

1. Gidley J. L., Holditch S. A., Nierode D. E., and Veatch R. W. *Recent advances in hydraulic fracturing*, p. 452. Monograph Series, SPE, Richardson, TX 12 (1989).

2. Rubin M. B. Experimental study of hydraulic fracturing in an impermeable material. *Journal of Energy Resources Technology* **105**, 116-124 (1983).

3. Scott P. P., Bearden W. G., and Howard C.G. Rock rupture as affected by fluid properties. *Trans., AIME* **198**, 111 (1953).

4. Haimson B. C. Hydraulic fracturing in porous and nonporous rock and its potential for determining in-situ stresses at great depth. Ph.D. Thesis, University of Minnesota, U.S.A. (1968).

5. Von Schonpeldt H. A. An experimental study of open-hole hydraulic fracturing as a stress measurement method–with particular emphasis on field tests. Ph.D. Thesis, University of Minnesota, U.S.A. (1970).

6. Daneshy A. A. A study of inclined hydraulic fractures. *Society of Petroleum Engineers Journal* **13**, 61-68 (1973).

7. Daneshy A. A. Experimental investigation of hydraulic fracturing through perforations. *Journal of Petroleum Technology* **25**, 1201-1206 (1973).

8. Komar C. A. and Frohne K. H. Factors controlling fracture orientation in sandstone. *Paper SPE 4567 presented at the 1973 SPE Annual Meeting*, Las Vegas, Nev., U.S.A. (1973).

9. Lockner D. and Byerlee J. D. Hydrofracture in Weber sandstone at high confining pressure and differential stress. *Journal of Geophysical Research* **82**, 2018-2026 (1977).

10. Solberg P., Lockner D., and Byerlee J. Shear and tension hydraulic fractures in low permeability rocks. *Pure and Applied Geophysics* **115**, 191-198 (1977).

11. Zoback M. D., Rummel F., Jung R., and Raleigh C. B. Laboratory hydraulic fracturing experiments in intact and pre-fractured rock. *Int. J. Rock Mech. Min. Sci. & Geomech. Abstr.* **14**, 49-58 (1977).

12. Medlin W. L. and Massé L. Laboratory investigation of fracture initiation pressure and orientation. *Society of Petroleum Engineers Journal* **19**, 129-144 (1979).

13. Avasthi J. M. Hydrofracturing in inhomogeneous, anisotropic and fractured rocks. Ph.D. Thesis, The University of Wisconsin-Madison, U.S.A. (1981).

14. Boyce G. M., Doe T. W., and Majer E. Laboratory hydraulic fracturing stress measurement in salt. *Rock Mechanics in Productivity and Protection, Proceedings of the 25th U.S. Symposium on Rock Mechanics*, Northwestern University, U.S.A., pp. 95-102 (1984).

15. Cheung L. S. and Haimson B. C. Laboratory study of hydraulic fracturing pressure data–how valid is their conventional interpretation? *Int. J. Rock Mech. Min. Sci. & Geomech. Abstr.* **26**, 595-604 (1989).

16. Schmitt D. R. and Zoback M. D. Poroelastic effects in the determination of the maximum horizontal principal stress in hydraulic fracturing tests—a proposed breakdown equation employing a modified effective stress relation for tensile failure. *Int. J. Rock Mech. Min. Sci. & Geomech. Abstr.* **26**, 499-506 (1989).

17. Behrmann L. A. and Elbel J. L. Effect of perforations on fracture initiation. *Journal of Petroleum Technology* **43**, 608-615 (1991).

18. Haimson B. C. and Zhao Z. Effect of borehole size and pressurization rate on hydraulic fracturing breakdown pressure. *Rock Mechanics as a Multidisciplinary Science, Proceedings of the 32nd U.S. Symposium on Rock Mechanics*, The University of Oklahoma, Norman, U.S.A., pp. 191-200 (1991).

19. Lamout N. and Jessen F. W. The effects of existing fractures in rocks on the extension of hydraulic fractures. *Trans., AIME* **228** (1963).

20. Anderson G. D. and Larson D. B. Laboratory experiments on hydraulic fracture growth near an interface. *Proceedings of the 19th U.S. Symposium on Rock Mechanics*, Mackay School of Mines, University of Nevada, U.S.A., pp. 333-339 (1978).

21. Daneshy A. A. Hydraulic fracture propagation in layered formations. *Society of Petroleum Engineers Journal* **18**, 33-41 (1978).

22. Anderson G. D. Effects of friction on hydraulic fracture growth near unbonded interfaces in rocks. *Society of Petroleum Engineers Journal* **21**, 21-29 (1981).

23. Hanson M. E., Shaffer R. J., and Anderson G. D. Effects of various parameters on hydraulic fracturing geometry. *Society of Petroleum Engineers Journal* **21**, 435-443 (1981).

24. Warpinski N. R., Clark J. A., Schmidt R. A., and Huddle L. W. Laboratory investigation on the effect of in situ stresses on hydraulic fracture containment. *Paper SPE 9834 presented at the 1981 SPE/DOE Low Permeability Symposium*, Renver, Colorado, U.S.A. (1981).

25. Blanton T. L. An experimental study of interaction between hydraulically induced and pre-existing fractures. *Paper SPE 10847 presented at the SPE/DOE Unconventional Gas Recovery Symposium*, Pittsburgh, PA, U.S.A. (1982).

26. Hanson M. E., Anderson G. D., Shaffer R. J., and Thorson L. D. Some effects of stress, friction, and fluid flow on hydraulic fracturing. *Society of Petroleum Engineers Journal* **22**, 321-332 (1982).

27. Teufel L. W. and Clark J. A. Hydraulic fracture propagation in layered rock: experimental studies of fracture containment. *Society of Petroleum Engineers Journal* **24**, 19-32 (1984).

28. Blanton T. L. Propagation of hydraulically and dynamically induced fractures in naturally fractured reservoirs. *Society of Petroleum Engineers Journal* **26**, 613-621 (1986).

29. Warpinski N. R. and Teufel L. W. Influence of geologic discontinuities on hydraulic fracture propagation. *Journal of Petroleum Technology* **39**, 209-220 (1987).

30. Blair S. C., Thorpe R. K., and Heuze F. E. Propagation of fluid-driven fractures in jointed rock. Part 2–physical tests on blocks with an interface or Lens. *Int. J. Rock Mech. Min. Sci. & Geomech. Abstr.* **27**, 255-268 (1990).

31. Biot M. A., Medlin W. L., and Massé L. Laboratory experiments in fracture propagation. *Paper SPE 10377 presented at the 1981 Eastern Regional Meeting*, Columbus, Ohio, U.S.A. (1981).

32. Medlin W. L. and Massé L. Laboratory experiments in fracture propagation. *Society of Petroleum Engineers Journal* **24**, 256-268 (1984).

33. Johnson E. and Cleary M. P. Implications of recent laboratory experimental results for hydraulic fractures. *Paper SPE 21846 presented at the Rocky Mountain Regional Meeting and Low-Permeability Reservoirs Symposium*, Denver, Colorado, U.S.A. (1991).

34. Majer E. L. and Doe T. W. Studying hydrofractures by high frequency seismic monitoring. *Int. J. Rock Mech. Min. Sci. & Geomech. Abstr.* **23**, 185-199 (1986).

35. Kosar K. M. and Been K. Large scale laboratory fracturing test in oil sands. *Paper in the 44th Annual Technical Meeting of the Petroleum Society of CIM*, Banff, Alberta, Canada (1989).

36. Indraratna B. Application of fully grouted bolts in yielding rock. Ph.D. Thesis, University of Alberta, Edmonton, AB, Canada (1987).

37. Indraratna B. Development and applications of a synthetic material to simulate soft sedimentary rocks. *Géotechnique* **40**, 189-200 (1990).

38. Kaiser P. K. and Morgenstern N. R. Time-dependent deformation of small tunnels–I. experimental facilities. *Int. J. Rock Mech. Min. Sci. & Geomech. Abstr.* **18**, 129-140 (1981).

Table 2.1. Properties of Gypstone

Bulk density (kg/m^3)	1780
Dry density (kg/m^3)	1730
Void ratio	0.503
Porosity %	33.45
Water content %	2.37
Degree of saturation %	12.3
Tensile strength[1] (kPa)	156 to 343
Tensile strength[2] (kPa)	113 to 154
Hydraulic conductivity (cm/s)	4.14×10^{-4} to 4.09×10^{-5}

---

[1] The tensile strength from the Brazilian tests

[2] The tensile strength from the splitting tests

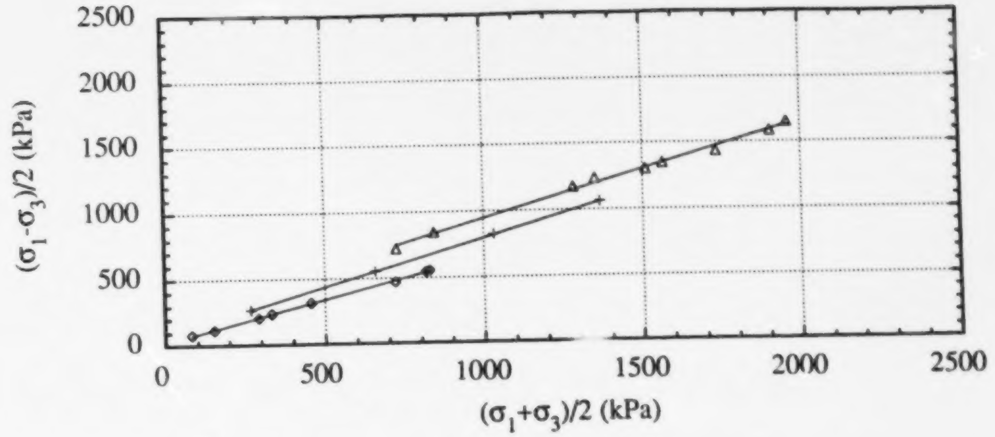

a. Shear Strength of Gypstone

—◆— saturated, drained (strain rate 1 x 10^{-6} s^{-1})

$c' = 29.4$ kPa, $\phi' = 39.6°$

—+— under natural water content (strain rate 8.4 x 10^{-6} s^{-1})

$c = 110.1$ kPa, $\phi = 46.4°$

—△— under natural water content (strain rate 8.4 x10^{-5} and 4.2 x 10^{-4} s^{-1}

$c = 333.9$ kPa, $\phi = 45.7°$

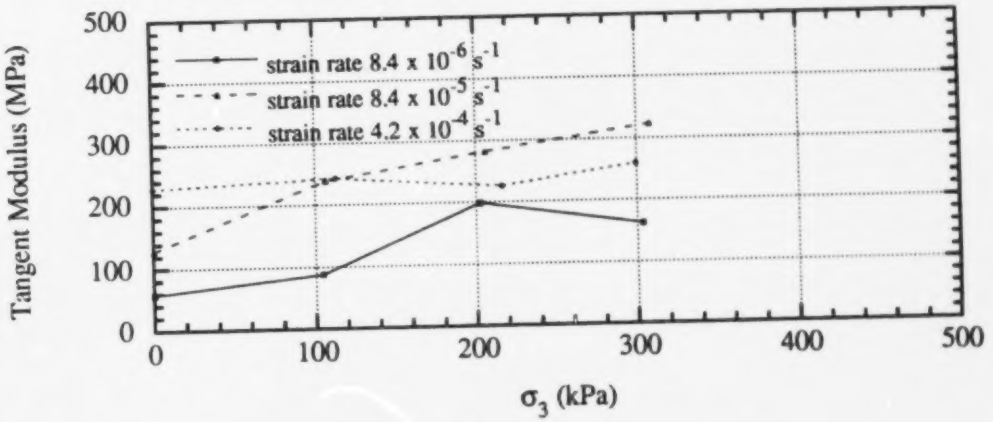

b. Tangent Modulus under Natural Water Content

Figure 2.1 Strength and Deformation of Gypstone

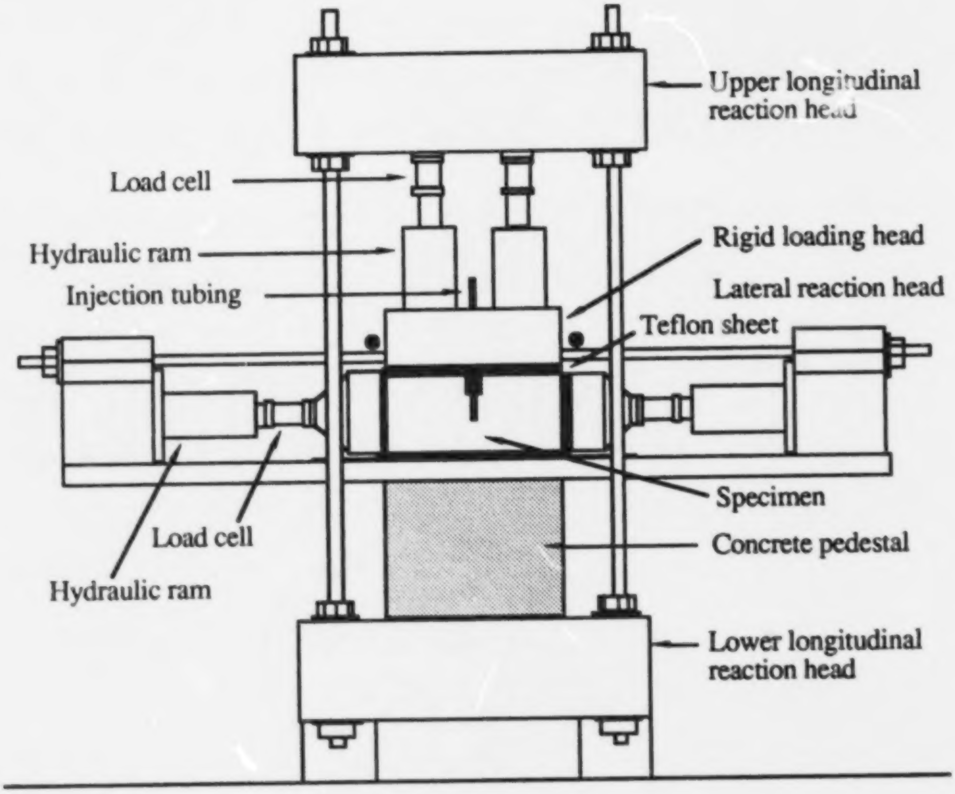
Upper longitudinal reaction head
Load cell
Hydraulic ram
Injection tubing
Rigid loading head
Lateral reaction head
Teflon sheet
Specimen
Load cell
Concrete pedestal
Hydraulic ram
Lower longitudinal reaction head

Figure 2.2 Hydraulic Fracture Test Frame

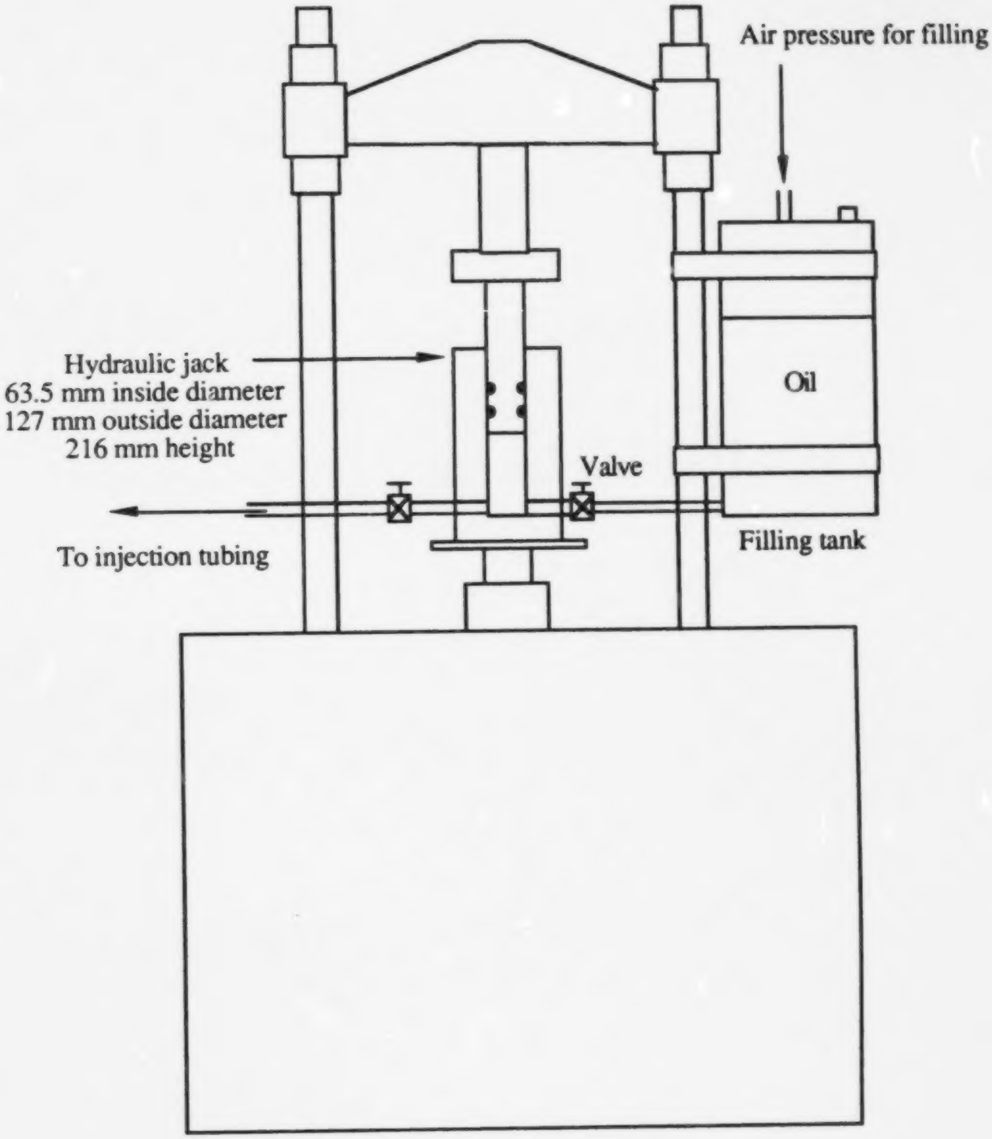
Air pressure for filling
Hydraulic jack
63.5 mm inside diameter
127 mm outside diameter
216 mm height
Oil
Valve
To injection tubing
Filling tank

Figure 2.3 Pump System

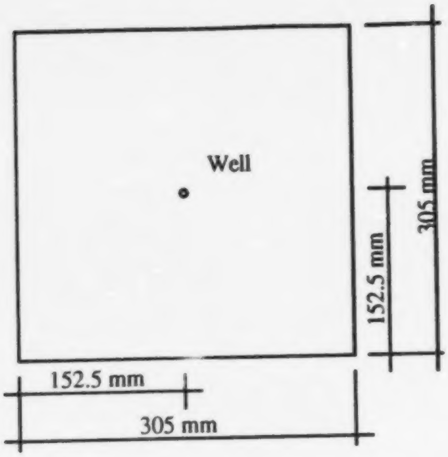
Well
152.5 mm
305 mm
152.5 mm
305 mm

a. Layout of Wells

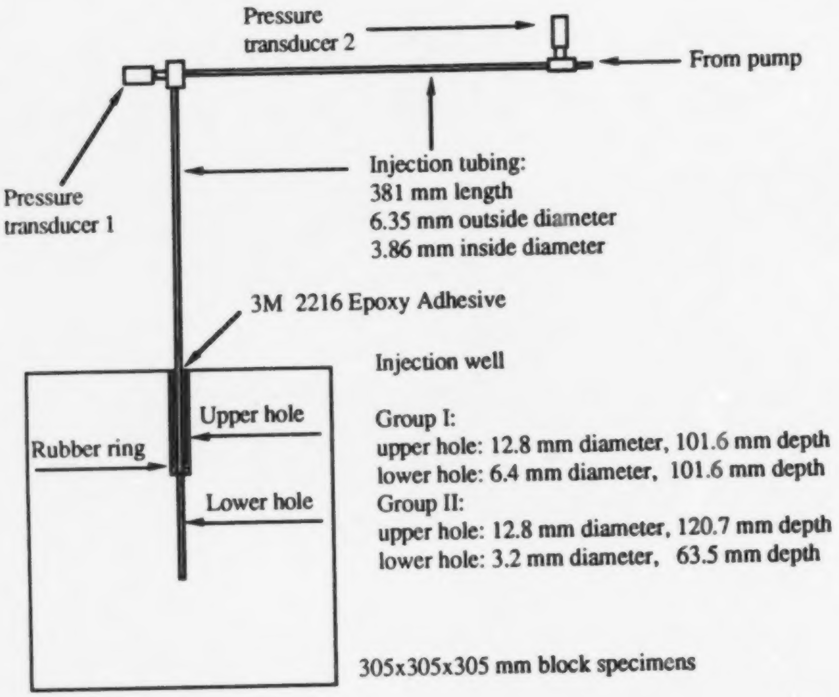
Pressure
transducer 2
From pump
Pressure
transducer 1
Injection tubing:
381 mm length
6.35 mm outside diameter
3.86 mm inside diameter
3M 2216 Epoxy Adhesive
Injection well
Upper hole
Rubber ring
Lower hole
Group I:
upper hole: 12.8 mm diameter, 101.6 mm depth
lower hole: 6.4 mm diameter, 101.6 mm depth
Group II:
upper hole: 12.8 mm diameter, 120.7 mm depth
lower hole: 3.2 mm diameter, 63.5 mm depth
305x305x305 mm block specimens

b. Injection Tubing, Sealing, and Pressure Transducers

Figure 2.4 Layout of Wells, Injection Tubing, and Sealing

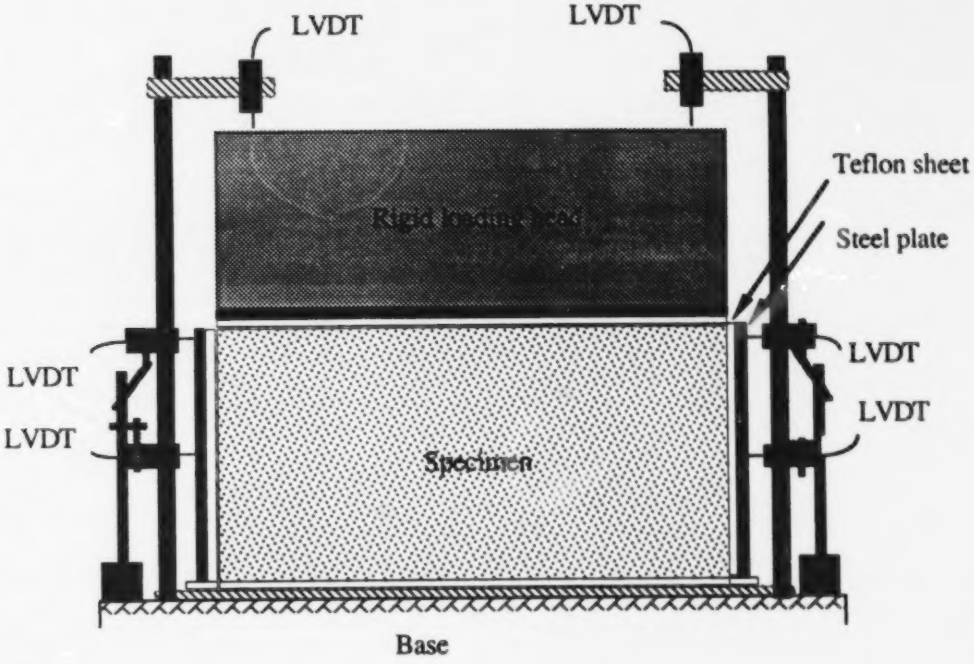
LVDT
LVDT
Teflon sheet
Rigid loading head
Steel plate
LVDT
LVDT
LVDT
LVDT
Specimen
Base

Figure 2.5 Deformation Monitoring

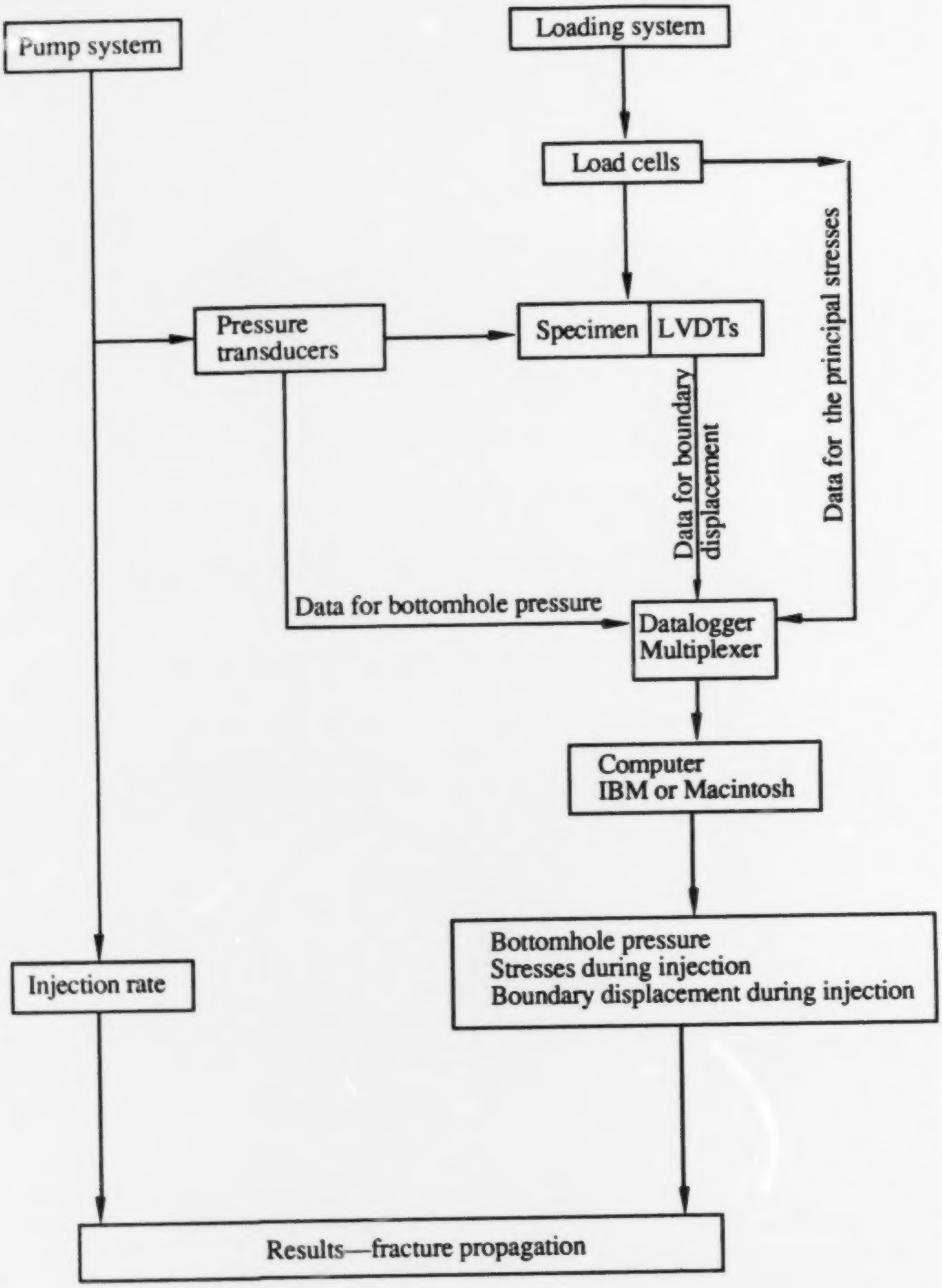
Pump system
Loading system
Load cells
Pressure transducers
Specimen
LVDTs
Data for boundary displacement
Data for the principal stresses
Data for bottomhole pressure
Datalogger Multiplexer
Computer IBM or Macintosh
Bottomhole pressure
Stresses during injection
Boundary displacement during injection
Injection rate
Results—fracture propagation

Figure 2.6 Schematic Diagram of Set-up and Data Acquisition for Hydraulic Fracture Tests

a. Bottomhole Pressure and Injection History

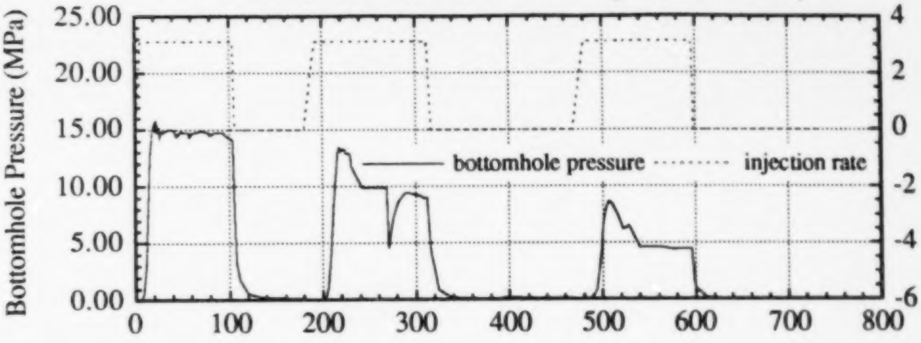

b. Principal Stresses

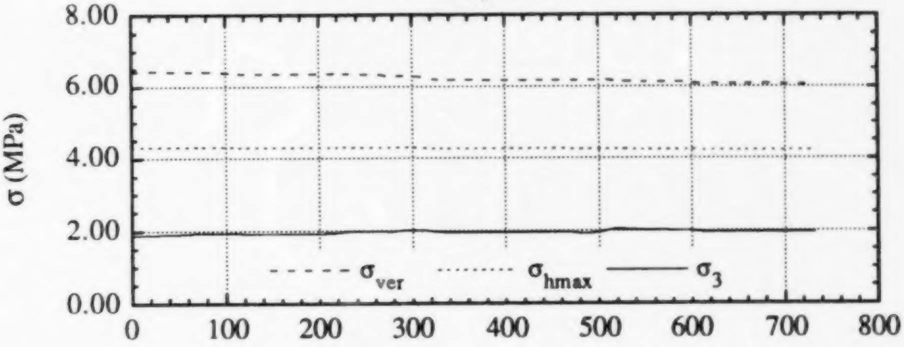

c. Boundary Displacement

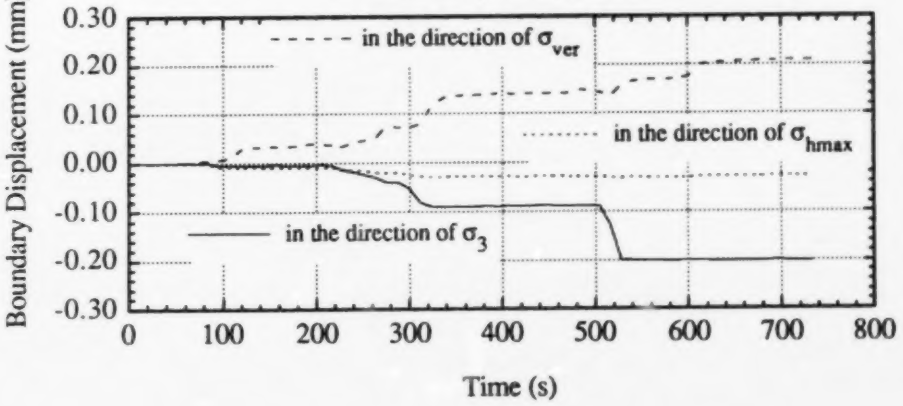

Figure 2.7 Hydraulic Fracture Test 3

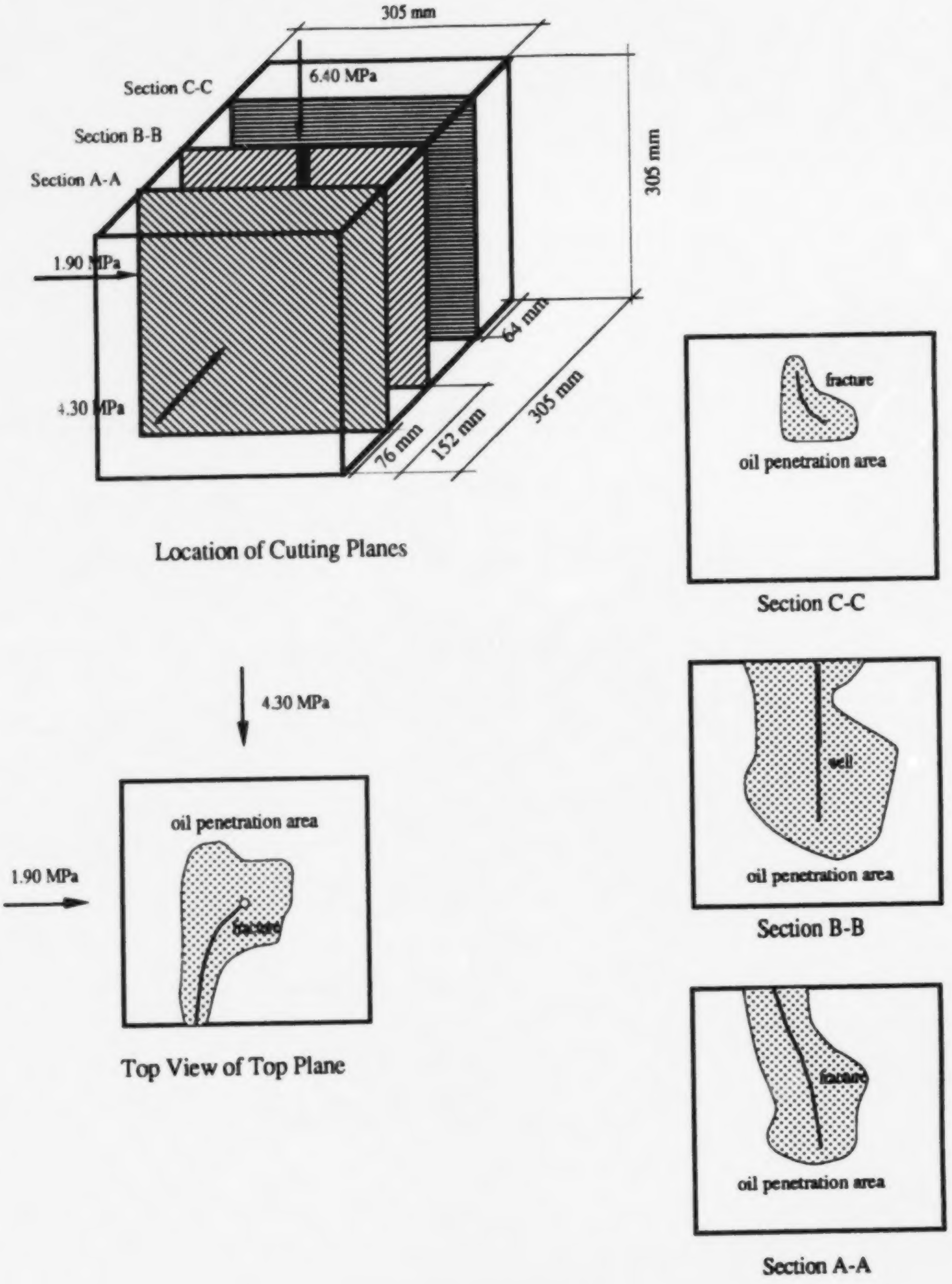
305 mm
6.40 MPa
Section C-C
Section B-B
Section A-A
305 mm
1.90 MPa
64 mm
305 mm
152 mm
4.30 MPa
76 mm
fracture
oil penetration area
4.30 MPa
1.90 MPa
oil penetration area
fracture
well
oil penetration area
fracture
oil penetration area

Location of Cutting Planes

Section C-C

Top View of Top Plane

Section B-B

Section A-A

d. Fracture Description

Figure 2.7 Continued

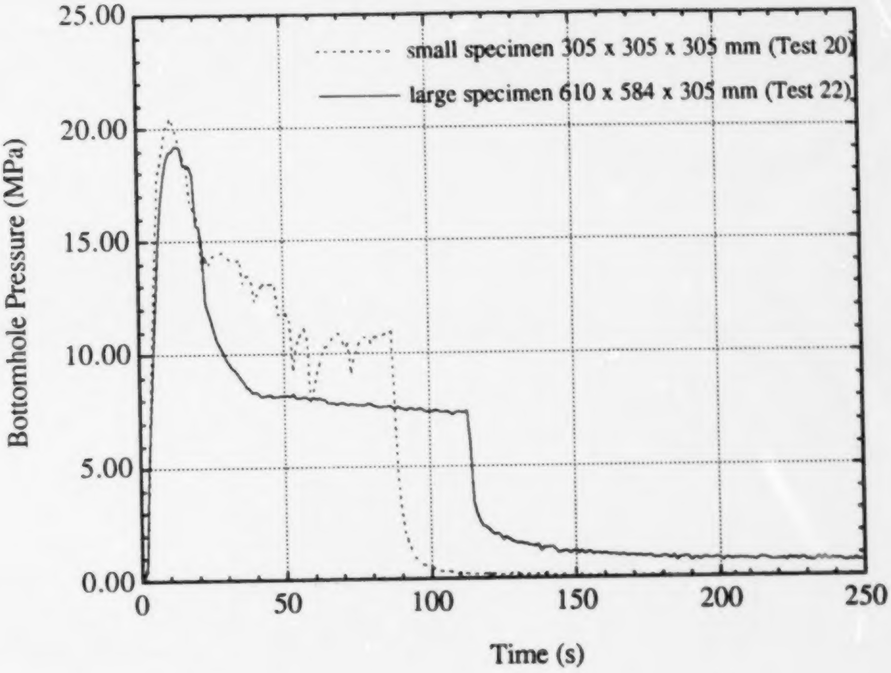

Test 20: σ_{ver}=4.88 MPa, σ_{hmax}=4. 68 MPa σ_3=2.95 MPa

Test 22: σ_{ver}=5.35 MPa, σ_{hmax}=5.01 MPa, σ_3=2.69 MPa

Fracture fluid: 1000 mPa•s

Injection rate: 3.186 cm^3/s
Borehole diameter: 3.2 mm

Figure 2.8 Hydraulic Fracture Tests under Different Specimen Size

Chapter 3

An Experimental Investigation into Hydraulic Fracture Propagation Part 2: Single Well Tests

3.1 Introduction

Since the development of hydraulic fracturing to enhance the production of oil or gas from a well, many fracture propagation models [1-4] have been put forward. They have advanced rapidly from simple two-dimensional theoretical models in the early 1960's, such as the PKN and the GdK models to complex three-dimensional numerical models. More than 2000 publications have been devoted to various aspects of hydraulic fracturing. However, practical methods of evaluating the theoretical and numerical models have been few. Mostly, they have been limited to indirect and generally inconclusive field evaluations. Only three significant laboratory research programs have been carried out (Biot and Medlin et al. [5-6], Rubin [7], and Johnson et al. [8]). Evidently experimental confirmation of the models has not been paid the attention that it deserves.

Many factors affect fracture propagation and fracture geometry, such as the state of stress, the injection rate, the fracture fluid, the Young's

Modulus, the fracture toughness of rocks or the tensile strength, the initial pore pressure, the leak-off coefficient, and the relative bed thickness of formations, the specimen size, and the like. It is impossible to cover all the factors in one program. The set of the experiments reported here mainly concentrated on the influence of the least principal stress and injection rate on fracture propagation.

In Chapter 2, the experimental facilities were described in detail. One typical experimental result was shown to illustrate data presentation, and the effect of specimen size on breakdown pressure was examined through comparison of hydraulic fracture tests under two different specimen sizes. No size effects were encountered. This chapter presents the experimental results from the single well hydraulic fracturing program. First, all hydraulic fracture tests are summarized. Subsequently, effects of the least principal stress and the injection rate on fracture propagation are discussed. Finally, several interesting observations are noted.

3.2 Summary of Hydraulic Fracture Tests

Twenty-three hydraulic fracture tests have been conducted. Twenty-one of them were run on 305 x 305 x 305 mm (12" x 12" x 12") block specimens, and the other two were run on 610 x 584 x 305 mm (24" x 23" x 12") block specimens. Three preliminary tests 0, 1, and 2 were conducted first. Through them, the experimental equipment was examined, and fracture fluid and injection tubing were chosen. Hydraulic oil with 30 mPa•s viscosity at room temperature was first used as the fracture fluid in Test 0. However, the experimental results showed that the viscosity of the oil was not high enough, and all the fracture fluid leaked off into the rock. A fracture could not be created. Although the hydraulic fracture test failed, it was possible to estimate hydraulic conductivity of Gypstone according to Hvorslev's theory [9]. The hydraulic conductivity obtained is 1.78×10^{-4} cm/s (0.182 μm^2) which confirms the measurement of hydraulic conductivity described in Chapter 2. Subsequently, more viscous gear oil with a viscosity of 460 mPa•s at room temperature was employed in Test 1. A fracture was created, but it did not extend to the surface of the specimen because of excessive leak-off. Finally a gear oil with 1000 mPa•s at room temperature was accepted as the fracture fluid, and it gave satisfactory results.

After the three preliminary tests were performed, five hydraulic fracture tests with injection rate of 3.114 cm^3/s under various σ_3 were conducted. They are hydraulic fracture tests 3, 5, 8, 9, and 18. Their objective was to study effects of the least principal stress on fracture propagation. Following that, 13 more hydraulic fracture tests 6, 7, 10 to 17, 19, 20, and 23 were performed to investigate effects of injection rate on fracture propagation. In addition, two hydraulic fracture tests were conducted in 610 x 584 x 305 mm (24" x 23" x 12") block specimens. By comparison with the results on 305 x 305 x 305 mm (12" x 12" x 12") block specimens, the effects of specimen size on breakdown pressure were investigated. These latter results have been presented in Chapter 2.

All hydraulic fracture tests are summarized in Table 3.1. Table 3.1 lists the three principal stresses applied on specimens, the oil viscosity (viscosity of fracture fluid), the injection rate, the diameter and the depth of injection well, the breakdown pressure, the oil penetration radius, and the fractures induced.

3.3 Hydraulic Fracturing Under Various σ_3

The state of in situ stress is one of the most important variables influencing hydraulic fracturing. It dominates not only the orientation of fracture initiation and propagation, but also fracture length and width. A successful model has to consider properly the influence of stresses. Theoretically, some insight on effects of stresses on fracture propagation have been obtained, but few experimental data are available to examine these effects. Hence, five hydraulic fracture tests were run to study the influence of the least principal stress on fracture propagation. In these tests, the same injection rate (3.114 cm^3/s) and the same well size (6.4 mm in diameter and 101.6 mm in depth) were used. The only difference was the state of stress applied to various specimens. The least principal stress in these tests ranged from 0 to 7.00 MPa (0 to 1,015 psi). The results of Test 3 have been shown in Chapter 2. The results of other two hydraulic fracture tests and comparison of the experimental results among the series are discussed in the following paragraphs.

Test 8 (Figure 3.1) was a test without stresses. The fracture created was vertical, and propagation was extremely fast. It extended over the whole specimen in only a few seconds. A noise accompanied this process. This rapid fracture propagation was also clearly reflected in the bottomhole pressure versus time curve. As shown in Figure 3.1 a, bottomhole pressure dropped to zero in a few seconds. The oil penetration area (Figure 3.1 b) was a circle around the injection well with radius of about 10 mm (0.4"). Beyond this area, oil also appeared in part of the fracture but only on the fracture wall, and there was no infiltration into the formation.

Test 5 (Figure 3.2) had 15.00 MPa (2,176 psi) vertical stress, 13.40 MPa (1,944 psi) and 7.00 MPa (1,015 psi) horizontal stresses. The fracture produced (Figure 3.2 d) was vertical and perpendicular to the least principal stress when it was initiated. It deviated from vertical when the fracture approached the bottom boundary. The oil penetration area was also interesting. It was not circular but more band-like and was evidently influenced by the presence of the fracture.

In the first three injection cycles, testing was run in the same way as Tests 3 and 8. However, the bottomhole pressure curve in these tests was completely different from that in Tests 3 and 8. There were no plunges or drops following an instantaneous rise in the bottomhole pressure curve. The bottomhole pressure after breakdown decreased so slowly that it was misinterpreted during testing by judging that the fracture could not extend any longer because of high σ_3. Consequently, σ_3 was unloaded by 1 to 2 MPa (145 to 290 psi). After testing, plotting of the results showed that the fracture was propagating, and the boundary displacement was advancing although the bottomhole pressure declined slowly. The fracture propagation was controlled. In the fifth injection cycle, a sudden drop in bottomhole pressure occurred, which indicated that the fracture extended to the surface of the specimen.

It is also of interest to note the difference between the bottomhole pressure at shut-in and the highest bottomhole pressure in the following injection cycle. The first injection cycle was shut in when bottomhole pressure was equal to 20.32 MPa (2,947 psi), and the highest bottomhole pressure achieved in the second injection cycle was 20.45 MPa (2,966 psi). They are approximately equal. The bottomhole pressure in the second injection cycle was 19.56 MPa (2,837 psi) at shut-in, and the highest bottomhole pressure in the third injection cycle was 19.65 MPa (2,850 psi). The same result was obtained, i.e. the two values are approximately equal. Between the third and fourth injection cycles, σ_3 was decreased by 0.74 MPa (107 psi). The bottomhole pressure in the third injection cycle was 19.05 MPa (2,763 psi) at shut-in, and the highest bottomhole pressure in the fourth injection cycle was 18.34 MPa (2,660 psi). Consequently, the highest bottomhole pressure in the fourth injection cycle was 0.71 MPa (103 psi) less than the bottomhole pressure at shut-in in the third injection cycle. σ_3 was lowered by 1.83 MPa (265 psi) between the fourth and fifth injection cycles. Similarly, the highest bottomhole pressure in the fifth injection cycle was 3.07 MPa (445 psi) less than the bottomhole pressure at shut-in in the fourth injection cycle (17.81 MPa). The experimental results show clearly that σ_3 controls the magnitude of bottomhole pressure during fracture propagation, and a low σ_3 leads to low bottomhole pressure.

Figure 3.3 illustrates the bottomhole pressure under various σ_3. The bottomhole pressure versus time curves for Tests 8, 3, and 5 (the first three cycles) are plotted in this figure. Figure 3.3 a was the result of Test 8 without stresses. The curve was pulse-like. The bottomhole pressure rose rapidly with injection, and plunged to zero in about three seconds after breakdown. The fracture was driven to the surface of the specimen in only one injection cycle. Fracture propagation was extremely rapid. The fracture extended over the whole specimen in about three seconds. Figure 3.3 b was the result of Test 3. The least principal stress was 1.90 MPa (276 psi). The bottomhole pressure versus time curve consists of plunges and drops following an instantaneous rise. The fracture propagated in a step-like manner. The rate of fracture propagation decreased in comparison with Test 8. Three injection cycles were required to extend a fracture to the boundary of the specimen. Figure 3.3 c was the bottomhole pressure of Test 5 (the first three injection cycles). The least principal stress was 7.00 MPa (1,015 psi). After breakdown, the bottomhole pressure dropped slowly. The fracture propagation was very slow and under control. The fracture was still within the specimen after three injection cycles. The rate of fracture propagation decreased again. In conclusion, the rate of fracture propagation obviously decreases with a rise in the least principal stress (σ_3). This decrease is characterized by the change in bottomhole pressure following breakdown. When the least principal stress is zero, the change in bottomhole pressure post breakdown is a sudden plunge from the breakdown pressure to zero (a surge in fracture length and width). For the low least principal stress, this change consists of small plunges and drops following an instantaneous rise. For the high least principal stress, the change is a gentle decline.

Figure 3.4 plots the boundary displacements in the direction of the least principal stress (perpendicular to the fracture) for Tests 3 and 5. Test 3 had the least principal stress of 1.90 MPa (276 psi). The boundary displacement in the direction of the least principal stress was around 0.20 mm (7.9×10^{-3} in.) at the end of the third cycle. Test 5 had the least principal stress of 7.00 MPa (1,015 psi). As it happened, the boundary displacement in the direction of the least principal stress was only 0.1 mm (3.9×10^{-3} in.) at the end of the third cycle. This indicates that a high least principal stress results in a reduced boundary displacement, that is, a narrow and short fracture; and a low least principal stress results in a large boundary displacement when a longer and wider fracture is induced.

Figure 3.5 presents the oil penetration area in a horizontal middle plane for Test 8 (Figure 3.5 a) and Test 5 (Figure 3.5 b). The two oil penetration zones have obviously different features. Oil penetration area for Test 8 was circular, and some part of the fracture was filled with oil, but oil was on the fracture wall and had not infiltrated into the rock. This indicates clearly that oil leaks off from the borehole into the rock, which forms the circular oil penetration area. Oil entering the fracture occurs suddenly so that the perfect circular oil penetration area is recorded. The oil enters the fracture after breakdown and fracture opening. The oil penetration area for Test 5 (Figure 3.5 b) was like a band. Obviously, oil leaks off from the fracture into the rock, which forms this penetration area. The linear flow along the fracture dominates oil leak-off in this test. If the bottomhole pressure curve in Figure 3.1 a is checked, it is found that in Test 8, the injection period before breakdown was 26 seconds, and the fracture extended over the whole specimen in 2 to 3 seconds. After that, oil flowed out of the specimen from the bottom. Hence the oil penetration area recorded mainly oil flow before breakdown. In contrast, the injection period before breakdown in Test 5 was 120 seconds, but the injection period after breakdown was 570 seconds. If leak-off after shut-in is considered, the injection period post breakdown and leak-off during shut-in dominated the whole injection process. Therefore, this oil penetration area represented mainly leak-off after breakdown. From the above analysis, it is concluded that radial flow dominates leak-off before breakdown. The linear flow along the fracture dominates the flow of the fracture fluid after breakdown, and the leak-off from the fracture into the rock is the main leak-off mode. The breakdown seems to be a transient point between the two flow modes.

The breakdown pressure is an important parameter for hydraulic fracturing stress measurements. To evaluate effects of the state of stress on them, Figure 3.6 is plotted, which covers the results of Tests 3, 5, 8, 9, 18, 2, and 14. Figure 3.6 a plots breakdown pressure against the least principal stress σ_3. The relative coefficient is 0.95 by the linear least squares fit. According to current hydraulic fracturing theories for stress measurements, breakdown pressure (for a vertical fracture) occurs when the minimum effective stress on the wall of a well reaches the tensile strength of the rock. The minimum effective stress on the wall of a well is approximately $3\sigma_3\text{-}\sigma_{hmax}$. Therefore, Figure 3.6 b plots the relation between breakdown pressure against $3\sigma_3\text{-}\sigma_{hmax}$. The relative coefficient is 0.89 by the linear least squares fit. This fact reveals that breakdown pressure depends more on the least principal stress rather than on the stress in the wall of a well ($3\sigma_3\text{-}\sigma_{hmax}$).

In the plot of breakdown pressure against $3\sigma_3\text{-}\sigma_{hmax}$, the breakdown pressure at $3\sigma_3\text{-}\sigma_{hmax}=0$ is the tensile strength (it is called the apparent tensile strength or hydraulic fracturing tensile strength) according to the hydraulic fracture theory. This value from Figure 3.6 b is 11.8 MPa (1,711 psi). However, the tensile strength measured by the Brazilian tests and the splitting tests is only 0.343 MPa (50 psi). "The tensile strength" from hydraulic fracturing is 34 times as high as the usual tensile strength from the Brazilian test. The breakdown pressure is extremely high and is not capable of being predicted by the tensile strength and the state of stress in the wall of a well according to common theories of hydraulic fracturing.

The five hydraulic fracture tests have been successfully conducted. From them, the following conclusions are drawn.

1. Five hydraulic fracture tests were successfully run. They produce data which may be used to check whether the influence of the least principal stress is formulated properly in numerical models.

2. The rate of fracture propagation decreases with a rise in the least principal stress (σ_3). This decrease is characterized by the change in bottomhole pressure post breakdown. When the least principal stress is zero or low, bottomhole pressure consists of plunges and drops following an instantaneous rise, and fractures propagate rapidly in a step-like manner. For the high least principal stress, like Tests 5 and 9, bottomhole pressure post breakdown drops gently. The fracture propagates slowly and under control, and the opportunity for leak-off is enhanced.

3. The decrease in the rate of fracture propagation is also characterized by boundary displacements perpendicular to the fracture. For the low least principal stress, a large boundary displacement appears, and a wide and long fracture is induced. For a high least principal stress, a small boundary displacement is produced, which implies that the fracture induced is short and narrow.

4. Through the evaluation of the oil penetration area, it is found that radial flow dominates leak-off before breakdown. The linear flow along the fracture dominates flow of the fracture fluid after breakdown, and leak-off from the fracture into the rock is the main leak-off mode after breakdown. The breakdown is a transient point between the two flow modes.

5. The breakdown pressure can be related to σ_3 rather than $3\sigma_3$-σ_{hmax} under some experimental conditions. "The tensile strength" calculated from hydraulic fracturing is 34 times as high as the usual tensile strength from the Brazilian test. The two facts indicates that breakdown pressure is extremely high for experiments reported here and is not capable of being predicted by the tensile strength and the state of stress on the wall of a well according to conventional theory.

3.4 Hydraulic Fracturing under Various Injection Rates

Injection rate is one of the most important controllable variables in hydraulic fracturing. In field hydraulic fracturing stimulation, injection rate and injection procedure are usually used to control fracture geometry. It is essential for a numerical model to formulate injection rate properly. Thirteen hydraulic fracture tests were performed under three different conditions to study the effects of injection rate on fracture propagation, which were Tests 6 to 8, 10 to 17, 19, and 20. The first set was under zero stress. They were hydraulic fracture tests 6 to 8, and 11 to 14. The injection rates ranged from 0.106 to 3.114 cm^3/s. The injection well was 6.4 mm (0.25") in diameter and 101.6 mm (4") in depth. Through these tests, effects of the injection rate under zero stresses were evaluated. Also another Test 10 was performed under step-rate injection. The injection rates were 0.317, 0.528, 1.056, and 3.166 cm^3/s, respectively. The three principal stresses on the specimen remained constant. The injection well was 6.4 mm (0.25") in diameter and 101.6 mm (4") in depth. This test was intended to reveal effects of injection rate on fracture propagation under constant stresses. Since subsequent injection cycles may be affected by the previous injection cycles, five other hydraulic fracture tests 15 to 17, 19, and 20 were conducted to avoid this interaction. The stresses on different specimens were similar. The injection rates were 2.164 and 3.186 cm^3/s. The injection well was 3.2 mm (0.125") in diameter and 63.5 mm (2.5") in depth. They were also intended to study effects of the injection rate under constant stresses on fracture propagation.

3.4.1 Hydraulic Fracturing under Various Injection Rates: without Stresses

Three representative results (Tests 8, 12, and 13) are shown in Figure 3.7 and 3.8. Figure 3.7 depicts the bottomhole pressure obtained and injection history in the three tests. Several features are apparent. The first feature is that the well storage and the compression of the fracture fluid control the bottomhole pressure at the beginning of injection. The three factors lead to a slow rise in bottomhole pressure. This period increases with decrease of the injection rate. Another feature is that when the wellbore was filled, leak-off of the fracture fluid and the compression of the fracture fluid dominate bottomhole pressure. During this duration, the bottomhole pressure increases rapidly. The final feature is that the fracture induced also affects bottomhole pressure. This is illustrated in Figure 3.7 a. A fracture opened and closed before breakdown, which resulted in two drops following an instantaneous rise in bottomhole pressure. Although the radial flow still dominates flow of the fracture fluid, as illustrated by the oil penetration area, there are many other factors which also influence bottomhole pressure.

Figure 3.8 presents the oil penetration area in the horizontal middle plane for the three tests. Tests 12 and 13 induced vertical fractures similar to Test 8. Fracture propagation was extremely fast, and it extended over the whole specimen in only two to three seconds. A noise accompanied this process. The bottomhole pressure dropped to zero in about three seconds (Figure 3.7). All the oil penetration areas were similar to Test 8 with radial penetration around wells. The oil penetration radius varied with injection rate, from 10 mm (0.4") at an injection rate of 3.114 cm^3/s to 25 mm (1") at an injection rate of 1.055 cm^3/s. Beyond this area, oil appeared on part of the fracture wall, and had not infiltrated into the formation. Similar fracture propagation and oil penetration areas were also obtained for an injection rate as low as 0.106 cm^3/s in Test 6. In Test 6, injection continued for one hour and 23 minutes, and the oil penetration radius was 70 mm (2.8"). These further proved that oil leaks off radially before breakdown, and oil enters fractures after breakdown even though the injection rate is as low as 0.106 cm^3/s.

The effect of injection rate on breakdown pressure also is of interest, especially for stress measurements. It is presented in Figure 3.9. The breakdown pressure from Tests 6 to 8, and 11 to 14 are plotted in this figure. When an injection rate increases from 0.106 to 3.114 cm^3/s, breakdown pressure rises from 3.88 MPa (563 psi) to 11.00 MPa (1,595 psi). The influence of the injection rate is striking.

This set of tests provides limited information for fracture propagation post breakdown because fracture propagation is so quick that a fracture extends to the boundary of the specimens in only a few seconds. However, it is informative with regard to the build-up of the bottomhole pressure and understanding of the breakdown pressure. The bottomhole pressure produces data for evaluation of flow theory before breakdown. The oil penetration area recorded supplies further evidence for the point that radial flow dominates leak-off before breakdown, and the fracture fluid enters a fracture at breakdown, which results in linear flow along the fracture. The relationship between the breakdown pressure and the injection rate provides data for verification of theories regarding breakdown pressure.

3.4.2 Hydraulic Fracturing under Various Injection Rates: a Step-Rate Test

Figure 3.10 provides the results of Test 10. A step-rate was used in this test. The injection rates were 0.317, 0.528, 1.056, and 3.166 cm^3/s, respectively. The three principal stresses were vertical stress of 13.20 MPa (1,914 psi), horizontal stresses of 9.70 MPa (1,407 psi) and 5.40 MPa (783 psi). The injection well was 6.4 mm (0.25") in diameter and 101.6 mm (4") in depth. The fracture induced was perpendicular to the least principal stress.

Four injection rates produced four different kinds of behavior of the bottomhole pressure versus time. In the first injection cycle, the bottomhole pressure increased continuously. When the bottomhole pressure reached 7.2 MPa (1,044 psi), the oil was used up, and the well was shut in. No features suggest that a fracture was initiated. In the second injection cycle, a sudden change in the slope of the bottomhole pressure versus time curve appeared when the bottomhole pressure was 10 MPa (1,450 psi). After that, the bottomhole pressure increased slowly. The highest bottomhole pressure had not been reached at shut-in. This sudden change in the slope indicates that a fracture was initiated before breakdown, which was identical with the conclusions drawn from AE monitoring by Zoback et al. [10]. It also reflects that an induced fracture will affect a build-up of bottomhole pressure. In the third injection cycle, the breakdown occurred when the bottomhole pressure rose to 13.83 MPa (2,006 psi). After that, the bottomhole pressure declined gently with injection. In the fourth injection cycle, the rate of decline in the bottomhole pressure increased. This test demonstrates the effects of the injection rate on hydraulic fracturing. When the injection rate is very low, as happened in the first injection cycle, the fracture fluid leaks off into the rock from the injection well. A fracture cannot be initiated, and the test is like a well test. For a higher injection rate, most of the fracture fluid still leaks off into the rock from the injection well so that a wedge effect cannot be formed. Consequently, as happened in the second injection cycle, the bottomhole pressure increases slowly with fracture propagation. The fracture should be extremely narrow under this injection rate. When the injection rate rises again, the amount of the fracture fluid entering the fracture increases, the wedge effect is formed so that the bottomhole pressure develops as happened in the third injection cycle. But the fracture is still narrow so that this wedge effect is small, and the bottomhole pressure declines slowly. For a higher injection rate, most of the fracture fluid enters into a fracture. Fracture wide increases rapidly with injection, which leads to a low loss of pressure in the fracture. The fracture propagates unstably under these conditions, as happened in the fourth injection cycle.

The boundary displacement perpendicular to the fracture (in the direction of σ_3) in Figure 3.10 b is consistent with the above explanation. There was no boundary displacement in the first injection cycle, which was identical with the fact that there was no fracture in the specimen. There still was no boundary displacement in the second injection cycle, which was also consistent with extremely narrow fractures deduced from bottomhole pressure. In the third injection cycle, a slight boundary displacement developed at the end of the injection cycle. The fracture induced was narrow. In the fourth injection cycle, the fracture fluid entered the fracture and a wide fracture developed, which led to a large boundary displacement. Therefore, boundary displacement, like bottomhole pressure, characterizes the fracture induced, but it is not sensitive to the narrow fracture as induced in the second and third injection cycles.

3.4.3 Hydraulic Fracturing under Various Injection Rates: with Similar Stresses

In the step-rate test, subsequent injection cycles may be affected by the previous injection cycle. To avoid this, five hydraulic fracture tests were conducted on different specimens. Two injection rates were used.

Tests 15 and 16 used an injection rate of 2.164 cm^3/s. Tests 17, 19, and 20 used an injection rate of 3.186 cm^3/s. The states of stress in all five tests were similar. The injection well was 3.2 mm (0.125") in diameter and 63.5 mm (2.5") in depth. The fracture fluid was still gear oil with 1000 mPa•s viscosity. In the following paragraphs, two of them (Tests 16 and 19) are compared and discussed.

Figure 3.11 shows the oil penetration area and the fracture induced in the two tests. Test 16 produced a fracture perpendicular to the least principal stress σ_3 (Figure 3.11 a). The fracture stopped extending due to low injection rate (2.164 cm^3/s). Finally oil leaked off radially so that approximately circular oil penetration was obtained. Test 19 created a vertical fracture. However, the orientation of this fracture was not perpendicular to the least principal stress. The low stress difference and nonhomogeneous permeability are perhaps the main factors which result in this deviation. In this test, a high injection rate (3.186 cm^3/s) created and opened the fracture rapidly so that the fracture fluid entered the fracture. Consequently, the oil penetration area was like a band, and the fracture propagated quickly. This comparison yields the same conclusion as the step rate test. A low injection rate leads to low fracture efficiency. Most of the fracture fluid leaks off into the rock. A high injection rate produces high fracture efficiency. Most of the fracture fluid is used to create a fracture.

Figure 3.12 plots bottomhole pressure produced and injection procedure used in two tests. Test 16 had eight injection cycles. However, the fracture was still within the specimen, as shown in Figure 3.11 a. In the first five injection cycles, the bottomhole pressure after breakdown pressure declined slowly. In the last three injection cycles, a balance was obtained, and the bottomhole pressure remained constant with injection. Unlike Test 16, the fracture in Test 19 was driven to the surface of the specimen by only two injection cycles. The bottomhole pressure declined rapidly after breakdown. This illustrates again that fracture efficiency increases with an rise in injection rate.

Figure 3.12 presents the boundary displacement in the direction of σ_3 monitored in the two tests. Eight injection cycles led to a maximum boundary displacement of 0.035 mm (1.4 x 10^{-3} in.) in Test 16. Conversely, only two injection cycles produced a maximum boundary displacement of 0.100 mm (3.9 x 10^{-3} in.) in Test 19. Obviously, the fracture in Test 19 was wider and longer than that in Test 16. A high injection rate leads to high fracture efficiency.

In conclusion, a low injection rate results in a slow decline in the bottomhole pressure post breakdown and a small boundary displacement. Most of the fracture fluid leaks off into rock. Fracture propagation is slow. Therefore, fracture efficiency is low. Conversely, a high injection rate leads to a quick decline in the bottomhole pressure post breakdown and a large boundary displacement. Most of the fracture fluid is used to create fractures, and fractures propagate rapidly. Hence fracture efficiency is high.

From hydraulic fracture tests under various injection rates, the following conclusions are drawn.

1. Thirteen hydraulic fracture tests were conducted. They produce a considerable amount of data to evaluate effects of the injection rate in numerical models.

2. For cases without stresses, fracture propagation post breakdown is always extremely rapid. Injection rate seems not to control the behavior of fracture propagation in this period. Injection rates have a strong influence on the breakdown pressure and the build-up of the bottomhole pressure before breakdown. The data produced by these tests is informative for understanding and interpretation of the breakdown pressure.

3. For cases with stresses, the conclusions from the step rate test and constant injection rate tests are the same. A low injection rate results in a slow decline in the bottomhole pressure post breakdown and a small boundary displacement. Most of the fracture fluid leaks off into rock. Fracture propagation is slow. Therefore, fracture efficiency is low. Conversely, a high injection leads to a quick decline in the bottomhole pressure post breakdown and a large boundary displacement. Most of the fracture fluid is used to create fractures and fractures propagate rapidly. Hence fracture efficiency is high, and at the same amount of fracture fluid, a longer and wider fracture is produced. It should also be pointed out that high breakdown pressure accompanies a high injection rate.

3.5 Discussion

3.5.1 Intersection of a Fracture with the Surface of Specimens

The identification of the intersection of a fracture with the surface of specimens is of importance to terminate injection. For tests without stresses such as Test 8, a fracture was visible when it intersected with the surface of the specimen. The bottomhole pressure plunged to zero, and continuing injection could not raise it. For low stress tests, a plunge in bottomhole pressure such as in Test 3 also indicated boundary contact. For high stress tests, bottomhole pressure dropped gently, and the high bottomhole pressure remained throughout testing although there also was a sudden drop in bottomhole pressure, as in Test 5. Does this sudden drop still indicate that the fracture induced extends to the surface of a specimen? The results of Tests 9 and 16 shown in Figure 3.14 answer this question. The difference between them is obvious. There was a sudden drop in bottomhole pressure, and the fracture extended to the surface of specimen in Test 9. Conversely, there was no sudden drop in Test 16, and the fracture was still in the specimen. Hence this sudden drop also indicates that a fracture extends to the surface of a specimen. When a fracture extends to the surface of the specimen, no tensile strength is required to be overcome, and the bottomhole pressure should have a sudden drop.

The remaining problem is how to explain the high bottomhole pressure after the plunge. The bottomhole pressure continued to remain as high as 12 MPa (1,740 psi) after the plunge in Test 9 even though the least principal stress was only 6.40 MPa (928 psi). If flow of fluid in the fracture is considered, this high bottomhole pressure seems to be reasonable. The flow of fluid in the fracture is similar to the flow of fluid in a duct after the fracture has extended to the surface of the specimen. When fluid is forced through a thin duct, the thinner the duct is, the larger the pressure loss in the duct. As a result, higher pressure is required. In this test, the fracture width was very narrow (The maximum boundary displacement is only 0.1 mm (3.9×10^{-3} in.)). Hence, high bottomhole pressure was required to drive the fracture fluid through this narrow fracture. That is why bottomhole pressure continued to remain as high as 12 MPa (1,740 psi) after the fracture had extended to the surface of the specimen.

Further evidence can be found in Tests 3 and 8. As stated in the previous section, a low σ_3 results in a wide fracture. σ_3 was equal to zero in Test 8 so the fracture should be the widest fracture. The pressure after the fracture extends to the boundary of the specimen should be the lowest according to the explanation in the above paragraph. The measured pressure, as expected, was zero in Test 8 (Figure 3.1 a). Test 3 had σ_3 of 1.90 MPa (276 psi) so the fracture induced should be wider than Test 9 and narrower than Test 8, and the pressure after the fracture extends to the surface of the specimen should be between that in Test 8 and Test 9. The pressure was about 4.5 MPa (653 psi), which is between zero and 12 MPa (1,740 psi). This further confirms the above explanation. The high bottomhole pressure after a fracture has extended to the surface of a specimen is caused by pressure loss in the fracture.

From the above analysis, it is concluded that the intersection of a fracture with the surface of a specimen is symbolized by a sudden drop in bottomhole pressure. The high bottomhole pressure after this plunge results from pressure loss in the fracture.

3.5.2 Boundary Displacements and Fractures

Boundary displacements are monitored to supply further information for fracture propagation. It is necessary to study to what degree boundary displacements can characterize a fracture. To achieve this goal, the boundary displacements under different fracture modes (vertical and horizontal) are compared, and the relationship between the boundary displacement and the bottomhole pressure is discussed in the following paragraphs.

One horizontal fracture was induced unexpectedly in hydraulic fracture test 15. This offers a chance to compare the boundary displacements for a horizontal fracture with that for a vertical fracture. The results are plotted in Figure 3.15. When a fracture is horizontal (Test 15), the two horizontal boundary displacements are always compressive throughout testing. The vertical boundary displacement is expansive during injection. On the other hand, when a fracture is vertical (Test 3), the vertical boundary displacement is compressive throughout testing. The boundary displacement in the direction of σ_3 (perpendicular to the fracture) is expansive. This clearly indicates that the fracture mode is characterized by the boundary displacements. The boundary displacement perpendicular to the fracture is always expansive during injection. In the other two directions, the boundary displacement in the direction with the higher stress is always compressive.

Boundary displacements are capable of not only characterizing fracture modes, but also characterizing fracture propagation like bottomhole pressure. This is illustrated in Figure 3.16. It is well known that the increase and the decrease in the bottomhole pressure characterize fracture propagation. A plunge in bottomhole pressure symbolizes the rapid opening or extension of fracture, and a rise in bottomhole pressure means the decrease of the speed of fracture propagation. Therefore, when a plunge occurs in the bottomhole pressure, the expansion in boundary displacement is expected. When a drop is followed by a rise in bottomhole pressure (a fracture opens, then stops or closes), boundary displacement should respond. Figure 3.16 illustrates this. The bottomhole pressure plunges from 8.7 to 4.6 MPa (1,262 to 667 psi) in the latter injection cycles, and the boundary displacement increases 0.11 mm (4.3 x 10^{-3} in.). A drop following a rise occurs in the former injection cycles. A steep slope in boundary displacement corresponds to a drop in bottomhole pressure, and a gentle slope to a rise in bottomhole pressure. These show that boundary displacements, like bottomhole pressure, are capable of characterizing fracture propagation. The measurement of boundary displacements has been successful and useful for interpreting fracture characteristics.

3.6 Conclusions

There are few laboratory tests which produce data for verification of hydraulic fracturing numerical models, especially with leak-off. These experiments have been undertaken to make such a contribution. Twenty-three hydraulic fracture tests have been conducted in a large test frame which is capable of taking a block specimen of 610 x 584 x 305 mm (24" x 23" x 12") and applying true triaxial stresses up to 10 MPa (1,450 psi). Leak-off was incorporated. Boundary displacements were measured. Effects of the least principal stress and the injection rate on fracture propagation were studied. Considerable data has been produced for interpretation. From these tests, the following conclusions were drawn.

Effects of the Least Principal Stress

•The rate of fracture propagation decreases with a rise in the least principal stress (σ_3). This decrease is characterized by the change in the bottomhole pressure post breakdown. When the least principal stress is zero or low, the bottomhole pressure consists of plunges and drops following an instantaneous rise, and a fracture rapidly propagates in a step-like manner. For the high least principal stress, the bottomhole pressure post breakdown drops gently and the fracture propagates slowly and under control.

•The decrease in the rate of fracture propagation is also characterized by boundary displacements perpendicular to the fracture. For the low least principal stress, a large boundary displacement appears. For a high least principal stress, a small boundary displacement is produced.

•Radial flow dominates leak-off before breakdown. The linear flow along the fracture dominates flow of fracture fluid after breakdown, and leak-off from the fracture into the rock is the main leak-off mode after breakdown. The breakdown is a transient point between the two flow modes.

•The breakdown pressure can be related to σ_3 rather than $3\sigma_3-\sigma_{hmax}$ under some experimental conditions. The tensile strength calculated from hydraulic fracturing is 34 times as high as the tensile strength from the Brazilian tests and the splitting tests. The breakdown pressure is extremely high and is not capable of being predicted by the tensile strength and the state of stress on the wall of a well according to common theories.

Effects of Injection Rate

•For cases without stresses, fracture propagation post breakdown is always extremely rapid. Injection rate seems not to control behavior of fracture propagation in this period. Injection rate has a strong influence on the breakdown pressure and the build-up of the bottomhole pressure before breakdown for cases without stresses. The data produced by this set of tests is informative for understanding and interpretation of the breakdown pressure.

•For cases with stresses, the conclusions from the step rate test and constant injection rate tests are the same. A low injection rate results in a slow decline in the bottomhole pressure post breakdown and a small boundary displacement. Most of the fracture fluid leaks off into the rock radially. Fracture propagation is slow. Therefore, fracture efficiency is low. Conversely, a high injection leads to a quick decline in the bottomhole pressure post breakdown and a large boundary displacement. Most of the fracture fluid is used to create a fracture. A fracture propagates rapidly. Hence, fracture efficiency is high, which means that at the same amount of fracture fluid in injection, a longer and wider fracture is produced. A high breakdown pressure accompanies a high injection rate.

In addition, the experimental results showed also that the intersection of a fracture with the surface of specimens is symbolized by a sudden drop in bottomhole pressure. The pressure loss in the fracture results in high bottomhole pressure after a fracture intersects with the surface of a specimen. Boundary displacements, like bottomhole pressure, are capable of characterizing fracture propagation.

3.7 References

1. Gidley J. L., Holditch S. A., Nierode D. E., and Veatch R. W. *Recent advances in hydraulic fracturing*, Monograph Series, SPE, Richardson, TX **12** (1989).

2. Mendelsohn D. A. A review of hydraulic fracture modeling–part I: general concepts, 2D models, motivation for 3D modeling. *ASME Journal of Energy Resources Technology* **106**, 369-376 (1984).

3. Mendelsohn D. A. A review of hydraulic fracture modeling–part II: 3D modeling and vertical growth in layered rock. *ASME Journal of Energy Resources Technology* **106**, 543-553 (1984).

4. Veatch Jr. R. W. and Moschovidis Z. A. An overview of recent advances in hydraulic fracturing technology. *Society of Petroleum Engineers Journal* **26**, 421-454 (1986).

5. Biot M. A., Medlin W. L., and Massé L. Laboratory experiments in fracture propagation. *Paper SPE 10377 presented at the 1981 Eastern Regional Meeting*, Columbus, Ohio, U.S.A. (1981).

6. Medlin W. L. and Massé L. Laboratory experiments in fracture propagation. *Society of Petroleum Engineers Journal* **24**, 256-268 (1984).

7. Rubin M. B. Experimental study of hydraulic fracturing in an impermeable material. *Journal of Energy Resources Technology* **105**, 116-124 (1983).

8. Johnson E. and Cleary M. P. Implications of recent laboratory experimental results for hydraulic fractures. *Paper SPE 21846 presented at the Rocky Mountain Regional Meeting and Low-Permeability Reservoirs Symposium*, Denver, Colorado, U.S.A. (1991).

9. Cedergren H. R. *Seepage, drainage, and flow nets*, John Wiley & Sons, New York (1977).

10. Zoback M. D., Rummel F., Jung R., and Raleigh C. B. Laboratory hydraulic fracturing experiments in intact and pre-fractured rock. *Int. J. Rock Mech. Min. Sci. & Geomech. Abstr.* **14**, 49-58 (1977).

Table 3.1 Summary of Hydraulic Fracture Tests

Specimen No.	Vertical stress MPa	Horizontal stress MPa	Horizontal stress MPa	Oil viscosity mPa•s	Injection rate cm^3/s	Diameter of wells mm	Depth of wells mm	Breakdown pressure MPa	Oil penetration radius mm	Fracture
0	6.40	5.10	3.30	30	1.100	6.4	101.6			no
1	6.40	4.30	2.20	460	2.640	6.4	101.6	14.30		vertical
2	5.70	3.90	1.30	1000	3.114	6.4	101.6	12.90		vertical
5	15.00	13.40	7.00	1000	3.114	6.4	101.6	20.80		vertical
9	14.60	11.30	6.40	1000	3.114	6.4	101.6	21.40		vertical
18	7.54	5.78	3.66	1000	3.114	6.4	101.6	13.90		vertical
3	6.40	4.30	1.90	1000	3.114	6.4	101.6	15.80		vertical
8	0.00	0.00	0.00	1000	3.114	6.4	101.6	10.80	10	vertical
14	0.00	0.00	0.00	1000	3.114	6.4	101.6	11.00	10	vertical
12	0.00	0.00	0.00	1000	2.110	6.4	101.6	9.61	15 to 20	vertical
13	0.00	0.00	0.00	1000	1.055	6.4	101.6	6.97	20 to 25	vertical
11	0.00	0.00	0.00	1000	0.528	6.4	101.6	6.26	25 to 30	horizontal
7	0.00	0.00	0.00	1000	0.528	6.4	101.6	5.92	25 to 30	vertical
6	0.00	0.00	0.00	1000	0.106	6.4	101.6	3.88	70	vertical
10	13.20	9.70	5.40	1000	0.317 to 3.166	6.4	101.6			vertical
15	5.15	5.31	3.01	1000	2.164	3.2	63.5	14.29		horizontal
16	5.12	4.93	2.92	1000	2.164	3.2	63.5	18.72		vertical
17	5.21	5.12	2.74	1000	3.186	3.2	63.5	12.16		vertical
19	4.39	4.53	2.99	1000	3.186	3.2	63.5	over 16		vertical
20	4.88	4.68	2.95	1000	3.186	3.2	63.5	20.50		vertical
23	0.00	0.00	0.00	1000	3.186	3.2	101.6	12.22		vertical
21*	4.67	4.37	2.77	1000	3.186	3.2	63.5	17.40		vertical
22*	5.35	5.01	2.69	1000	3.186	3.2	63.5	19.23		vertical

---

* Hydraulic fracture test 21 and 22 were conducted on 610 x 584 x 305 mm block specimens, and the other on 305 x 305 x 305 mm block specimens.

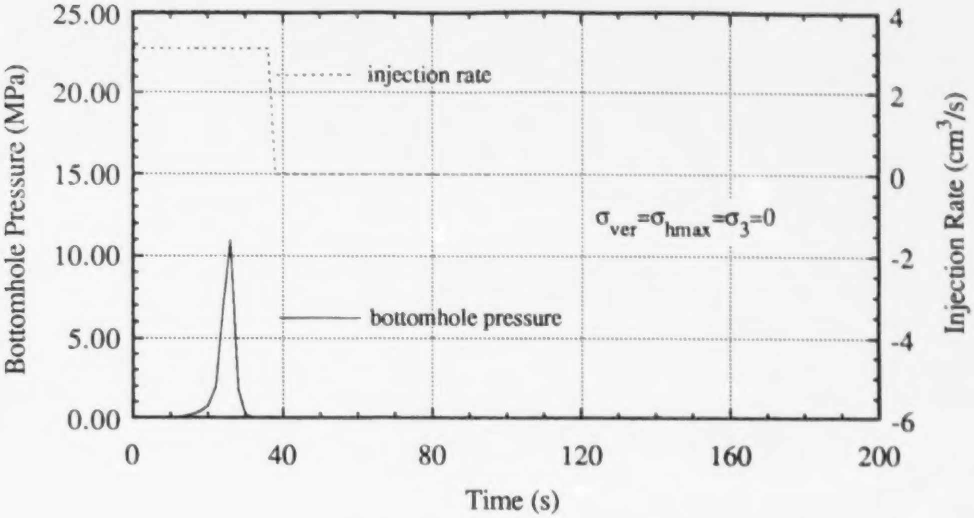

a. Bottomhole Pressure and Injection History

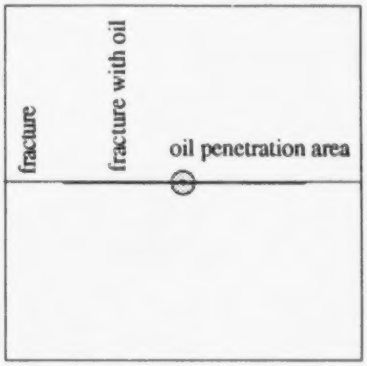
fracture
fracture with oil
oil penetration area

Top View of Horizontal Middle Plane

b. Fracture Description

Figure 3.1 Hydraulic Fracture Test 8

a. Bottomhole Pressure and Injection History

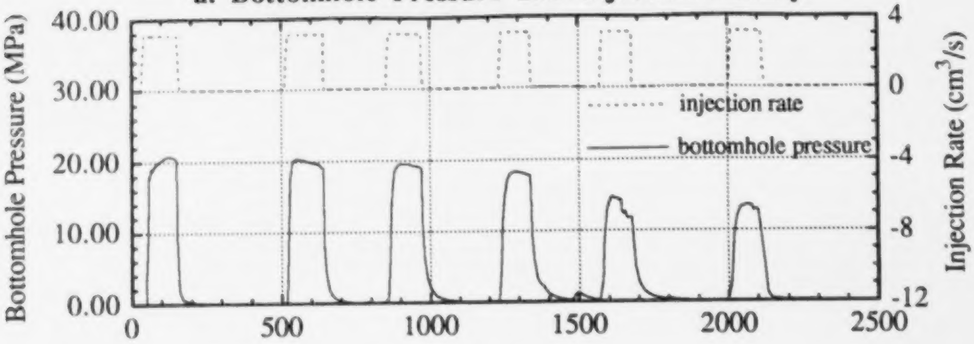

b. Principal Stresses

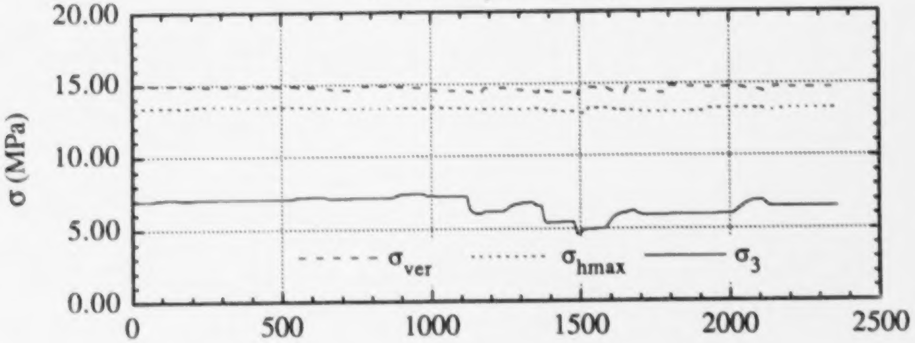

c. Boundary Displacement

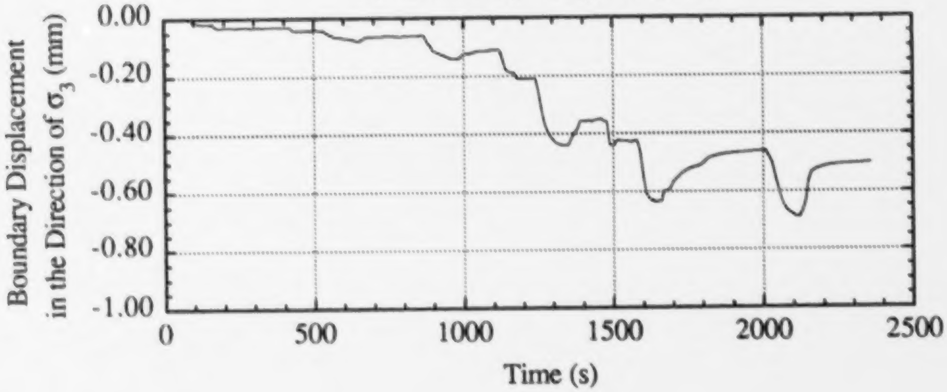

Figure 3.2 Hydraulic Fracture Test 5

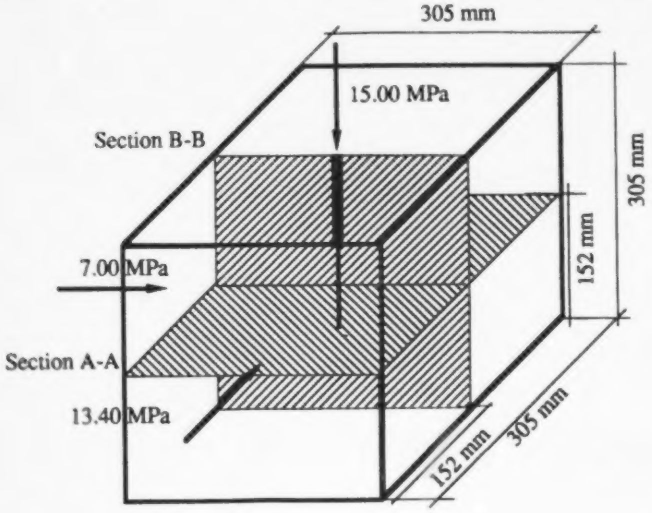
305 mm
15.00 MPa
Section B-B
305 mm
152 mm
7.00 MPa
Section A-A
13.40 MPa
152 mm
305 mm

Location of Cutting Planes

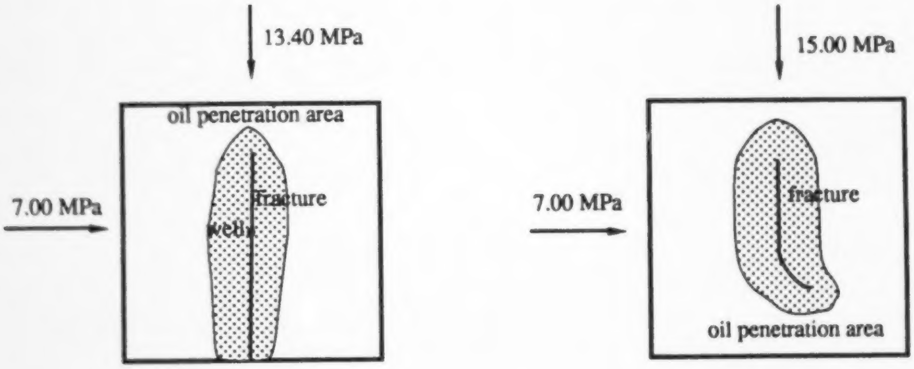
13.40 MPa
oil penetration area
7.00 MPa
fracture
well
15.00 MPa
7.00 MPa
fracture
oil penetration area

Section A-A

Section B-B

d. Fracture Description

Figure 3.2 Continued

a. Hydraulic Fracture Test 8

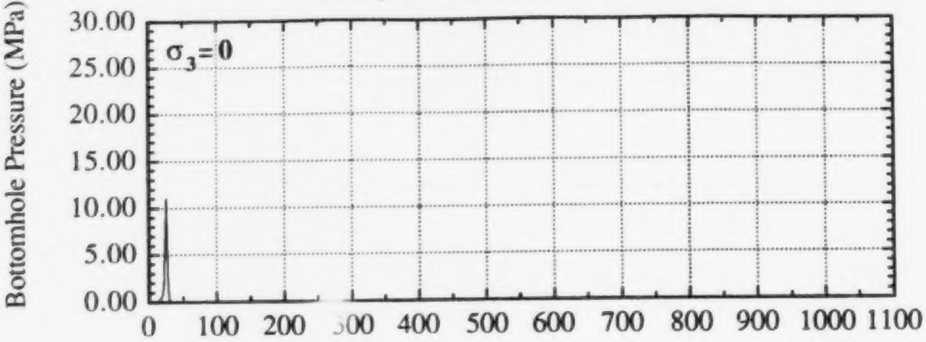

b. Hydraulic Fracture Test 3

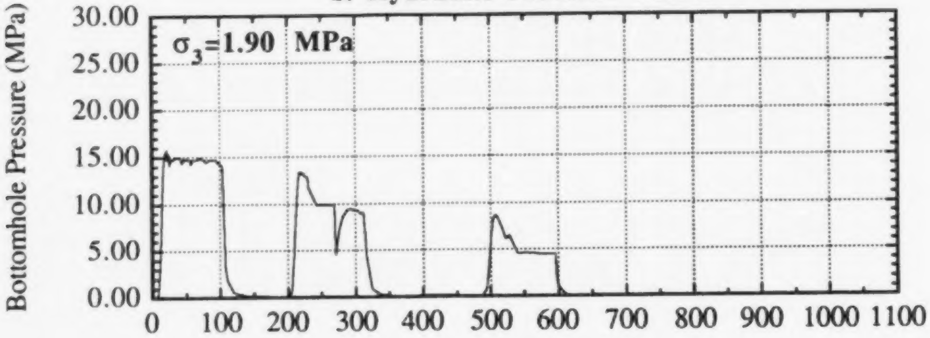

c. Hydraulic Fracture Test 5

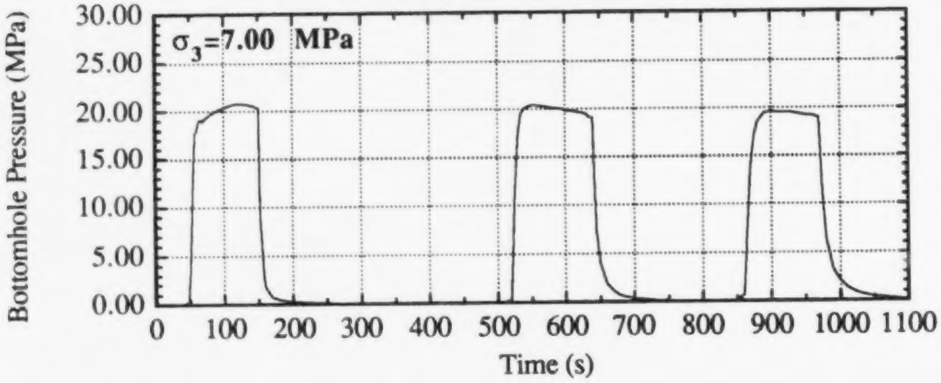

Figure 3.3 Bottomhole Pressure under Various σ_3

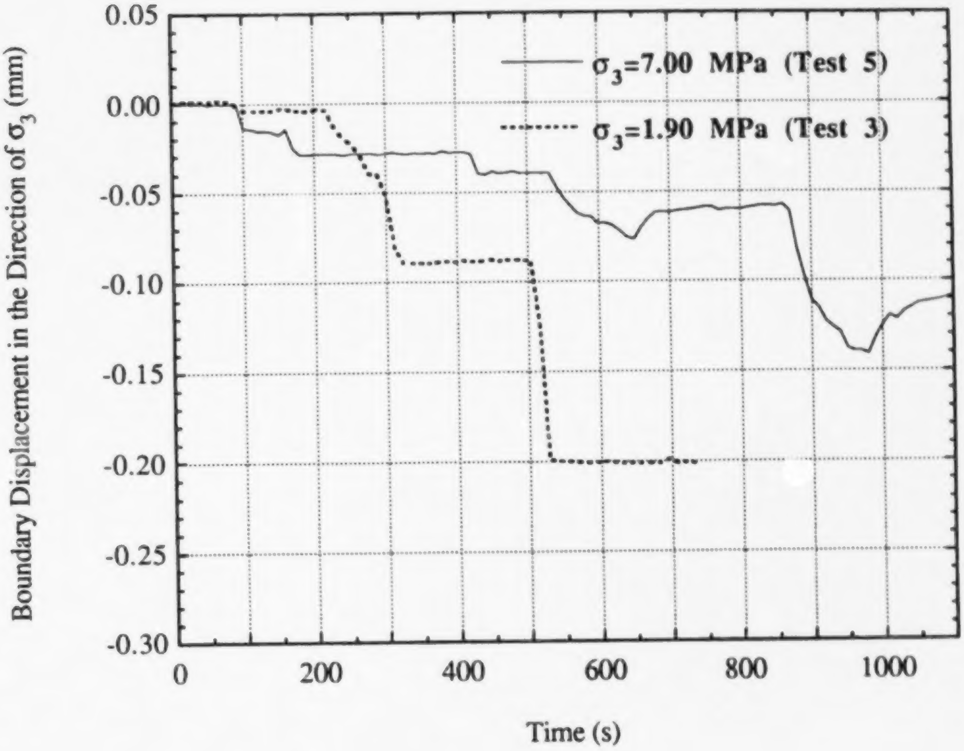

Figure 3.4 Boundary Displacement under Various σ_3

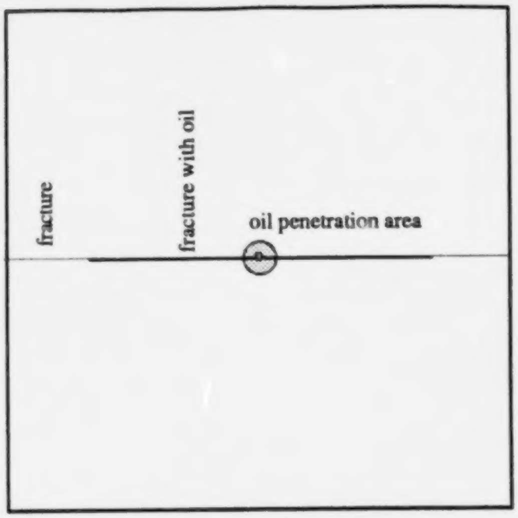
fracture
fracture with oil
oil penetration area

Top View of Horizontal Middle Plane

a. Hydraulic Fracture Test 8 (σ_3=0)

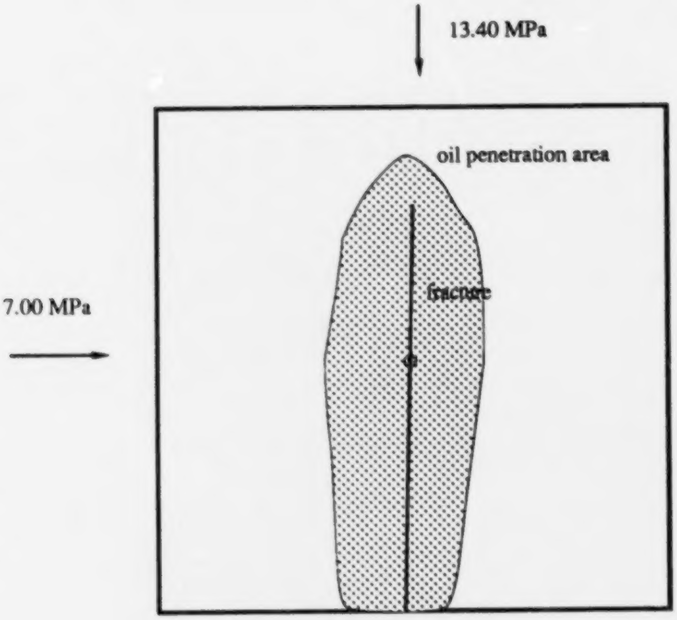
13.40 MPa
oil penetration area
fracture
7.00 MPa

Top View of Horizontal Middle Plane

b. Hydraulic Fracture Test 5 (σ_3=7.00 MPa)

Figure 3.5 Oil Penetration Area under Various σ_3

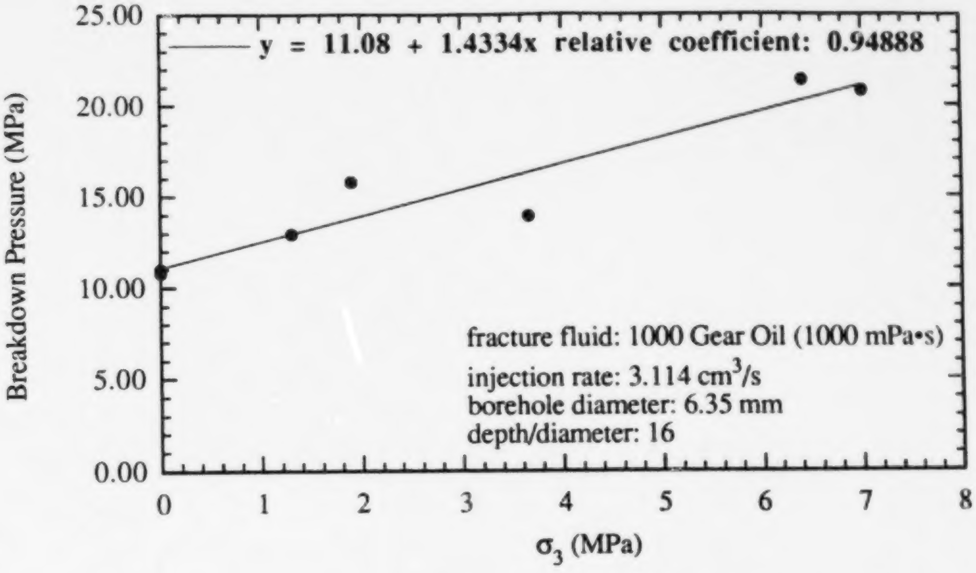

a. Breakdown Pressure against σ_3

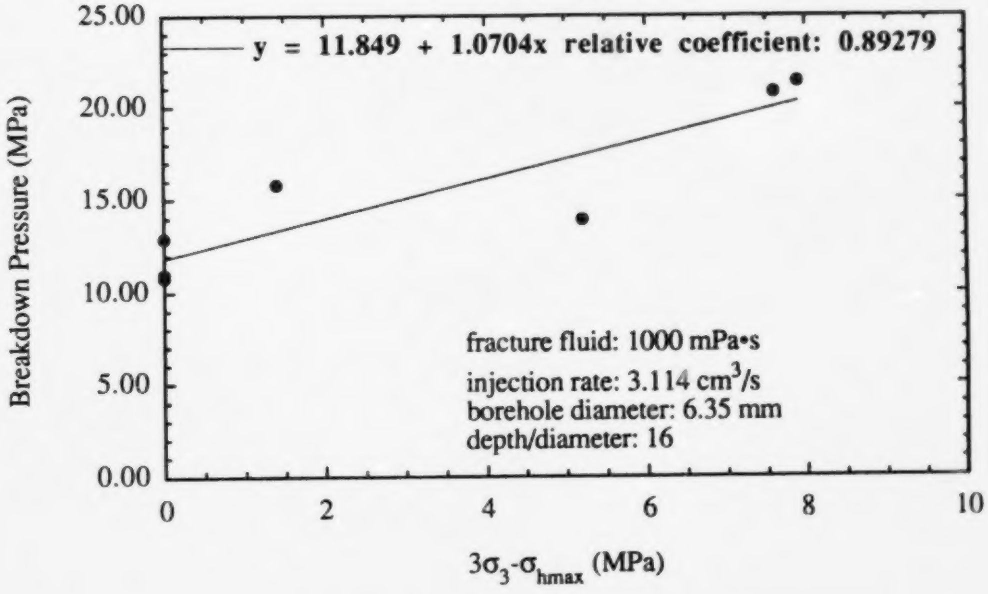

b. Breakdwon Pressure against $3\sigma_3$-σ_{hmax}

Figure 3.6 Breakdown Pressure against Stresses

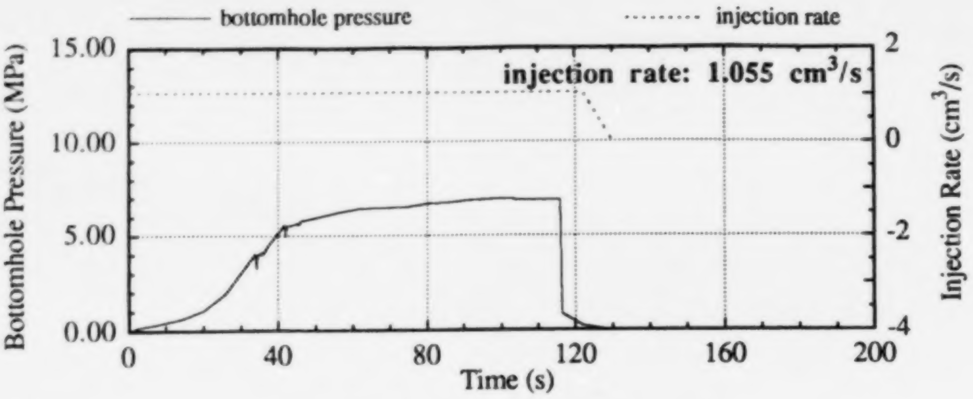

a. Hydraulic Fracture Test 13

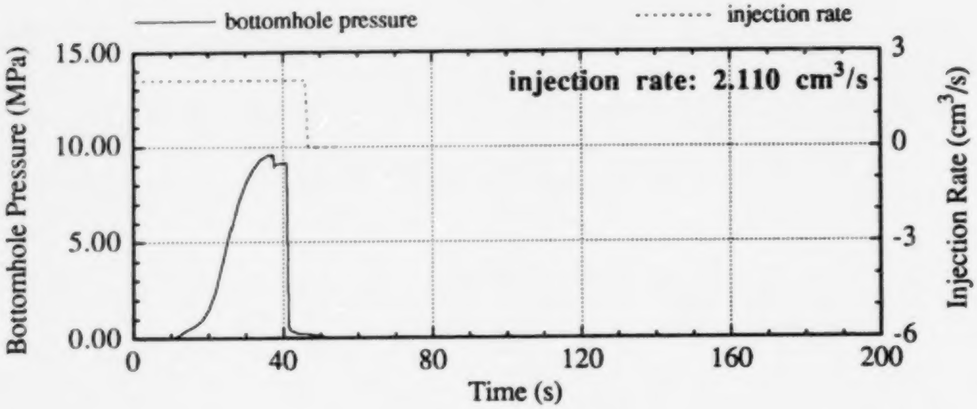

b. Hydraulic Fracture Test 12

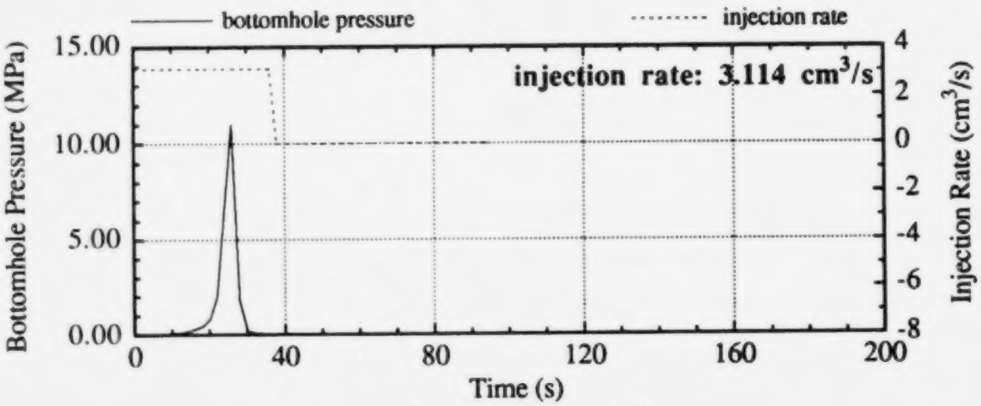

c. Hydraulic Fracture Test 8

Figure 3.7 Bottomhole Pressure under Various Injection Rates: without Stresses

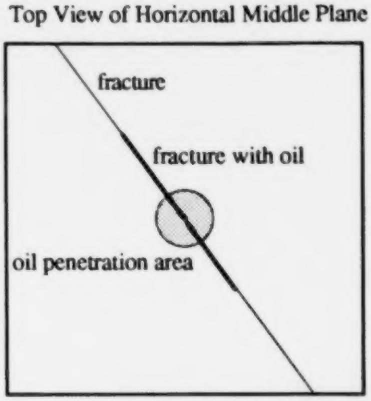
Top View of Horizontal Middle Plane
fracture
fracture with oil
oil penetration area

a. Hydraulic Fracture Test 13
(Injection Rate: 1.055 cm^3/s)

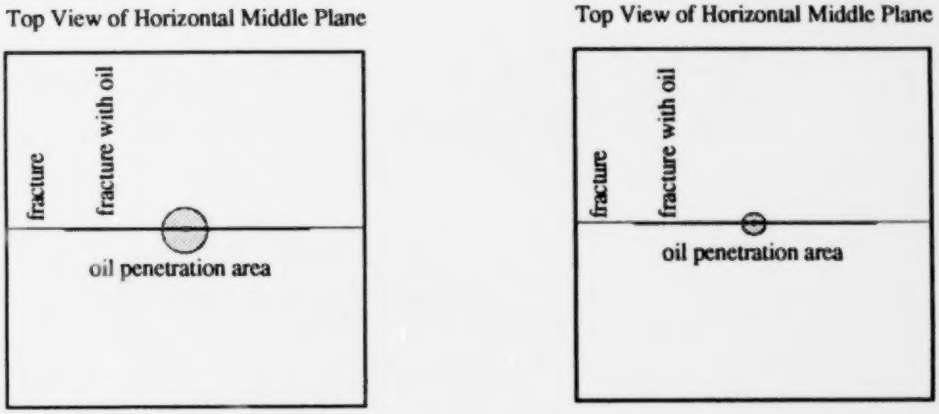
Top View of Horizontal Middle Plane
fracture
fracture with oil
oil penetration area
Top View of Horizontal Middle Plane
fracture
fracture with oil
oil penetration area

b. Hydraulic Fracture Test 12
(Injection Rate: 2.110 cm^3/s)

c. Hydraulic Fracture Test 8
(Injection Rate: 3.114 cm^3/s

Figure 3.8 Oil Penetration Area under Various Injection Rates: without Stresses

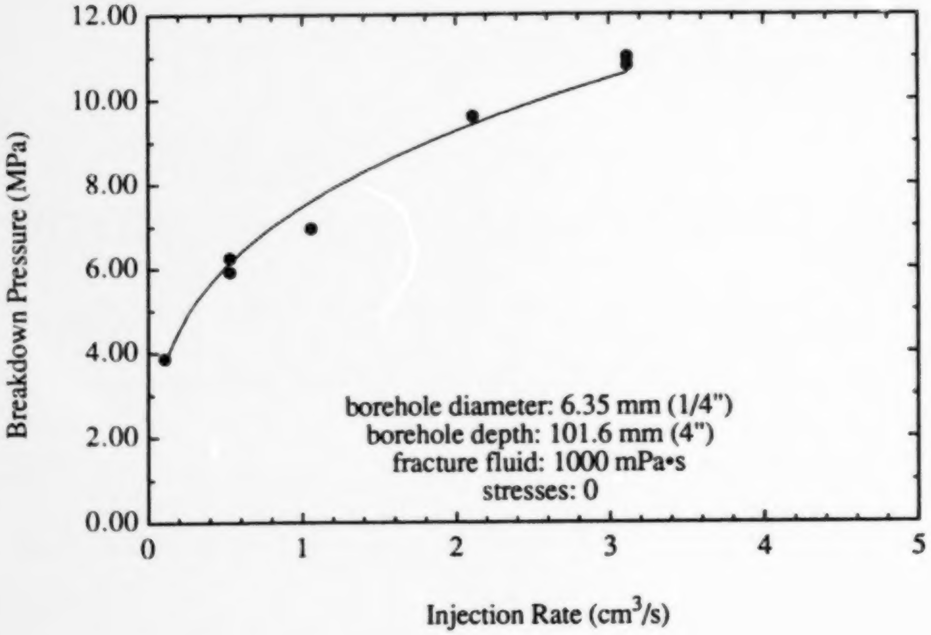

Figure 3.9 Breakdown Pressure against Injection Rate

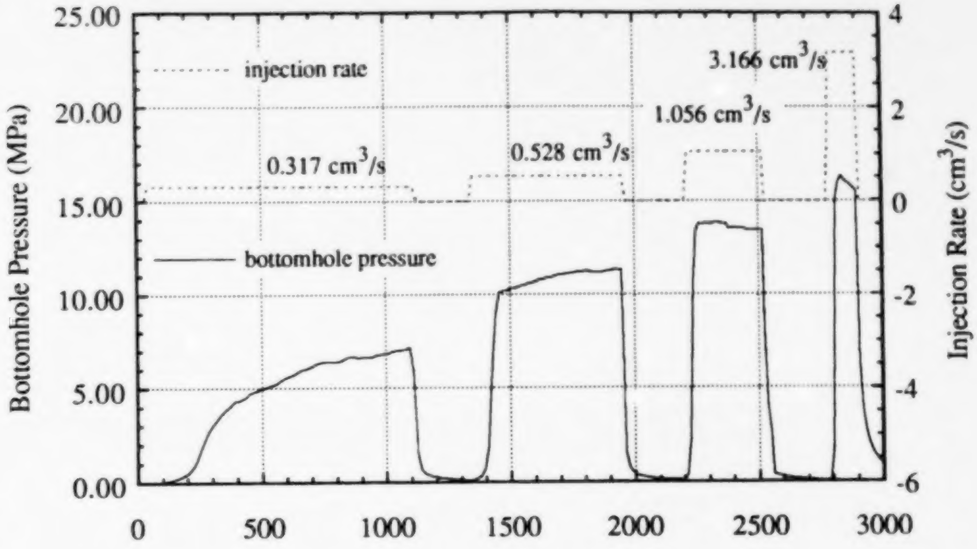
a. Bottomhole Pressure and Injection History

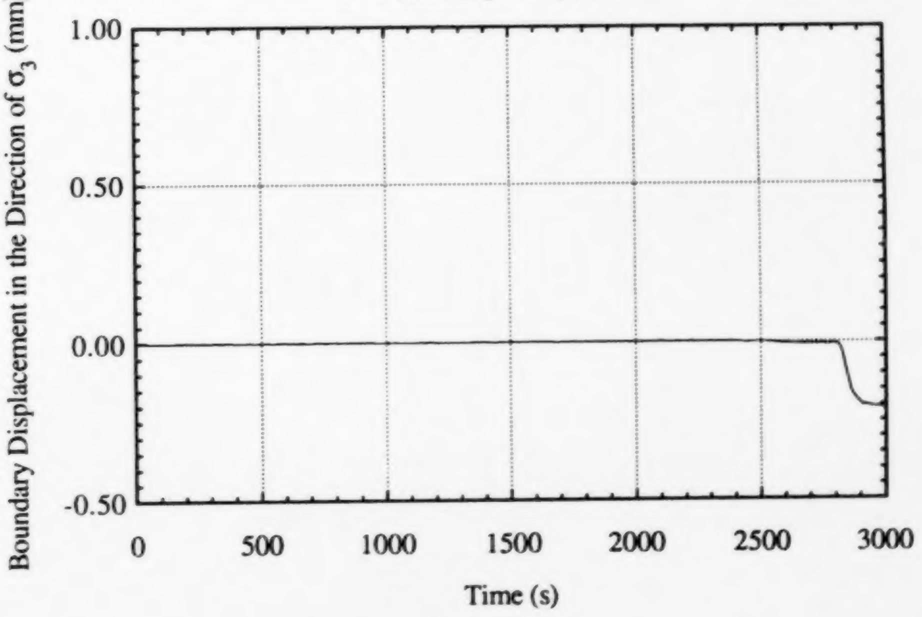
b. Boundary Displacement

σ_{ver}=13.20 MPa, σ_{hmax}=9.70 MPa, σ_3=5.40 MPa

Figure 3.10 Hydraulic Fracture Test 10

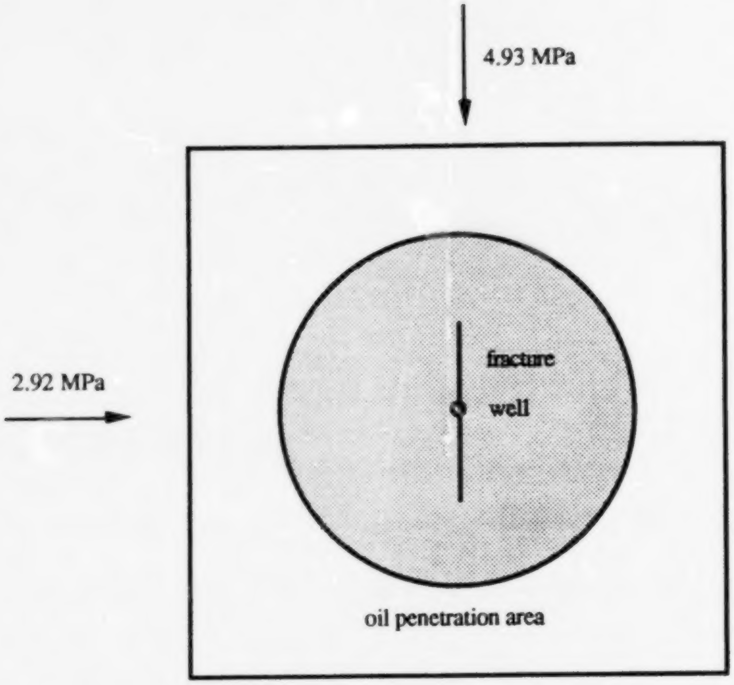
4.93 MPa
2.92 MPa
fracture
well
oil penetration area

Top View of Horizontal Middle Plane

a. Hydraulic Fracture Test 16 (Injection rate: 2.164 cm^3/s)

$\sigma_{ver} = 5.12$ MPa, $\sigma_{hmax} = 4.93$ MPa, $\sigma_3 = 2.92$ MPa

Figure 3.11 Oil Penetration Area and Fractures under Various Injection Rates: with Similar Stresses

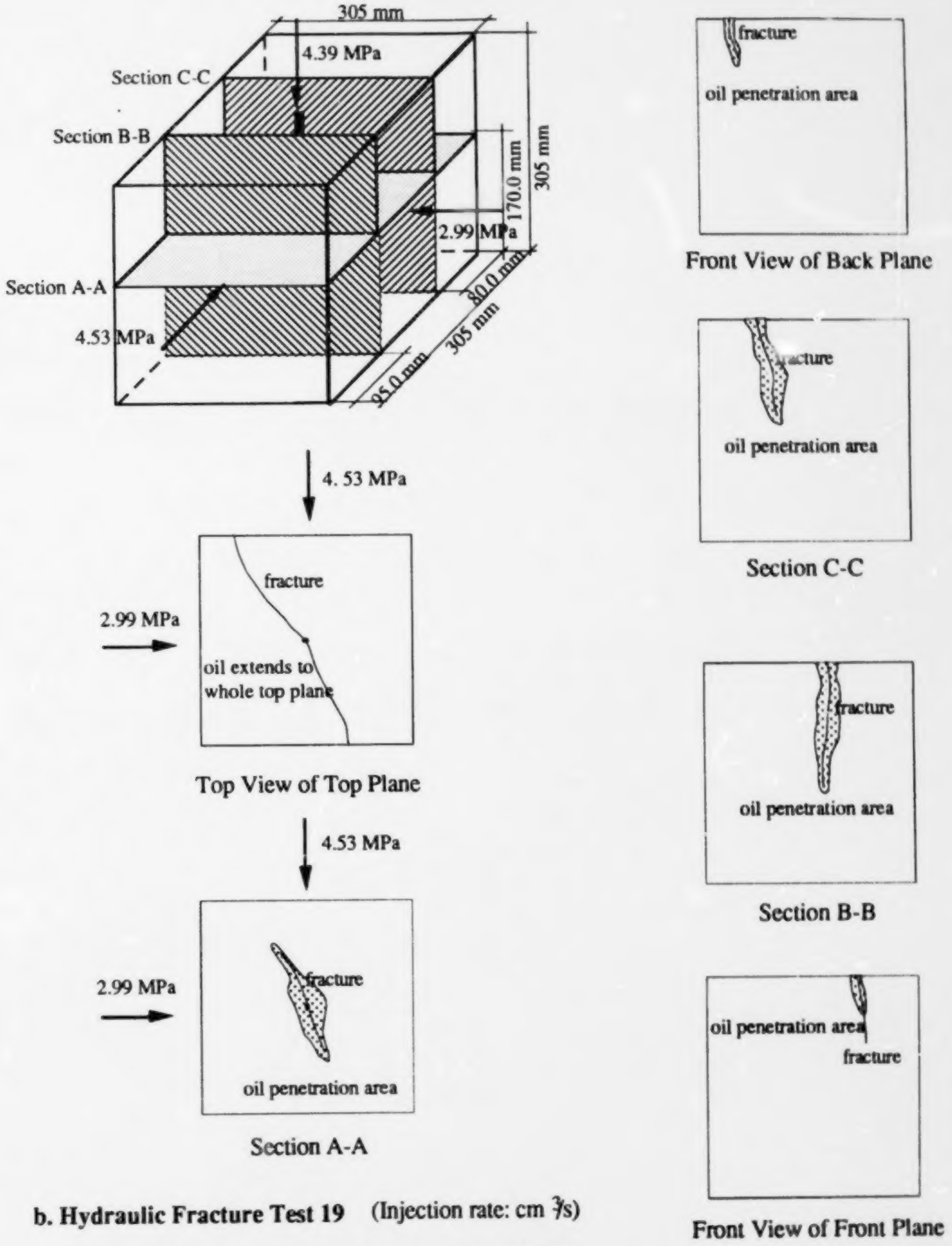
305 mm
4.39 MPa
Section C-C
Section B-B
170.0 mm
305 mm
2.99 MPa
Section A-A
80.0 mm
305 mm
4.53 MPa
95.0 mm
fracture
oil penetration area
Front View of Back Plane
fracture
oil penetration area
Section C-C
4. 53 MPa
fracture
2.99 MPa
oil extends to whole top plane
Top View of Top Plane
fracture
oil penetration area
Section B-B
4.53 MPa
2.99 MPa
fracture
oil penetration area
Section A-A
oil penetration area
fracture
Front View of Front Plane

b. Hydraulic Fracture Test 19 (Injection rate: cm^3/s)

$\sigma_{ver} = 4.39$ MPa, $\sigma_{hmax} = 4.53$ MPa, $\sigma_3 = 2.99$ MPa

Figure 3.11 Continued

a. Hydraulic Fracture Test 16

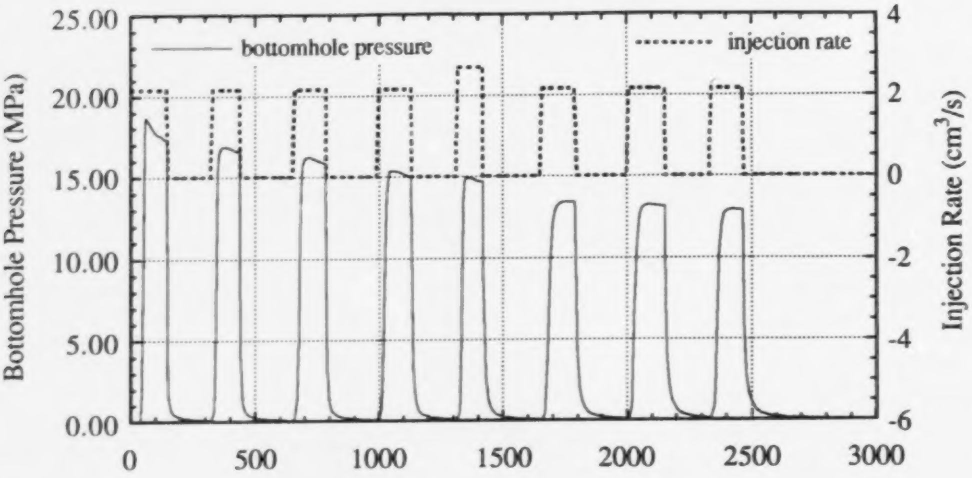

b. Hydraulic Fracture Test 19

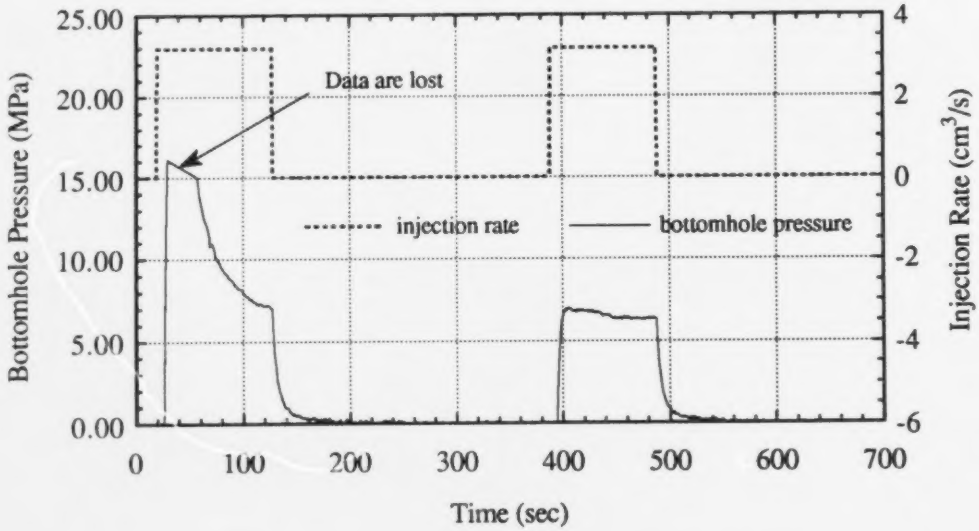

Test 16: σ_{ver}=5.12 MPa, σ_{hmax}=4.93 MPa, σ_3=2.92 MPa

Test 19: σ_{ver}=4.39 MPa, σ_{hmax}=4.53 MPa, σ_3=2.99 MPa

Figure 3.12 Bottomhole Pressure under Various Injection Rates: with Similar Stresses

a. Hydraulic Fracture Test 16

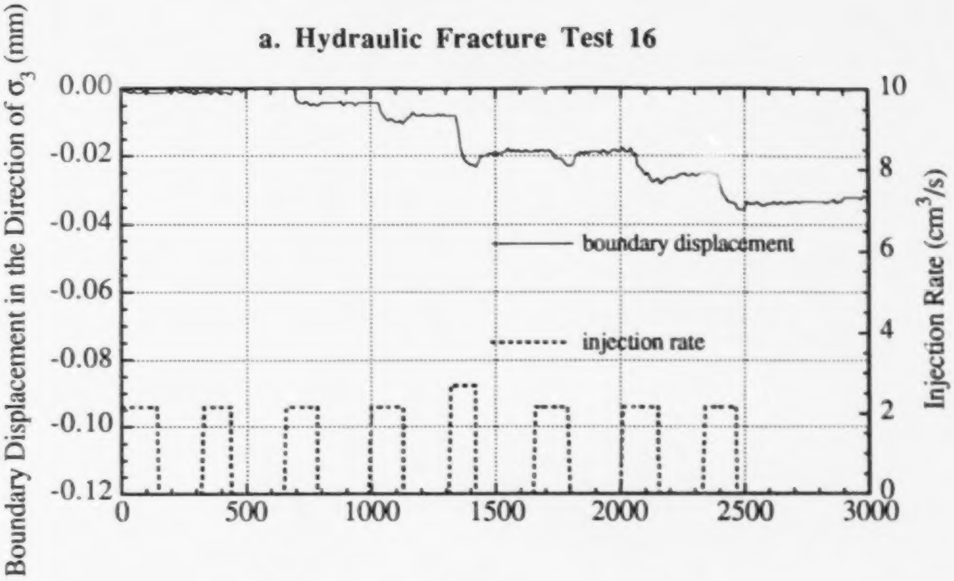

b. Hydraulic Fracture Test 19

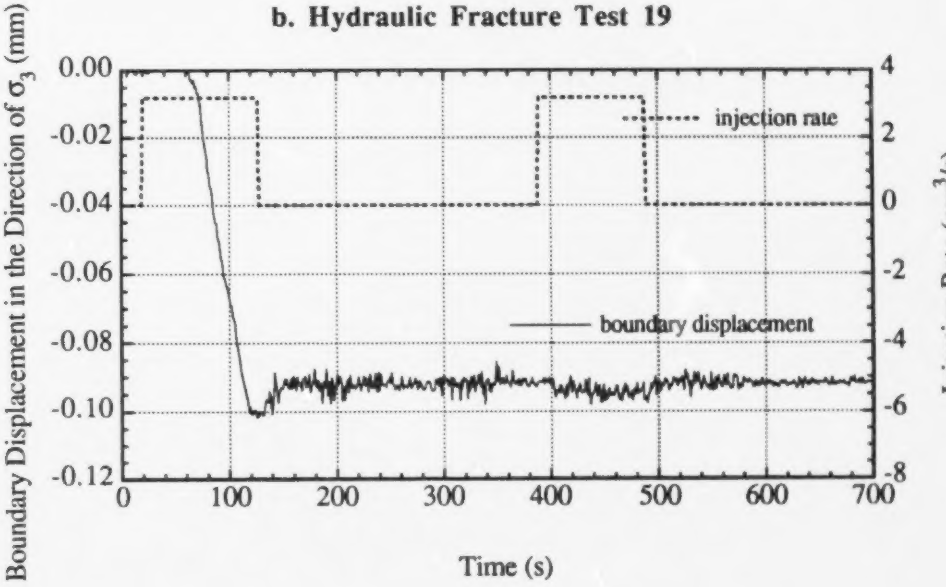

Test 16: σ_{ver}=5.12 MPa, σ_{hmax}=4.93 MPa, σ_3=2.92 MPa

Test 19: σ_{ver}=4.39 MPa, σ_{hmax}=4.53 MPa, σ_3=2.99 MPa

Figure 3.13 Boundary Displacement under Various Injection Rates: with Similar Stresses

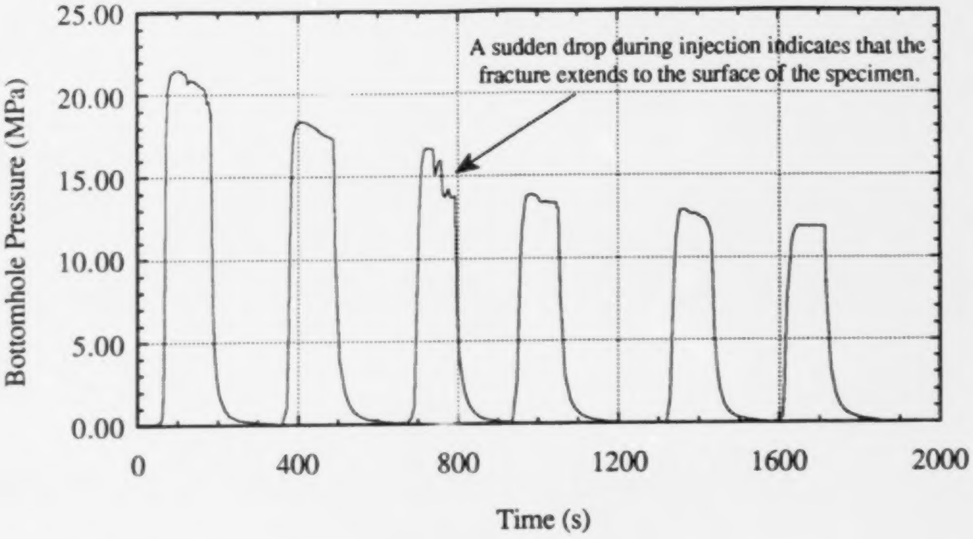

a. Hydraulic Fracture Test 9

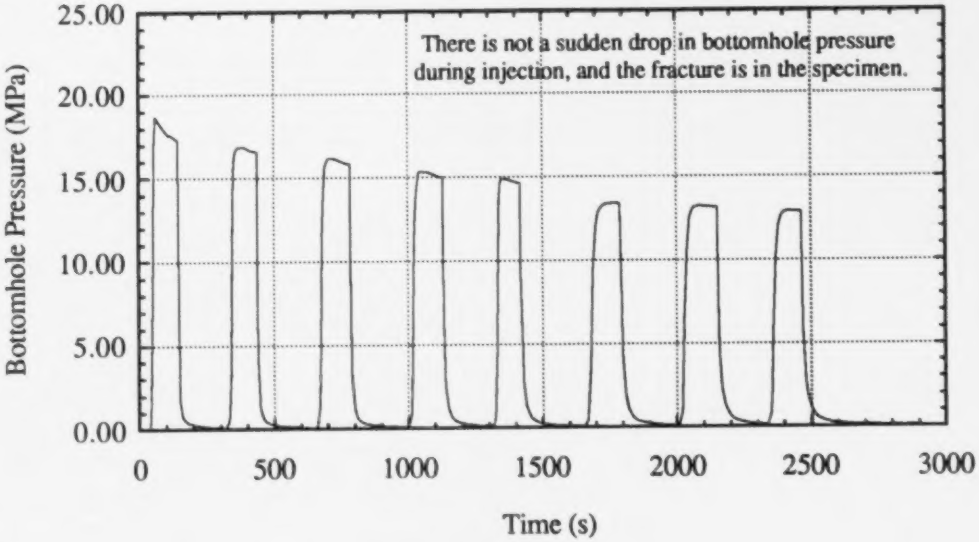

b. Hydraulic Fracture Test 16

Figure 3.14 Intersection of a Fracture with the Surface of a Specimen

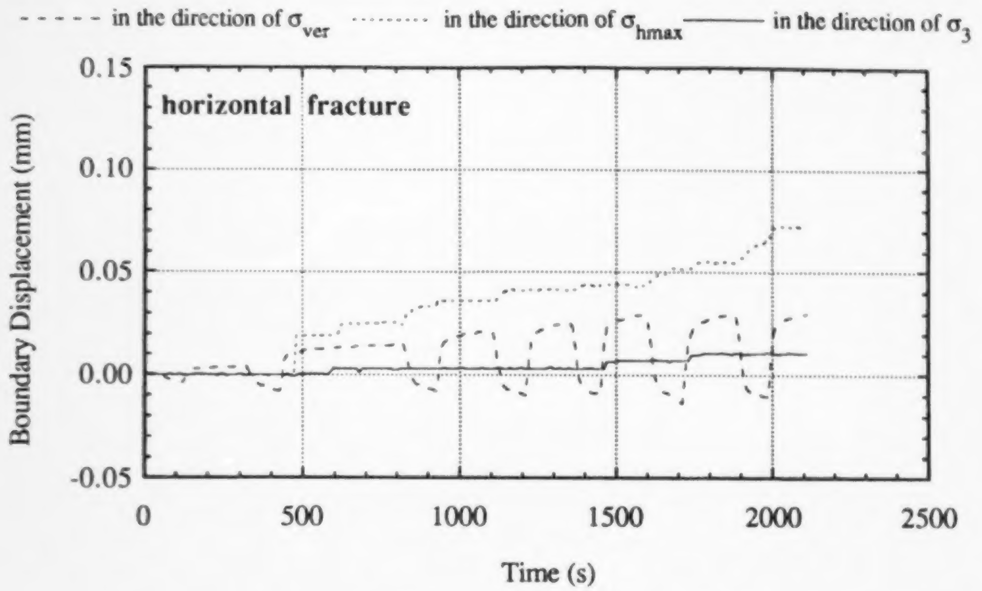

a. Hydraulic Fracture Test 15

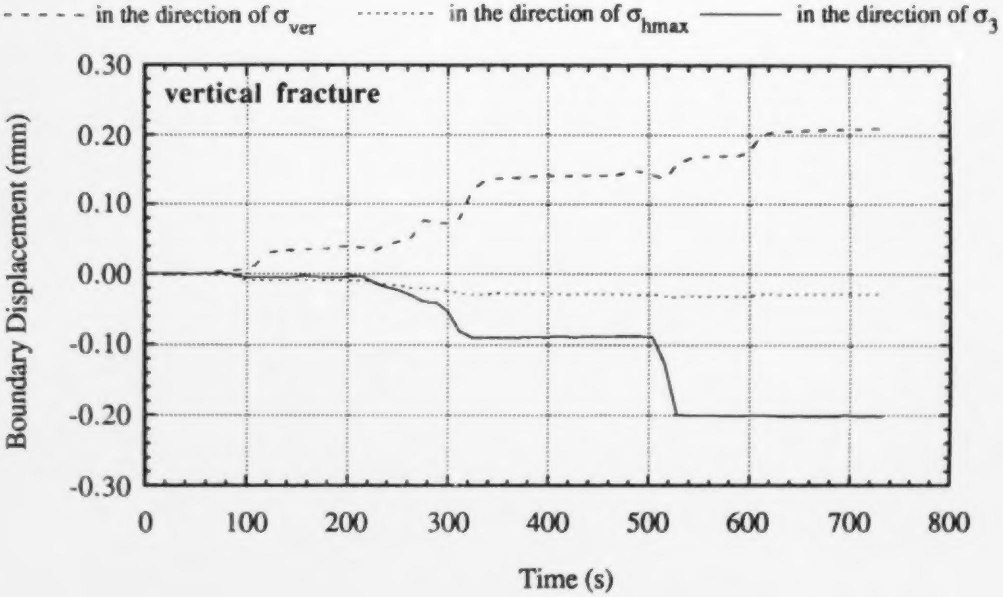

b. Hydraulic Fracture Test 3

Figure 3.15 Boundary Displacements for Vertical and Horizontal Fractures

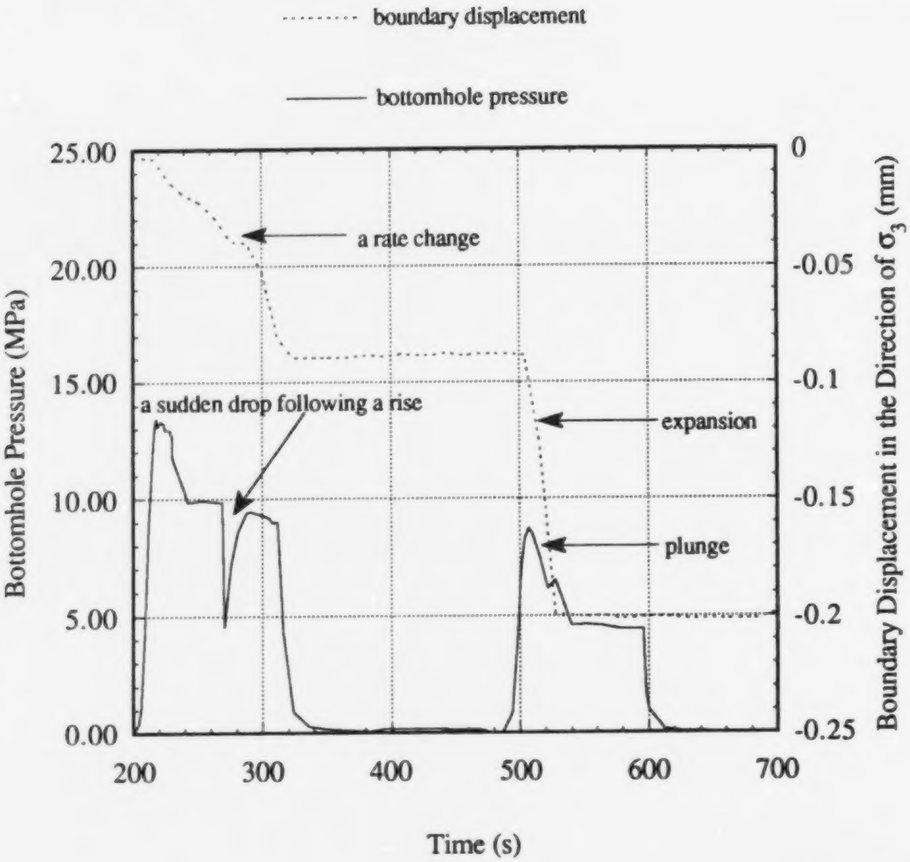

Figure 3.16 Bottomhole Pressure and Boundary Displacement of Hydraulic Fracture Test 3

Chapter 4

An Experimental Study of Well Communication by Hydraulic Fracturing

4.1 Introduction

Steamflooding is one of the most important recovery processes for deep oil sands [1]. The recovery concept envisioned is to establish communication between wells by hydraulic fracturing. These fractures are then converted into hot communication paths, leading to bitumen recovery by steam drive. The key to this process is in developing and maintaining well communication.

Development of well communication depends on fracture orientation and fracture propagation. When fractures are initiated and propagated horizontally, well communication is easily obtained. This has been proven by most of the pilot projects [1]. However, when the vertical stress is not the least principal stress, fractures induced are not horizontal. Well communication by a horizontal fracture driven hydraulically from an injection well usually is impossible. As happened in the Gregoire Lake In Situ Steam Pilot (GLISP) [1], well communication through the base of the oil sands is not obtained due to isotropic in situ stresses. At depth more than 250 m (920 ft), the vertical stress in oil sands deposit is close to or more than the minimum horizontal stress [2-3]. Consequently, the orientation of fractures is unpredictable, or vertical fractures are expected. Obviously, the original concepts regarding well communication are questionable under these stress conditions.

The concept of extracting heat from hot dry rock masses was originated at the Los Alamos Scientific Laboratory in New Mexico. The basic idea is to establish an artificial circulation loop in hot dry rock masses [4-5]. Murphy [5] stated clearly:

> "Basically, hot dry rock reservoirs are formed by drilling into low-permeability basement rock to a depth where the temperature is high enough to be useful, creating the necessary permeability, i.e., flow paths, by hydraulic fracturing, and then completing the circulation loop with a second well which intercepts the fractured region."

The major technical problem in this energy extraction scheme is also establishment of well communication. The usual practice, as stated by Cornet et al. [6], is to drill the first borehole for stress measurement purposes. A large hydraulic fracture is then developed from this borehole, and its geometry is determined. Finally, a second borehole is drilled to intersect the fracture. However, the techniques available for marking the direction of the fractures and for directional drilling, as stated by Bouteca et al. [7] do not provide sufficient resolution. For low permeability rocks, a several meter deviation from the fracture is a disaster for the completion of the circulation loop [5]. Obviously, it is necessary to look for a new method to encourage well communication.

There are two possibilities for hydraulic fracturing to link two wells. One possibility is to create a hydraulic fracture between two wells. Another is to try to improve the permeability of the rock by increasing microcracking through the application of pore pressure cycles. Lessi et al. [8] examined the two possibilities in the laboratory. They tried the former on a model material–a mixture of cement and 10% Bentonite. The experiments were performed on blocks of 300 x 300 x 500 mm (12" x 12" x 20") without stresses applied. The well spacing was 150 mm (6"). The testing procedure used was as follows.

> "One well is fractured and the pressure is kept constant while the second one is fractured. Then the two fractures are alternatively developed by pumping the fracture fluid in one well and keeping in the other one a pressure lower than the propagation pressure in the other."

The experiments showed that it was always possible to connect the two wells by hydraulic fracturing.

The latter possibility was examined by microfracturing experiments on granite. A prior fracturing test was conducted first, which gives an estimate of the tensile strength. From the tensile strength, the range, within which the change of injection pressure caused fatigue and avoided an outright break, was defined. Following, cyclical injections were carried out in the pressure range defined above so that microcracks were initiated and developed. The experiments found that this method was not feasible.

Lessi's experiments were performed without stresses, which corresponds to an experiment under isotropic stresses. Bouteca et al. [7] conducted further laboratory experiments with stress differences. The experiments were performed in sandstone blocks of 1000 x 400 x 100 mm (39" x 16" x 4"). The vertical stresses (parallel to wells) on 1000 x 400 mm faces was 6 to 12 MPa (870 to 1,740 psi). The horizontal stress on 400 x 100 mm faces was 1 MPa (145 psi). There was no stress on the other faces. The well spacing was 120 mm (4.7"). The wells had the diameter of 3 mm (0.12"). The angle (ß) between the well line and the direction of the maximum horizontal stress was 10°. They first performed an experiment in which injection was carried out in only one well. The fracture created was not influenced by the presence of the other well, and was perpendicular to σ_3. Subsequently, the testing procedure was changed. They injected simultaneously in both wells before fracturing. However, the following procedure was not described in detail in their paper. One experimental result reported showed that two wells were linked for ß of 10°.

Because the previous studies are limited, a double well hydraulic fracturing program was carried out to check the possibility of well communication by vertical fractures driven hydraulically. The strategy envisioned is to induce and drive two fractures in two wells simultaneously. When two fractures are approaching each other, they will interact; consequently, the stress at the tip of the fractures is changed. This change will lead to a change in the direction of fracture propagation. It is believed that this change in the direction of fracture propagation will encourage intersection of fractures.

This chapter presents experimental apparatus and results for a double well hydraulic fracturing program. It begins with a discussion of factors that control well communication by hydraulic fracturing and the choice of these factors in the research program. This is followed by a description of the experimental apparatus. After that, the experimental results are discussed.

4.2 Research Strategy

When a vertical fracture is initiated and driven from an injection well, the orientation of the fracture is perpendicular to the minimum horizontal stress if the state of stress is not isotropic and the rock is homogeneous and isotropic. To change this direction of fracture propagation into the direction along the well line is the key to develop communication when the well line is not aligned with the direction of the maximum horizontal stress.

There are several factors which apparently affect the change of the orientation of fracture propagation. The first factor is the angle (ß) between the well line and the direction of the maximum horizontal stress. For ß of 0°, a fracture from one well propagates toward the other well, so it is unnecessary to change the direction of fracture propagation for communication between two wells. For ß of 90°, two fractures from different wells will propagate in a parallel manner, so it is most difficult to encourage well communication if not impossible. The second factor is the stress difference between the maximum and the minimum horizontal stresses. When two stresses are equal or close, the stress change caused by injection controls the stress field. Well communication is easily obtained if the proper injection procedure is used, as Lessi's experiments showed [8]. If the stress difference is very high, the stress change caused by injection will be slight in comparison with the in situ stress, so that the in situ stress field will control fracture propagation, and the change in the direction of fracture propagation is slight, and well communication is difficult. Well spacing is also an important factor. Obviously, the possibility for well communication increases with decrease of well spacing, especially in the field. Another important factor is injection procedure. Injection may be carried out only in one well or in two wells simultaneously, etc.. The different injection procedures will result in entirely different results. When injection is carried out in one well, the other well has little influence on the orientation of fracture propagation. This has been illustrated experimentally by Bouteca et al. [7]. When injection is carried out in two wells, Bouteca's experiments [7] have also shown that the change of the orientation of fracture propagation occurred and well communication was obtained for ß of 10°. The other factor is injection rate and fracture fluid. When injection rate is high, and an extremely viscous fracture fluid is used, bottomhole pressure is rapidly built up, and high bottomhole pressure is produced. Hence, injection will influence strongly the in situ stress field around the borehole. The influenced zone will enlarge with fracture propagation. When the injection rate is low, and a light viscous fracture fluid is used, most of the fracture fluid leaks into the rock. Injection will exert a weak influence on the in situ stress field but the affected area will be large [8-9]. Other factors, such as the properties of rocks, the homogeneity and the isotropy of rocks, the discontinuities in rocks, and the relative thickness of the formation, all may have some influences on well communication. It is out of the scope of this research to discuss each factor in detail.

In this research program, the angle (ß) between the well line and the direction of the maximum horizontal stress is chosen as the controlling variable due to its importance. A high stress difference is unfavorable to well communication. If well communication by hydraulic fracturing is possible for high stress differences, then well communication must be feasible for low stress differences under the same conditions. The objective of the study is to investigate well communication for various unfavorable in situ conditions. Hence, a considerable stress difference was applied. In practical applications, well spacing usually is determined by economic feasibility. To simulate as large a well spacing as possible, the maximum well spacing which the apparatus permits is used. Injection procedure, injection rate, and fracture fluid are the main controllable variables. Whether well communication can be achieved, to a large extent, depends on how to control these variables. The change of the orientation of fracture propagation depends on the interaction of fractures. Interaction of fractures only can be achieved through driving two fractures at the same time. Therefore, injection is carried out in two wells simultaneously at the same injection rate. High injection rate will lead to high bottomhole pressure, which changes the in situ stress field around wells. This affected zone will extend with fracture propagation. Therefore, the injection rate used is as high as possible to obtain well communication under a high stress difference. In brief, in this research program, double well hydraulic fracture tests will be conducted through injecting oil simultaneously into two wells at a high injection rate. The tests concentrate on the effects of the angle (ß) between the well line and the direction of the maximum horizontal stress.

4.3 Experimental Facilities

Artificial Rock: The experiments were performed on Gypstone [9-10] that consists of 10% gypsum, 14.15% water, 75.8% quartz sand and 0.05% retarder, Na_2HPO_4, by mass. In comparison with natural rocks, its homogeneity and isotropy, which result in improved repeatability of experiments and simplified interpretation of experimental results, are an advantage. Its properties are similar to sedimentary rocks, which ensured that the fracture behavior produced is similar to that in rocks. The physical and mechanical properties of Gypstone have been studied comprehensively in a single well hydraulic fracturing program, and are summarized again in Table 4.1.

Test Frame: The three principal stresses (external pressure) were applied by a large test frame (Figure 4.1) developed by Kaiser and Morgenstern [11] at the University of Alberta. The large test frame can take block specimens up to 610 x 584 x 305 mm (24" x 23" x 12"), and is capable of applying true triaxial stresses up to 10 MPa (1,450 psi) on specimens.

Pump System: Injection was carried out by two pumps. A pump (Figure 4.2) consists of a compression test machine and a hydraulic jack. The hydraulic jack was controlled by the compression test machine. Various constant injection rates were obtained by changing the displacement rate of the compression test machine. Injection rate was calculated by the displacement rate of the compression test machine times the inside area of hydraulic jack.

Specimen and Layout of Injection Wells: All double well hydraulic fracture tests were conducted on 610 x 584 x 305 mm (24" x 23" x 12") Gypstone blocks. The layout of injection wells is shown in Figure 4.3.

Injection Well and Sealing: An injection well consists of an upper hole and a lower hole. The upper hole is used to install injection tubing, and the lower hole serves as the injection segment. The upper hole was drilled vertically in the designated location. The lower hole was drilled concentrically at the bottom of the upper hole. The distance between bottom of the lower hole and the bottom of specimens is equal to the depth of the upper hole. The injection segment is in the middle of the specimens. A piece of tubing, with a 381 mm (15") length, a 6.4 mm (0.25") outside diameter and a 3.86 mm (0.152") inside diameter, was cemented to the wall of the upper hole of each injection well with 3M 2216 Epoxy Adhesive. This tubing serves as injection tubing, and the 3M 2216 Epoxy Adhesive as sealant. At the top of the injection tubing, a pressure transducer, which was called pressure transducer 1, was installed to monitor injection pressure. To obtain bottomhole pressure, another piece of 381 mm (15") tubing and another pressure transducer, which was called pressure transducer 2, was connected to the previous pressure transducer. Injection tubing, sealing, and pressure transducers are shown in Figure 4.4.

Bottomhole Pressure: Bottomhole pressure in each injection well was obtained from data recorded by two pressure transducers (see Figure 4.4).

The pressure loss between pressure transducer 1 and the sealed well segment is equal to the pressure difference between the two pressure transducers because the two pieces of tubing have the same size and length. Therefore, the bottomhole pressure is equal to the pressure at pressure transducer 1 minus the pressure difference between two pressure transducers. If p_1 expresses the pressure recorded by pressure transducer 1, and p_2 is the pressure recorded by pressure transducer 2, then the bottomhole pressure is equal to $2p_1$-p_2.

Boundary Displacements: Displacement on the five moveable faces of a specimen in the direction of the three principal stresses was monitored by 16 LVDTs. Four LVDTs which were installed vertically at the four top corners of the rigid loading head were used to obtain vertical displacements. The average gives the vertical boundary displacement. The other 12 LVDTs which were installed horizontally on four sides of the specimen (three LVDTs each side) were used to monitor horizontal displacement. Three LVDTs on each side were installed at the upper corners and center of the side, respectively. The average of three recorded displacements provides the horizontal displacement on the corresponding side. Summation of displacement on two opposite sides in the direction of each principal stress gives the total displacement along that principal stress, which is called boundary displacement.

Stresses: During injection, the three principal stresses were also monitored by 12 load cells. Four of them measured vertical stress, and the other eight load cells monitored the two horizontal stresses.

Data Acquisition: The data acquisition system consists of a Macintosh IIx, NB-MIO-16x board, and a Multiplexer. Signals from load cells, LVDTs, and pressure transducers entered the NB-MIO-16x board through the Multiplexer. After the signals were converted from analogue into digital by the NB-MIO-16x Board, they were sent into the Macintosh microcomputer. The whole process was controlled by the Macintosh microcomputer through LabVIEW software. The system is able to scan 64 channels at a rate of one sample per second. The data were stored on disk and were accessible by popular data analysis/graphics applications software. Bottomhole pressure and other variables were shown on the screen of the microcomputer during testing. The scan speed used in the tests was one sample per second.

Fracture Mapping: After testing, a specimen was cut. The fracture induced and the oil penetration area were described. The fracture is expressed as a line, and the oil penetration area is a shaded zone. The location of cutting planes is shown in a cavalier oblique projection.

Fracture Fluid: Gear oil with viscosity of 1000 mPa•s at room temperature was used as fracture fluid.

Testing Procedure: The following testing procedure was used in double well hydraulic fracture tests.

1. Installation of Injection Tubing: After wells was drilled at the designated locations, they were cleaned by compressed air. Then, injection tubing was cemented to the wall of the upper holes with 3M 2216 Epoxy Adhesive. The specimen was left at room temperature overnight or for about 12 hours to allow the adhesive to harden.

2. Set-up of Loading System and Instrumentation: After the adhesive had hardened, the specimen was placed into the test frame, and the load system, load cells, LVDTs, and pressure transducers were set up.

3. Loading: The three principal stresses were hydrostatically applied at an increment of 0.5 MPa (73 psi) until σ_3 was up to the designated value. Subsequently, σ_1 and σ_2 were synchronically increased up to the designated σ_2 at an increment of 0.5 MPa (73 psi). Finally, σ_1 was raised to the required value at an increment of 0.5 MPa (73 psi). To minimize the effect of creep on boundary displacement, the applied stresses were maintained for 24 hours before hydraulic fracturing.

4. Fracturing: Fracture fluid was injected simultaneously into two injection wells at the same injection rate of 3.186 cm^3/s until fractures intersect or fracture fluid leaks out of the surface of the specimen.

5. Description of Fractures: After the specimen was taken out of the test frame, it was cut into slices to describe the fracture. This step was completed on the day after fracturing.

4.4 Experimental Results and Discussions

4.4.1 Summary of Double Well Hydraulic Fracturing

Ten double well hydraulic fracture tests were conducted in this program. The angles (ß) between the well line and the direction of the maximum horizontal stress were 0°, 15°, 30°, 45°, and 60°, respectively. The injection rate was 3.186 cm^3/s. The viscosity of the fracture fluid was

1000 mPa•s. The injection well was 3.2 mm (0.125") in diameter. Two states of stress were applied. The first six tests had a low stress difference, and the other tests had a high stress difference. The angle ß, the three principal stresses, the diameter and the depth of injection wells, the injection rate, the oil viscosity, and the fractures are listed in Table 2.

4.4.2 Double Well Hydraulic Fracturing Tests under a Low Stress Difference

A low stress difference was applied first (σ_1/σ_3 around 1.5). The experimental results are shown in the following paragraphs.

Test 1: Figure 4.5 shows the fractures induced in Test 1. ß in this test is 0°, i.e. the well line is aligned with the direction of the maximum horizontal stress. The two vertical fractures were initiated at the two wells. They propagated then in the direction of the maximum horizontal stress (Figure 4.5 b). The two fractures intersected between the wells. When the fractures extended toward the boundary, the orientation of the fractures rotated. They deviated from the direction of the maximum horizontal stress.

Test 2: Figure 4.6 presents the fractures created in Test 2 with ß of 15°. The fracture at Well 1 was initiated vertically. It propagated in the direction of the maximum horizontal stress in the horizontal plane. When it migrated upward and downward, the fracture deviated from the direction of the maximum horizontal stress. The fracture at Well 2 had two branches. One branch propagated in the direction of the maximum horizontal stress. The deep oil penetration area around it (Section A-A in Figure 4.6 b) showed that it was contained during propagation. The other branch was an inclined fracture. Fracture propagation at Well 2 mainly developed in this direction. The recorded stress showed that a hydraulic ram above this branch was leaking during testing. Only half load was maintained by this ram. This led to the particular mode of fracture propagation at Well 2. Although two fractures had not intersected, Section A-A in Figure 4.6 b illustrated that it was possible for the two fractures to intersect.

Test 3: Figure 4.7 shows the fractures produced in Test 3. ß is 30° in this test. Unexpectedly, two horizontal fractures were initiated (Sections B-B, C-C, and D-D in Figure 4.7 b). Then the fractures rotated toward the direction perpendicular to the least principal stress. This process was demonstrated in Sections B-B, C-C, and D-D in Figure 4.7 b. The fractures intersected between two wells (Section C-C in Figure 4.7 b). Well communication was achieved.

Test 4: Figure 4.8 demonstrates the fractures in Test 4 with ß of 45°. The oil penetration area has not suggested the modes of fracture initiation. The observation of the fractures has not supplied any significant evidence for the mode of fracture initiation, either. Hence, the orientation of the fractures was unknown. However, the oil penetration area illustrated that two fractures propagated horizontally in the same horizontal plane (Sections A-A, B-B, and D-D in Figure 4.8 b). This is unexpected. The vertical stress was the maximum principal stress (σ_1) in this test. Although the two fractures did not intersect (Section C-C), fracture intersection was possible.

Test 5: Figure 4.9 illustrates the fractures induced in Test 5. ß is 60° in this test. Two vertical fractures were initiated (Sections A-A and C-C in Figure 4.9 b). When the fracture extended away from Well 1, it rotated and became an inclined fracture (Sections B-B and D-D). The fracture at Well 2 also changed orientation during propagation. It rotated 90° and become a horizontal fracture (Sections A-A and C-C). Two fractures intersected during rotation (Section C-C). Well communication was obtained.

Test 8: Figure 4.10 shows the fractures produced in Test 8. ß is 30° in this test. Like the previous other tests, Two fractures rotated during propagation. Although the orientation of fracture initiation at Well 1 was unknown, the fracture rotation was apparent. It was an inclined fracture in Sections D-D and C-C, and a horizontal fracture in Section B-B. The fracture at Well 2 was initiated vertically, and propagated in the direction of the maximum horizontal stress. It changed from a vertical fracture at initiation (Section C-C) into an inclined fracture (Section D-D) when migrating downward. Two fractures intersected between two wells (Section C-C). Well communication was achieved.

In conclusion, six double well hydraulic fracture tests were conducted under various ß (0°, 15°, 30°, 45°, and 60°). A low stress difference (σ_1/σ_3 about 1.5) was applied in these tests. The experimental results show that intersection of two fractures is possible for ß as high as 60°. Although two fractures intersect for ß as high as 60° in six double well hydraulic fracture tests, fracture initiation and propagation are unexpected. Horizontal fractures in some cases are initiated, even though the vertical stress is far higher than the minimum horizontal stress. As happened in Test 3, the vertical stress was 4.39 MPa (637 psi), and the minimum horizontal stress was 2.99 MPa (437 psi), but two horizontal fractures were initiated. Most of the fractures then turn toward the direction perpendicular to the least principal stress. Intersection of two fractures happens during the rotation of fracture orientation. However, the fractures do not always rotate toward the direction perpendicular to the least principal stress. The fractures rotate sometimes to the direction perpendicular to σ_1 or σ_2. For example, two fractures in Test 4 propagated horizontally. The vertical stress was σ_1 in this test. The fracture at Well 2 in Test 5 changed from a vertical fracture to a horizontal stress. The vertical stress was σ_2 in this test.

4.4.3 Double Well Hydraulic Fracturing Tests under a High Stress Difference

To control the orientation of fracture initiation and fracture propagation, the vertical stress (σ_{ver}) and the maximum horizontal stress (σ_{hmax}) were increased to around 5 MPa, and the minimum horizontal stress (σ_3) was decreased to around 2.5 MPa. The ratio of σ_{ver} and σ_{hmax} to σ_3 is around 2. At the same time, the depth of the sealed-off well was increased from 63.5 mm (2.5") to 101.6 mm (4"). Four more tests were conducted.

Test 6: Figure 4.11 shows the fractures induced in Test 6. ß is 15° in this test. Two vertical fractures were initiated. They propagated in the direction perpendicular to the least principal stress. The fractures intersected between the two wells. This was observed in Sections A-A and C-C in Figure 4.11 b. Obviously, fracture initiation and fracture propagation were under control for this high stress difference. The rotation of fractures disappeared.

Test 7: Figure 4.12 shows the fractures induced in Test 7. β is 30° in this test. Two vertical fractures were initiated. The fractures propagated approximately in the direction perpendicular to the least principal stress. When fractures started to interact, a new fracture was initiated in the bottom. This new fracture was a vertical fracture, and had an angle of around 60° with the maximum horizontal stress. Well communication was obtained.

Test 9: Figure 4.13 presents the fracture produced in Test 9. β is 45° in this test. The orientation of fracture initiation was vertical. The fracture at Well 1 rotated towards the horizontal during propagation. The fracture at Well 2 passed by the fracture at Well 1, and propagated continuously in the direction perpendicular to the least principal stress. The fractures did not intersect between the wells (Section A-A in Figure 4.13). Well communication was not obtained.

Test 10: Figure 4.14 shows the fractures in Test 10. β is 60° in this test. Two vertical fractures were initiated again. However, the two fractures rotated towards the horizontal during propagation. In the horizontal middle plane, they become horizontal fractures. The possible reason is non-homogeneity of material. Although the fractures rotated, and were contained by the horizontal middle plane, the two fractures were still vertical between the wells (Section C-C in Figure 4.14 b). They seemed to be avoiding each other (Section A-A in Figure 4.14 b). There was no evidence that implied that they were going to intersect. Therefore, well communication was not obtained.

Fracture initiation was controlled after the stress difference was increased. The vertical fractures were initiated in all four tests. For ß less than and equal 30°, two vertical fractures from two injection wells intersect, and well communication was obtained. For ß more than 30°, two fractures from two injection wells will not intersect between wells, and well communication is not obtained. These tests demonstrates clearly the effect of ß (the angle between the well line and the direction of the maximum horizontal stress) on well communication.

The tests characterize not only the effect of ß, but also the effect of stress difference on well communication. Well communication is possible for ß as high as 60° in the first six tests with a low stress difference (σ_1/σ_3 is around 1.5). Well communication is obtained only for ß up to 30° in the last four tests with a high stress difference (σ_1/σ_3 is around 2). A low stress difference makes well communication easy, and a high stress difference makes well communication difficult.

4.4.4 Fracture Initiation

Although considerable stress differences were applied, the orientation of fracture initiation was completely different in the two sets of experiments. For a low stress difference (σ_1/σ_3 around 1.5), the orientation of fracture initiation was unpredictable. Horizontal fractures were sometimes initiated. For the high stress difference, the orientation of fracture initiation was under control. Vertical fractures were always initiated.

It is of interest to note the stress on the wall of wells before injection. The vertical stress can be regarded as vertical stress on the wall of the wells because well depth is far larger than diameter of wells. The specimen size is much larger than the diameter of the wells, so the minimum horizontal stress on the wall of wells may be expressed by $3\sigma_3$-σ_{hmax}. The vertical stress and the minimum horizontal stress on the wall of wells ($3\sigma_3$-σ_{hmax}) and the orientation of fracture initiation observed are summarized in Table 4.3. The two sets of experiments have different state of stresses in the wall of the wells. For the tests with the low stress difference, the vertical stress and the minimum horizontal stress on the wall of wells are close, and the orientation of fracture initiation is unpredictable. For example, the minimum horizontal stress on the wall of wells was 0.35 MPa (51 psi) higher than the vertical stress in Test 1, but two vertical fractures were initiated. Similar phenomenon happened in Test 8. However, the minimum horizontal stress on the wall of wells was also 0.17 MPa (25 psi) higher than the vertical stress in Test 3, two horizontal fractures were initiated. The orientation of fracture initiation is not capable of being predicted by the state of stress on the wall of wells because of the low difference between the vertical stress and the minimum horizontal stress on the wall of wells. For tests with the high stress difference, the vertical stress is higher than the minimum horizontal stress on the wall of wells. Consequently, the orientation of fracture initiation is always vertical and identical with the direction predicted by the state of stress on the wall of wells. The comparison seems to illustrate that there are many factors that affect fracture initiation, but the state of stress on the wall of wells is an extremely important one. When the difference between the vertical stress and the minimum horizontal stress on the wall of wells is apparent, the orientation of fracture initiation is controlled by the state of stress. If the difference is not apparent, the state of stress on the wall of wells will not dominate the orientation of fracture initiation, and other factors, such as anisotropy and non-homogeneity in strength and permeability, may have a dominant role on the orientation of fracture initiation.

4.4.5 A Representative Instrumentation

The fractures induced have been discussed in the previous section. In the experiments, other variables such as bottomhole pressure and boundary displacements also were monitored. One of the monitored results (Test 8) will be discussed in the following paragraphs.

Figure 4.15 a is the injection history of Test 8. This is a representative injection procedure. Two wells were injected simultaneously at a constant injection rate of 3.186 cm^3/s, and were shut in at the same time. This process was repeated until the fractures intersected or extended to the surface of the specimen. The bottomhole pressure produced at two wells by this injection procedure is illustrated in Figure 4.15 b. The two wells were under the same state of stress and had the same size and the same injection rate so that a similar breakdown pressure was obtained. The breakdown pressure in the other tests (Table 4.3) also had similar results. After breakdown, the two fractures propagated along different paths (Section A-A in Figure 4.10 b); consequently, two different bottomhole pressure curves were produced (the first three injection cycles in Figure 4.15 b). When the two fractures intersected, the bottomhole pressure at the two wells became the same again (the fourth injection cycle in Figure 4.15 b). The change of bottomhole pressure reflects the path of fracture propagation.

Figure 4.15 c is the three principal stresses during injection. The vertical stress and the maximum horizontal stress changed little. The least principal stress had a slight increase during injection. This is identical with the fractures perpendicular to the least principal stress. This change is so small that the constant stress condition is still maintained. The corresponding boundary displacement is presented in Figure 4.10 d. There were no boundary displacements in the first injection cycle due to the short injection time. In the second injection cycle, a negative boundary displacement (expansion) occurred in the direction of σ_3, and two positive boundary displacements occurred in the other directions. This illustrates that the fractures had not started to rotate. In the following two injection cycles, boundary displacement expanded during injection in the vertical direction. This implied that the fractures were no longer vertical and had rotated into an inclined or horizontal fracture. Boundary displacements again demonstrate fracture rotation. This is consistent with the fractures observed after testing (Figure 4.10 b).

4.5 Conclusions

The possibility of well communication by hydraulic fracturing depends on the interaction of fractures driven hydraulically. The interaction of fractures is affected by many factors. Among the more important are the angle between the well line and the direction of the maximum horizontal stress, the state of stress (the ratio among three principal stresses, or stress difference), the well spacing, the injection procedure, and the injection rate. In this research program, a new injection procedure–injecting simultaneously oil into two wells–was used. The effect of the angle between the well line and the direction of the maximum horizontal stress on well communication was studied systematically. The angle ranged from 0° to 60°. Two states of stress were applied. From the ten double well hydraulic fracture tests conducted on 610 x 584 x 305 mm (24" x 23" x 12") Gypstone blocks, the following conclusions are drawn.

•For a low stress difference (σ_1/σ_3 around 1.5), well communication by hydraulic fracturing is possible for ß as high as 60°. The orientation of fracture initiation under this low stress difference is hard to predict by the state of stress on the wall of the wells because other factors such as anisotropy of permeability and strength of rock play a dominant role. Rotation of fractures was observed during fracture propagation.

•For a high stress difference (σ_1/σ_3 around 2), well communication by hydraulic fracturing is possible for ß up to 30°. A high stress difference makes well communication difficult. The orientation of fracture initiation is under control for this high stress difference. The orientation of fracture initiation is capable of being predicted by the state of stress on the wall of wells.

•One set of the monitored results is shown. It illustrates that bottomhole pressure reflects the path of fracture propagation, and boundary displacements imply fracture rotation.

4.6 References

1. *A 15 Year Portfolio of Achievement*, AOSTRA (1990).

2. Chhina H. S. and Agar J. G. Potential use of fracture technology for recovery of bitumen from oil sands. *Paper presented at the 3rd International Conference on Heavy Crude and Tar Sands*, Long Beach, California, U. S. A. (1985).

3. Proskin S. A., Scott J. D., and Chhina H. S. Current practice in the interpretation of microfrac tests in oil sands. *Paper SPE 20040 presented at the 60th California Regional Meeting*, Ventura, California, U.S.A. (1990).

4. Nemat-Nasser S. Thermally induced cracks and heat extraction from hot dry rocks. *Proceedings of the First Japan-United States Joint Seminar on Hydraulic Fracturing and Geothermal Energy*, pp. 11-32, Tokyo, Japan, (1982).

5. Murphy H. Hot dry rock reservoir development and testing in the U.S.A.. *Proceedings of the First Japan-United States Joint Seminar on Hydraulic Fracturing and Geothermal Energy*, pp. 33-58, Tokyo, Japan, (1982).

6. Cornet F. H., Hosanski J. M., Bernaudat F., and Ledoux E. Shallow depth experimentation on the concept of energy extraction from deep hot dry rocks. *Proceedings of the First Japan-United States Joint Seminar on*

Hydraulic Fracturing and Geothermal Energy, pp. 73-93, Tokyo, Japan, (1982).

7. Bouteca M., Lessi J., and Sarda J. P. Étude Théorique et Expérimentale de la Liaison de Deux Puits par Fracturation Hydraulique. *REVUE DE L'INSTITUTE FRANCAIS DU PETROLE* **39**, 433-444 (1984).

8. Lessi J. and Sarda J. P. Scale models studies of well linking by hydraulic fracturing and fatigue microfracturing. *Advances in European Geothermal Research*, 957-966 (1980).

9. Indraratna B. Application of fully grouted bolts in yielding rock. Ph.D. Thesis, University of Alberta, Edmonton, AB, Canada (1987).

10. Indraratna B. Development and applications of a synthetic material to simulate soft sedimentary rocks. *Géotechnique* **40**, 189-200 (1990).

11. Kaiser P. K. and Morgenstern N. R. Time-dependent deformation of small tunnels–I. experimental facilities. *Int. J. Rock Mech. Min. Sci. & Geomech. Abstr.* **18**, 129-140 (1981).

Table 4.1. Properties of Gypstone

Bulk density (kg/m^3)	1780
Dry density (kg/m^3)	1730
Void ratio	0.503
Porosity %	33.45
Water content %	2.37
Degree of saturation %	12.3
Tensile strength[1] (kPa)	113 to 343
Cohesion (kPa)[2]	334
Friction angle[2]	45.7°
Tangent modulus (MPa)[3]	179
Hydraulic conductivity (cm/s)	4.14×10^{-4} to 4.09×10^{-5}

---

[1] The tensile strength from Brazilian tests and splitting tests

[2] The shear strength from triaxial tests under natural water content with strain rate 8.4×10^{-5} and $4.2 \times 10^{-4}\ s^{-1}$

[3] The tangent modulus from uniaxial tests under natural water content with strain rate 8.4×10^{-5} and $4.2 \times 10^{-4}\ s^{-1}$

Table 4.2 Summary of Double Well Hydraulic Fracture Tests*

Specimen No.	ß**	σ_{ver} MPa	σ_{hmax} MPa	σ_3 MPa	Diameter/depth mm	Injection rate cm^3/s	Oil viscosity mPa*s	Fractures intersect
1	0	4.42	4.50	3.09	3.2/63.5	3.186	1000	yes
2	15	4.49	4.44	2.97	3.2/63.5	3.186	1000	not yet, but possible
3	30	4.39	4.41	2.99	3.2/63.5	3.186	1000	yes
4	45	4.46	4.23	3.01	3.2/63.5	3.186	1000	not yet, but possible
5	60	4.57	4.79	2.61	3.2/63.5	3.186	1000	yes
8	30	4.49	4.49	3.27	3.2/63.5	3.186	1000	yes
6	15	5.11	4.91	2.55	3.2/101.6	3.186	1000	yes
7	30	5.15	4.95	2.63	3.2/101.6	3.186	1000	yes
9	45	5.14	4.98	2.50	3.2/101.6	3.186	1000	no
10	60	4.86	4.74	2.42	3.2/101.6	3.186	1000	no

---

* Specimen size: 610 x 584 x 305 mm (24" x 23" x 12")

** ß: the angle between the well line and the direction of the maximum horizontal principal stress.

Table 4.3 Orientation of Fracture Initiation and Breakdown Pressure:

Specimen No.	β	σ_{ver} MPa	$3\sigma_3$-σ_1 MPa	Fracture initiation at Well 1	Fracture initiation at Well 2	Breakdown pressure at well 1 MPa	Breakdown pressure at well 2 MPa
Tests under a low stress difference							
1	0°	4.42	4.77	vertical	vertical	15.35	15.61
2	15°	4.49	4.47	vertical	vertical	16.54	15.84
3	30°	4.39	4.56	horizontal	horizontal	16.32	14.36
4	45°	4.46	4.80	unknown	unknown	16.51	15.00
5	60°	4.57	3.04	vertical	vertical	16.27	14.25
8	30°	4.49	5.32	unknown	vertical	20.37	20.80
Tests under a high stress difference							
6	15	5.11	2.74	vertical	vertical	15.69	16.08
7	30	5.15	2.94	vertical	vertical	14.51	13.76
9	45	5.14	2.52	vertical	vertical	13.73	15.20
10	60	4.86	2.52	vertical	vertical	15.56	16.32

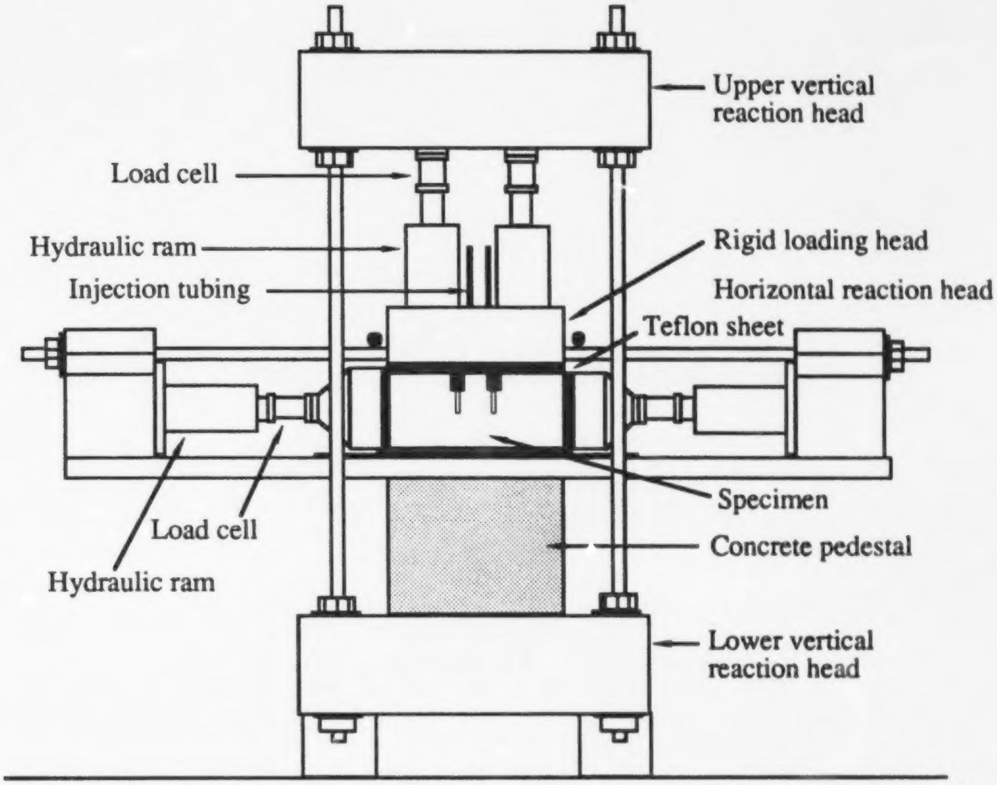
Upper vertical reaction head
Load cell
Hydraulic ram
Rigid loading head
Injection tubing
Horizontal reaction head
Teflon sheet
Specimen
Load cell
Concrete pedestal
Hydraulic ram
Lower vertical reaction head

Figure 4.1 Hydraulic Fracture Test Frame

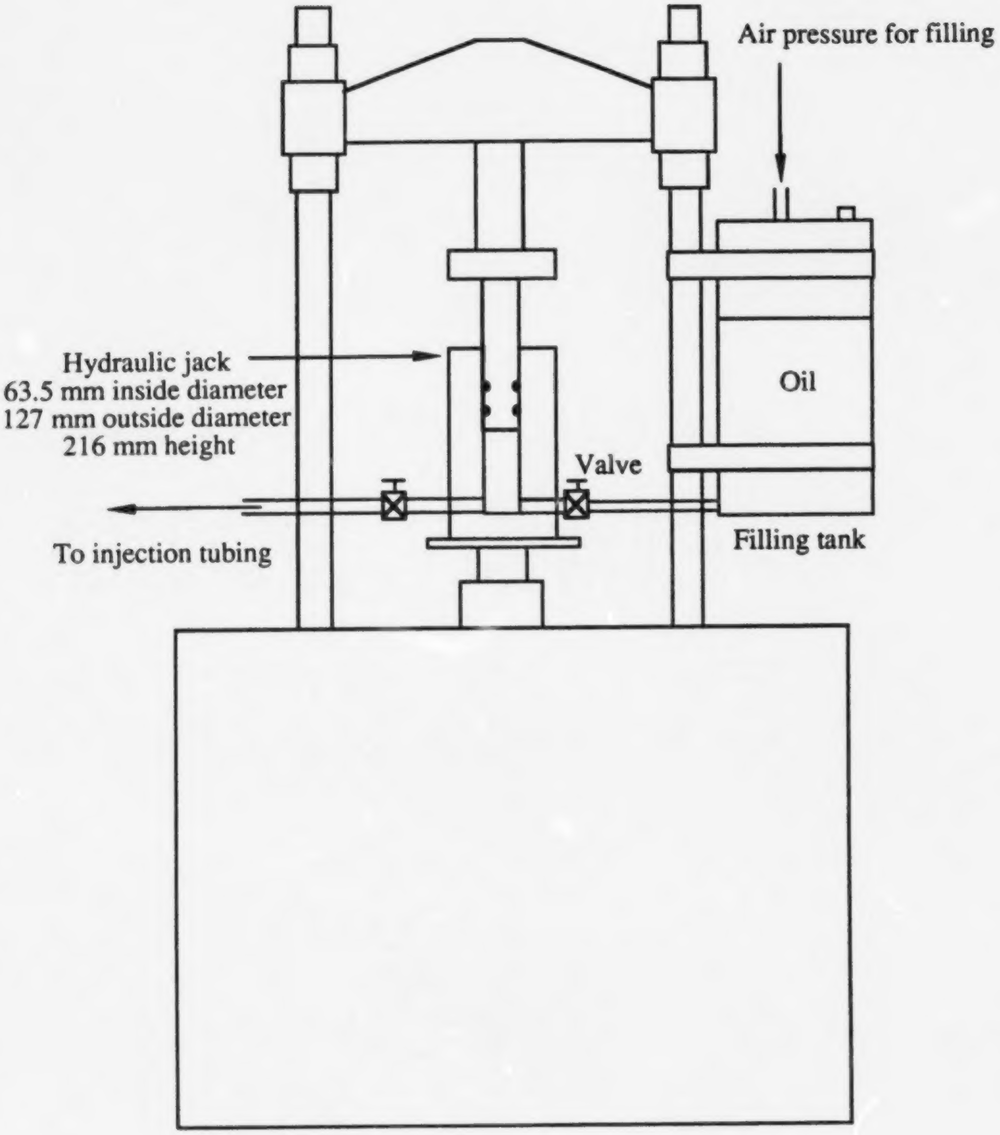
Air pressure for filling
Hydraulic jack
63.5 mm inside diameter
127 mm outside diameter
216 mm height
Oil
Valve
To injection tubing
Filling tank

Figure 4.2 Pump System

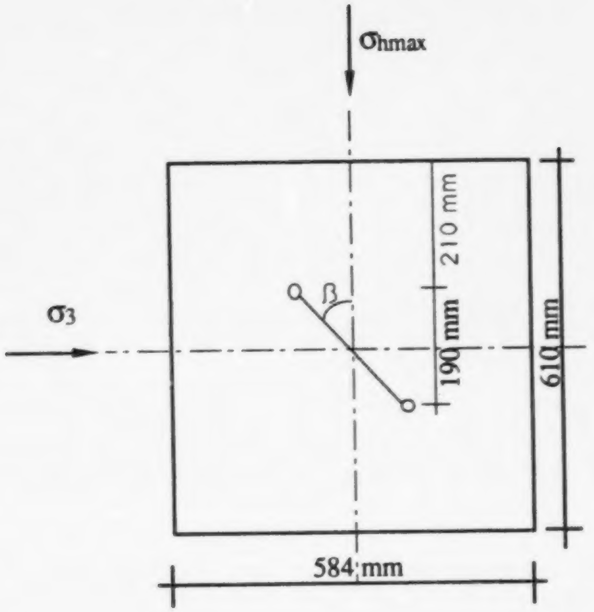
σhmax
σ3
β
210 mm
190 mm
610 mm
584 mm

Figure 4.3 Layout of Injection Wells

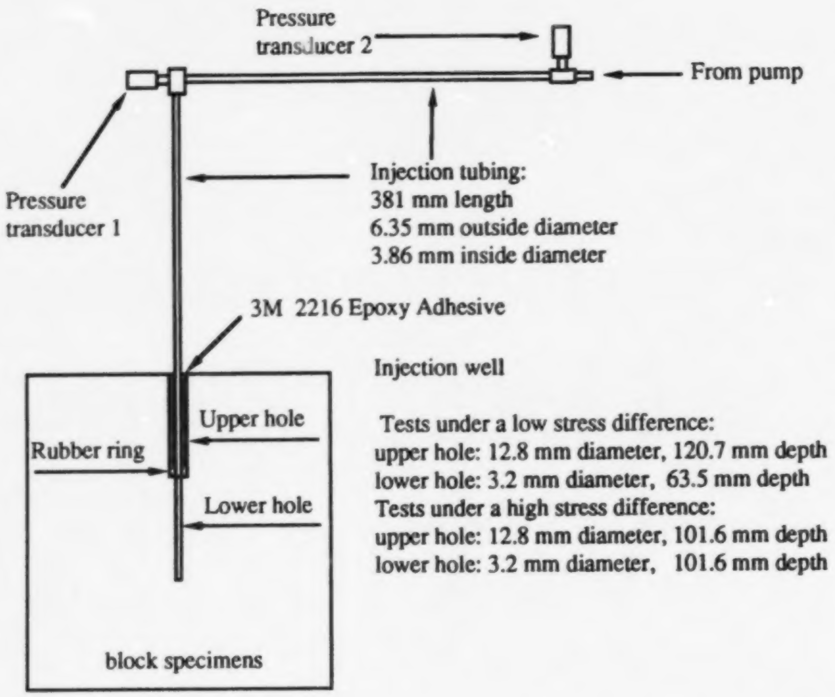
Pressure
transducer 2
From pump
Pressure
transducer 1
Injection tubing:
381 mm length
6.35 mm outside diameter
3.86 mm inside diameter
3M 2216 Epoxy Adhesive
Injection well
Upper hole
Rubber ring
Lower hole
Tests under a low stress difference:
upper hole: 12.8 mm diameter, 120.7 mm depth
lower hole: 3.2 mm diameter, 63.5 mm depth
Tests under a high stress difference:
upper hole: 12.8 mm diameter, 101.6 mm depth
lower hole: 3.2 mm diameter, 101.6 mm depth
block specimens

Figure 4.4 Injection Tubing and Sealing

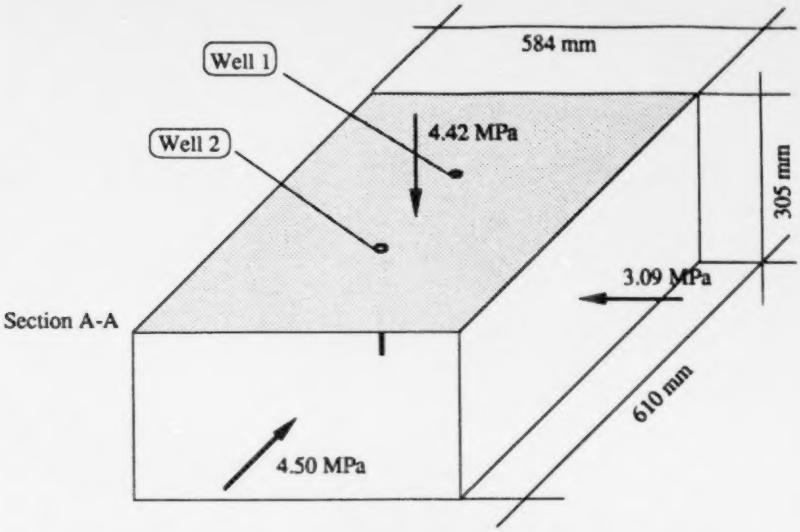
584 mm
Well 1
Well 2
4.42 MPa
305 mm
3.09 MPa
Section A-A
610 mm
4.50 MPa

a. Location of Cutting Planes

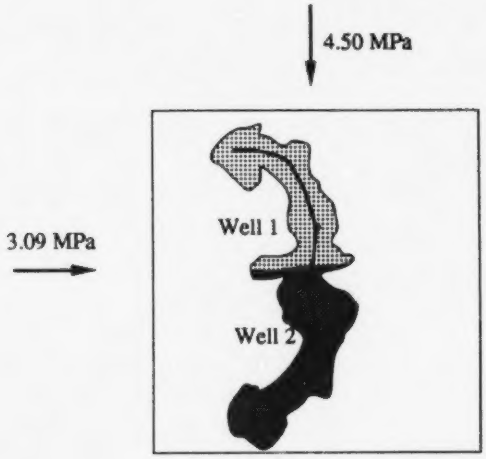
4.50 MPa
3.09 MPa
Well 1
Well 2

Section A-A (Top View of Top Plane)

▨ oil penetration area at Well 1

■ oil penetration area at Well 2

b. Fracture Description

Figure 4.5 Double Well Hydraulic Fracture Test 1 (ß=0°)

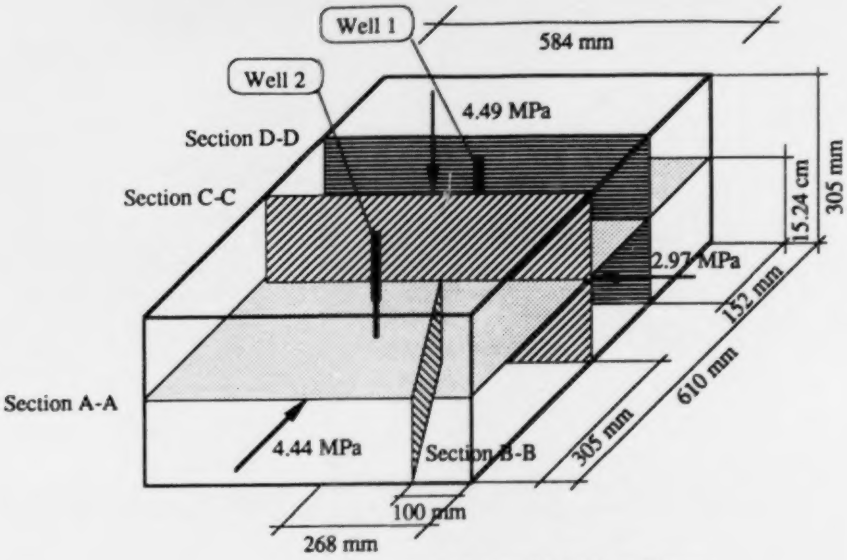
Well 1
584 mm
Well 2
4.49 MPa
Section D-D
Section C-C
15.24 cm
305 mm
2.97 MPa
152 mm
610 mm
Section A-A
305 mm
4.44 MPa
Section B-B
100 mm
268 mm

a. Location of Cutting Planes

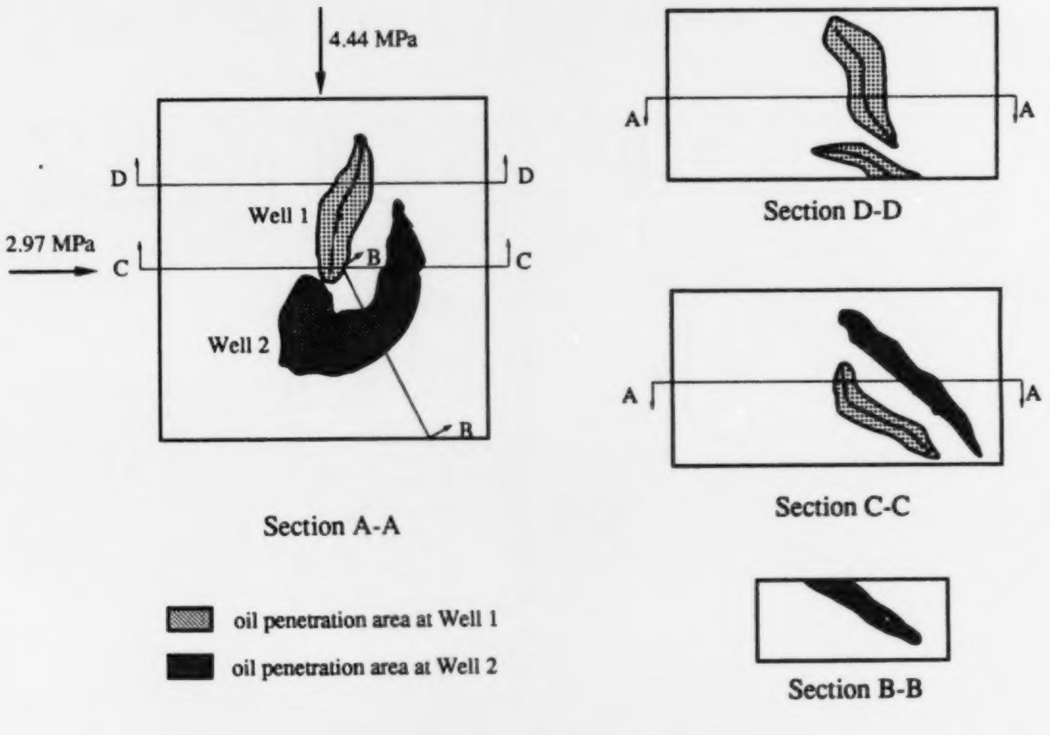
4.44 MPa
D
D
Well 1
2.97 MPa
C
B
C
Well 2
B
Section A-A
A
A
Section D-D
A
A
Section C-C
Section B-B
oil penetration area at Well 1
oil penetration area at Well 2

b. Fracture Description

Figure 4.6 Double Well Hydraulic Fracture Test 2 (ß=15°)

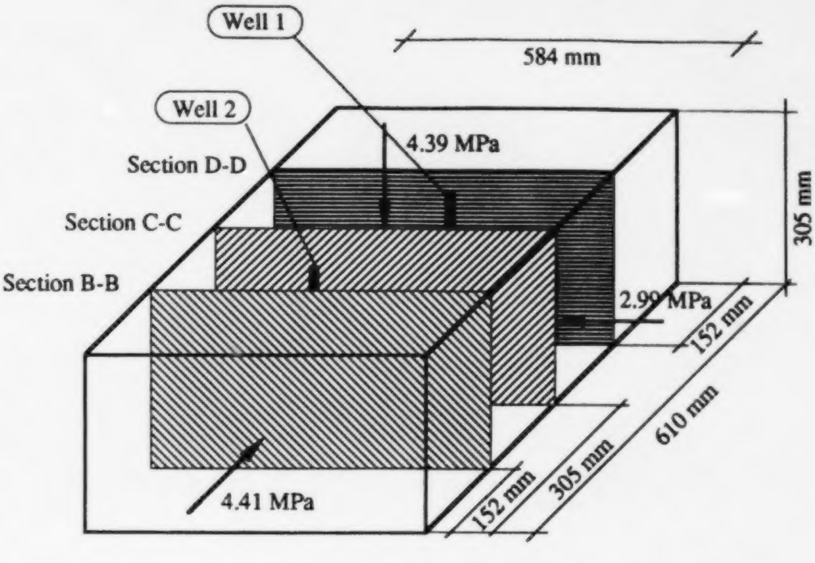
Well 1
584 mm
Well 2
4.39 MPa
Section D-D
Section C-C
305 mm
Section B-B
2.99 MPa
152 mm
610 mm
305 mm
152 mm
4.41 MPa

a. Location of Cutting Planes

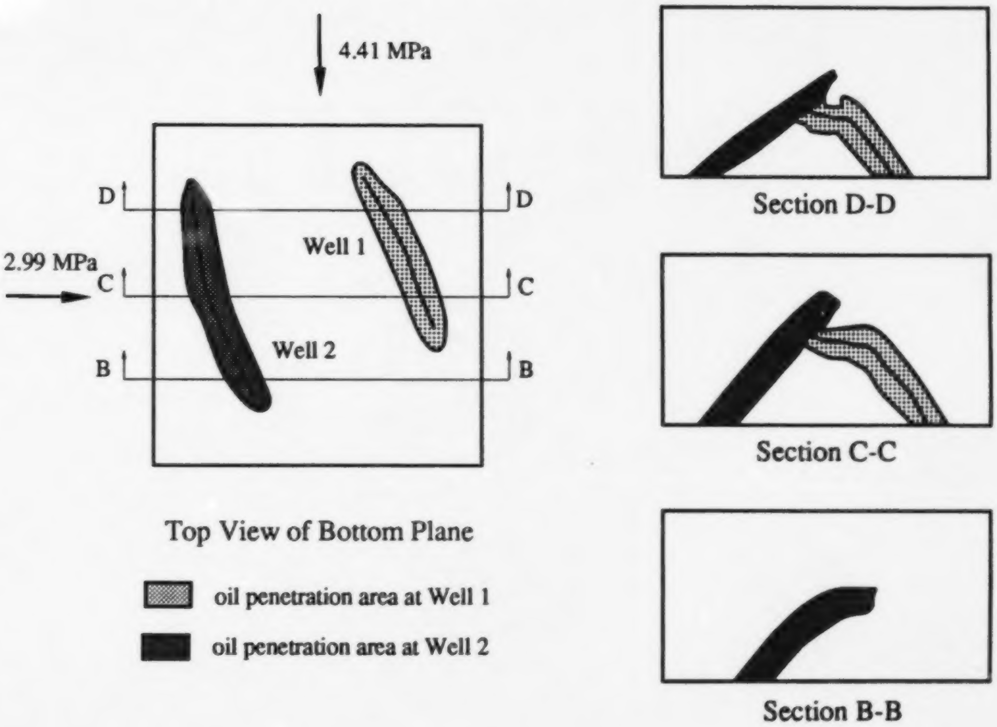
4.41 MPa
D
D
Well 1
2.99 MPa
C
C
Well 2
B
B
Top View of Bottom Plane
▨ oil penetration area at Well 1
■ oil penetration area at Well 2
Section D-D
Section C-C
Section B-B

b. Fractur Description

Figure 4.7 Double Well Hydraulic Fracture Test 3 (ß=30°)

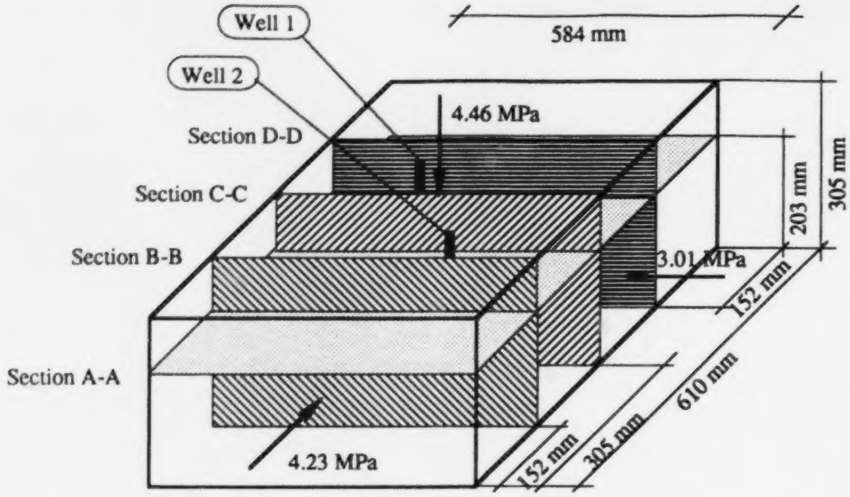
Well 1
Well 2
584 mm
4.46 MPa
Section D-D
Section C-C
Section B-B
Section A-A
203 mm
305 mm
3.01 MPa
152 mm
610 mm
305 mm
152 mm
4.23 MPa

a. Location of Cutting Planes

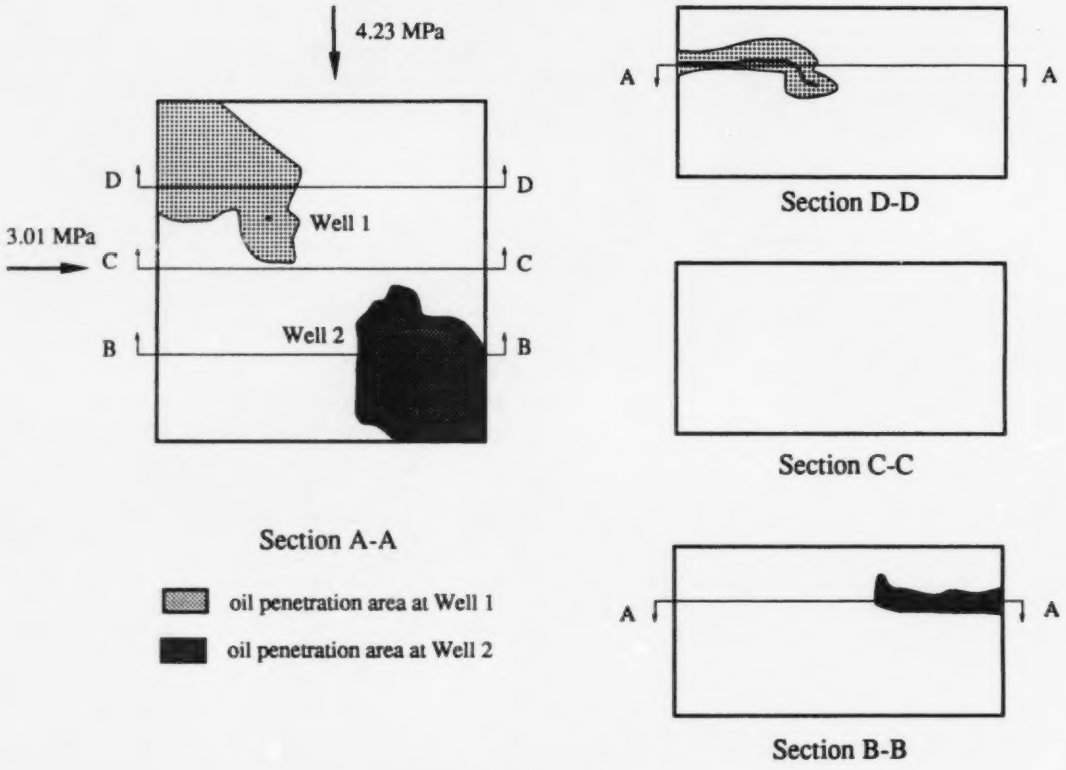
4.23 MPa
D
D
Well 1
3.01 MPa
C
C
Well 2
B
B
Section A-A
oil penetration area at Well 1
oil penetration area at Well 2
A
A
Section D-D
Section C-C
A
A
Section B-B

b. Fracture Description

Figure 4.8 Double Well Hydraulic Fracture Test 4 (ß=45°)

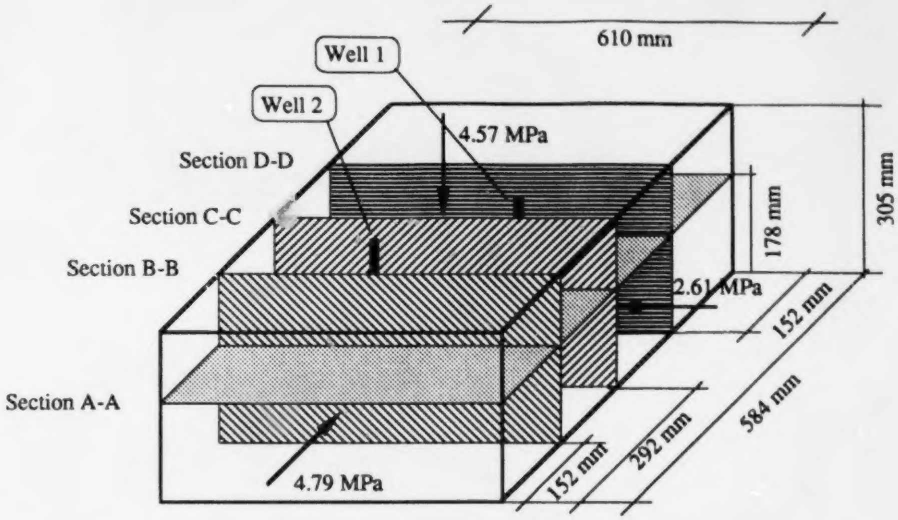
610 mm
Well 1
Well 2
4.57 MPa
Section D-D
Section C-C
Section B-B
Section A-A
178 mm
305 mm
2.61 MPa
152 mm
584 mm
292 mm
152 mm
4.79 MPa

a. Location of Cutting Planes

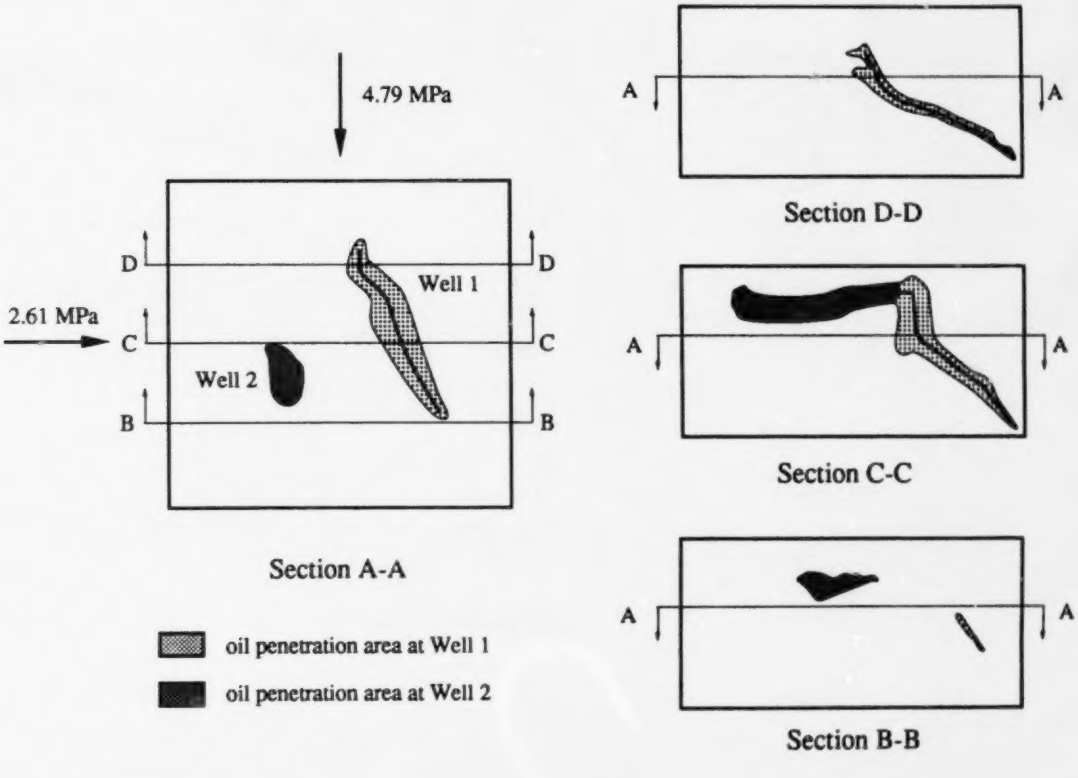
4.79 MPa
2.61 MPa
D
D
C
C
B
B
Well 1
Well 2
Section A-A
▨ oil penetration area at Well 1
■ oil penetration area at Well 2
A
A
Section D-D
A
A
Section C-C
A
A
Section B-B

b. Fracture Description

Figure 4.9 Double Well Hydraulic Fracture Test 5 (ß=60°)

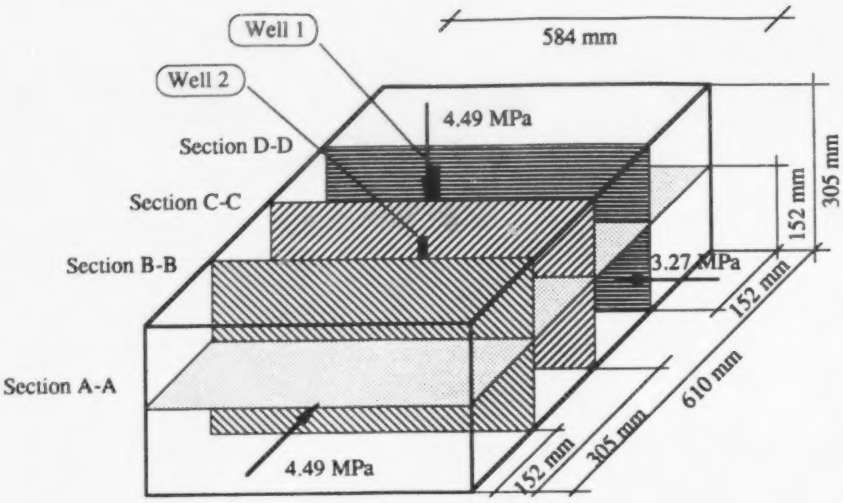
Well 1
Well 2
584 mm
4.49 MPa
Section D-D
Section C-C
Section B-B
Section A-A
3.27 MPa
152 mm
305 mm
152 mm
610 mm
305 mm
152 mm
4.49 MPa

a. Location of Cutting Planes

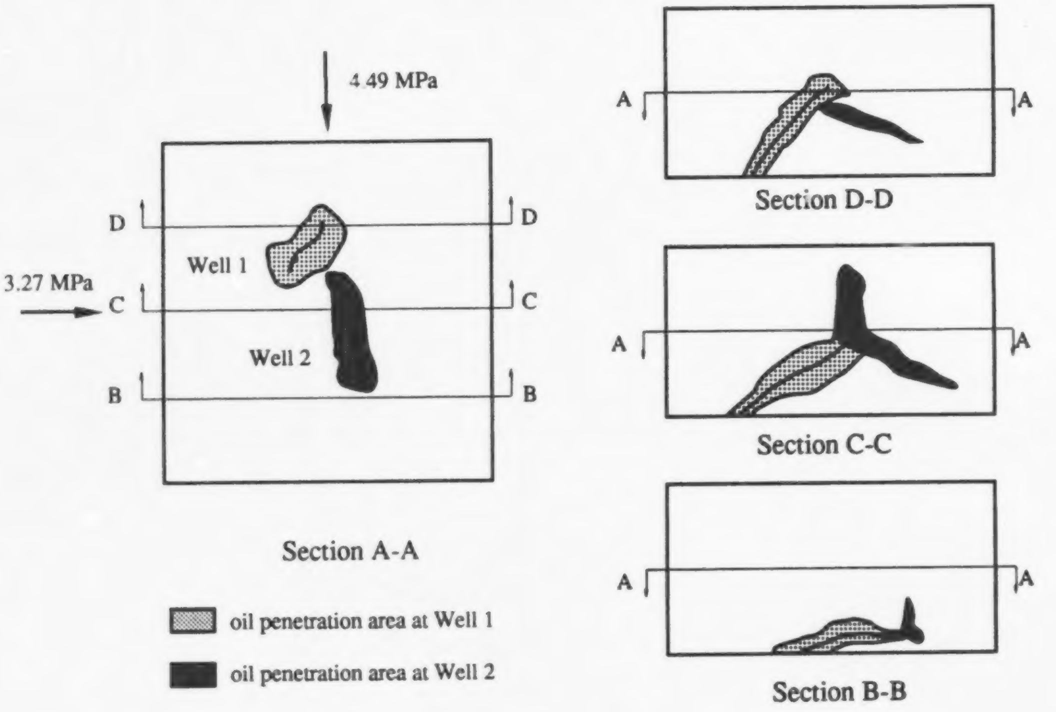
4.49 MPa
D
D
Well 1
3.27 MPa
C
C
Well 2
B
B
Section A-A
oil penetration area at Well 1
oil penetration area at Well 2
A
A
Section D-D
A
A
Section C-C
A
A
Section B-B

b. Fracture Description

Figure 4.10 Double Well Hydraulic Fracture Test 8 (ß=30°)

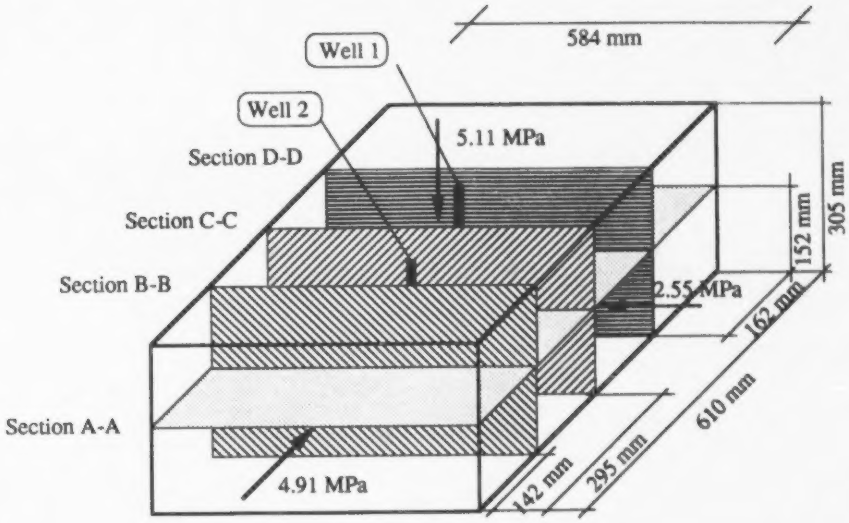
584 mm
Well 1
Well 2
5.11 MPa
Section D-D
Section C-C
Section B-B
Section A-A
2.55 MPa
4.91 MPa
152 mm
305 mm
162 mm
610 mm
295 mm
142 mm

a. Location of Cutting Planes

Figure 4.11 Double Well Hydraulic Fracture Test 6 (ß=15°)

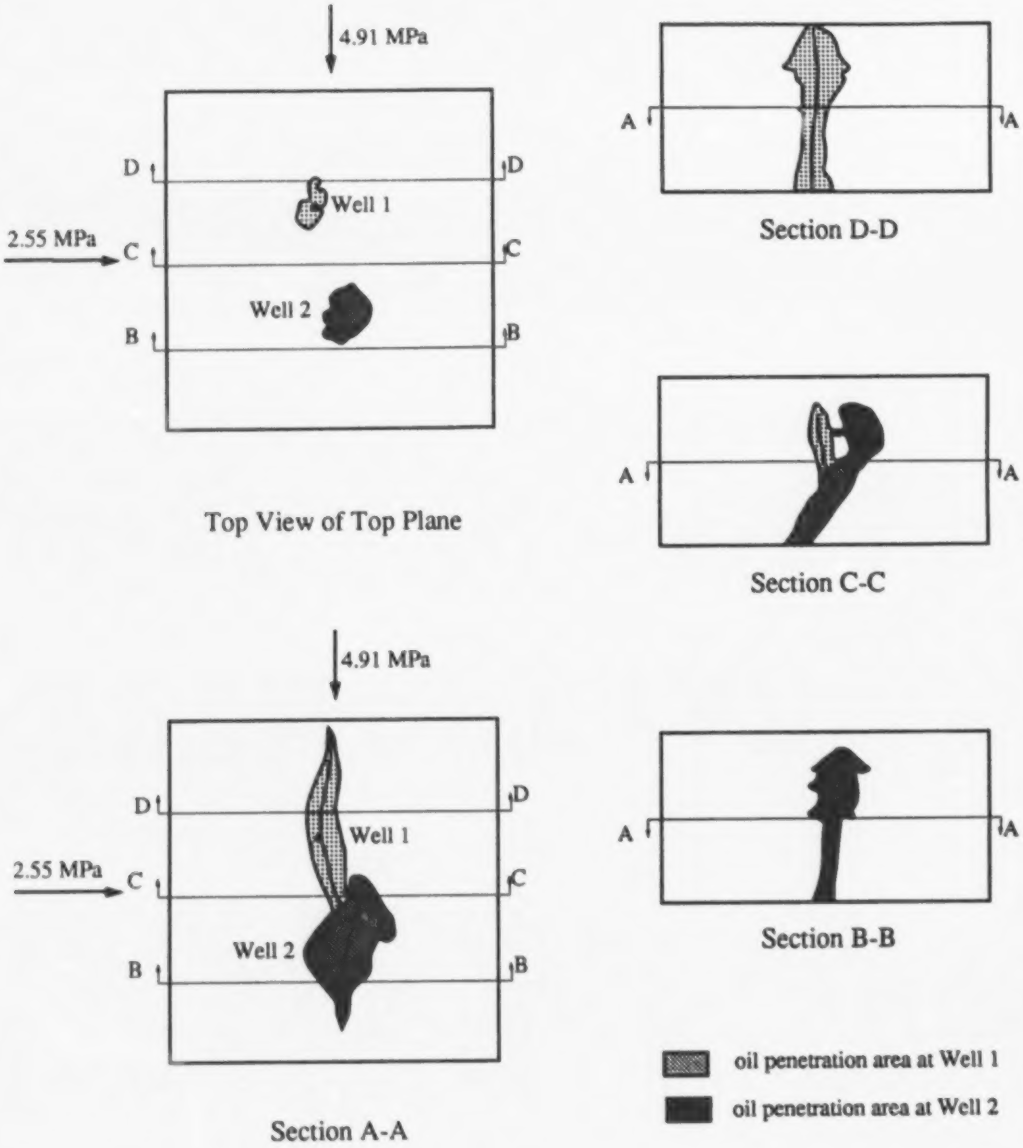
4.91 MPa
2.55 MPa
D
D
C
C
B
B
Well 1
Well 2
A
A
oil penetration area at Well 1
oil penetration area at Well 2

Top View of Top Plane

Section D-D

Section C-C

Section B-B

Section A-A

b. Fracture Description

Figure 4.11 Continued

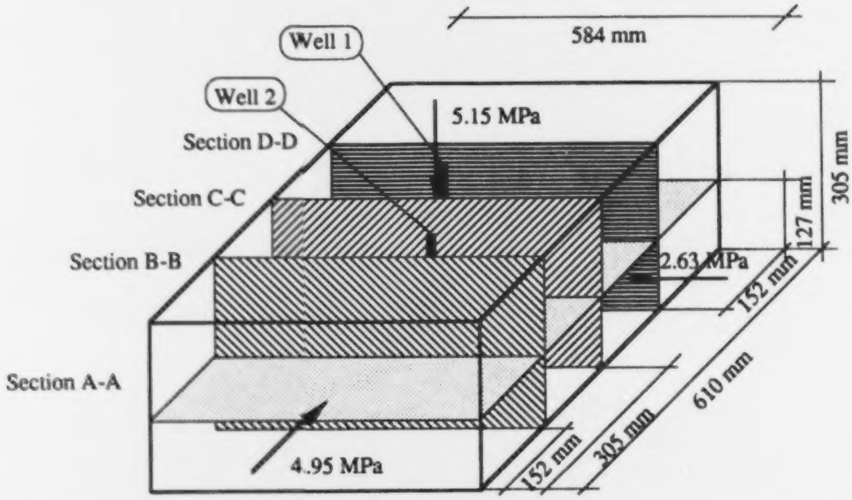
Well 1
584 mm
Well 2
5.15 MPa
Section D-D
Section C-C
Section B-B
Section A-A
305 mm
127 mm
2.63 MPa
152 mm
610 mm
305 mm
152 mm
4.95 MPa

a. Location of Cutting Planes

Figure 4.12 Double Well Hydraulic Fracture Test 7 (ß=30°)

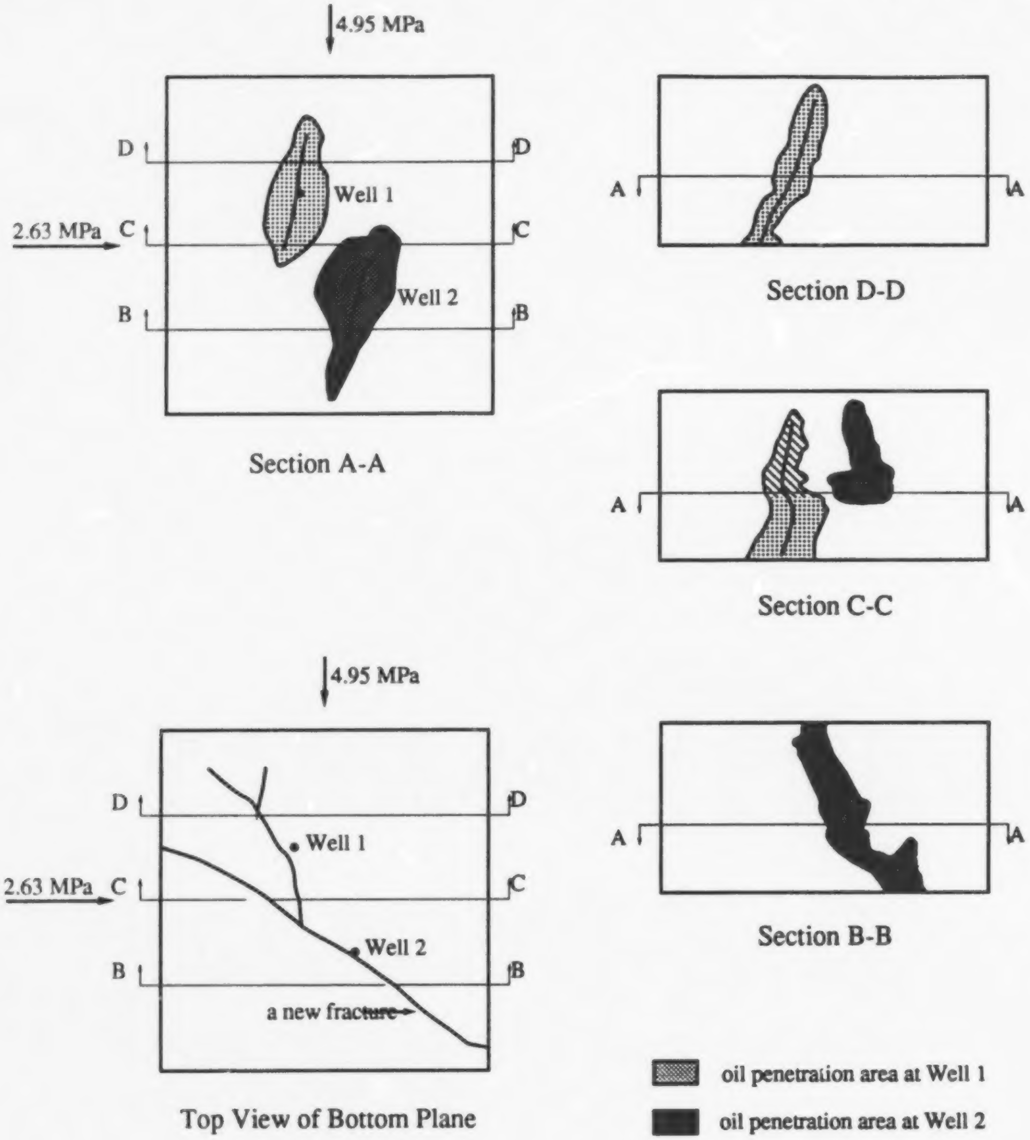
4.95 MPa
2.63 MPa
D
C
B
Well 1
Well 2
A
a new fracture
oil penetration area at Well 1
oil penetration area at Well 2

Section A-A

Section D-D

Section C-C

Top View of Bottom Plane

Section B-B

b. Fracture Description

Figure 4.12 Continued

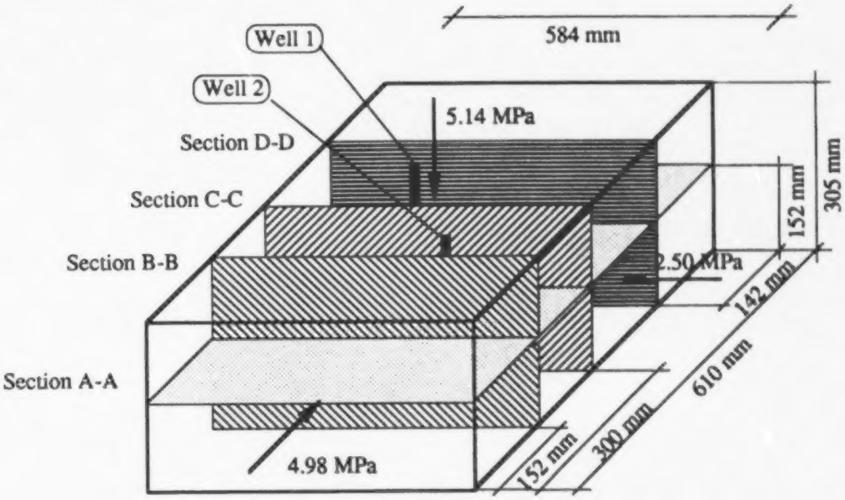
Well 1
Well 2
584 mm
5.14 MPa
Section D-D
Section C-C
Section B-B
Section A-A
2.50 MPa
152 mm
305 mm
142 mm
610 mm
300 mm
152 mm
4.98 MPa

a. Location of Cutting Planes

Figure 4.13 Double Well Hydraulic Fracture Test 9 (ß=45°)

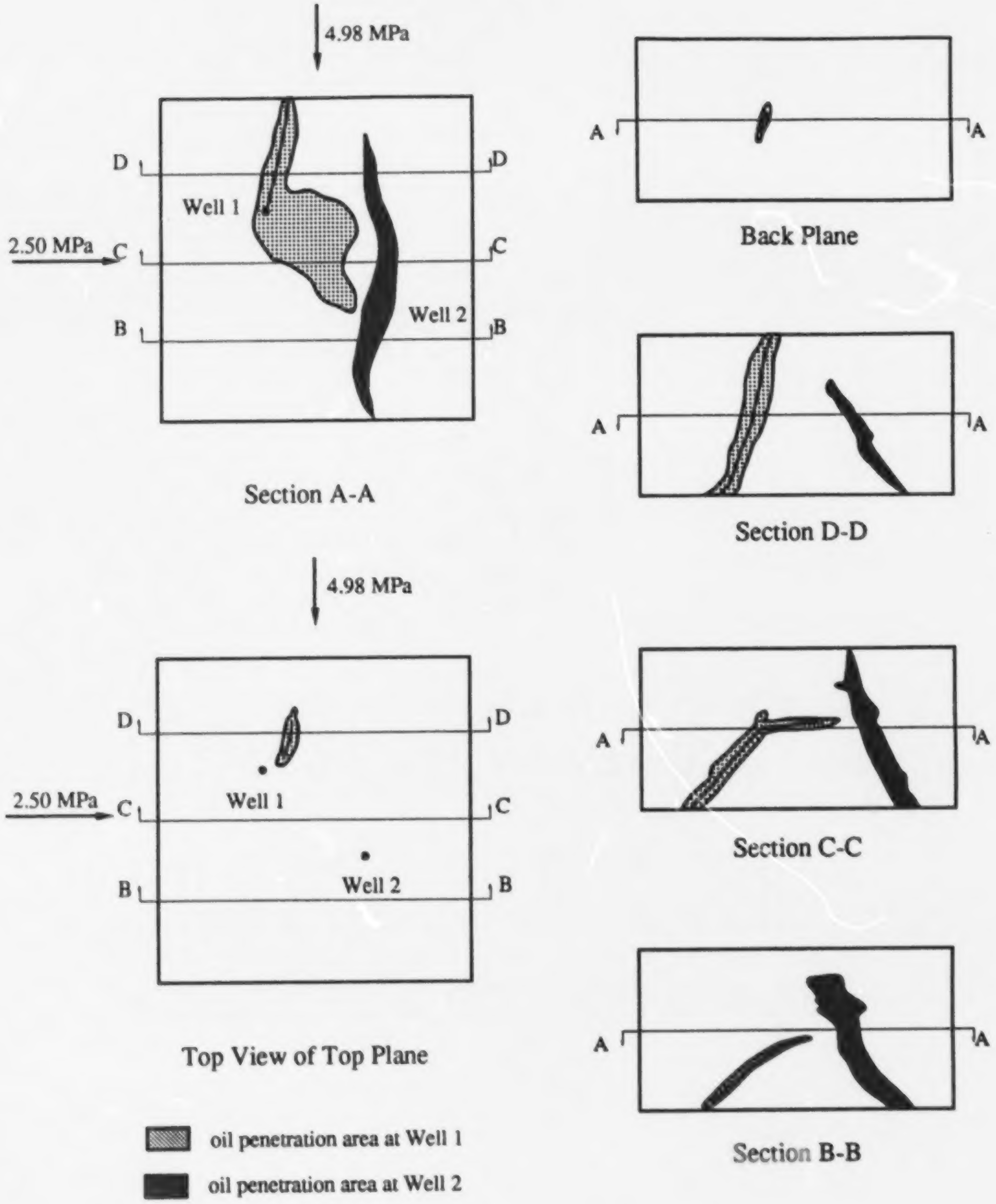
4.98 MPa
2.50 MPa
D
C
B
Well 1
Well 2
A
4.98 MPa
2.50 MPa
D
C
B
Well 1
Well 2

Back Plane

Section A-A

Section D-D

Section C-C

Top View of Top Plane

Section B-B

▨ oil penetration area at Well 1

■ oil penetration area at Well 2

b. Fracture Description

Figure 4.13 Continued

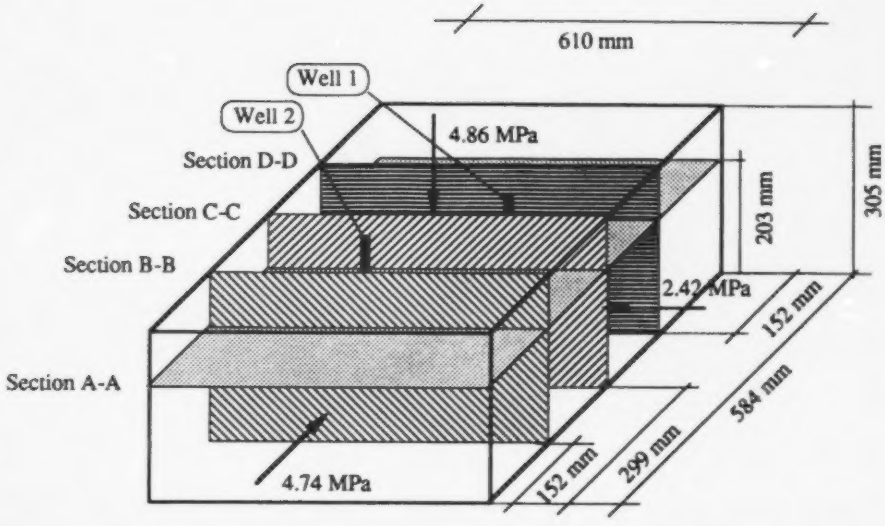
610 mm
Well 1
Well 2
4.86 MPa
Section D-D
Section C-C
Section B-B
Section A-A
203 mm
305 mm
2.42 MPa
152 mm
584 mm
299 mm
152 mm
4.74 MPa

a. Location of Cutting Planes

Figure 4.14 Double Well Hydraulic Fracture Test 10 (ß=60°)

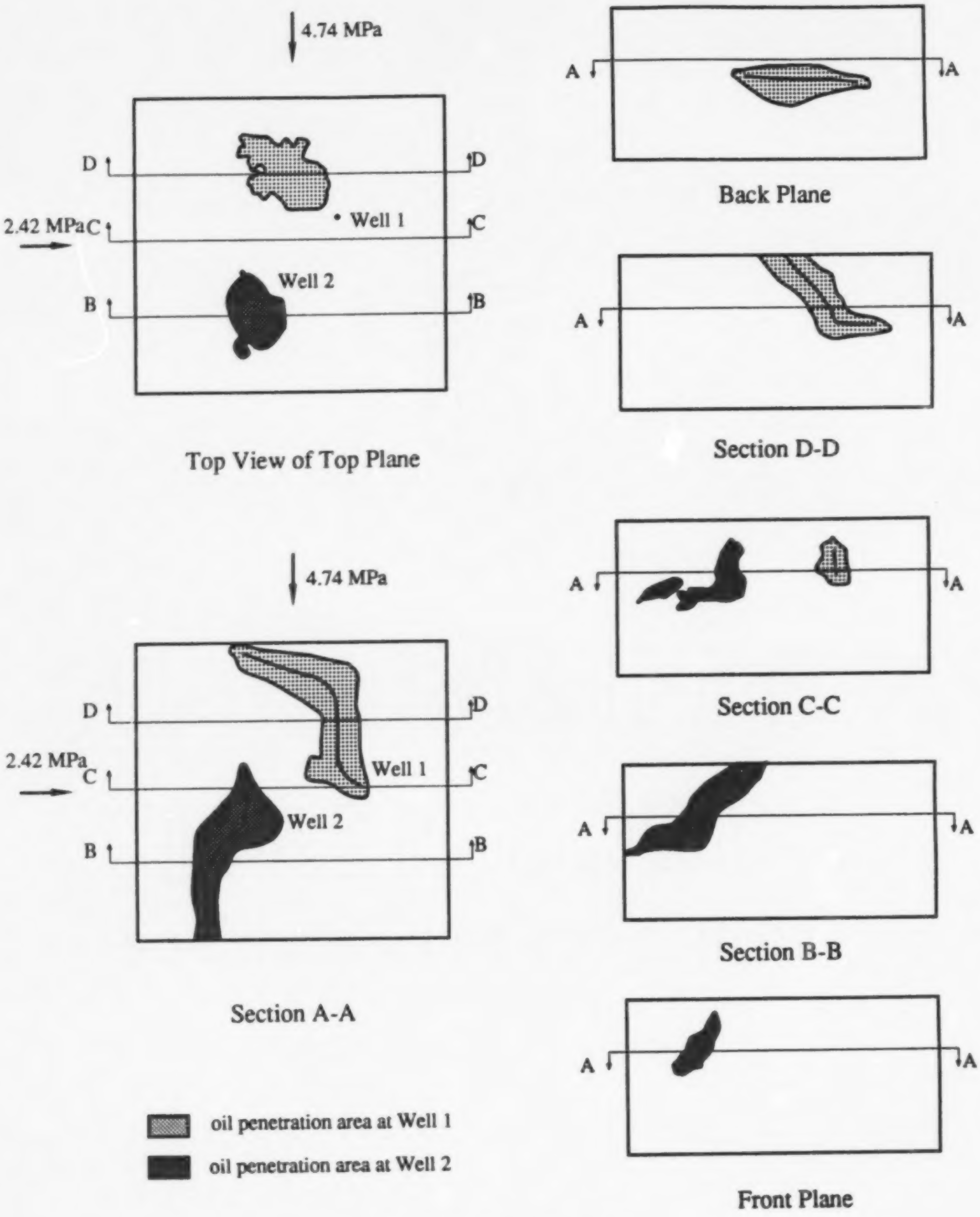
4.74 MPa
2.42 MPa
D
C
B
A
Well 1
Well 2
oil penetration area at Well 1
oil penetration area at Well 2

Top View of Top Plane

Back Plane

Section D-D

Section C-C

Section A-A

Section B-B

Front Plane

b. Fracture Description

Figure 4.14 Continued

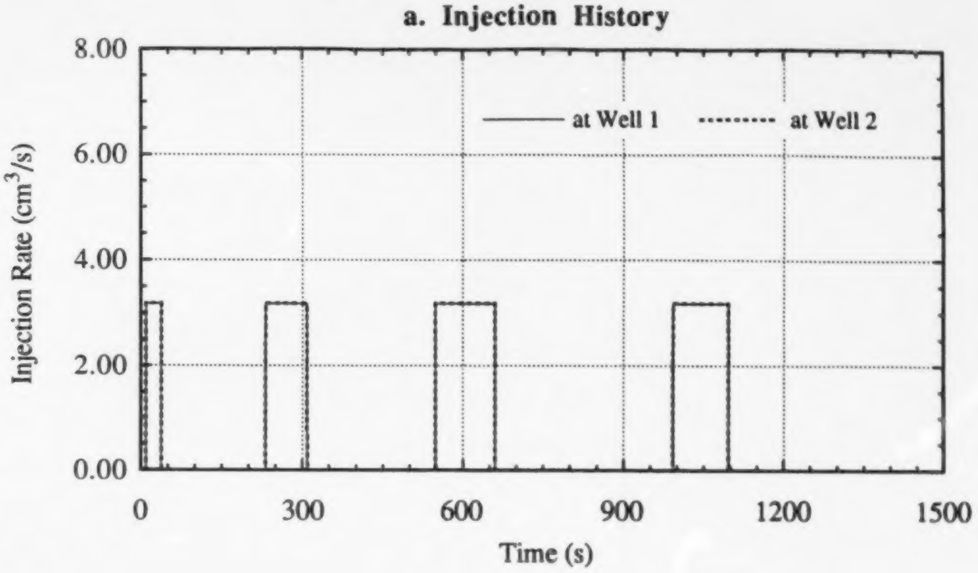

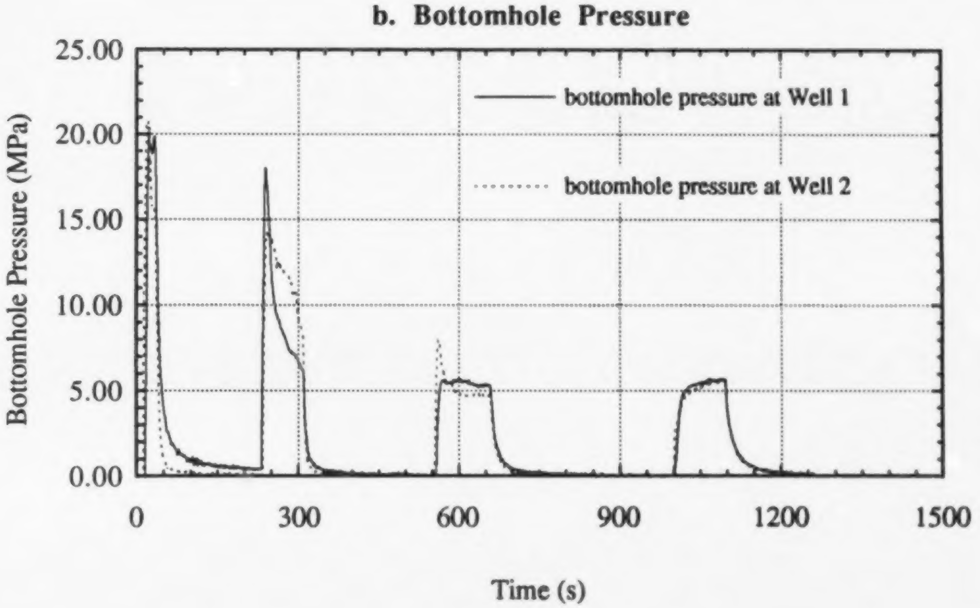

Figure 4.15 Double Well Hydraulic Fracture Test 8

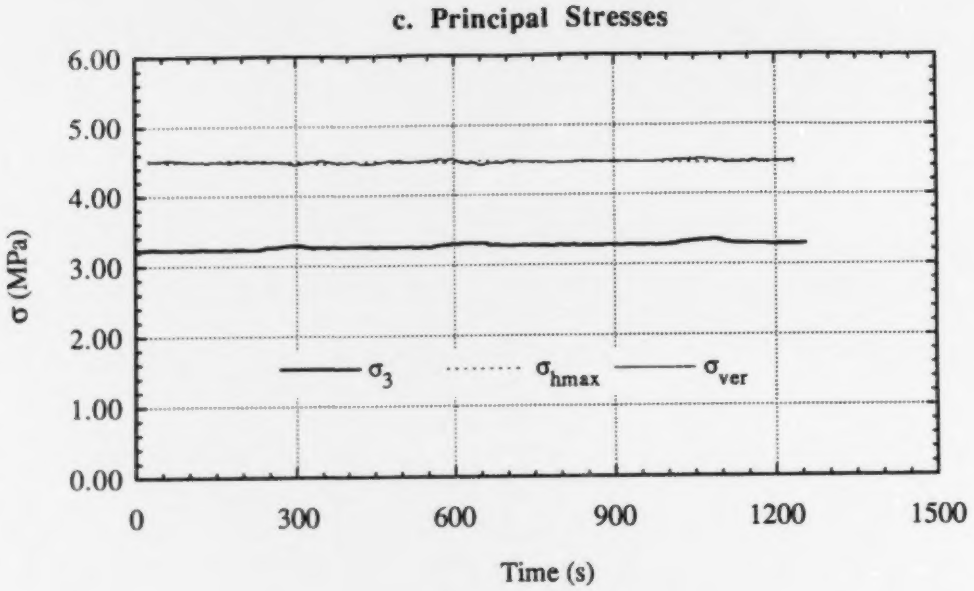

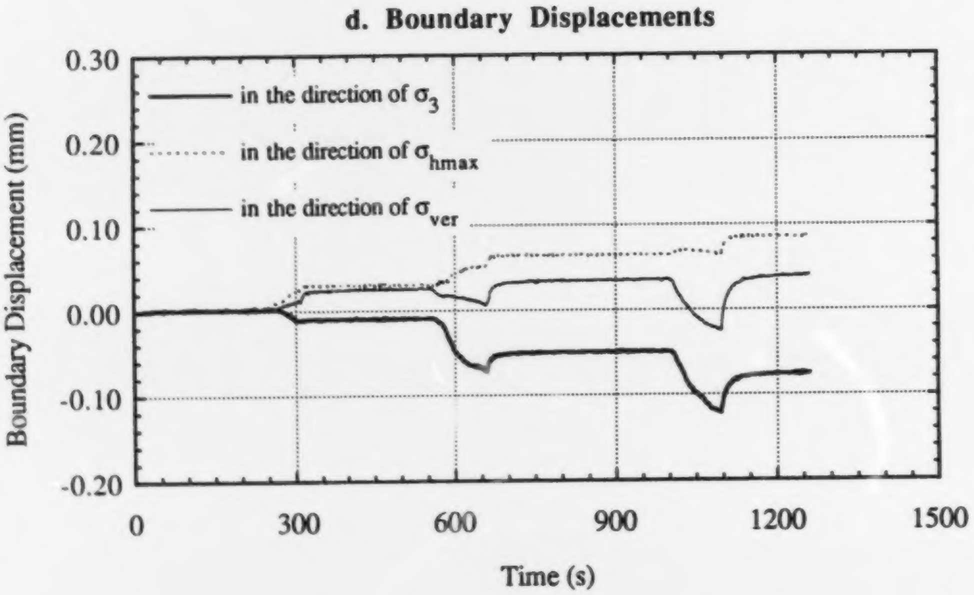

Figure 4.15 Continued

Chapter 5

Interpretation of Bottomhole Pressure

5.1 Introduction

Bottomhole pressure during hydraulic fracturing is informative. Breakdown pressure depends on the two horizontal principal stresses and the tensile strength for a vertical fracture; consequently, it is used to evaluate the maximum horizontal stress. Bottomhole pressure post breakdown characterizes the manner in which a fracture is propagating; therefore, it is used to diagnose the fracture and to provide design parameters for subsequent treatment. The shut-in pressure is equal to the least principal stress, so the shut-in curve is usually analyzed to determine the least principal stress. Many theories have been developed to achieve these objectives. The intent of this chapter is to compare some of them with the experimental results obtained in the single well hydraulic fracturing program. The analysis begins with the bottomhole pressure before breakdown. Build-up of the bottomhole pressure and factors which affect the build-up are studied. Subsequently, the breakdown models are checked by the experimental results. After that, fracture pressure analysis based on 2D hydraulic fracturing models is used to study the bottomhole pressure.

Finally, the shut-in curve is analyzed, and the methods to determine the least principal stress are evaluated.

5.2 Build-up of Bottomhole Pressure before Breakdown

5.2.1 Introduction

Bottomhole pressure before breakdown is important to understand the breakdown process. It is impossible to predict breakdown pressure without knowledge of the build-up of the bottomhole pressure. The current method to predict the build-up of the bottomhole pressure in hydraulic fracturing stress measurements is to accept one of the existing theories. One of the most current theories is Biot's poroelastic theory [1]. Another theory is the flow theory of a slightly compressible fluid in porous media [2-3]. Unfortunately, there are few studies which devote to check whether these predictions are identical with that observed during fracturing. In addition, poroelastic theory is a complex coupled theory. A complex numerical calculation is required to obtain the pore pressure distribution around a well. It is still unknown whether the bottomhole pressure can be predicted by simple uncoupled theories such as the flow theory of a slightly compressible fluid in porous media. Therefore, this section compares the build-up of the bottomhole pressure predicted by uncoupled radial flow theory with the measured behavior.

5.2.2 Theoretical Considerations

Build-up of the bottomhole pressure before breakdown is one kind of unsteady well-flow problem. This problem has been studied in detail in well test analysis. Many analysis techniques are available [4-8]. The interpretation of the pressure versus time data is based on the flow theory of a slightly compressible fluid in porous media. The governing equation is obtained by combining the law of mass conservation, the equation of state, and Darcy's law [4]. The resulting equation in cylindrical coordinates is

$$\frac{\partial^2 p}{\partial r^2} + \frac{1}{r}\frac{\partial p}{\partial r} = \frac{\phi \; C_t \; \mu}{k}\frac{\partial p}{\partial t} \quad \ldots\ldots\ldots\ldots\ldots\ldots 5.1$$

where p is the pore pressure in the formation, r is the radius co-ordinate, ϕ is the porosity of the formation, μ is the viscosity of the fluid, C_t is the compressibility of the fluid, k is the permeability of the formation, and t is the time.

The derivation of the above equation is based on the assumption of single phase fluid flow. For a single phase fluid, the mass conservation requires that the difference between the amount flowing-into a unit and that flowing-out of a unit is equal to the change of the fluid volume in the unit, i.e. compression of the fluid. For hydraulic fracturing under saturated conditions, the above equation may continue to predict the bottomhole pressure. However, for hydraulic fracturing under dry conditions, the mechanism of flow is completely different. When the fracture fluid leaks off into the formation, it fills the pores in the formation first, but does not compress the fluid existing in the formation. The injection amount is not balanced by the compression of the fluid in the formation but by the pores in the formation. Therefore, two different responses of the bottomhole pressure are expected. For the above reason, a formula is derived for the flow into a dry formation. It, then, is applied to interpret the pressure versus time data from the single well hydraulic fracture tests.

Fracture fluid with viscosity μ is injected at a constant rate q_i into a well of radius r_w and depth h which is located in a dry formation. The formation has porosity, ϕ, and absolute permeability, k. Fracture fluid flows radially into the formation, and infiltration upwards and downwards is negligible. Darcy's law is valid, and the fracture fluid is incompressible. R is the boundary of the oil penetration area, i.e. $p = 0$, at $r = R$. p_w represents bottomhole pressure. In the fluid penetration area, the fluid occupies the whole pore space.

Darcy's law may be expressed as $q_i = - \frac{k}{\mu} \frac{\partial P}{\partial r} A$. This equation is valid for all $r < R$ because the fracture fluid is incompressible. From this equation and the boundary condition $p = 0$ at $r = R$ and $A = 2\pi rh$, the equation below is obtained.

$$p = \frac{q_i \mu}{2\pi hk} \ln \frac{R}{r} \quad \text{.......} 5.2$$

Thus,

$$p_w = \frac{q_i \mu}{2\pi hk} \ln \frac{R}{r_w} \quad \text{.......} 5.3$$

From the assumptions that the fluid is incompressible, and the formation is fully saturated in the oil penetration area, the mass conservation requires that the amount of the fluid injected is equal to the volume of the pores in the oil penetration area. That is

$$q_i t = \pi(R^2 - r_w^2)h\phi \quad \text{.......... 5.4}$$

Thus,

$$R = \sqrt{\frac{q_i t}{\pi h \phi} + r_w^2} \quad \text{.......... 5.5}$$

Substituting equation 5.5 into equation 5.3, the following equation for the build-up of the bottomhole pressure is obtained.

$$p_w = \frac{q_i \mu}{4\pi hk} \ln\left(\frac{q_i t}{\pi h \phi r_w^2} + 1\right) \quad \text{.......... 5.6}$$

5.2.3 Application to the Hydraulic Fracture Tests

Equation 5.6 will be applied to the single well hydraulic fracture tests to understand factors that dominate the build-up of the bottomhole pressure before breakdown. As well test analysis shows [5-8], the wellbore storage and the skin effect influence strongly the behavior of the build-up of the bottomhole pressure. To predict the behavior of the build up of the bottomhole pressure, they must be incorporated into the equation.

Wellbore Storage: In hydraulic fracture tests, the well and the injection tubing are dry before pumping to avoid oil infiltration into the formation before injection. Therefore, this space must firstly be filled during pumping. This is one kind of wellbore storage. This effect is incorporated into equation 5.6 through replacing t by $t - t_0$, i.e. the fluid enters the formation after t_0. When the fracture fluid is pumped into the injection well, the bottomhole pressure will be built up. In turn, the oil in the pump, the injection tubing, and the injection well will be compressed, and the wellbore will also expand under this pressure. This is another kind of wellbore storage. This effect is considered through correcting injection rate q_i.

Skin Effect: The skin effect is incorporated into equation 5.6 by introducing a constant term s, as in well test analysis. Now equation 5.6 becomes

$$p_w = \frac{q\mu}{4\pi hk}[\ln(\frac{q(t-t_0)}{\pi h\phi r_w^2} + 1)+s] \quad \text{.......... 5.7}$$

where q is flow rate flown into the formation, i.e. the injection rate after correction. This is the equation used in analysis of the build-up of the bottomhole pressure.

Correction of Injection Rate q_i: If the compressibility of the oil is assumed as a constant, the effect of compressibility of the fluid in the pump, the injection tubing, and the injection well on injection rate can be expressed as

$$- C_t \frac{dp_w}{dt} V \quad \text{.......... 5.8}$$

where C_t is the compressibility of the fluid, V is the oil volume compressed, and p_w is the bottomhole pressure. The wellbore storage caused by well deformation may be expressed as

$$- h[\pi(r_w + du_r)^2 - \pi r_w^2]/dt \quad \text{.......... 5.9}$$

where u_r is radial displacement of the wall of the injection well, h is height of injection segment that is depth of the injection well. If it is assumed that the well deformation can be approximately expressed by the solution for a hole in an infinite media under internal pressure p_w [9], then,

$$u_r = \frac{r_w}{2G} p_w \quad \text{.......} 5.10$$

where G is the shear modulus of the formation. Because du_r is small, $(du_r)^2$ is negligible. Therefore, the change of injection rate resulted from well deformation is

$$- \pi r_w^2 h \frac{1}{G} \frac{dp_w}{dt} \quad \text{.......} 5.11$$

Thus, the flow rate into the formation becomes

$$q = q_i - C_t \frac{dp_w}{dt} V - \pi r_w^2 h \frac{1}{G} \frac{dp_w}{dt} \quad \text{.......} 5.12$$

In calculations, V takes the value of 400 cm^3 and G is 68.85 MPa (9,986 psi), which is equivalent to a Young's modulus of 179 MPa (25,962 psi) and a Poisson's ratio of 0.3. C_t is equal to 4.2 x 10^{-4} MPa^{-1} (2.9 x 10^{-6} psi^{-1}). dp_w/dt is obtained from the measured bottomhole pressure.

Determination of t_0 and s: After the injection rate is corrected, a plot of $4\pi hkp_w/q\mu$ vs $\ln[q(t-t_0)/\pi h\phi r_w^2+1]$ is made. From equation 5.7, it is obvious that the radial flow region is a straight line with unit slope in this plot, and the y-intercept gives the value of s. When t_0 changes, the curve will vary its form (a straight line or a curve). t_0 is determined by trial and error so that the curve becomes a straight line in the plot of $4\pi hkP_w/q\mu$ vs $\ln[q(t-t_0)/\pi h\phi r_w^2+1]$ after the initial wellbore storage effect. Similarly, if the true values of h, q, μ, and k are applied, the slope of the straight line should be unity. h, μ, and q are known. Although the measured k is also available, it is variable and ranges from 4.09×10^{-5} to 4.14×10^{-4} cm/s (0.0417 to 0.422 μm^2). Hence, k is chosen so that the slope becomes unity. Then, the corresponding y-intercept is s.

The analysis results of six hydraulic fracture tests are shown in Figure 5.1 to 5.6. A negative skin effect is obtained for all tests. For three tests without stress, it increases from -0.74707 at an injection rate of 0.528 cm^3/s to -2.617 at an injection rate of 3.186 cm^3/s. For the three tests with stress, the s value is slightly high, and ranges from -3.38 to -3.99. For the tests without stress, the permeability obtained is 1.78×10^{-4} cm/s (0.182 μm^2) and 1.21×10^{-4} cm/s (0.123 μm^2), which is in the measured range. The permeability obtained is 2.70×10^{-4} cm/s (0.275 μm^2) and 2.43×10^{-4} cm/s (0.248 μm^2) for Tests 21 and 22, which is also in the measured range. The permeability is 4.22×10^{-4} cm/s (0.430 μm^2) for the second injection cycle of Test 20, which is slightly higher than the maximum value measured, 4.14×10^{-4} cm/s (0.422 μm^2). Considering the variable permeability of Gypstone, the permeability from the pressure analysis is similar to the measured values.

It is of interest to compare the bottomhole pressure predicted with the measured values (Figure 5.1 b to Figure 5.6 b). At the beginning of pumping, the bottomhole pressure vs time curve is concave. The wellbore storage has such a strong influence on the build-up of the bottomhole pressure that the radial flow theory cannot predict the behavior. After this period, the bottomhole pressure rapidly increases with injection, and the radial flow dominates the leak-off behavior. One point which should be stressed is that during this period, the bottomhole pressure increases rapidly, which results in considerable compression of the fracture fluid and well deformation so that wellbore storage caused by them must be considered. Following this period, the bottomhole pressure deviates again from that predicted by the radial flow theory. This deviation is large. The radial flow model can predict pressure several megapascals higher than the true bottomhole pressure. One possible reason is that a fracture occurs in the formation, which contains fracture fluid, so that the bottomhole pressure is lower than that predicted. However, the observed oil penetration area does not support this explanation. The oil penetration area is basically a circle around the well. If the fluid enters into the fracture, the amount is also very small because the oil penetration area has not been affected. A more reasonable explanation may be the decrease of tangential effective stress during pumping, which leads to a rapid increase in the permeability. This increase in the permeability affects the behavior of bottomhole pressure in this phase. In fact, Roegiers [10] had produced experimental evidence which illustrates the increase in permeability with the decrease of effective stress.

The analysis clearly illustrates that the build-up of the bottomhole pressure is a complex process. Several factors strongly affect this process. One of them is the change of the permeability with effective stress around the well. This change makes the bottomhole pressure less than that predicted by the radial flow theory. The deviation is up to several megapascals near breakdown. Another important factor is the wellbore storage effect. This results in an initially complex behavior. To understand its effect on the bottomhole pressure, the monitoring of flow rate is necessary. Skin effect is another important factor. Several possible reasons for the skin effect are inexact well radius, damage caused by a high hydraulic gradient and application of stress, and so on. The radial flow model is capable of predicting the build-up of the bottomhole pressure after initial wellbore storage and before the large permeability change close to breakdown if the wellbore storage and the skin effect are considered.

5.3 Breakdown Pressure

5.3.1 Introduction

The breakdown is an important process in hydraulic fracturing. The breakdown pressure is regarded as a function of the state of stress. When a vertical fracture is induced, the maximum horizontal stress can be determined from the breakdown pressure if the minimum horizontal stress and the properties of rocks, such as the tensile strength or the fracture toughness, are known. On the other hand, breakdown is an complex process. The injection rate, the fracture fluid, the wellbore size, the state of stress, the properties of rocks, and the like have influences on this process. As a result, numerous breakdown models prevail. Although there exist many models, such as the classical breakdown model, the poroelastic model, the shear failure model, the point stress model, and the fracture mechanics model, none of these models are generally accepted because they cannot explain the observed breakdown phenomena. Therefore, the estimation of σ_{hmax} has least confidence, and the prediction of the breakdown pressure is still an open question [11-12].

Abnormally high breakdown pressures were observed in the single well hydraulic fracture tests reported in chapters 2 and 3. The statistical analysis revealed that the breakdown pressure is more straight related to σ_3 rather than $3\sigma_3 - \sigma_{hmax}$. These results offer an opportunity to test the various breakdown models. This section evaluates these models through experimental results and theoretical analysis.

5.3.2 Review of Breakdown Models

The first breakdown model was put forward by Hubbert and Willis [13]. It is often referred as the classic or conventional breakdown model. The model assumes that when the minimum tangential compressive stress in the wall of a well is equal to the tensile strength of the rock, a fracture is initiated, and breakdown occurs. Stress analysis is conducted under linear elastic conditions, and the rock is considered as an impermeable material. If there is no initial pore pressure in the rock, then the breakdown pressure is

$$p_b = 3\,\sigma_{hmin} - \sigma_{hmax} + \sigma_t \quad \text{.........} \quad 5.13$$

If there is an initial pore pressure in the rock, the breakdown equation is

$$p_b = 3\,\sigma_{hmin} - \sigma_{hmax} + \sigma_t - p_0 \quad \text{.........} \quad 5.14$$

where p_b is the breakdown pressure, σ_t is the tensile strength of the rock, p_0 is the initial pore pressure, and σ_{hmin} and σ_{hmax} is the minimum and maximum horizontal stress.

The tensile strength is usually considered as an extremely variable parameter. Therefore, it is often eliminated from the breakdown equation by the introduction of fracture reopening pressure. This concept was introduced by Bredehoeft et al. [14]. They stated that

> "During the first cycle of pumping into an initially intact interval of rock, the rock must be broken. In theory, the difference in breakdown pressure between the first and later cycles of pumping is equal to the tensile strength."

From this concept, the following breakdown equation is obtained

$$p_b\ (\sigma_t = 0) = 3\ \sigma_{hmin} - \sigma_{hmax} - p_0 \quad \text{..................................} 5.15$$

Usually, the peak bottomhole pressure in the second or third injection cycle is used as $p_b\ (\sigma_t = 0)$. This method was further improved by Hickman and Zoback [15]. They thought that $P_b\ (\sigma_t = 0)$ was the pressure at which the initial borehole pressurization rate in the later cycles deviated from that established in the first cycle prior to breakdown.

The second model is Haimson's model [1]. The same concept as the first model is accepted, i.e. when the minimum tangential effective stress in the wall of a well reaches the tensile strength of the rock, breakdown occurs. The difference between them is that the latter analyzes stress in the rock by Biot's poroelastic theory. The breakdown equation is

$$p_b = \frac{3\ \sigma_{hmin} - \sigma_{hmax} + \sigma_t - \alpha\ \frac{1-2\upsilon}{1-\upsilon}\ p_0}{2 - \alpha\ \frac{1-2\upsilon}{1-\upsilon}} \qquad \text{......................5.16}$$

where υ is Poisson's ratio, and α is Biot's poroelastic parameter. The tensile strength in the breakdown equation is the apparent tensile strength rather than the tensile strength from the Brazilian test or the direct tensile test.

Schmitt and Zoback [16] argued that the Terzaghi effective stress is inappropriate for low-porosity rocks. They thought that a modified effective stress law for tensile failure $\sigma' = \sigma - \beta\ p$, where $0 \le \beta \le 1$, may be more appropriate. After introduced this concept, they obtained the following breakdown equation:

$$p_b = \frac{3\ \sigma_{hmin} - \sigma_{hmax} + \sigma_t - \alpha\ \frac{1-2\upsilon}{1-\upsilon}\ p_0}{1 + \beta - \alpha\ \frac{1-2\upsilon}{1-\upsilon}} \qquad \text{......................5.17}$$

Another model is the fracture mechanics model [17-18]. The model assumes that breakdown occurs when a fracture starts unstable extension. Following this assumption, the breakdown equation is derived from $K_I = K_{Ic}$. The breakdown equation is

$$p_b = \frac{1}{h_0(L,r_w) + h_a(L,r_w)} \left[\frac{K_{Ic}}{\sqrt{r_w}} + \sigma_{hmax} f(L,r_w) + \sigma_{hmin} g(L,r_w)\right] \qquad \text{........5.18}$$

where L is the fracture length, r_w is the well radius, K_{Ic} is the fracture toughness, and h_0, h_a, g, and f are the function of the fracture length and the well radius.

Another interesting model is Ito's point stress model [3]. The model assumes that fracture initiation occurs when the minimum effective stress reaches the tensile strength of a rock at a point that is not on the wellbore surface, but is inside the rock. The distance between that point and the point of stress concentration is a material constant. Stress analysis was carried out by linear elastic stress analysis.

Shear failure criteria are also used to predicted the breakdown pressure [19-24]. This model assumes that when the stress in the wall of a well reaches the shear strength of rocks, breakdown occurs.

Before discussion, it is necessary to clarify the definition of the breakdown pressure again. In the following discussion, the breakdown pressure refers to the peak bottomhole pressure induced during injection of the fracture fluid.

In following paragraphs, the classical breakdown equation and the various methods related to the tensile strength are first evaluated. Subsequently, the poroelastic model, the shear failure model, the point stress model, and the fracture mechanics model are considered.

5.3.3 Tensile Strength and Classical Breakdown Model

Fracture Reopening Pressure: Bredehoeft et al. [14] first suggested that the tensile strength could be obtained from the recorded bottomhole pressure curve. The rock is intact during the first injection, so it must be broken, and the tensile strength must be overcome. A fracture exists in the borehole during the subsequent injection cycles, and the tensile strength is zero. From this assumption, they concluded that the difference between the first peak bottomhole pressure (p_{b1}) and the subsequent peak bottomhole pressure (p_{b2}, p_{b3}, and the like) is equal to the tensile strength.

Figures 5.7 and 5.8 shows the four bottomhole pressure curves from Tests 3, 5, 16, and 20. Table 5.1 presents the peak bottomhole pressure in various injection cycles and the tensile strength obtained from them. The experimental results are not consistent with the above conclusion. The first fact that contradicts Bredehoeft's conclusion is the decrease of the peak bottomhole pressure in various injection cycles with increase in cycle number (Figures 5.7 and 5.8). For example, p_{b2} is 13.41 MPa (1,945 psi), and p_{b3} is 8.70 MPa (1,262 psi) for Test 3 (Table 5.1). If p_{b2} is used as the fracture reopening pressure, then the tensile strength is 2.39 MPa (347 psi) (Table 5.1). If p_{b3} is used as the fracture reopening pressure, the tensile strength will be 7.10 MPa (1,030 psi) (Table 5.1). The second fact is that the tensile strength from the fracture reopening pressure will change with the stress applied on the specimen. Tests 3 and 5 have the same conditions except for the state of stresses. The tensile strength from them is completely different. When p_{b2} is used as the fracture reopening pressure, the tensile strength from Test 5 is 0.35 MPa (51 psi). It is much lower than 2.39 MPa (347 psi) from Test 3 (Table 5.1). A similar result is obtained when p_{b3} is used as the fracture reopening pressure. The other fact that contradicts Bredehoeft's conclusion is that the tensile strength from the fracture reopening pressure varies with injection rate. Test 20 has an injection rate of 3.186 cm^3/s, and Test 16 has an injection rate of 2.164 cm^3/s. The other conditions in both tests are similar. However, when p_{b2} is used as the fracture reopening pressure, the tensile strength from Test 20 is

1.84 MPa (267 psi), while that from Test 16 is 9.30 MPa (1,349 psi). A similar result is obtained when p_{b3} is used as the fracture reopening pressure. The above three facts illustrate that the concept of fracture reopening pressure is questionable. The tensile strength from this concept is too variable. It ranges from 0.35 to 11.75 MPa (51 to 1,704 psi), as illustrated in Table 5.1.

The improved method by Hickman and Zoback [15] cannot be checked because the single well hydraulic fracture tests were conducted in dry specimens. It is well-known that the build-up of the bottomhole pressure follows different mechanisms in dry and saturated formations. The experimental results in Figure 5.9 further prove this point. A dry cylindrical specimen (37.5 mm in diameter and 64.5 mm in length) was set up in a triaxial cell, and 1 MPa (145 psi) confining pressure was applied to the specimen. Then oil with 1000 mPa•s viscosity was pumped, at a constant rate of 0.111 cm^3/min, into the specimen from its bottom with its top maintained open (zero pressure). When the oil flowed out from the top of the specimen, the injection was stopped, and the pore pressure was released. After 12 hours, the injection was restarted. Figure 5.9 is the monitored pressure at the bottom of the specimen. The two completely different curves clearly prove the above conclusion. In the hydraulic fracture tests, the process is the same as the above test. In the first injection cycle, the specimen is dry, and the fracture fluid mainly fills the pores of the rock. It is similar to injection into a dry sample (the first injection cycle in the above). In the subsequent injection cycles, the pores in the formation have been filled partially or fully by fracture fluid, and the compression of the fracture fluid controls the build-up of the bottomhole pressure. The behavior of the build-up of the bottomhole pressure is more like that in the second injection cycle in the above test. Therefore, the comparison between the bottomhole pressure curves from the first and the subsequent injection cycles is meaningless. Although the method cannot be checked, this phenomenon reminds one that when the rock around a well is not saturated, the improved method should be applied with care.

Tensile Strength from Brazilian Test: There are several methods to determine the tensile strength such as the Brazilian test, the direct tensile tests, and the splitting tests. Because it is widely accepted in rock engineering and has a little requirements for equipment, the Brazilian tests were undertaken. The tensile strength from the Brazilian tests is also variable. It ranges from 0.156 to 0.343 MPa (23 to 50 psi). This scatter is so small that the tensile strength can be regarded as a parameter. In the following analysis, the tensile strength of Gypstone will be considered as 0.343 MPa (50 psi). The breakdown pressure predicted by this tensile strength and the classical breakdown equation is plotted in Figure 5.10 (bold dash line). The figure illustrates that the predicted value is too low and the classical breakdown equation and the tensile strength cannot predict the breakdown pressure obtained from the single well hydraulic fracturing program. Actually, this is not a new fact. The first set of the laboratory hydraulic fracture tests conducted by Scott et al. [25] had demonstrated the same conclusion. Their results are summarized in Table 5.2. There was one order of magnitude difference between the predicted and measured breakdown pressure.

Apparent Tensile Strength*: The apparent tensile strength was measured on two different specimens. One was a cylindrical specimen 140 mm (5.5") in diameter and 152.4 mm (6") in height, and the other ones were 305 x 305 x 305 mm (12" x 12" x 12") block specimens. The hydraulic fracture tests with stresses were conducted on block specimens of 305 x 305 x 305 mm (12" x 12" x 12"). The fracture fluid, the injection rate, and the well size in these specimens were the same as that in the hydraulic fracture tests. The apparent tensile strength is 1.68 MPa (244 psi) for the small cylindrical specimen and is 10.90 MPa (1,581 psi) for the large block specimen. The breakdown pressure predicted by the two apparent tensile strengths and the classical model is also shown in Figure 5.10. The breakdown pressure predicted by the apparent tensile strength from the small cylindrical specimen is still too low. That predicted by the apparent tensile strength from the large blocks is close to the experimental results. Hence, this figure illustrates that if the same specimen sizes are used for hydraulic fracturing and for the determination of the apparent tensile strength, the breakdown pressure is capable of being predicted approximately by the apparent tensile strength. This conclusion is similar to Haimson's [1]. However, it also reveals that the apparent tensile strength is dependent on specimen size, which indicates that the apparent tensile stress is not applicable for the interpretation of field hydraulic fracturing data.

---

* According to Haimson's concept, the apparent tensile strength is the tensile strength of the rock measured under conditions similar to those of hydraulic fracturing. The determination of it follows the procedure below. A well, with the same size as that in the hydraulic fracture tests, is drilled and sealed in a sample without stresses applied. Then, the same fluid as the fracture fluid is injected at the same rate as that in the hydraulic fracture tests into the well. The breakdown pressure induced is the apparent tensile strength.

Statistical Analysis: The breakdown pressure was plotted against the least principal stress σ_3, and that data were fitted by the linear least squares method. Unexpectedly, it was found that the breakdown pressure could be related to the least principal stress σ_3 rather than the minimum tangential compressive stress in the wall of a well, $3\sigma_3$ - σ_{hmax}, i.e. the relative coefficient for breakdown pressure versus σ_3 was higher than that for breakdown pressure versus $3\sigma_3$ - σ_{hmax}. If this is true, then the determination of σ_{hmax} from the breakdown pressure is questionable. Hence data from hydraulic fracture tests under true triaxial stresses were collected from hydraulic fracturing literature. The results are listed in Table 5.3. Table 5.3 illustrates that it is true under some conditions that the breakdown pressure is related to the least principal stress rather than the minimum tangential compressive stress in the wall of a well. Although this phenomenon has not been discovered before, it indeed exists. It appears to be associated with a high loading rate. As shown in Table 5.3, Haimson [1] used a low rate of pressurization; consequently, the breakdown pressure is related to $3\sigma_3$ - σ_{hmax}. Avasthi [26] employed a high rate of pressurization, the breakdown pressure is related to σ_3. Cheung et al. [27] used a constant rate in the tests. From the fracture fluid, the permeability of the rock, and the injection rate, a high rising rate in bottomhole pressure is also expected. Consequently, the breakdown pressure is related to σ_3. The highest rising rate in bottomhole pressure is up to 3 MPa/s (435 psi/sec) in our tests. Similarly, the breakdown pressure is related to σ_3. This phenomenon, like the tensile strength, challenges the classical breakdown equation or validity of the strength theory again.

In brief, the classical breakdown model cannot predict the breakdown pressure satisfactorily. The tensile strength from Brazilian tests predicts too low a breakdown pressure. The various improved methods have their limitations. The apparent tensile strength depends on specimen size, which limits its practical application. Bredehoeft's fracture reopening pressure gives an extremely variable tensile strength (0.35 to 11.75 MPa). In addition, they all cannot explain the phenomenon that the breakdown pressure can be related to σ_3 rather than $3\sigma_3 - \sigma_{hmax}$.

5.3.4 Pore Pressure Effect and Poroelastic Model

Fluid penetration into the rock is an important factor which complicates the breakdown process. Its effect can be assessed in terms of the governing equations and the boundary conditions. Fluid penetration will cause a change of the pore pressure in the formation. If the poroelastic effect is neglected and the effective stress law is accepted, the change of the pore pressure affects only the equilibrium and the boundary conditions. The change in the equilibrium equations and the boundary conditions can be illustrated by the axially symmetrical plane problem. The equilibrium equation for the axially symmetrical plane problem is

$$\frac{\partial \sigma_r}{\partial r} + \frac{\sigma_r - \sigma_\theta}{r} + F_r = 0 \quad \text{.....5.19}$$

where F_r is the radial body force. When the fracture fluid does not penetrate into the formation, the effective stress is equal to the total stress minus the initial pore pressure, i.e. $\sigma' = \sigma - p_0$. Because p_0 is constant, the equilibrium equation becomes

$$\frac{\partial\sigma'_r}{\partial r} + \frac{\sigma'_r - \sigma'_\theta}{r} + F_r = 0 \quad \text{.......} 5.20$$

It has the same form as equation 5.19. When the fracture fluid penetrates into the formation, the effective stress is still equal to the total stress minus the pore pressure, i.e. $\sigma' = \sigma - p(r,t)$. $p(r,t)$ is no longer constant, but changes with time and radial distance. The equilibrium equation becomes

$$\frac{\partial\sigma'_r}{\partial r} + \frac{\sigma'_r - \sigma'_\theta}{r} + F_r + \frac{\partial p(r,t)}{\partial r} = 0 \quad \text{.......} 5.21$$

In comparison with equation 5.20, a new term $\partial p(r,t)/\partial r$ is added into the equation. It is analogous to a body force.

Turning to the boundary conditions, when the fracture fluid does not penetrate, it is

$$\sigma'_r = p_w, \text{ at } r = r_w \quad \text{.......} 5.22$$

The infinite boundary condition has not been changed during injection so it is not considered here. When the fracture fluid penetrates into the formation, the radial total stress on the wall of a well is equal to the pore pressure, so the effective stress is always equal to zero, i.e.

$$\sigma'_r = 0, \text{ ar } r = r_W \quad \text{.......} 5.23$$

In comparison with boundary condition 5.22, the surface force acting on the wall of a well disappears. When the equilibrium equation and the boundary conditions are considered together, the fluid penetration transfers a surface force acting on the wall of a well, p_w, into a body force, $\partial p/\partial r$. The conclusion can be extended to 3-dimensional problems.

The effect of fluid penetration on the breakdown pressure is illustrated by the breakdown equation based on a poroelastic theory such as Haimson's equation [1], Medlin and Massé's [2] as well as Schmitt and Zoback's [16]. The consideration of fluid penetration reduces the breakdown pressure predicted. Therefore, fluid penetration and the poroelastic effect are not the reason for the high breakdown pressure found in the tests although they have a strong influence on the breakdown pressure.

5.3.5 Shear Failure Model

Some investigators [19-24] argued that a hydraulic fracture is induced by shear failure rather than tensile failure. Therefore, a shear failure criterion should be used.

It is necessary to study stress paths during hydraulic fracturing to evaluate this argument. The stress path on the wall of a well during hydraulic fracturing is shown in Figure 5.11. When a well is drilled, the stress redistributes in the rock around the well. The state of stress will move along the path a-b-c if the rock has yielded or along the path d-e if the rock has not yielded. When pumping, the stress will move along the σ'_θ axis because σ'_r is equal to zero. With pumping, the state of stress moves towards tension. When it reaches f, the rock fails. The state of stress at f is uniaxial tensile, so the failure is tensile. From the stress paths, it appears that shear failure is impossible if a fracture is initiated on the wall of a well.

If the strength envelope is replaced by a shear failure criterion, Point f usually moves to Point g due to the tensile cut-off (Figure 5.11). This simplification leads to an overestimation of the breakdown pressure. It may be of interest to check whether this overestimation can predict the high breakdown pressure mathematically. For Gypstone, the tensile strength ranges from 113 to 343 kPa (the value at f), the value deduced from the shear strength is 300 kPa (the value at g). They are of the same order. If the tensile failure criterion cannot predict the observed high breakdown pressure, the shear failure criterion is not better.

The above analysis illustrates that if a failure starts from the wellbore, shear failure seems impossible. However, there are two extreme cases to contradict the above analysis. It is of interest to evaluate whether they lead to shear failure or to a high breakdown pressure. One case is impermeable rocks or non-penetrating fluid. The radial effective stress at the wellbore is equal to the bottomhole pressure. The stress should follow the path in Figure 5.12. The stress changes along the path a-b-c-f for the yielded rock before injection, and along the path d-e-d-f' for the non-yielded rock before injection. If the tensile failure criterion is used for these cases, f is replaced by g, and f' by g'. The application of the tensile failure criterion results in a higher value. The failure mode may still be tensile because the rocks usually fail by cleavage under uniaxial load when the loading rate is high. The other case is that the injection rate is so low or the rock is so permeable that the pore pressure develops almost uniformly in the formation. It is similar to a decrease of σ_{hmax} and σ_{hmin} in the same increment. Failure will not occur at the wellbore but in the formation in shear if there is an adequate stress difference. When this happens, the breakdown pressure is low, lower than σ_{hmin}. This has been shown experimentally by Solberg and Lockner et al.[28-29]. Therefore, these two extreme cases also cannot predict a high breakdown pressure.

5.3.6 Nonlinear (softening) and Point Stress Model

Boone and Ingraffea [30] thought that when the stress in the rock reaches the tensile strength, the rock does not collapse, i.e. a true crack (no capacity to carry the load) does not occur. Instead the rock starts strain-softening. When the strain-softening zone develops to some extent, the stress decreases to zero, and a true crack is induced (Figure 5.13). One advantage of this concept is that it provides a promising explanation for well size effects. As Ingraffea illustrated [31], the development of displacement in the strain-softening zone requires a large rise in load for a small wellbore, and requires little rise in load for a large wellbore. Hence, for a small wellbore, inducing a true crack requires a much higher load than inducing a stress equal to the tensile strength; while for a large wellbore, the load inducing a true crack is similar to the load inducing a stress equal to the tensile strength. However, this concept must overcome two problems if it is to be used to explain the high breakdown pressure. One problem is when breakdown occurs. The other problem is whether strain-softening under tensile load is apparent for hydraulic fracturing. The strain-softening zone under tensile load is observed in a displacement controlled test. For hydraulic fracturing, the loading rate before breakdown is usually high whether fracturing is at a constant injection rate or at a constant rate of pressurization, especially for extremely high breakdown pressures. Rock mechanics experience strongly indicates that a high loading rate leads to little strain-softening.

Although it had not been stated, Ito and Hayashi's breakdown equation [3] used the same concept as Boone and Ingraffea's. When strain-softening happens, the stress will redistribute. The peak of the tangential stress will move towards the formation. When the peak moves to the distance d, i.e. $r = r_w + d$, the stress at the wellbore decreases to zero, and a true crack occurs. Ito and Hayashi thought that the breakdown occurs at this moment. The value of d was measured experimentally, and the stress field was analyzed by linear elastic theory. A breakdown equation was established. Ito and Hayashi reported that the breakdown pressure observed is identical with that predicted by the above equation. Although the breakdown pressure was used, the breakdown pressure did not refer to the peak bottomhole pressure during pumping. Their experiments were conducted at a constant rate of pressurization. The breakdown pressure refers to the pressure where the injection rate rises abruptly or the accumulated AE energy increases abruptly. This pressure usually indicates fracture initiation, and is much lower than the breakdown pressure for a high injection rate and viscous fracture fluid [32]. Therefore, although strain-softening has some influence on the breakdown pressure, it is not the reason for the high breakdown pressure.

5.3.7 Stable Fracture Propagation and Fracture Mechanics Model

The most promising explanation is the fracture mechanics model. In the existing fracturing mechanics model for breakdown pressure, a commonly accepted concept is that when $K_I = K_{Ic}$, the fracture starts unstable propagation [17-18, and 32]. Breakdown corresponds to the onset of this unstable fracture propagation. The analysis procedure is as follows. A fracture length and the fluid pressure distribution in the fracture are assumed, and then the fracture criterion, $K_I = K_{Ic}$, is applied to obtain the expression for breakdown pressure. Finally, fracture length is regarded as a material parameter [18, 33]. Before the feasibility of this model is evaluated, it is necessary to check the above concept.

First of all, the concept of unstable fracture propagation should be clarified. There are two aspects for unstable fracture propagation. The first refers to the phenomenon that the fracture is propagating with decline of the load. Propagation may require new energy input to drive fracture extension. This is the concept used in the following discussion. The other refers to the phenomenon that the fracture is propagating without energy input into the system. A rock-burst is one example.

The bottomhole pressure increases before breakdown, which indicates that the fracture is not propagating or is propagating stably. The bottomhole pressure decreases after the breakdown, which indicates that the fracture is propagating unstably. Therefore, the breakdown pressure is the onset of the unstable fracture propagation. This is identical with the assumption in the fracture mechanics model. Hence, attention is only paid to the criterion for unstable fracture propagation. When $K_I = K_{Ic}$, the fracture starts propagating unstably. This is a concept from opening mode or mode I in linear elastic fracture mechanics. The typical opening mode is a line crack under a uniform tensile stress perpendicular to the crack line.

The stress intensity factor is $K_I = \sigma\sqrt{L}$. K_I increases with the fracture length so the fracture propagates unstably once $K_I = K_{Ic}$. This is the source of the above concept. Actually, $K_I = K_{Ic}$ is not a criterion for unstable fracture propagation but a criterion for fracture growth. When $K_I = K_{Ic}$, a fracture does not need propagating unstably. It may first propagate stably, then extend unstably when the fracture extends to some length. One good example is that the loading distribution changes with fracture extension. This can be demonstrated by considering a case with a uniform load p acting on part of a fracture, L_0. The stress intensity factor for this problem is

$$K_I = \frac{2}{\pi} p \sqrt{L} \sin^{-1}\left(\frac{L_0}{L}\right) \quad \text{5.24}$$

When L_0/L is small,

$$K_I = \frac{2}{\pi} p \frac{L_0}{\sqrt{L}} \quad \text{5.25}$$

K_I decreases with an increase of the fracture length. If the fracture toughness is constant, the fracture propagation is stable when $K_I = K_{Ic}$. This indicates that the pressure must be increased if the fracture is to be extended. When L_0/L is unity, the stress intensity factor becomes

$$K_I = p\sqrt{L} \quad \text{5.26}$$

It increases with a fracture lengthening. When $K_I = K_{Ic}$, a fracture propagates unstably. If L_0/L increases with fracture extension, a fracture will firstly propagate stably, and then it will propagate unstably when L_0/L reaches some value. This example indicates that $K_I = K_{Ic}$ is the criterion for fracture growth. It is not the criterion for unstable fracture propagation. The completion criterion, as stated by Gdoutos [34], should be

$$K_I - K_{Ic} = 0, \quad \text{...} 5.27\ a$$

and

$$\frac{\partial(K_I - K_{Ic})}{\partial L} \geq 0 \quad \text{.................................} 5.27\ b$$

The introduction of equation 5.27 b makes it possible to explain the high breakdown pressure using fracture mechanics criterion. Theoretically, when $K_I = K_{Ic}$, a fracture starts propagating. When $K_I = K_{Ic}$ and $\partial(K_I - K_{Ic})/\partial L \geq 0$, a fracture propagates unstably. Between them, a fracture propagates stably. The load must be increased to extend the fracture in this period. Therefore, a large difference can occur between the load at which the fracture starts propagating and the load at which the fracture propagates unstably. For hydraulic fracturing, the former load corresponds to fracture initiation, and the latter corresponds to the breakdown pressure. Therefore, this criterion is able to explain the large difference between the fracture initiation pressure and the breakdown pressure, in other words, the high breakdown pressure.

The experimental observations supply the evidence for this explanation. One proof is the stable fracture propagation observed before breakdown. Zoback's [32] and Majer's [35] experiments both demonstrated that the fracture is initiated before breakdown. Following the fracture initiation, the bottomhole pressure increases continuously. The fracture propagates stably. The hydraulic fracture tests reported in chapter 3. present further evidence. The oil penetration area is a circle before breakdown, which indicates that the fracture fluid leaks off radially. When the fracture fluid leaks off radially, the load exerted by it is also radial, and decays rapidly with the distance away from the wellbore. This indicates that the load is concentrated on the area around the well. This pressure distribution is identical to that for stable fracture propagation. After breakdown, the linear flow along the fracture dominates the flow of the fracture fluid, which applies a more uniform pressure in the fracture. Consequently, the fracture propagates unstably.

This explanation is identical with the fact that a high breakdown pressure occurs with a viscous fracture fluid and a high injection rate. When the flow is radial, the viscous fracture fluid will limit the penetration depth of the fracture fluid. Hence the load exerted by the fluid injection concentrates at the wellbore. For a narrow fracture just initiated, the viscous fracture fluid limits the entrance of the fracture fluid into the fracture, so the load is limited again at the wellbore. All these actions prefer the occurrence of stable fracture propagation. Hence, the bottomhole pressure must be raised to force the fracture fluid to enter the fracture and to propagate the fracture unstably. The extreme case is the pressuremeter, where the fluid cannot enter the rock and the fracture so that there is no visible breakdown. Similarly, a high injection rate also raises the breakdown pressure.

This explanation is also consistent with the phenomenon that the breakdown pressure is dependent on σ_3 rather than $3\sigma_3 - \sigma_{hmax}$ under some conditions. The stress intensity factor K_I, as stated by Rummel [18], can be formulated using the principal of superposition of stress intensity factors from each loading source: σ_3, σ_{hmax}, and the pressure in the well and the fracture. From Rummel's formulas for $K_I(\sigma_3)$ and $K_I(\sigma_{hmax})$, it can be found that $K_I(\sigma_3)/K_I(\sigma_{hmax})$ increases rapidly with fracture length. For example, when L/r_w is 1.3, $K_I(\sigma_3)/K_I(\sigma_{hmax})$ is as high as 165. When L/r_w is up to 2.0, $K_I(\sigma_3)/K_I(\sigma_{hmax})$ is as high as 258. The contribution of σ_{hmax} to K_I is negligible if the fracture has a considerable length. The fracture has indeed a considerable length at breakdown. The stable fracture propagation has driven the fracture to some length, which depends on the viscosity of the fracture fluid, the injection rate, and the rock properties. Therefore, K_I is controlled by σ_3 and the pressure in the well and the fracture. This is why the breakdown pressure is related to σ_3 rather than 3 $\sigma_3 - \sigma_{hmax}$ under some conditions.

The size effect is another important phenomenon observed for the breakdown pressure [1, 12, and 33]. It can easily be explained by the above concept. The size effect of the breakdown pressure usually is described as the effect of borehole size. Exactly speaking, this size effect is also caused by the fracture size. If size effect is only caused by the borehole size, then after a fracture extends away from wellbore the fracture pressure should go back to the least principal stress. In fact, in the second and subsequent injection cycles, the peak bottomhole pressure is far higher than the least principal stress. In addition, the decline of the peak bottomhole pressure in the subsequent injection cycles with the number of cycles also suggests that the size effect of the breakdown pressure is also caused by the fracture size. The fracture mechanics explanation for this size effect is as follows. When the fracture length is short, the fracture width, w, is also narrow according to Sneddon's solution for uniform load [36]. The pressure gradient is proportional to $1/w^3$. Therefore, the pressure distribution is not uniform for a short fracture. As a result, a high bottomhole pressure is required to open the fracture and form a uniform pressure distribution, which drives the fracture to propagate unstably. For a long fracture, the fracture width is wider. A small pressure gradient exists in the fracture. Hence, the pressure distribution in the fracture is more uniform Consequently, a lower breakdown pressure is required to drive the fracture to propagate unstably. For small wellbore sizes, the crack opening displacement at a well is small and develops slowly, as illustrated by Ingraffea [31]. It limits the entrance of the fracture fluid into the fracture. Hence a high bottomhole pressure is required to form a pressure distribution which prefers an unstable fracture propagation. For large wellbore sizes, the crack opening displacement at a well is large and develops rapidly. The fracture fluid enters into the fracture just after the fracture is initiated. Hence, the breakdown pressure is low.

The above analysis shows that the fracture mechanics model is a promising model. The stable fracture propagation may be the reason for high breakdown pressures. After the fracture is initiated, the high viscosity of the fracture fluid, the high injection rate, or low fracture opening displacement caused by a short fracture or a small wellbore radius restricts the fracture fluid entering the fracture. A concentrated pressure is produced around the wellbore. That results in the stable fracture propagation.

5.3.8 Conclusions

The breakdown pressure is an interesting parameter for hydraulic fracturing stress measurements. It is thought that the maximum horizontal stress can be calculated from the breakdown pressure, the least principal stress, and the properties of the rocks. On the other hand, the breakdown is a complex process. The breakdown pressure is rate-dependent, size-dependent, fracture fluid-dependent, and σ_3-dependent. As a result, many breakdown models prevail. This section evaluates the various models experimentally and theoretically. From the analysis, the following conclusions are drawn.

The classical breakdown model cannot predict the breakdown pressure satisfactorily. The tensile strength from Brazilian tests predicts too low a breakdown pressure. The various improved methods have their own limitation. The apparent tensile strength depends on specimen size, which limits its practical application. Bredehoeft's fracture reopening pressure gives an extremely variable tensile strength (0.35 to 11.75 MPa). In addition, they all cannot explain the phenomenon that the breakdown pressure can be related to σ_3 rather than $3\sigma_3 - \sigma_{hmax}$ under some conditions such as a high rate of pressurization or a high injection rate.

The effect of fluid penetration complicated the explanation of fracturing process. The fluid penetration changes the pore pressure in the formation. This change in the pore pressure is equivalent to transferring a surface load acting on the wall of a well and the fracture into a distributing body force $\partial p/\partial r$. The effect of it on the breakdown pressure is illustrated by the breakdown equation based on the poroelastic theory. The breakdown pressure is decreased. Shear failure is possible when the injection rate and the viscosity of the fracture fluid are so low that the pore pressure increase in the formation is almost uniform. Shear failure also results in a low breakdown pressure. Ito's point stress model predicts the fracture initiation pressure, not the breakdown pressure. All these models cannot explain the abnormally high breakdown pressure.

The fracture mechanics model is a promising model. The bottomhole pressure increases before breakdown, which indicates that the fracture is propagating stably. The bottomhole pressure decreases after breakdown, which indicates that the fracture is propagating unstably. Therefore, the breakdown pressure is the onset of the unstable fracture propagation. This is identical with the assumption in the fracture mechanics model. It should be stressed that fracture criterion for the unstable fracture propagation is $K_I - K_{Ic} = 0$ and $\partial(K_I - K_{Ic})/\partial L \geq 0$, not only $K_I - K_{Ic} = 0$. Introduction of $\partial(K_I - K_{Ic})/\partial L \geq 0$ makes it possible to explain the several phenomena such as rate-dependent, size-dependent, fracture fluid-dependent, and σ_3-dependent responses and the high breakdown pressure.

5.4 Fracture Pressure Analysis

5.4.1 Introduction

The change in bottomhole pressure during injection reflects the manner in which the fracture is propagating. Hence, fracture pressure analysis provides a powerful tool to determine the manner in which a fracture is developing. The basic principles and application are analogous to those for the pressure analysis of transient fluid flow in the reservoir. Both provide a means to interpret complex phenomena occurring underground by the pressure resulting from fluid movement in rock formations. The difference is that fracture pressure analysis involves the process of fracture propagation. Therefore, fracture mechanics, fluid mechanics, and flow in porous media must be incorporated.

Fracture pressure analysis is based on three 2D-hydraulic fracturing models: the PKN, the GdK, and the radial models [37-41]. The PKN model has the following assumptions [37, 42-46] .

1. The fracture is a rectangle with a fixed height, independent of fracture length.

2. The fluid pressure in the fracture is constant in vertical cross section perpendicular to the direction of propagation.

3. Deformation of reservoir rock prevails in the vertical plane. In other words, each vertical cross section deforms individually and is not hindered by its neighbors.

4. Rock compliance is obtained by England and Green's solution for a line plane-strain crack.

5. The fluid pressure gradient in the fracture during the propagation is determined by the flow resistance in a narrow, elliptical flow channel.

6. The fluid pressure in the fracture falls off toward the tip such that $p = \sigma_3$ at the tip for unspecified reasons.

7. Fracture fluid is injected at a constant rate.

The solutions for the fracture length, the fracture width, and the bottomhole pressure are obtained by incorporating these assumptions with the mass conservation equation, boundary conditions, and initial conditions. The model predicts an exponential rise in the bottomhole pressure with increase of the fracture length or the injection time [37], that is

$$\Delta p \propto t^m \qquad \frac{1}{4(n+1)} \le m \le \frac{1}{2n+3}$$

where Δp is the fracture pressure equal to the bottomhole pressure minus the fracture closure pressure, p_c ($p_c = \sigma_3$ for a uniform stress field), and n is the power-law exponent for the fracture fluid. n ranges usually from 0.5 to 1 and is equal to 1 for a Newtonian fluid. Therefore, m ranges from 0.125 to 0.25.

The GdK model [37, 42-44, 47-48] uses the following assumptions:

1. The fracture is a rectangle with a fixed height, independent of fracture length.

2. The fluid pressure in the fracture and the fracture width are constant in vertical cross section perpendicular to the direction of propagation.

3. Rock stiffness is taken into account in the horizontal plane. In other words, each horizontal cross section deforms individually and is not hindered by its neighbors.

4. Rock compliance is obtained by England and Green's solution for a line plane strain crack. However, it is applied in a horizontal plane unlike the PKN model.

5. The fluid pressure gradient in the fracture during the propagation is determined by the flow resistance in a narrow rectangular slit of variable width in the vertical direction.

6. Barenblatt's equilibrium condition is applied.

$$\int_{x=0}^{L} \frac{p(x,t)}{\sqrt{L^2-x^2}}\,dx = \frac{\pi}{2}\sigma_3 + \frac{\pi K_{Ic}}{2\sqrt{L}} \quad \text{.......................................5.28}$$

7. Fracture fluid is injected at a constant rate.

The solutions for the fracture length, the fracture width, and the bottomhole pressure are obtained by incorporating these assumptions with the mass conservation equation, boundary conditions, and initial conditions. The model predicts a decline in the bottomhole pressure with an increase of the fracture length or the injection time [37], that is

$$\Delta p \propto t^m \qquad\qquad \frac{-n}{2(n+1)} \geq m \geq \frac{-n}{n+2}$$

where Δp is the fracture pressure equal to the bottomhole pressure minus the fracture closure pressure, n is the power-law exponent for the fluid. Therefore, m usually ranges from -0.3 to -0.167.

There are three types of radial models [37, 45, 48]. Common to them is that all three models assume that the fracture propagates radially, and Sneddon's solution for a penny-shape crack under an arbitrary distribution pressure is used for fracture compliance. The PKN model assumes that the fluid pressure in the fracture reduces logarithmically from the bottomhole pressure at the wellbore to σ_3 at the tip of the fracture. The GdK model also assumes that the fluid pressure in the fracture decreases logarithmically. The pressure reduces to zero at some r, a value close to the fracture length. Barenblatt's equilibrium condition is applied. The model predicts that the bottomhole pressure reduces with an increase of the fracture length. Nolte simplifies the fluid pressure distribution in a fracture. The pressure reduces exponentially is accepted in his model. From this assumption, The relationship [37]

$$\Delta p \propto t^{-m} \qquad \frac{-3n}{8(n+1)} \geq m \geq \frac{-n}{n+2}$$

is obtained again, and m ranges from -0.3 to -0.125.

The more appropriate of these 2D models is the one for which the physical dimensions of the fracture more closely represent the assumptions of the 2D fracture. As indicated by Perkins [49], Geertsma and Haafkens [50], the GdK model is more appropriate when the fracture length is smaller than the height, while the PKN model is more appropriate when the fracture length is much larger than the height. The radial model is most appropriate when the total length is approximately equal to the height. These conditions occur for fracture propagation from a point source of injection, as the case for a horizontal fracture, or as an intermediate condition between the two limiting cases of 2D models.

All three models predict an exponential change in the fracture pressure. Hence, they should be straight lines with slopes equal to m in the plot of log (p_w-p_c) vs log t,. This notion forms a basis for fracture pressure analysis, and is analogous to the log-log diagnostic plot for reservoir flow. In brief, fracture pressure analysis is based on three 2D models. It is conducted in a plot of log (p_w-p_c) vs log t. By comparing the slope in the plot with m in models, the fracture propagation mode is identified. m ranges from 0.125 to 0.25 for the PKN model, from -0.3 to -0.167 for the GdK model, and from -0.3 to -0.125 for the radial model.

5.4.2 Behavior of Fracture Pressure

Five representative experimental results (Tests 3, 9, 16, 19, and 22) are analyzed. The results are shown in Figures 5.14 to 5.18. The analysis indicates that the behavior of the fracture pressure may be divided into five regions. Region I has a positive slope in the plot of log (p_w-σ_3)) vs log t. It occurs before breakdown. Region II has a zero slope. It follows Region I or occurs in the last injection cycle. Region III is a region where the slope is negative, and its absolute value is far larger than the value predicted by the models. Region IV is a region where the slope is negative and falls in the range predicted by the GdK and the radial models. In region V the slope is negative but its absolute value is far less than that predicted by the models. Fracture pressure declines after breakdown. The fracture seems to propagate in the manner described by the GdK model or the radial models. This result is identical with Biot and Medlin's [51-52] and Rubin's [53] experimental findings.

The behavior of the fracture pressure is dependent on testing conditions such as the injection rate and the least principal stress. Test 3 (Figure 5.14) has a low σ_3. After the initial positive slope (Region I), as shown by Figure 5.14, a rapid decline (Region III) occurs frequently, and it often occurs alternatively with a positive or zero slope (Regions I and

II). The slope between the range predicted by the models (Region IV) occurs occasionally. In comparison with Test 3, Test 9 (Figure 5.15) has the same testing conditions except a high σ_3. After the initial positive slope and following the zero slope, the slope falls in the range predicted by the models. A rapid decline (Region III) occurs occasionally. Finally, at injection cycle 7, the slope maintains at zero after the initial positive slope.

Test 16 (Figure 5.16) has a low injection rate. After the initial positive slope and following the zero slope, the fracture pressure starts to decline. However, the slope is beyond the range predicted by the GdK and the radial models. At the last three injection cycles, the decline disappears and the slope maintains at zero after the initial positive slope. Tests 19 and 22 (Figures 5.17 and 5.18) have similar test conditions to Test 16 except a high injection rate. The behavior of the fracture pressure is different. After the initial positive slope and following the zero slope, a rapid decline (Region III) occurs. After that, the slope decreases and falls in the range predicted by the GdK and the radial models.

In brief, the experimental results demonstrate the following behavior of the fracture pressure. The initial positive slope appears in each test whether the least principal stress and the injection rate are high or low. Following that, a zero slope occurs. For the low least principal stress and high injection rate, this region is short or just a point as in Test 3. The decline of the fracture pressure will start after this zero slope. When the least principal stress is low, and the injection rate is high; a rapid decline will appear (Test 22), or it appears alternatively with a positive or zero slope (Test 3). When the injection rate is extremely low, the decline may be so slow that it is beyond the range predicted by the GdK and the radial models (Test 16). When a high least principal stress is applied, the slope will decrease. It falls in the range predicted by the models (Test 9). Finally, the zero slope usually is maintained (Tests 16 and 9).

5.4.3 Discussion

Region I–the positive slope: In all the tests, the positive slope appears first. Nolte explained this initial positive slope. He stated [37],

> "The increasing net pressure during the first 2 hours of the treatment indicates that the PK model..., for a confined-height fracture in the vertical plane, is the most applicable basic model. This is the only model that predicts increasing pressure with increasing penetration; ..."

where the net pressure means the fracture pressure (p_w-p_c), and the PK model refers to the PKN model. Nolte thought that in this region the fracture propagates according to conditions prescribed by the PKN models. This explanation is questionable. It is well-known that the PKN model requires that the fracture length is far larger than the fracture height. Only when this condition is satisfied, is the assumption that each vertical cross section deforms individually and is not hindered by its neighbors acceptable. However, the above assumption is unacceptable when a vertical fracture is just initiated from a well and the fracture is still short. Instead, the GdK model seems to be the acceptable model for this condition. Unfortunately, the existing solution for the GdK model predicts a decrease in the fracture pressure with injection time. All the models fail to predict the behavior in this region.

It is of interest to understand the mechanism of this positive slope. The GdK model has the best assumption with regard to fracture dimensions in this region. The fracture pressure in this region increases with injection time. The fracture propagates stably. Therefore, a fracture criterion must be used to predict the fracture length. The GdK Model employs Barenblatt's equilibrium condition (Equation 5.28) as the fracture criterion, which is equivalent to $K_I = K_{Ic}$ if K, Barenblatt's cohesion, is replaced by fracture toughness K_{Ic} times a constant $\sqrt{2}/\pi$. If the assumption of the fluid pressure in the fracture by Geertsma [48], $p(x,t) = p(t)$ for $0 < x < L_0$, and $p = 0$ for $L_0 < x < L$, is accepted, then the fracture criterion becomes the following expression.

$$p(t) = \frac{1}{\sin^{-1}\frac{L_0}{L}} \frac{\pi}{2} (\sigma_3 + \frac{K_{Ic}}{\sqrt{L}}) \quad \text{..........} 5.29$$

When $L_0/L << 1$, $\sin^{-1}\frac{L_0}{L}$ can approximately be replaced by L_0/L. Then,

$$p(t) = \frac{L}{L_0} \frac{\pi}{2} (\sigma_3 + \frac{K_{Ic}}{\sqrt{L}}) \quad \text{..........} 5.30$$

This expression predicts that the fracture pressure increases with fracture extension. The fracture length will increase or does not change with injection time. Hence, this expression also indicates that the fracture pressure will increase with the injection time, i.e. the slope should be positive in the plot of log $(p_w - p_c)$ vs log t.

$L_0/L << 1$ is also possible in practice. The experimental results reported in Chapter 3 showed that the radial leak-off controls the flow mode of the fracture fluid, and the fracture is narrow and long before breakdown, i.e. in this region. When the flow is radial, the corresponding load is also radial, and decays rapidly with radial distance. $\partial P/\partial r$ is proportional to $1/w^3$, where w is the fracture width. The fluid pressure also decays rapidly with radial distance in a narrow fracture. These two facts prefer that the fluid pressure in the fracture decays rapidly with distance from the well. This implies that L_0 is small. Therefore, L_0/L is also small with fracture extension.

The above analysis clearly indicates that the initial increase in the fracture pressure may result from the fluid pressure distribution in a fracture. The fluid pressure assumption in the GdK model is not appropriate in this region so the model cannot predict the behavior of the fracture pressure in this region. The concept that only the PKN model can predict the positive slope should be corrected. The GdK model can also predict a positive slope in the plot of log (p_w-p_c) vs log t, provided that there is a proper fluid pressure distribution in the fracture. This indicates that the fluid pressure distribution in the fracture is extremely important for the response of the bottomhole pressure.

Region II–the zero slope: There are two kinds of zero slope: one follows an initial positive slope, and the other one occurs at the end of testing. Although both regions have a zero slope, the mechanism is completely different. This part discusses the first.

The above explanation can be extended to explain this zero slope. The case for a small L_0/L has been reviewed. The fracture criterion requires that the fracture pressure increases with time. However, fracture width will increase with the fracture length and the injection time. Consequently, the fracture fluid will enter the fracture, and L_0/L will increase. Considering an extreme case, $L_0/L=1$, then Barenblatt's equilibrium condition becomes

$$p(t) - \sigma_3 = \frac{K_{Ic}}{\sqrt{L}} \quad \ldots\ldots 5.31$$

Fracture propagation is unstable and the fracture pressure will decrease with the fracture length and the injection time. Between these two cases, there should be a value of L_0/L, where the fracture pressure will be independent of the fracture length and the injection time, and fracture propagation changes from stable to unstable. This appears to be the reason for a zero slope following the initial positive slope.

Region III–the rapid decline: The possible reason for this rapid decline is rapid fracture extension. Fracture extension is so rapid that the rate of the increase in fracture volume surpasses the rate of the fluid injection.

In this region, the fracture pressure declines with injection time. The fracture is propagating unstably. When a fracture propagates stably, the fracture criterion must be satisfied, and the fracture geometry is dominated by the fracture criterion. However, when it propagates unstably, the fracture criterion must still be satisfied, but it no longer controls the fracture geometry. This is because once the fracture criterion is satisfied the fracture will extend continuously if the load distribution maintains constant. An alternative for the fracture criterion is the mass conservation. Through the mass conservation equation, a balance is obtained among the rate of increase in the fracture volume, the leak-off rate, and the injection rate. However, when a fracture propagates so rapidly that the rate of increase of the fracture volume surpasses the injection rate, the balance is not maintained. The fracture fluid cannot fill the whole fracture space. The restriction on the fracture fluid disappears. Consequently, the pressure in the fracture will fall rapidly. Before breakdown, the fracture is narrow, which restricts the entrance of the fracture fluid so that an high pressure is built-up when a high viscosity oil or a high injection rate is used. At breakdown, the fracture width increase leads to entrance of the fracture fluid, which results in a high pressure region in the fracture. When the least principal stress is low, this high pressure may produce an extremely high rate of increase in fracture volume. This is perhaps the reason for the rapid decline in the fracture pressure.

An experimental observation reported in Chapter 3 gives further evidence for this explanation. Test 8 was a test without stresses. The fracture extended over the whole specimen in only a few seconds. Corresponding to this process, the bottomhole pressure dropped to zero in a few seconds (a rapid decline). Observation of oil penetration after testing showed that the fracture fluid only penetrated part of the fracture (the fracture fluid could not fill the whole fracture space). This clearly illustrates that when a rapid decline occurs, the fluid front cannot catch up the fracture front, i.e. the rate of increase of the fracture volume is more than the rate of the fluid injection.

Region IV–the slope between the range predicted by the model. In this region, the assumptions in the models may be satisfied so an identical slope is obtained.

Region V–the slow decline: In this region, the fracture pressure declines slowly. The slope is far higher than the range predicted by the models. The possible reason for this slow decline is the leak-off behavior used by the models. The upper bound for the slope is given by zero fracture efficiency. Hence, this explanation also can be illustrated by an analysis for zero fracture efficiency.

A zero fracture efficiency means that all the fracture fluid injected is leaked off. Under this assumption, the mass conservation equation become

$$q_f = q_i - q_l = q_i - 2hC \int_{x=0}^{x} \frac{dx}{\sqrt{t-\tau(x)}} \quad \text{..................................} 5.32$$

where q_f is the flow rate through the fracture, q_i is injection rate, q_l is leak-off rate, C is the leak-off coefficient, and h is the height of injection segment or the depth of wells. From this equation and the condition $q_f(L,t) = 0$, the solution, $L \propto t^{0.5}$ is obtained [46]. It is of interest to note that although all the fracture fluid leaks off into the formation, the fracture still extends at a rate. This seems a paradox. In fact, it results from the assumption of the leak-off behavior. In the above mass conservation equation, the rate of leak-off per unit area is assumed equal to

$$\frac{C}{\sqrt{t}} \quad \text{..} 5.33$$

When a fracture fluid is injected into a unit area at a rate q_i, the injection volume is $q_i t$. However, the amount of leak-off is only $2C\sqrt{t}$. Equilibrium cannot be obtained, and the area must increase to balance the injection amount. Similarly, when injecting into a fracture, the fracture area must increase to balance the injection amount. This is the physical background for the solution of $L \propto t^{0.5}$.

When there is no filtercake on the wall of a fracture, the flow theory in porous media will play a main role. The total leak-off rate from a fracture is adjusted by two factors: pressure gradient and area. When the fracture area reaches some value, the rate of leak-off will be equal to the injection rate. The pressure in the fracture cannot be increased. Consequently, the fracture is contained. Therefore, the upper limit for the rate of decline in the fracture pressure should be zero.

The above analysis illustrates that the leak-off model used in the 2D models is not identical with what happens in testing. Hence, the experimental results cannot be predicted. It also provides a rationale for the zero slope at the end of testing.

5.4.4 Conclusions

The analysis of the five experimental results shows that the fracture pressure declines after breakdown. The GdK or the radial models gives a more appropriate prediction for the fracture pressure than the PKN model. This is identical with Biot and Medlin's, and Robin's experimental results [51-53].

Many assumptions are introduced in the 2D models and the fracture pressure analysis to obtain closed-form solutions. These assumptions limit the applicable scope of the models. One of them is the leak-off model. The leak-off model used assumes that leak-off velocity is equal to $C/\sqrt{t}$, where C, a constant, is called the leak-off coefficient. It is not related to the pressure or hydraulic gradient, the viscosity of the fracture fluid, or the permeability of the formation. One important concept from this assumption is that a fracture will continuously propagate provided that the fracture fluid is injected continuously. This is unacceptable. The applicability of this model should be limited to the case where a filtercake is formed. Darcy's law may be a more acceptable model for most fracture fluids.

The second assumption that limits the models is the mass conservation equation. The mass conservation equation in the hydraulic fracturing models assumes that the injection rate is equal to the rate of leak-off plus the rate of change in fracture volume. It implies that the fracture fluid fills all the fracture space. As the experimental results illustrated, the fracture fluid does not always fill the whole fracture space, especially in the region just after breakdown pressure for a high injection rate and a low least principal stress. When this phenomenon happens, the fracture pressure usually declines at a higher rate than that predicted by the models.

Another assumption that limits the applicable scope of the models is the fluid pressure distribution in a fracture. The assumption of the pressure distribution in a fracture is based on the fact that the fracture fluid flows along the fracture. As reported in Chapter 3, this is true after breakdown. However, the fracture fluid leaks off into the formation radially before breakdown. Therefore, the conclusion from this assumption is limited to post breakdown, i.e. the models are applicable for post breakdown. It should also be pointed out that the decline or increase of the fracture pressure with fracture extension, to a large extent, depends on the fluid pressure distribution in a fracture. When the fluid pressure in a fracture results in stable fracture propagation, the fracture pressure will increase with fracture extension. If the fluid pressure in a fracture results in unstable fracture propagation, the fracture pressure will decline with fracture extension.

The other points which should be stressed are the fracture criterion (Barenblatt's equilibrium condition) and the mass conservation equation. When a fracture propagates stably, as happens before breakdown, the fracture criterion is the condition which specifies the fracture length and direction. However, when a fracture propagates unstably, as happens post breakdown, the fracture criterion no longer predicts the fracture length although it must be satisfied. Conversely, although the mass conservation must be satisfied before breakdown, it gives little information about the fracture geometry, partially because the fracture volume is quite small, and partially because the fracture is free of the fracture fluid. Post breakdown, the fracture propagates unstably, and the mass conservation equation dominates the rate of fracture propagation.

5.5 Shut-in Pressure and σ_3

5.5.1 Introduction

The least principal stress is an important factor in the design of underground openings and massive hydraulic fracturing. Hydraulic fracturing is one of the most promising methods to determine the least principal stress, especially at great depth. In hydraulic fracturing stress measurements, the least principal stress is assumed to be equal to the shut-in pressure. This concept is attributed to Kehle [54]. One important premise of this concept is that leak-off into the formation is negligible. As hydraulic fracturing practice illustrates [55-56], an indistinct shut-in pressure appears if leak-off is not negligible. To deal with the indistinct shut-in pressure, numerous methods have been put forward. A comparison among various methods has also been made by Aggson et al. [57] and Proskin et al. [58]. However, the comparison was performed on field hydraulic fracturing data. The least principal stress was unknown in these tests, and it is difficult to obtain a persuasive conclusion from the comparisons.

Considerable shut-in pressure responses were obtained in the single well hydraulic fracturing program. All the curves yielded indistinct shut-in pressure because a high leak-off was incorporated in the tests. Therefore, the data provide an opportunity to evaluate the analysis techniques to deal with indistinct shut-in pressure. This section compares the shut-in pressure evaluated by eight different methods with the least principal stress applied on a specimen.

5.5.2 Shut-in Pressure Identification Techniques

Various investigators have proposed methods to identify indistinct shut-in pressure. Proskin [59] has summarized the various methods developed by hydraulic fracturing practitioners to determine shut-in pressure. Eight of these methods will be described in the following paragraphs.

Pressure vs time (Inflection Point Method)

The inflection point method suggested by Gronseth and Kry [60-61] is a simple graphical technique. The construction consists of drawing a tangent line to the pressure-time record immediately after shut-in. The pressure at which the pressure-time record departs from the tangent line is defined as the shut-in pressure. This method was suggested to interpret low rate hydraulic fracturing data (<50 L/min). Figure 5.19 illustrates the application of this method.

p_w vs $\log(t+\Delta t)/\Delta t$ (Horner's plot)

McLennan and Roegiers [62] suggested that the inflection point (a slope change) in the plot of p_w vs $\log (t+\Delta t)/\Delta t$ represents the shut-in pressure, where p_w is the bottomhole pressure, t is the time of injection, and Δt is the time since shut-in. Figure 5.20 shows how to determine the shut-in pressure from the plot of p_w vs $\log (t+\Delta t)/\Delta t$.

p_w vs $\log \Delta t$

Doe et al. [63] obtained the shut-in pressure using the plot of the p_w vs $\log \Delta t$ for the period immediately following the first breakdown, where Δt is the time since shut-in. The shut-in pressure corresponds to a break in the slope in the plot. The method was recommended to interpret hydraulic fracturing under slow pumping cycles. Figure 5.21 demonstrates the application of this method.

log (p_w-p_a) vs Δt (Muskat method)

Aamodt and Kuriyagawa [64] thought that the pressure after shut-in approaches some value asymptotically. A trial value for this asymptotic pressure, p_a, is chosen and the logarithm of the pressure, p_w, minus p_a, is plotted against time. p_a is varied until the curve, after an initial transient, is best fitted by a straight line. The straight line is extrapolated back to the time of shut-in, giving a pressure. Then, this pressure plus p_a is taken as the shut-in pressure. This method is shown in Figure 5.22.

log p_w vs log t

As stated by Zoback and Haimson [65], Haimson recommended selecting the shut-in pressure from the plot of log p_w vs log t, where p_w is the bottomhole pressure, and t is the time since pumping. The pressure vs time curve in this plot is bilinear. The shut-in pressure is the intersection of the bilinear lines. Figure 5.23 illustrates this method.

$\frac{dp_w}{dt}$ vs p_w

Tunbridge [66] assumed that the shut-in curve is bilinear in the plot of $\frac{dp_w}{dt}$ vs p_w, where p_w is the bottomhole pressure. The intersection of the two lines corresponds to the shut-in pressure. Figure 5.24 is a plot of $\frac{dp_w}{dt}$ vs p_w and the corresponding shut-in pressure.

p_w vs $\sqrt{\Delta t}$

Fracture linear flow will lead to a linear relation between the pressure and $\sqrt{\Delta t}$. Therefore, when the plot of p_w vs $\sqrt{\Delta t}$ departs from a straight line, the fracture closes. The corresponding bottomhole pressure is the fracture closure pressure or the shut-in pressure [67]. This method is illustrated in Figure 5.25.

Maximum Curvature Method

The bottomhole pressure at the point of the maximum curvature in the shut-in curve is also recommended as the shut-in pressure [68]. Figure 5.26 illustrates the shut-in pressure determined through the maximum curvature method.

5.5.3 Results and Discussion

The shut-in pressure obtained by the various methods and the true least principal stress applied on the specimens are summarized in Table 5.4.

Inflection Point Method: This method always produces a high shut-in pressure, especially for a low stress. For example, it gives a shut-in pressure of 8.0 to 9.5 MPa (1,160 psi to 1,378 psi) in Test 16, but the least principal stress was only 2.92 MPa (424 psi). The shut-in pressure obtained by this method is 8.0 to 9.0 MPa (1,160 to 1,305 psi) in Test 5; while the actual least principal stress was 7.0 MPa (1,015 psi). This method depends strongly upon the time scale used in the plot. When the time scale used expands, the shut-in pressure determined by this method increases. The reason is that the slope of the pressure vs time curve is not constant after immediate shut-in, and it increases rapidly with time (Figure 5.27). The shut-in pressure determined by this method is subjective.

p_w vs log $(t+\Delta t)/\Delta t$ Method: This method is a promising method. It produces a slightly high shut-in pressure. For example, Test 3 has a σ_3 of 1.9 MPa (276 psi), and the shut-in pressure obtained by this method is 2.6 MPa (377 psi). Test 5 has a σ_3 of 7.0 MPa (1,015 psi), and the shut-in pressure is 7.0 MPa (1,015 psi). Test 16 has a σ_3 of 2.92 MPa (424 psi), and the shut-in pressure is 3.8 MPa (551 psi). Under various stress conditions the linear feature of p_w vs log $(t+\Delta t)/\Delta t$ is obvious, and the shut-in pressure can easily be identified.

p_w vs log Δt Method: This method, like p_w vs log $(t+\Delta t)/\Delta t$, produces good results. Test 3 has a σ_3 of 1.9 MPa (276 psi), and the shut-in pressure obtained by this method is 3.0 MPa (435 psi). Test 5 has a σ_3 of 7.0 MPa (1,015 psi), and the shut-in pressure is 6.5 MPa (943 psi). Test 16 has a σ_3 of 2.92 MPa (424 psi), and the shut-in pressure is 3.0 MPa (435 psi). However, it should be pointed out that the p_w vs log Δt curve is not bilinear. In this analysis, the shut-in pressure is considered as the pressure at which the p_w vs log Δt curve departs from a straight line.

log (p_w-p_a) vs Δt Method: This is also a promising method. It is capable of providing a reasonable σ_3, as illustrated in Table 5.4. It should be stressed that the shut-in curve from the first injection cycle usually underestimates the shut-in pressure. For example, while test 5 has a σ_3 of 7.0 MPa (1,015 psi), the shut-in pressure from the first injection cycle is only 1.0 MPa (145 psi). The subsequent injection cycles usually give good estimations of σ_3. For example, the shut-in pressure from the second and the third injection in Test 5 is 7.0 MPa (1,015 psi). They are equal to σ_3. If the injection rate is low, the shut-in curve after several injection cycles can produce a shut-in pressure close to σ_3 as shown by Test 16. The shut-in curve after the fourth injection cycle gives a shut-in pressure close to σ_3.

Log p_w vs log t Method: This method produces little significant results. The plot of log p_w vs log t is usually a smooth curve. It is difficult to draw a bilinear relation. Therefore, the shut-in pressure is considered as the pressure at which the curve departs from the line. As shown in Table 5.4, the results are not stable. For some tests like Tests 3 and 16, the shut-in pressure obtained is close to σ_3. However, for the other tests like Test 5, the shut-in pressure obtained is meaningless.

dp_w/dt vs p_w Method: For high stress, this method provides a reasonable shut-in pressure. For example, Test 5 has a σ_3 of 7.0 MPa (1,015 psi), while the shut-in pressures obtained by this method are 7.0, 6.5 and 6.5 MPa (1,015 psi and 943 psi). Test 9 has a σ_3 of 6.4 MPa (928 psi), and the shut-in pressures are 6.9, 7.0, and 6.8 MPa (1,001, 1,015, and 986 psi). The bilinear feature is distinct. However, this method produces a high shut-in pressure under low stress, as happened in Tests 3 and 16. In addition, the bilinear feature is sometimes indistinct under a low stress.

p_w vs $\sqrt{\Delta t}$ Method: This method sometimes produces a reasonable shut-in pressure. As in Test 9 and the second shut-in of Test 3, the shut-in pressure is close to σ_3. However, some shut-in curves have no linear period as in Test 16, so the shut-in pressure cannot be determined. In addition, the bilinear features are not distinct. Therefore, the shut-in pressure is regarded as the pressure at which the curve departs from the linear segment.

The Maximum Curvature Method: Although this method has an exact definition, it produces poor results. The main error may result from the calculation of the curvature. The curvature depends on the second derivative of pressure versus time, so a little noise on the pressure data will lead to a large fluctuation in curvature. This fluctuation often masks the true maximum curvature. Therefore, while the definition is clear, the determination of shut-in pressure is still subjective.

In conclusion, the shut-in pressure obtained from eight methods has been compared with the least principal stress. The results show that the p_w vs log $(t+\Delta t)/\Delta t$ method, the p_w vs log Δt method, and the log (p_w-p_a) vs Δt method obtain the shut-in pressure close to σ_3 if the shut-in curve following the first injection cycle is used in the plot of p_w vs log $(t+\Delta t)/\Delta t$ and the plot of p_w vs log Δt, and the shut-in curves in the subsequent injection cycles are used in the plot of log (p_w-p_a) vs Δt. The log p_w vs log t method, the dp_w/dt vs Δt method, the p_w vs $\sqrt{\Delta t}$ method, and the maximum curvature method can sometimes obtain a shut-in pressure close to σ_3. However, the results are unstable. For some tests, the results are meaningless. The inflection point method is also subjective because of nonlinear shut-in curves immediately after shut-in.

5.6 Conclusions

Bottomhole pressure is an informative parameter. For example, the least principal stress can be estimated from the shut-in curve. The maximum horizontal stress can be interpreted from the breakdown pressure. The manner of fracture propagation can be characterized by the whole bottomhole pressure versus time curve. On the other hand, its interpretation is complex. Fracturing is a process of fracture propagation. The application of fracture mechanics is necessary. Fracture propagation is driven by the injection of the fracture fluid. Therefore, fluid mechanics and flow theory in porous media must also be incorporated. All these make the bottomhole pressure a sensitive variable to the fracture fluid, the injection rate, the wellbore geometry, and the properties of the formation. To interpret this complex process, many theories and models have been developed. This chapter compared some models with the experimental observation. The following conclusions are drawn from this comparison.

The existing methods are capable of estimating the least principal stress from the shut-in curve even though leak-off is incorporated and the shut-in pressure is indistinct. Eight methods are compared with the experimental results. The comparison shows that the p_w vs log $(t+\Delta t)/\Delta t$ method, the p_w vs log Δt method, and the log (p_w-p_a) vs Δt method are able to obtain a shut-in pressure close to σ_3 if the shut-in curve following the first injection cycle is used in the plot of p_w vs log $(t+\Delta t)/\Delta t$ and the plot of p_w vs log Δt, and the shut-in curves in the subsequent injection cycles are used in the plot of log (p_w-p_a) vs Δt. The inflection point method, the log p_w vs log t method, the dp_w/dt vs Δt method, the p_w vs $\sqrt{\Delta t}$ method, and the maximum curvature method can sometimes obtain a shut-in pressure close to σ_3. However, the results are unstable.

Fracture pressure analysis based on 2D hydraulic fracturing models is used to study the bottomhole pressure. Five experimental results are analyzed. The fracture pressure declines after breakdown. The fracture propagates in a manner which is similar to the GdK or the radial models. However, the models are able to predict only part of the curve due to the introduction of many simplifications to obtain closed-form solutions. One of them is the leak-off model used. The leak-off model assumes that the leak-off velocity is equal to $C/\sqrt{t}$, where C is a constant called the leak-off coefficient. It is not related to the pressure or hydraulic gradient, the viscosity of the fracture fluid, or the permeability of the formation. This leak-off model underestimates the upper limit of the decline in the fracture pressure so that the slow decline cannot be predicted. The second assumption is the mass conservation. The mass conservation equation in the hydraulic fracturing models assumes that the injection rate is equal to the rate of leak-off plus the rate of change in fracture volume. It implies that the fracture fluid fills all the fracture space. Actually, the fracture fluid does not always fill the whole fracture space, especially in the region just after breakdown pressure for a high injection rate and a low least principal stress. As a result, the model is not able to predict the rapid decline in the fracture pressure.

The interpretation of the breakdown pressure is still an open question. The classical breakdown equation and various methods to determine the tensile strength are evaluated. Bredehoeft's fracture reopening pressure gives an extremely variable tensile strength (0.35 to 11.75 MPa). The tensile strength from Brazilian tests predicts too low a breakdown pressure. The apparent tensile strength seems to make sense.

However, it depends on specimen size, which limits its practical application. A statistical analysis was conducted. It reveals that the breakdown pressure can be related to the least principal stress rather than 3 σ_3 - σ_{hmax} under some conditions, such as a high rate of pressurization or a high injection rate. This phenomenon, like the tensile strength, challenges the classical strength theory.

The effect of fluid penetration and several other breakdown models have also been evaluated. Fluid penetration changes the pore pressure in the formation. This change in pore pressure is equivalent to transferring a surface load acting on the wall of a well and the fracture into a distributing body force $\partial p/\partial r$. The effect of it is illustrated by the breakdown equation based on the poroelastic theory. The breakdown pressure is decreased. Shear failure is possible when the injection rate and the viscosity of the fracture fluid are so low that the increase in pore pressure in the formation is almost uniform. Shear failure also results in low breakdown pressure. Ito's point stress model predicts the fracture initiation pressure, not breakdown pressure. The fracture mechanics model is promising. The breakdown occurs when a fracture starts propagating unstably. This is an acceptable concept whether considering it from theoretical or mechanistic views. It should be stressed that the fracture criterion for unstable fracture propagation is $K_I - K_{Ic} = 0$ and $\partial(K_I - K_{Ic})/\partial L \geq 0$, not only $K_I - K_{Ic} = 0$. Introduction of $\partial(K_I - K_{Ic})/\partial L \geq 0$ makes it possible to explain high breakdown pressure as well as several phenomena such as rate-dependent, size-dependent, σ_3-dependent, and fracture fluid-dependent responses.

It is also necessary to know the build-up of the bottomhole pressure before breakdown in order to predict the breakdown pressure. Few studies were found on this aspect. This study shows that the build-up of the bottomhole pressure depends not only on the radial flow theory, but also on the wellbore storage, the skin effect, and the change in permeability. It is impossible to predict the build-up of the bottomhole pressure without consideration of the latter factors.

5.7 References

1. Haimson B. C. Hydraulic fracturing in porous and nonporous rock and its potential for determining in-situ stresses at great depth. Ph.D. Thesis, University of Minnesota, U.S.A. (1968).

2. Medlin W. L. and Massé L. Laboratory investigation of fracture initiation pressure and orientation. *Society of Petroleum Engineers Journal* **19**, 129-144 (1979).

3. Ito T. and Hayashi K. Physical background to the breakdown pressure in hydraulic fracturing tectonic stress measurements. *Int. J. Rock Mech. Min. Sci. & Geomech. Abstr.* **28**, 285-293 (1991).

4. Van Everdingen F. A. and Hurst W. The application of the Laplace transformation to flow problems in reservoirs. *Petroleum Transactions, AIME* **194**, 305-324 (1949).

5. Earlougher R. C. *Advances in well test analysis*, p. 264. SPE Monograph Series, the America Institute of Mining, Metallurgical, and Petroleum Engineers, (1977).

6. Streltsova T. D. *Well testing in heterogeneous formations*, p. 413. An Exxon Monograph, John Wiley & Sons (1988).

7. Da Prat G. *Well test analysis for fractured reservoir evaluation*, p. 210. Developments in Petroleum Science, **27**, Elsevier Science Publishers B.V. (1990).

8. Sabet M. A. *Well test analysis*, p. 460. Contributions in Petroleum Geology & Engineering, **8**, Gulf Publishing Company, (1991).

9. Rekach V. G. *Manual of the theory of elasticity*, Mir Publishers, (1979).

10. Roegiers J.-C. The development and evaluation of a field method for in-situ stress determination using hydraulic fracturing. Ph. D. Thesis, University of Minnesota, U.S.A. (1974).

11. Enever J. R., Cornet F., and Roegiers J. C. ISRM: Hydraulic fracture records. *Int. J. Rock Mech. Min. Sci. & Geomech. Abstr.* **29**, 69-72 (1992).

12. Cuisiat F. D. and Haimson B. C. Scale effects in rock mass stress. *Int. J. Rock Mech. Min. Sci. & Geomech. Abstr.* **29**, 99-117 (1992).

13. Hubbert K. M. and Willis D. G. Mechanics of hydraulic fracturing. *Petroleum Transactions, AIME* **210**, 153-166 (1957).

14. Bredehoeft J. D., Wolff R. G., Keys W. S., and Shuter E. Hydraulic fracturing to determine the regional in situ stress field, Piceance Basin, Colorado. *Geol. Soc. America Bull.* **87**, 250-258 (1976).

15. Hickman S. H. and Zoback M. D. The interpretation of hydraulic fracturing pressure-time data for in-situ stress determination. *Proc. Workshop on Hydraulic Fracture Stress Measurements*, Monterey, CA, pp.44-54 (1981).

16. Schmitt D. R. and Zoback M. D. Poroelastic effects in the determination of the maximum horizontal principal stress in hydraulic fracturing tests—a proposed breakdown equation employing a modified

effective stress relation for tensile failure. *Int. J. Rock Mech. Min. Sci. & Geomech. Abstr.* **26**, 499-506 (1989).

17. Abou-sayed A. S., Brechtel C. E., and Clifton R. J. In situ stress determination by hydrofracturing: a fracture mechanics approach. *J. Geophys. Res.* 83, 2851-2862 (1978).

18. Rummel F. Fracture mechanics approach to hydraulic fracturing stress measurements. *Fracture mechanics of rock* (B. K. Atkinson, Ed), Chapter 6, pp. 217-239. Academic Press, London (1987).

19. Morgenstern N. R. A relation between hydraulic fracture pressure and tectonic stresses. *Geofisica Pura e Applicata* **52**, p.104 (1962).

20. Callanan M. J. Hydraulic fracture initiation by shear failure in formation at great depths. *Proc. a Workshop on Hydraulic Fracture Stress Measurements*, Monterey, CA, U.S.A. pp.181-189 (1981).

21. Ljunggren C, Amadei B, and Stephansson O. Use of the Hoek and Brown failure criterion to determine in-situ stresses from hydraulic fracturing measurements. *Proc. CARE 88 (Conference on Applied Rock Engineering)*, Newcastle, pp. 133-142 (1988).

22. Panah A. K. and Yanagisawa E. Laboratory studies on hydraulic fracturing criteria in soil. *Soils and Foundations* **29**, 14-22 (1989).

23. Lo K. Y. and Kaniaru K. Hydraulic Fracture in earth and rock-fill dams. *Can. Geotech. J.* **27**, 496-506 (1990).

24. Mori A., Tamura M., and Fukui Y. Fracturing pressure of soil ground by viscous materials. *Soils and Foundations* **30**, 129-136 (1990).

25. Scott P. P., Bearden W. G., and Howard C. G. Rock rupture as affected by fluid properties. *Petroleum Transactions, AIME* **198**, 111-124, (1953).

26. Avasthi J. M. Hydrofracturing in inhomogeneous, anisotropic and fractured rocks. Ph.D. Thesis, The University of Wisconsin-Madison, U.S.A. (1981).

27. Cheung L. S. and Haimson B. C. Laboratory study of hydraulic fracturing pressure data–how valid is their conventional interpretation? *Int. J. Rock Mech. Min. Sci. & Geomech. Abstr.* **26**, 595-604 (1989).

28. Lockner D. and Byerlee J. D. Hydrofracture in Weber sandstone at high confining pressure and differential stress. *Journal of Geophysical Research* **82**, 2018-2026 (1977).

29. Solberg P., Lockner D., and Byerlee J. Shear and tension hydraulic fractures in low permeability rocks. *Pure and Applied Geophysics* **115**, 191-198 (1977).

30. Boone T. J. and Ingraffea A. R. *Simulation and visualization of hydraulic fracture propagation in poroelastic rock*. The report to NSF Grant 8351914 (1989).

31. Ingraffea A. R. Theory of rock initiation and propagation in rock. *Fracture mechanics of rock* (B. K. Atkinson, Ed), Chapter 3, pp. 71-110. Academic Press, London (1987).

32. Zoback M. D., Rummel F., Jung R., and Raleigh C. B. Laboratory hydraulic fracturing experiments in intact and pre-fractured rock. *Int. J. Rock Mech. Min. Sci. & Geomech. Abstr.* **14**, 49-58 (1977).

33. Haimson B. C. and Zhao Z. Effect of borehole size and pressurization rate on hydraulic fracturing breakdown pressure. *Rock Mechanics as a Multidisciplinary Science, Proceedings of the 32nd U.S. Symposium on Rock Mechanics*, The University of Oklahoma, Norman, U. S. A., pp. 191-200 (1991).

34. Gdoutos E. E. *Fracture mechanics criteria and applications*, Kluwer Academic Publishers (1990).

35. Majer E. L. and Doe T. W. Studying hydrofractures by high frequency seismic monitoring. *Int. J. Rock Mech. Min. Sci. & Geomech. Abstr.* **23**, 185-199 (1986).

36. Sneddon I. N. and Elliott H. A. The opening of a Griffith crack under internal pressure. *Quarterly of Applied Math.* **4**, 262-268 (1946).

37. Gidley J. L., Holditch S. A., Nierode D. E., and Veatch R. W. *Recent advances in hydraulic fracturing*, p. 452. Monograph Series, SPE, Richardson, TX 12 (1989).

38. Nolte K. G. Determination of fracture parameters from fracturing pressure decline. *Paper SPE 8341* (1979).

39. Nolte K. G. and Smith M. B. Interpretation of fracturing pressures. *Journal of Petroleum Technology (JPT)* **33**, 1767-1775 (1981)

40. Nolte K. G. A general analysis of fracturing pressure decline. *Paper SPE 12941* (1986).

41. Nolte K. G. and Economides M. J. *Fracturing diagnosis using pressure analysis*. Dowell Schlumberger.

42. Mendelsohn D. A. A review of hydraulic fracture modeling–part I: general concepts, 2D models, motivation for 3D modeling. *ASME Journal of Energy Resources Technology* **106**, 369-376 (1984).

43. Mendelsohn D. A. A review of hydraulic fracture modeling–part II: 3D modeling and vertical growth in layered rock. *ASME Journal of Energy Resources Technology* **106**, 543-553 (1984).

44. Veatch Jr. R. W. and Moschovidis Z. A. An overview of recent advances in hydraulic fracturing technology. *Society of Petroleum Engineers Journal* **26**, 421-454 (1986).

45. Perkins T. K. and Kern L. R. Widths of hydraulic fractures. *Journal of Petroleum Technology* (JPT) **13**, 937-949 (1961).

46. Nordgren R. P. Propagation of a vertical hydraulic fracture. *Society of Petroleum Engineers Journal* **12**, 306-314 (1972).

47. Barenblatt G. I. The mathematical theory of equilibrium cracks in brittle fracture. *Advances in Applied Mechanics* **VII**, 56-129 (1962).

48. Geertsma J. and de Klerk F. A rapid method of predicting with and extent of hydraulically induced fractures. *Journal of Petroleum Technology (JPT)* **21**, 1571-1581 (1969).

49. Perkins T. K. Discussion to paper, *Journal of Petroleum Technology (JPT)* **25**, 93-95 (1973).

50. Geertsma J. and Haafkens R. A comparison of the theories to predict width and extent of vertical, hydraulically induced fractures. *Trans., ASME* **101**, 8-19 (1979).

51. Biot M. A., Medlin W. L., and Massé L. Laboratory experiments in fracture propagation. *Paper SPE 10377 presented at the 1981 Eastern Regional Meeting*, Columbus, Ohio, U.S.A. (1981).

52. Medlin W. L. and Massé L. Laboratory experiments in fracture propagation. *Society of Petroleum Engineers Journal* **24**, 256-268 (1984).

53. Rubin M. B. Experimental study of hydraulic fracturing in an impermeable material. *Journal of Energy Resources Technology* **105**, 116-124 (1983).

54. Kehle R. O. The determination of tectonic stresses through analysis of hydraulic well fracturing. *Journal of Geophysical Research* **69**, 259-273 (1964).

55. *Hydraulic fracturing stress measurements*, Proceedings of a workshop on Hydraulic Fracturing Stress Measurements, National Academy Press, Washington, D. C. (1983).

56. Haimson B. C., Roegiers J. C., and Zoback M. D. *Hydraulic fracturing stress measurements*, Proceedings of the Second International Workshops on Hydraulic Fracturing Stress Measurements, (1988).

57. Aggson J. R. and Kim K. Analysis of hydraulic fracturing pressure histories: A comparison of five methods used to identify shut-in pressure. *Int. J. Rock Mech. Min. Sci. & Geomech. Abstr.* **24**, 75-80 (1987).

58. Proskin S. A., Scott J. D., and Chhina H. S. Interpretation of the minimum principal stress from microfrac tests, Rock at Great Depth, Proceedings of The International Symposium on Rock Mechanics and Rock Physics ar Great Depth, Pau, France, pp.1509-1519 (1990).

59. Proskin S. In situ stress determination in oil sands. MSc. Thesis, Department of Civil Engineering, University of Alberta, Alberta, Canada (1989).

60. Gronseth J. M. and Kry P. R. Instantaneous shut-in pressure and its relationship to the minimum in-situ stress. *Proc. Workshop on Hydraulic Fracture Stress Measurements*, Monterey, CA, U.S.A. pp.55-60 (1981).

61. Gronseth J. M. Determination of the instantaneous shut-in pressure from hydraulic fracturing data and its reliability as a measure of the minimum principal stress. *Issues in Rock Mechanics, Proc. of the 23rd U.S. Symposium on Rock Mechanics*, pp. 183-189, University of California, Berkeley, U. S. A. (1982).

62. McLennan J. D. and Roegiers J.-C. Do instantaneous shut-in pressures accurately represent the minimum principal stress. *Proc. Workshop on Hydraulic Fracture Stress Measurements*, Monterey, CA, U.S.A. pp.68-78 (1981).

63. Doe W. T. and Hustrulid W. A. Determination of the state of stress at the Stripa Mine, Sweden. *Proc. Workshop on Hydraulic Fracture Stress Measurements*, Monterey, CA, U.S.A. pp.119-129 (1981).

64. Aamodt R. L. and Kuriyagawa M. Measurement of instantaneous shut-in pressure in crystalline rock. *Proc. Workshop on Hydraulic Fracture Stress Measurements*, Monterey, CA, U.S.A. pp.139-142 (1981).

65. Zoback M. D. and Haimson B. C. Status of the hydraulic fracturing method for in-situ stress measurements. *Issues in Rock Mechanics, Proc. of the 23rd U.S. Symposium on Rock Mechanics*, University of California, Berkeley, U.S.A. pp. 143-156 (1982).

66. Tunbridge L. W. Interpretation of the shut-in pressure from the rate of pressure decay. *Int. J. Rock Mech. Min. Sci. & Geomech. Abstr.* **26**, 457-459 (1989).

67. Sookprasong P. A. Plot procedure finds closure pressure. *Oil & Gas Journal* **84** Sept. 8, 110-112 (1986).

68. Hayashi K. and Sakurai I. Interpretation of hydraulic fracturing shut-in curves for tectonic stress measurements. *Int. J. Rock Mech. Min. Sci. & Geomech. Abstr.* **26**, 477-482 (1989).

Table 5.1: Fracture Reopening Pressure

Specimen No.	σ_3 MPa *Injection rate cm^3/s*	p_{b1}[*] MPa	p_{b2}[*] MPa	p_{b3}[*] MPa	$p_{b1}-p_{b2}$ MPa	$p_{b1}-p_{b3}$ MPa
3	1.90	15.80	13.41	8.70	2.39	7.10
5	7.00	20.80	20.45	19.65	0.35	1.15
20	*3.186*	18.72	16.88	16.19	1.84	2.53
16	*2.164*	20.50	11.20	8.75	9.30	11.75

---

[*] p_{b1}, p_{b2}, and p_{b3} are the peak bottomhole pressure in the first, second, and third injection cycles, respectively.

Table 5.2: Comparison of Observed and Calculated Internal Rupturing Pressure (breakdown pressure) of Cylinders of Rock (after Scott et al.)

					Internal Pressure (psi)					
Cylinder radii(in)					Calculated					Observed
Internal	External	Type rock formation	Tensile strength (psi)	Shear strength (estimated)(psi)	Max. Principal stress	Max. shear	Max. strain	Max. strain energy	Plastic	
Nonpenetrating fluid										
0.19	2.0	Neat Cement	182	1400	179	1390	143	115	494	700
0.19	1.75	Sandstone	504	3000	495	2960	396	342	1290	4200
0.19	1.75	Sandstone	378	2000	368	1970	298	240	968	5550
0.19	2.13	Shale	20	500	20	20	16	13	56	886
3.0	Infinite	Sandstone	360	1800	360	1800	288	228	infinite	>3500
Penetrating fluid										
0.19	1.0	Sandstone	200	850	186	820	151	122	386	258
0.19	1.0	Sandstone	120	400	112	385	91	73	232	166

Table 5.3: Statistical Analysis of Breakdown Pressure

Author (date)	Rock	Viscosity of fracture fluid	Rate	c_1	c_4^2	c_3	c_4^2
Guo (1992)	Gypstone	1000 mPa•s	3.114 ml/s	1.433	**0.900**	1.070	0.797
Cheung (1989)	Niagara Dolomite	90 cSt	0.04 to 0.08ml/s	1.452	**0.921**	0.843	0.856
Avasthi (1981)	Revett Quartzite		80 psi/s	1.051	**0.728**	0.662	0.711
	Revett Quartzite		80 psi/s	1.412	**0.946**	0.855	0.924
	Martinsburg slate		80 psi/s	1.046	**0.916**	0.543	0.885
	Martinsburg slate		80 psi/s	1.106	**0.928**	0.536	0.889
Haimson (1968)	Tennessee Marble		7 to 15psi/s	1.473	0.928	0.679	**0.983**
	Charcoal Granite		6 to 10 psi/s	1.548	0.926	0.810	**0.968**
	Mankato Pink Dolomite		10 to 15 psi/s	1.487	0.480	0.560	**0.717**
	Hydrostone 30%		4 to 15psi/s	1.493	0.876	0.566	**0.947**
	Hydrostone 32%		4 to 20psi/s	1.510	0.931	0.732	**0.955**
	Hydrostone 35%		4 to 15psi/s	1.8072	0.838	0.82572	**0.890**

Note: $p_b = c_0 + c_1 \sigma_{hmin}$, $p_b = c_2 + c_3 (3\sigma_{hmin} - \sigma_{hmax})$, and c_4 is relative coefficient.

Table 5.4 Determination of σ_3

		Shut-in pressure (MPa)							
Method	Cycle 1	2	3	4	5	6	7	8	Comment
Test 3 σ_3 = 1.90 MPa									
Inflection point	7.0	4.8							not suggested
p vs log (t+Δt)/Δt	2.6	*							suggested
p vs log Δt	3.0	*							suggested
log (p-p_a) vs Δt	1.3	1.8							suggested
log p vs log t	2.0	*							suggested
dp/dt vs p	4.5	?							not suggested
p vs √Δt	5.3	2.4							not suggested
Maximum curvature	4.6	4.6							not suggested
Test 5 σ_3 = 7.00 MPa									
Inflection point	9.0	9.9	9.9						not suggested
p vs log (t+Δt)/Δt	7.0	*	*						suggested
p vs log Δt	6.5	*	*						suggested
log (p-p_a) vs Δt	1.0	7.0	7.0						suggested
log p vs log t	3.5	*	*						not suggested
dp/dt vs p	7.0	6.5	6.5						suggested
p vs √Δt	8.0	9.0	8.5						not suggested
Maximum curvature	?	5.6	7.0						not suggested
Test 9 σ_3 = 6.40 MPa									
Inflection point		9.0	12.5	9.0					not suggested
p vs log (t+Δt)/Δt		*	*	*					
p vs log Δt		*	*	*					
log (p-p_a) vs Δt		6.9	7.0	6.8					suggested
log p vs log t		*	*	*					
dp/dt vs p		7.0	7.8	5.8					suggested
p vs √Δt		7.3	5.5	5.9					suggested
Maximum curvature		5.4	7.4	5.7					suggested
Test 16 σ_3 = 2.92 MPa									
Inflection point	8.0	8.0	8.0	9.0	9.5	9.5	9.5	9.0	not suggested
p vs log (t+Δt)/Δt	3.8	*	*	*	*	*	*	*	suggested
p vs log Δt	3.0	*	*	*	*	*	*	*	suggested
log (p-p_a) vs Δt	1.0	1.2	1.0	1.9	2.9	*	3.0	3.1	suggested
log p vs log t	2.0	*	*	*	*	*	*	*	suggested
dp/dt vs p	3.3	4.0	4.8	4.0	3.7	3.9	4.6	3.2	not suggested
p vs √Δt	?	5.0	?	?	?	4.2	?	?	not suggested
Maximum curvature	3.9	5.0	4.1	5.9	4.4	4.2	7.1	4.8	not suggested

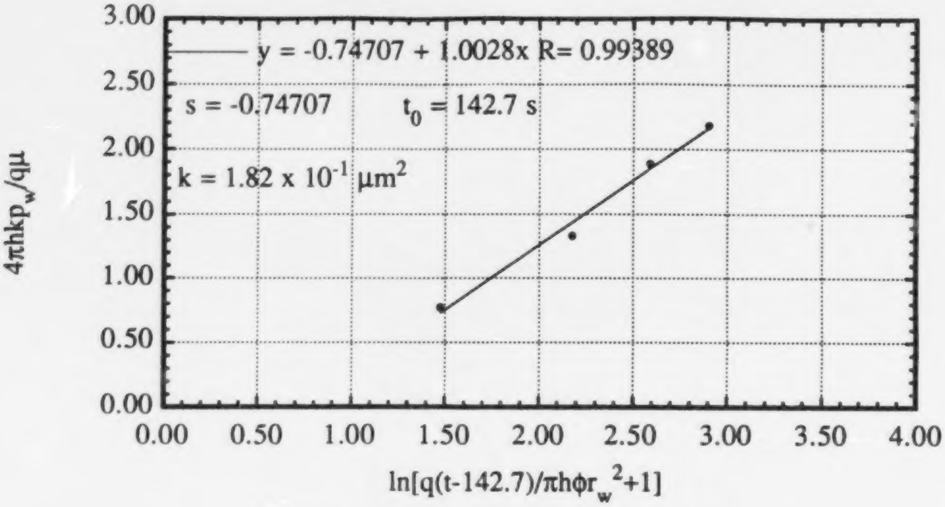

a. Determination of s and t_0

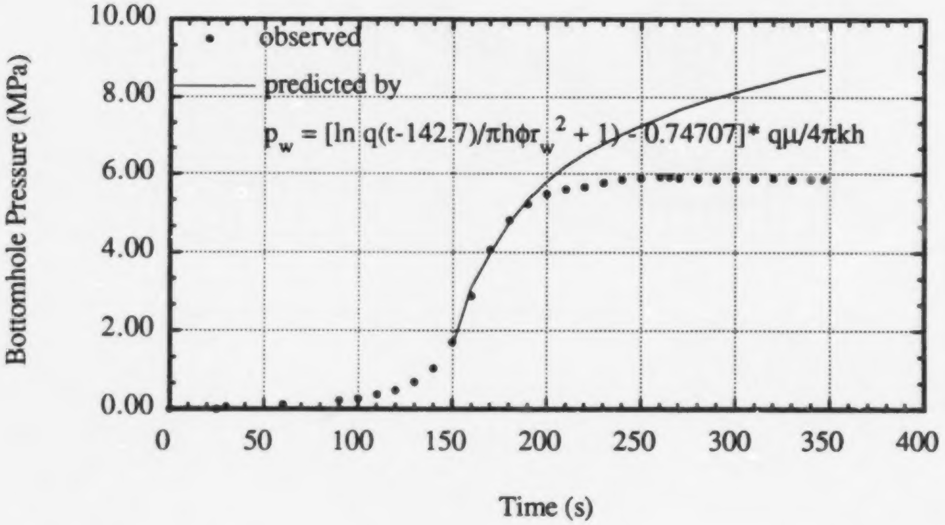

b. Build-up of Bottomhole Pressure

Figure 5.1 Build-up of Bottomhole Pressure: Test 7

(Test 7: Without stress and $q_i = 0.528\ cm^3/s$)

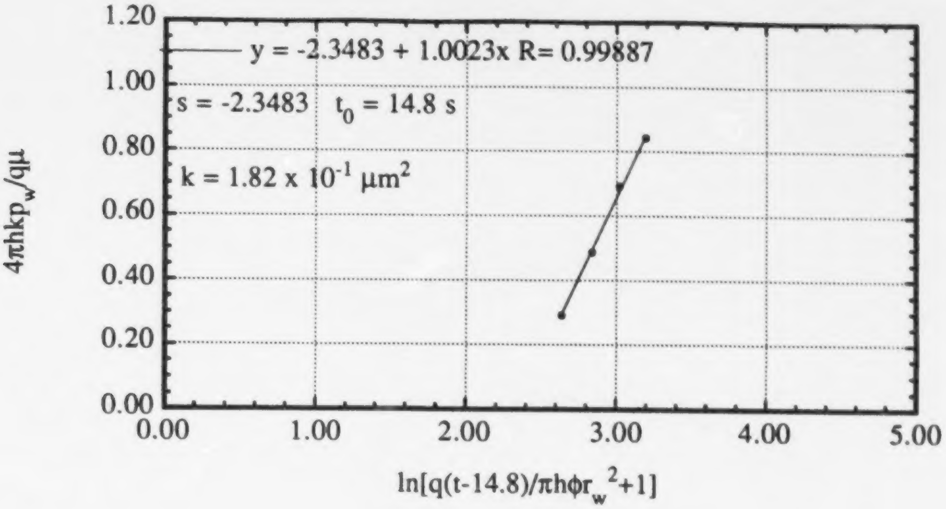

a. Determination of s and t_0

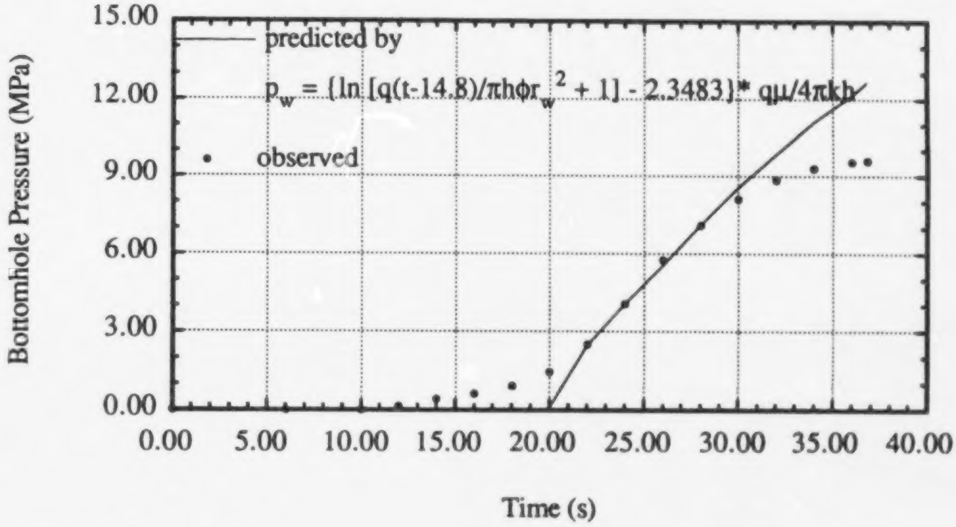

b. Build-up of Bottomhole Pressure

Figure 5.2 Build-up of Bottomhole Pressure: Test 12

(Test 12: Without stress and $q_i = 2.110$ cm^3/s)

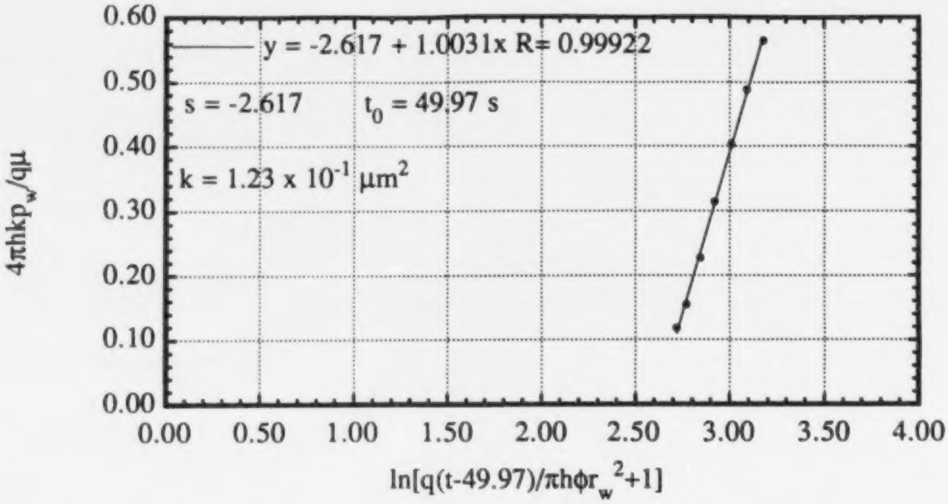

a. Determination of s and t_0

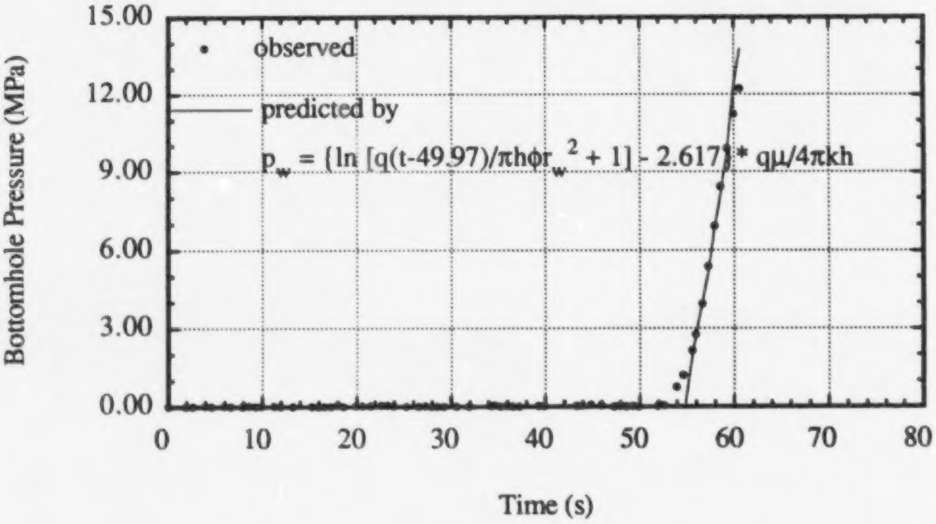

b. Build-up of Bottomhole Pressure

Figure 5.3 Build-up of Bottomhole Pressure: Test 23

(Test 23: Without stress and q_i = 3.186 cm^3/s)

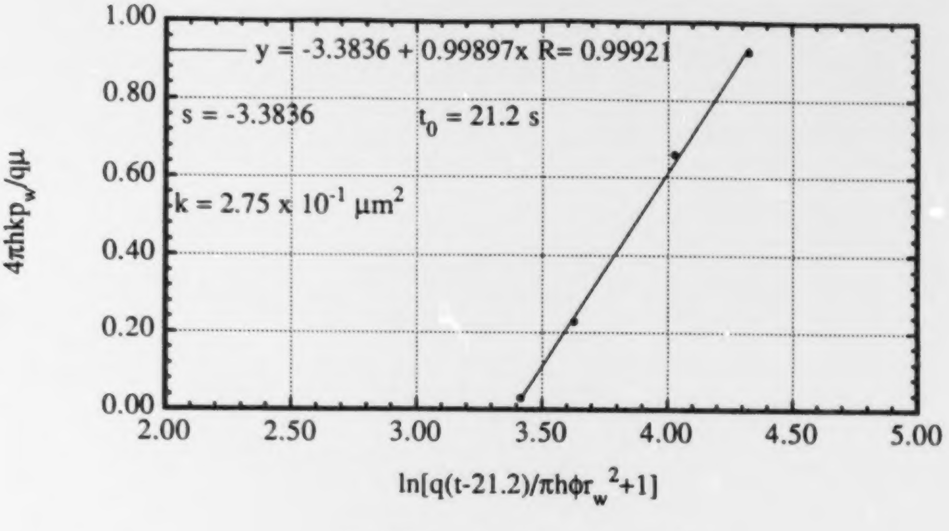

a. Determination of s and t_0

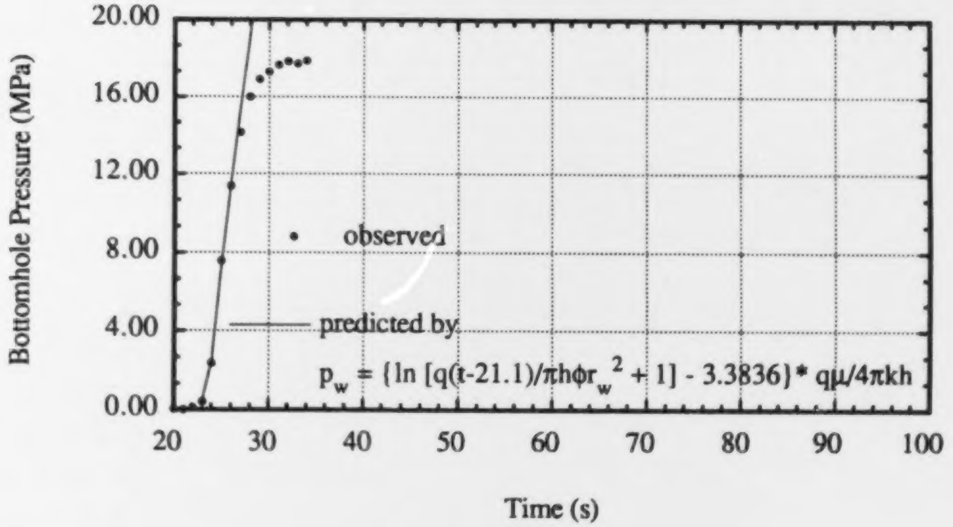

b. Build-up of Bottomhole Pressure

Figure 5.4 Build-up of Bottomhole Pressure: Test 21

Test 21: σ_{ver} = 4.67 MPa, σ_{hmax} = 4.37 MPa, σ_{hmin} = 2.77 MPa, q_i = 3.186 cm^3/s

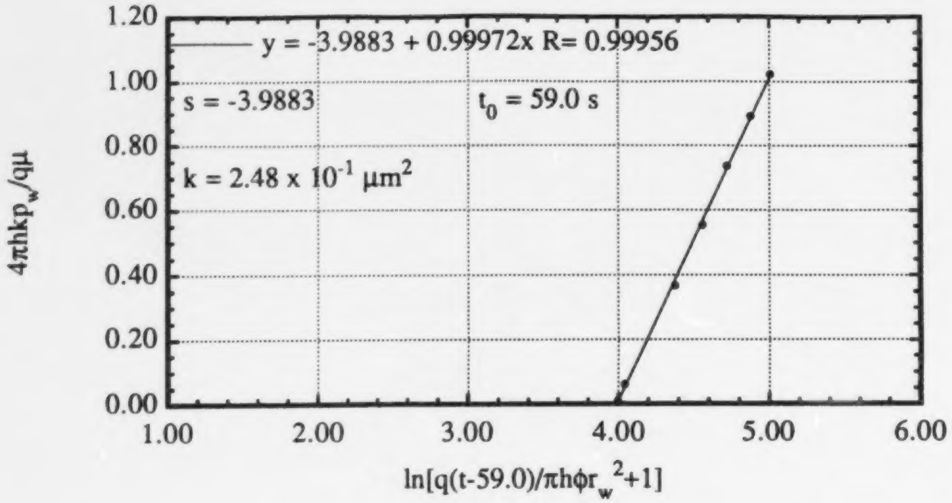

a. Determination of s and t_0

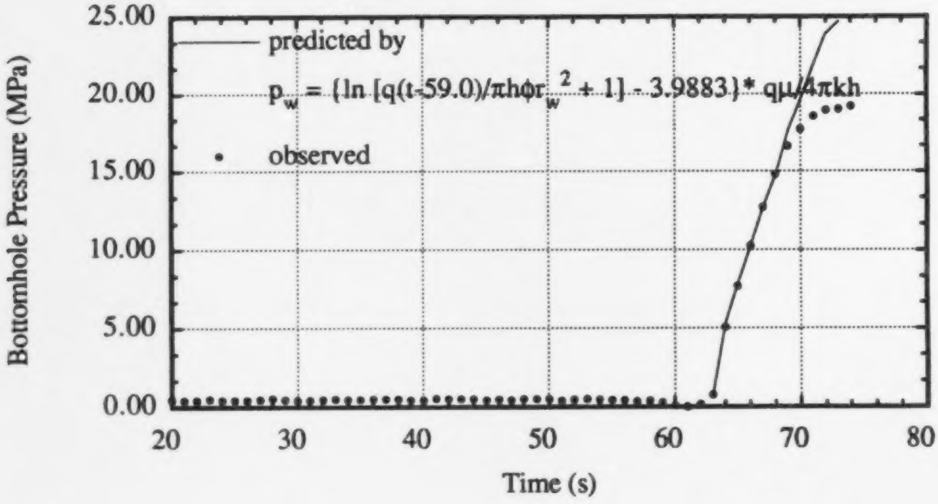

b. Build-up of Bottomhole Pressure

Figure 5.5 Build-up of Bottomhole Pressure: Test 22

Test 22: σ_{ver} = 5.35 MPa, σ_{hmax} = 5.01 MPa, σ_{hmin} = 2.69 MPa, q_i = 3.186 cm³/

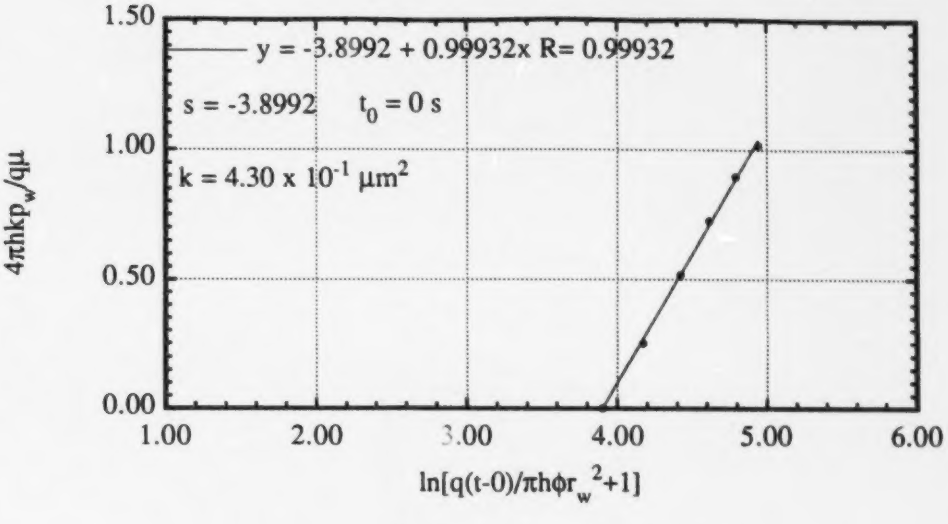

a. Determination of s and t_0

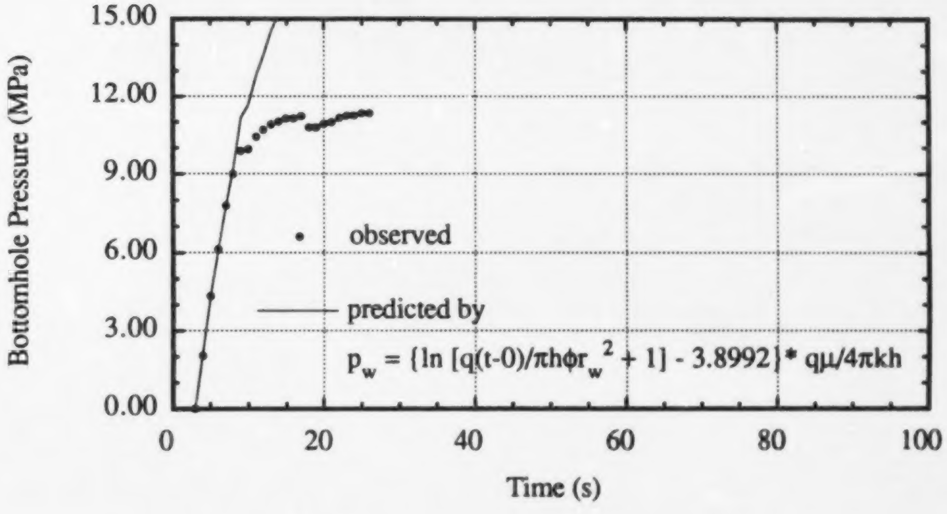

b. Build-up of Bottomhole Pressure

Figure 5.6 Build-up of Bottomhole Pressure: the Second Injection Cycle of Test 20

Test 20: σ_{ver} = 4.88 MPa, σ_{hmax} = 4.68 MPa, σ_{hmin} = 2.95 MPa, q_i = 3.186 cm^3/s

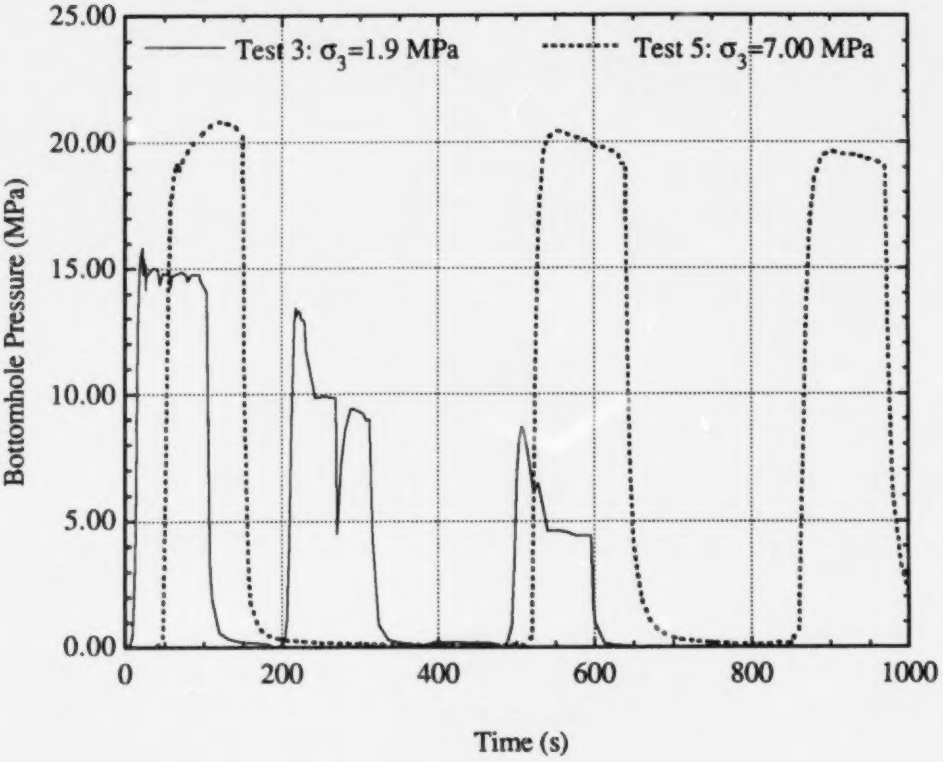

Figure 5.7 Bottomhole Pressure of Tests 3 and 5

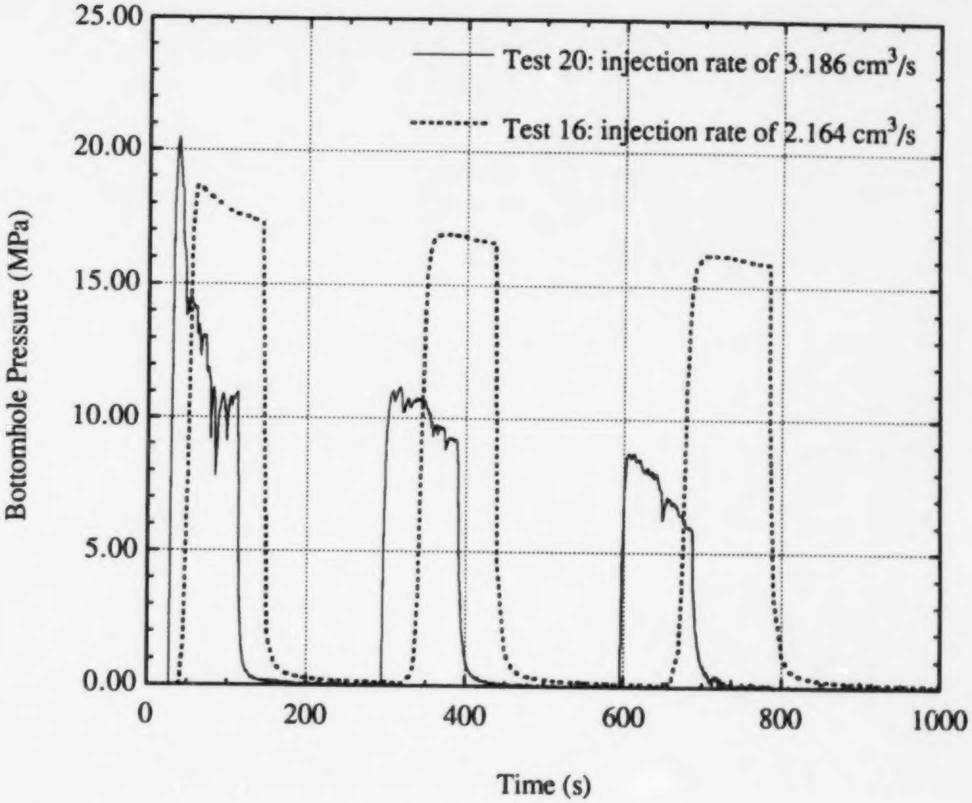

Figure 5.8 Bottomhole Pressure of Tests 16 and 20

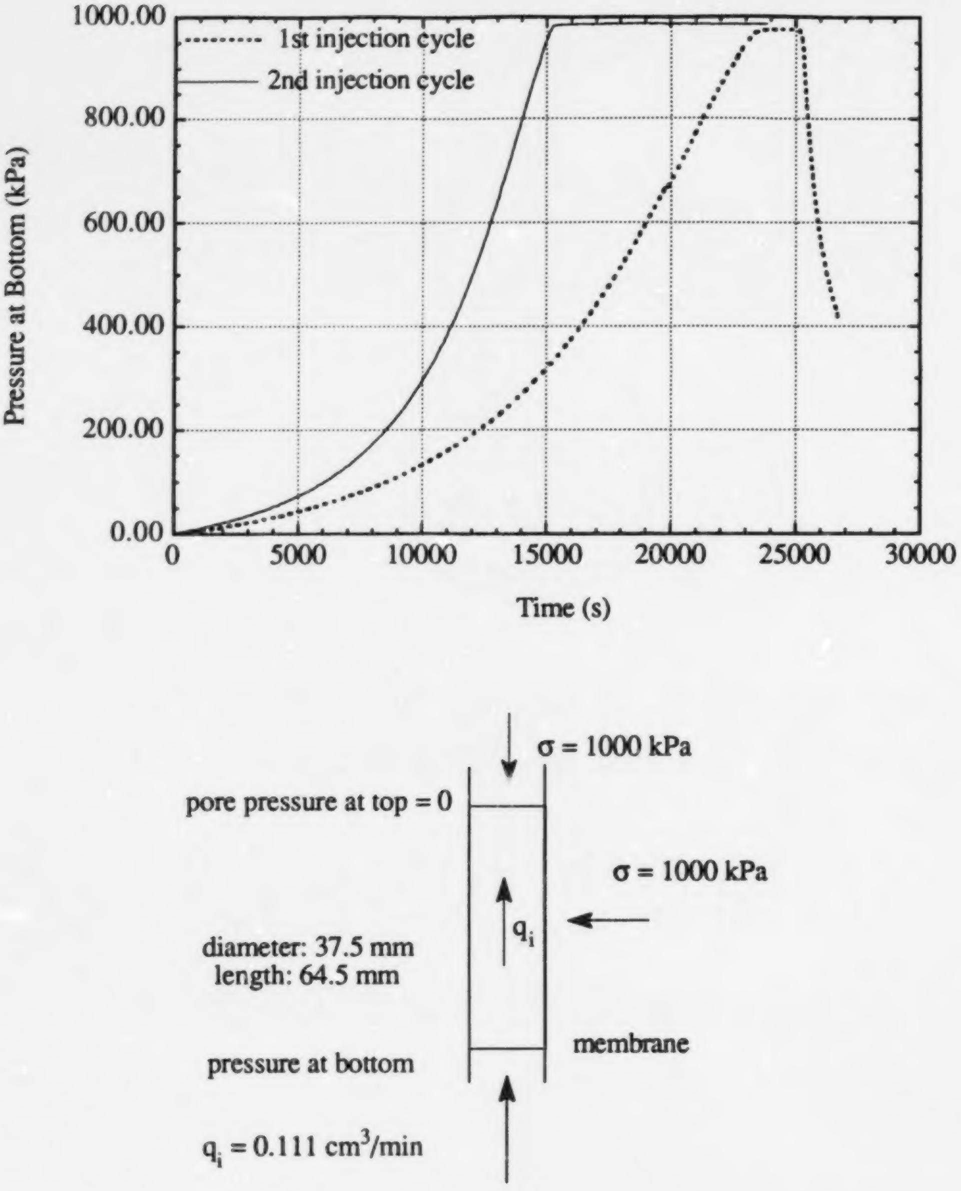

Figure 5.9 Leak-off Test 2

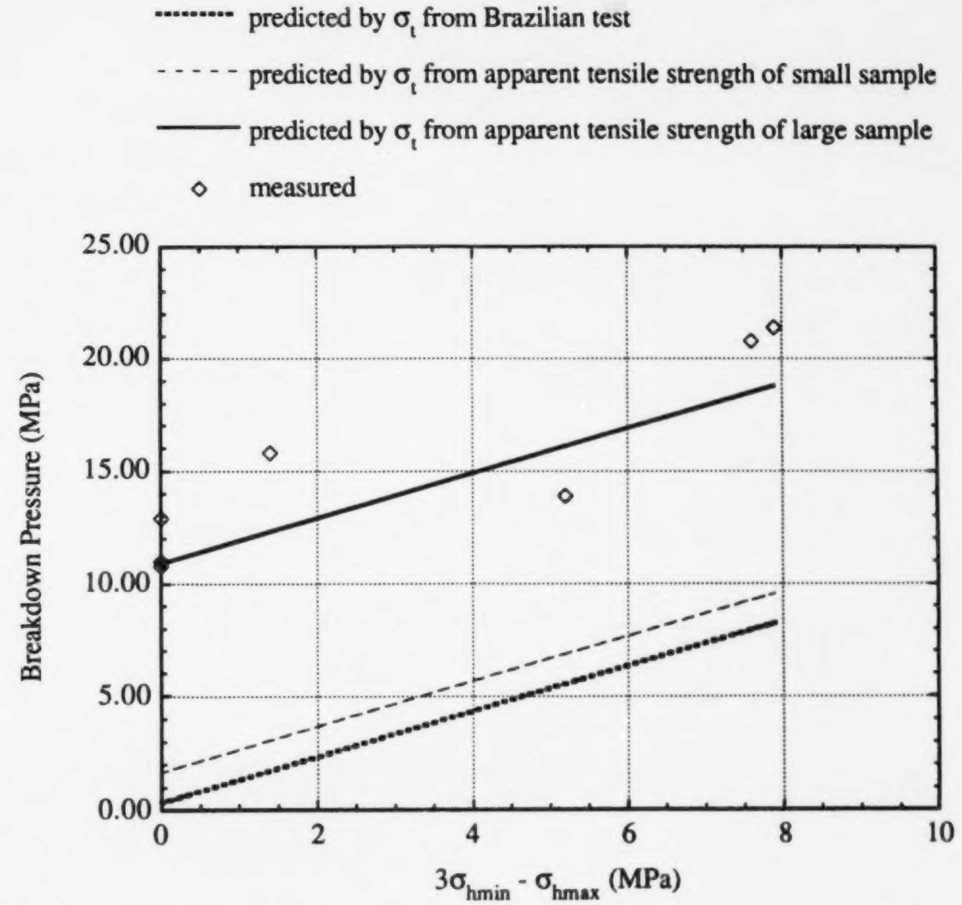

Figure 5.10 Breakdown Pressure Measured and Predicted by the Classical Breakdown Model

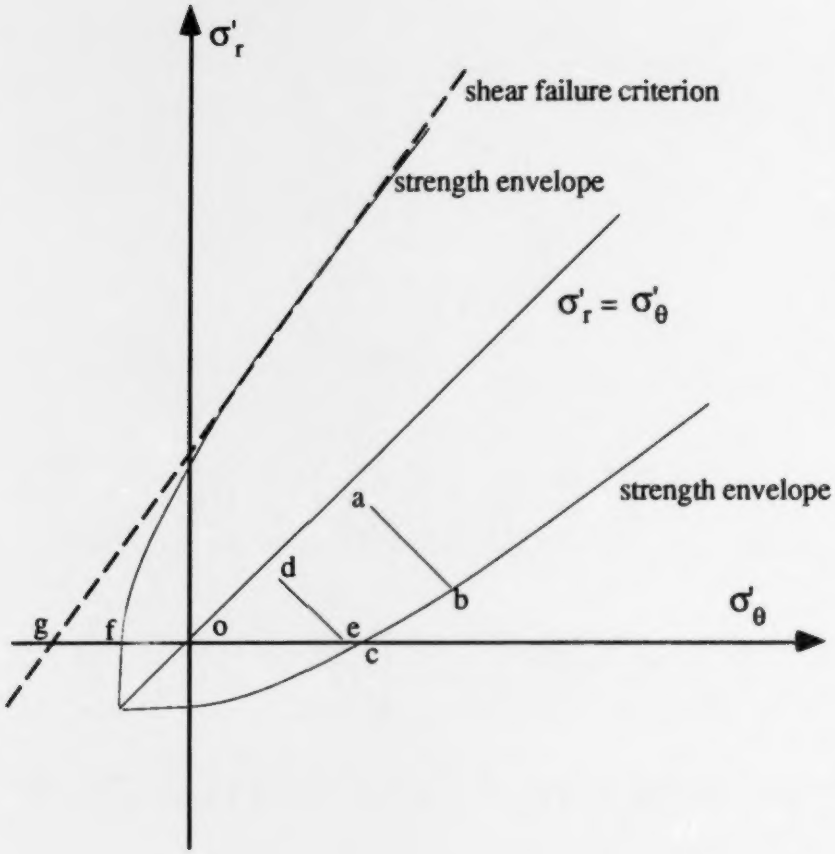
σ'r
shear failure criterion
strength envelope
σ'r = σ'θ
strength envelope
a
d
b
g
f
o
e
c
σ'θ

Figure 5.11 Stress Path during Fracturing for Permeable Case

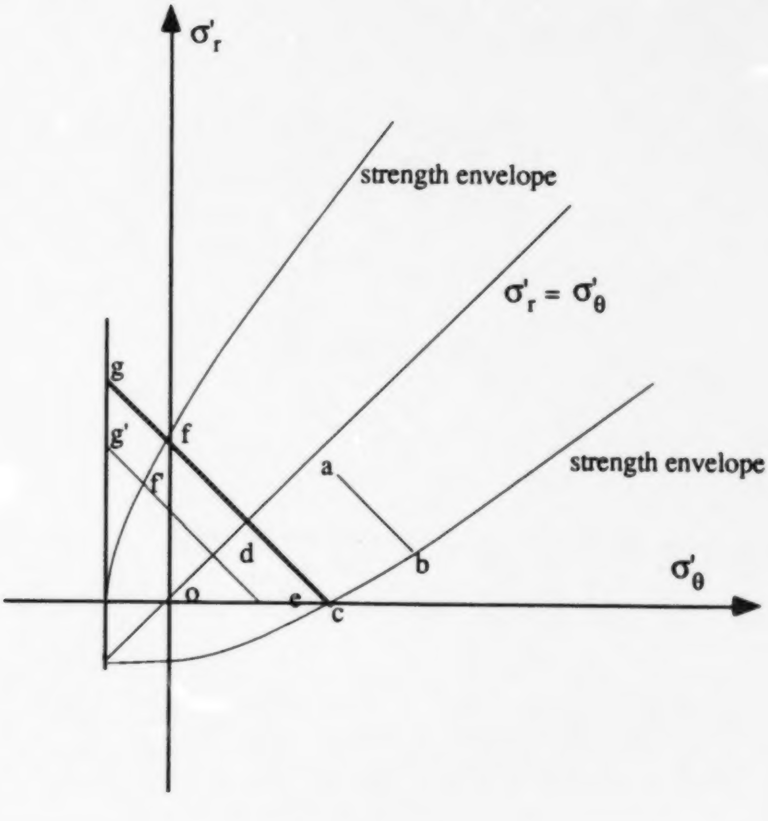
σ'r
strength envelope
σ'r = σ'θ
strength envelope
σ'θ
g
g'
f
f'
a
b
d
o
e
c

Figure 5.12 Stress Path during Fracturing for Impermeable Case

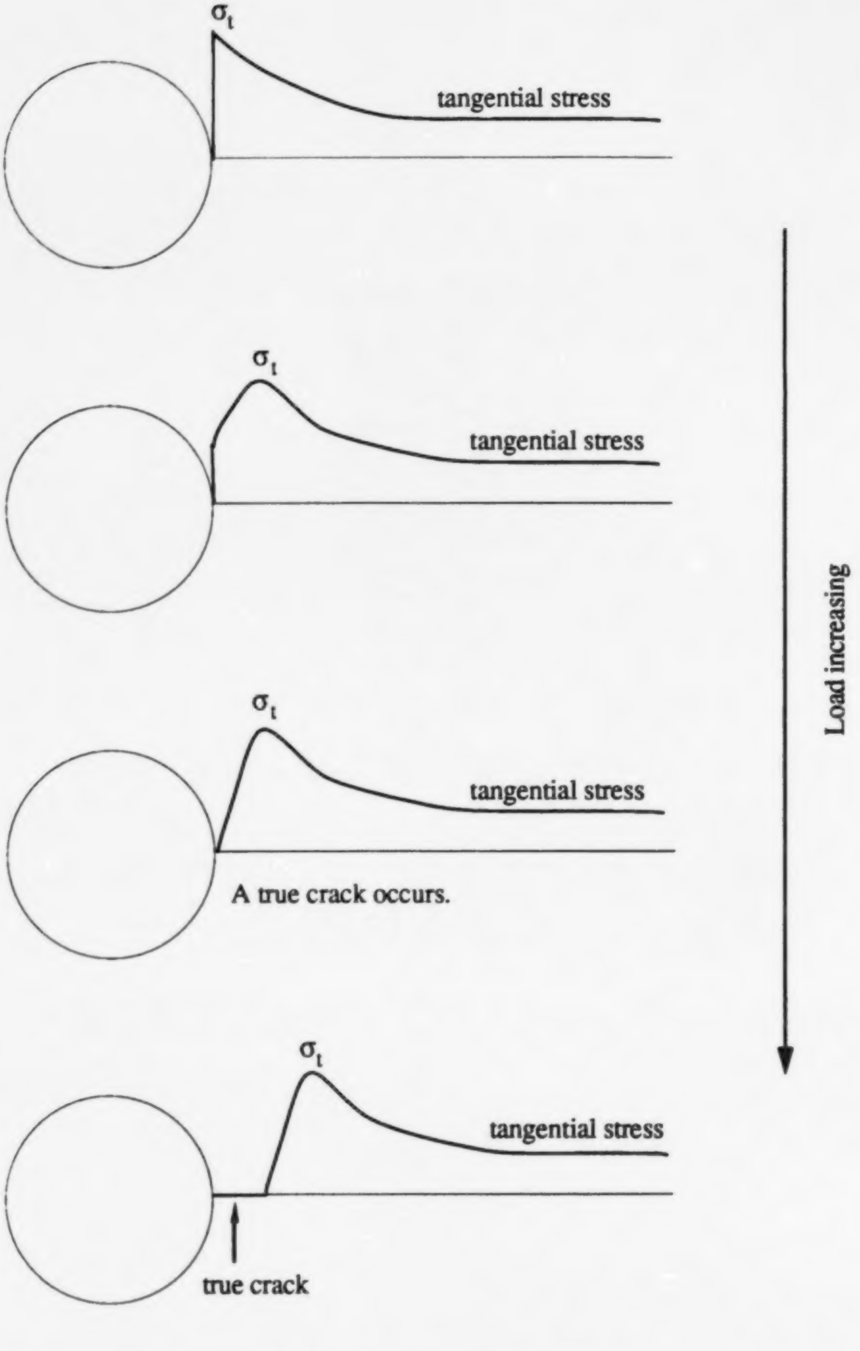
σt
tangential stress
σt
tangential stress
σt
tangential stress
A true crack occurs.
σt
tangential stress
true crack
Load increasing

Figure 5.13 Development of a True Crack

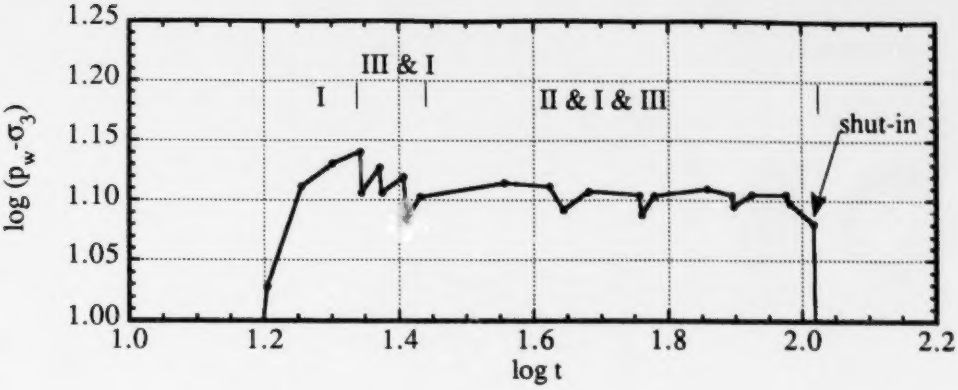

a. Hydraulic Fracture Test 3 Cycle-1

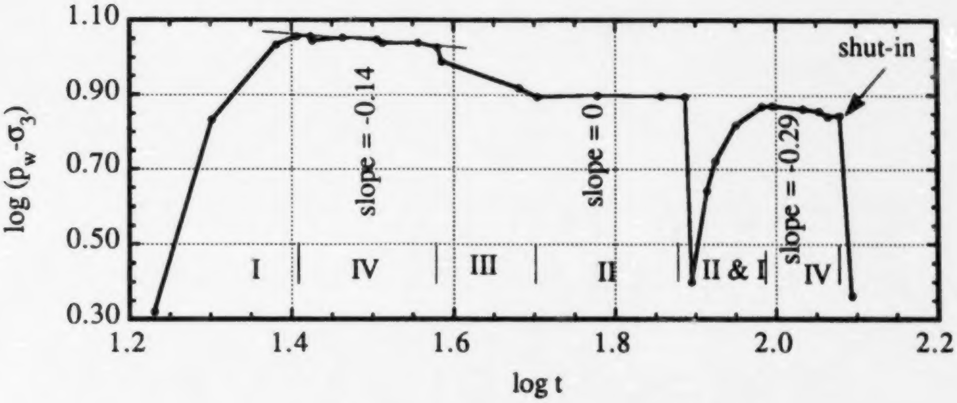

b. Hydraulic Fracture Test 3 Cycle-2

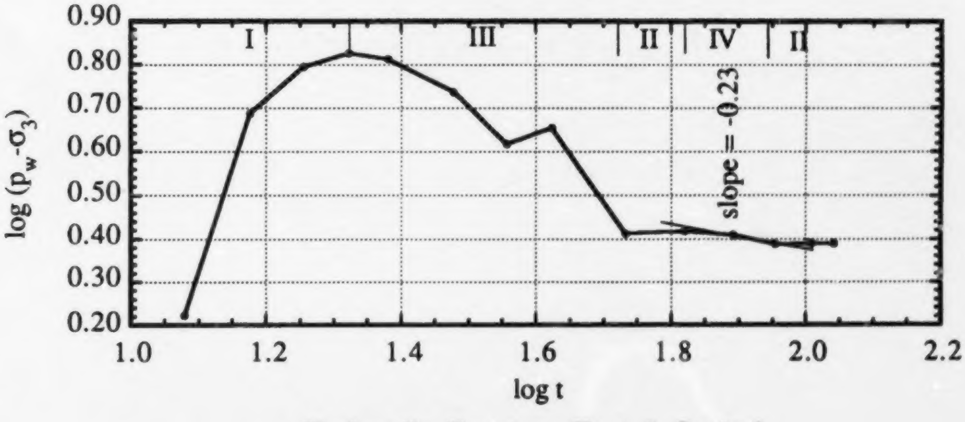

c. Hydraulic Fracture Test 3 Cycle-3

Figure 5.14 Fracture Pressure Analysis: Test 3

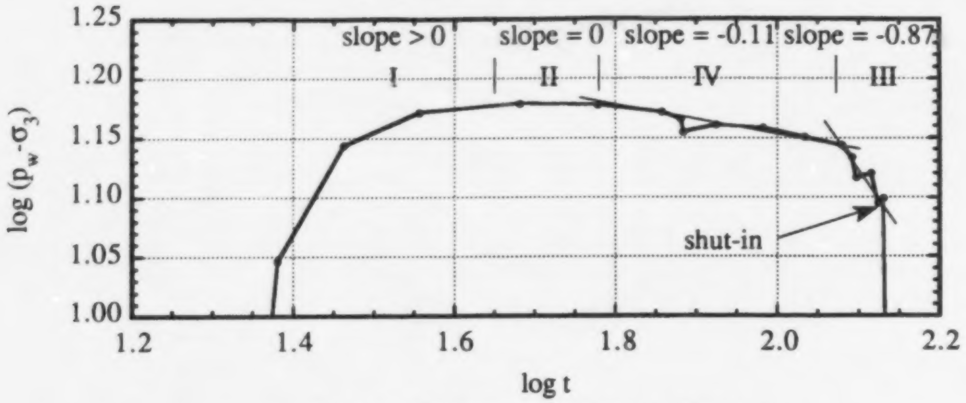

a. Hydraulic Fracture Test 9 Cycle-2

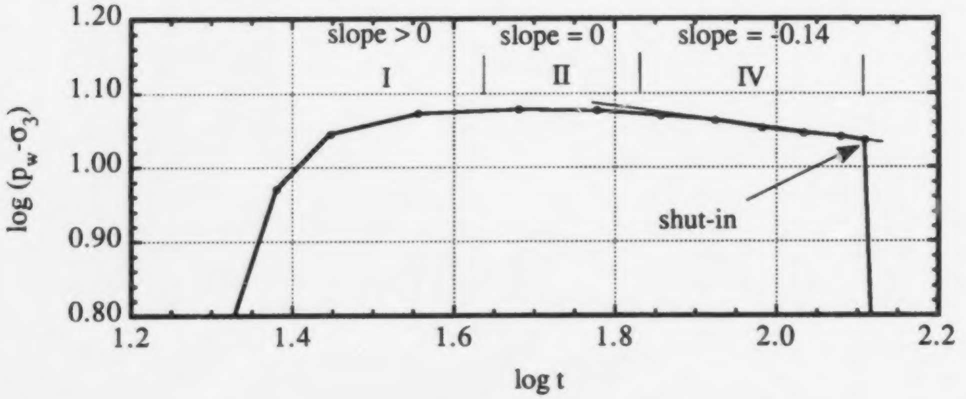

b. Hydraulic Fracture Test 9 Cycle-3

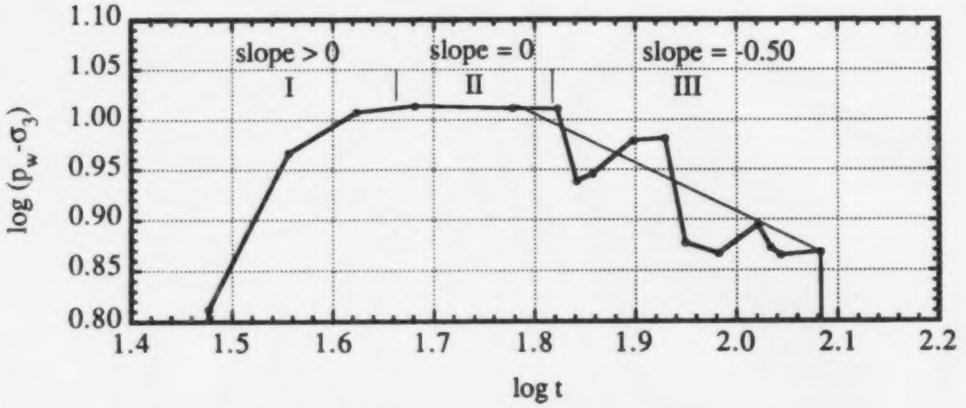

c. Hydraulic Fracture Test 9 Cycle-4

Figure 5.15 Fracture Pressure Analysis: Test 9

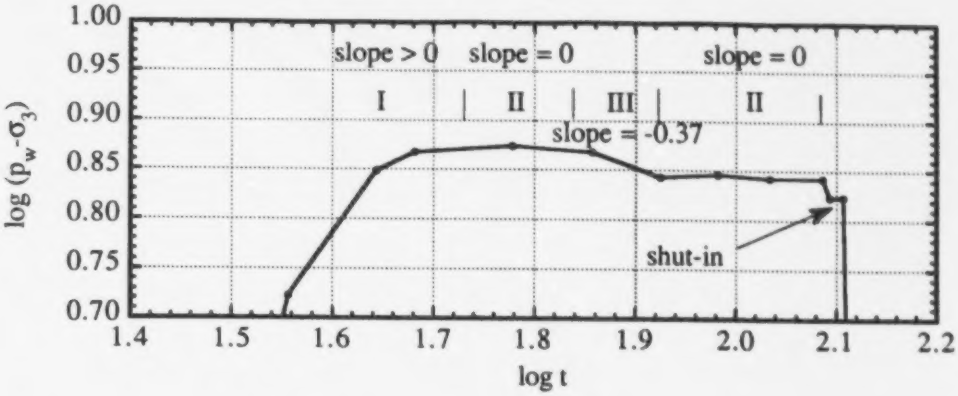

d. Hydraulic Fracture Test 9 Cycle-5

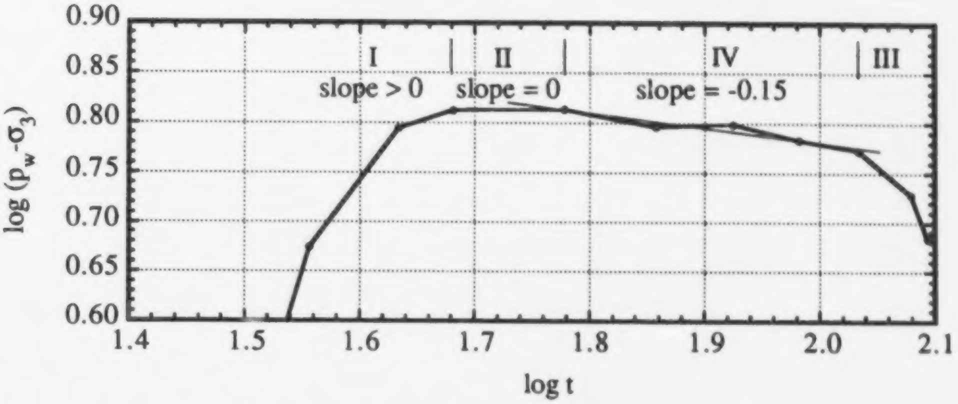

e. Hydraulic Fracture Test 9 Cycle-6

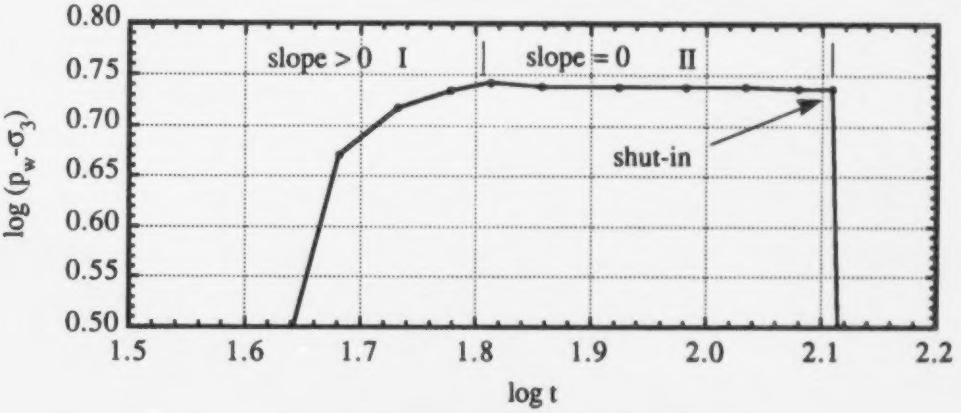

f. Hydraulic Fracture Test 9 Cycle-7

Figure 5.15 Continued

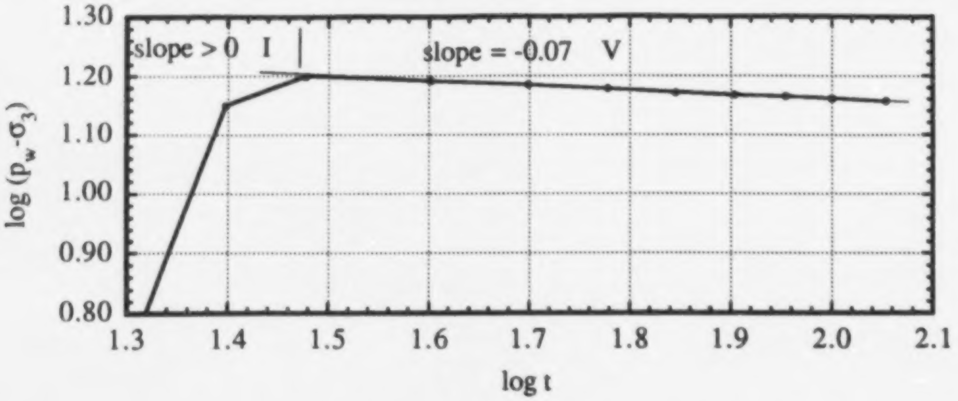

a. Hydraulic Fracture Test 16 Cycle-1

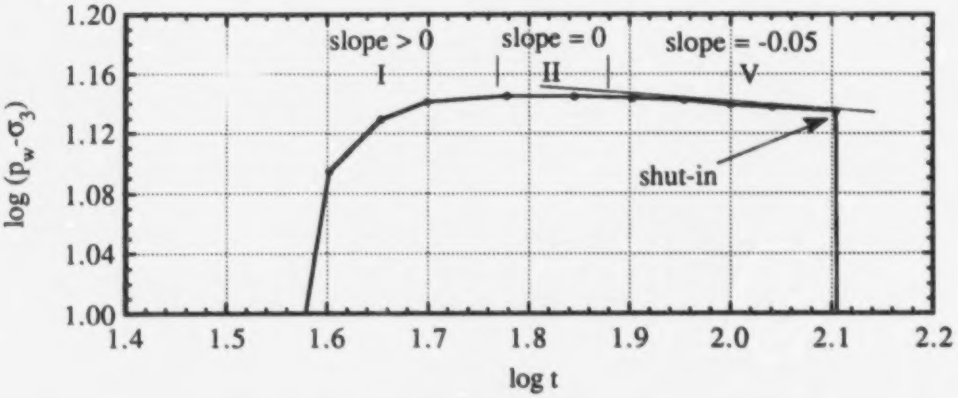

b. Hydraulic Fracture Test 16 Cycle-2

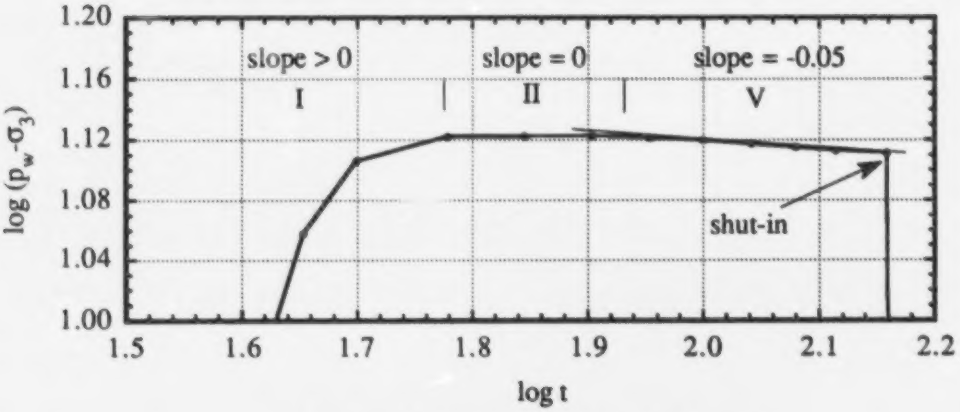

c. Hydraulic Fracture Test 16 Cycle-3

Figure 5.16 Fracture Pressure Analysis: Test 16

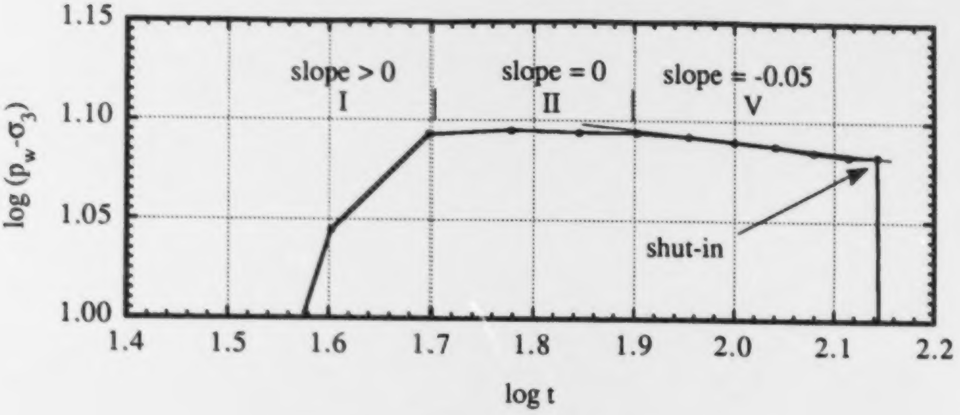

d. Hydraulic Fracture Test 16 Cycle-4

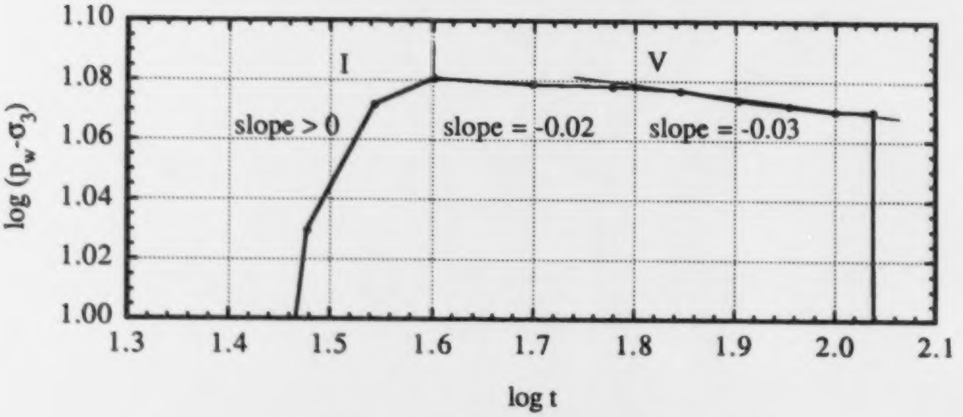

e. Hydraulic Fracture Test 16 Cycle-5

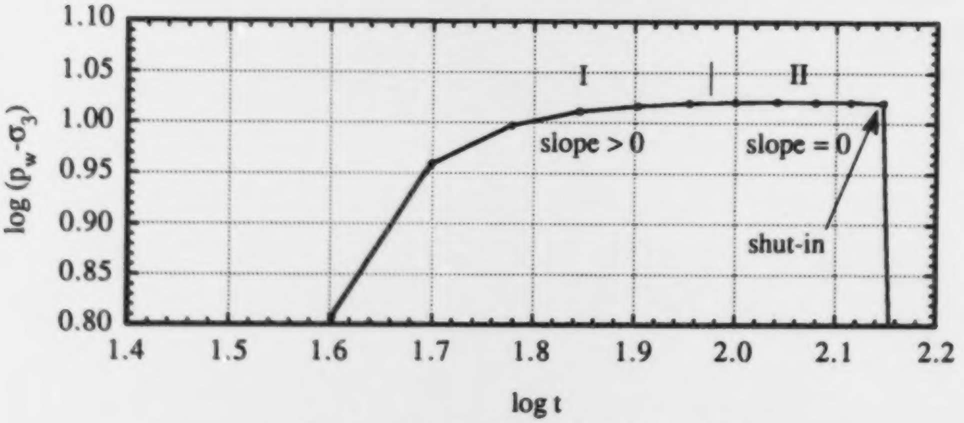

f. Hydraulic Fracture Test 16 Cycle-6

Figure 5.16 Continued

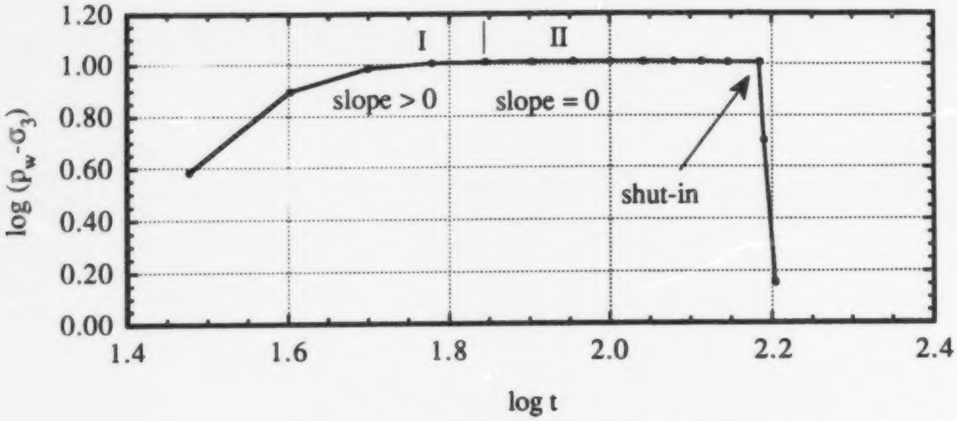

g. Hydraulic Fracture Test 16 Cycle-7

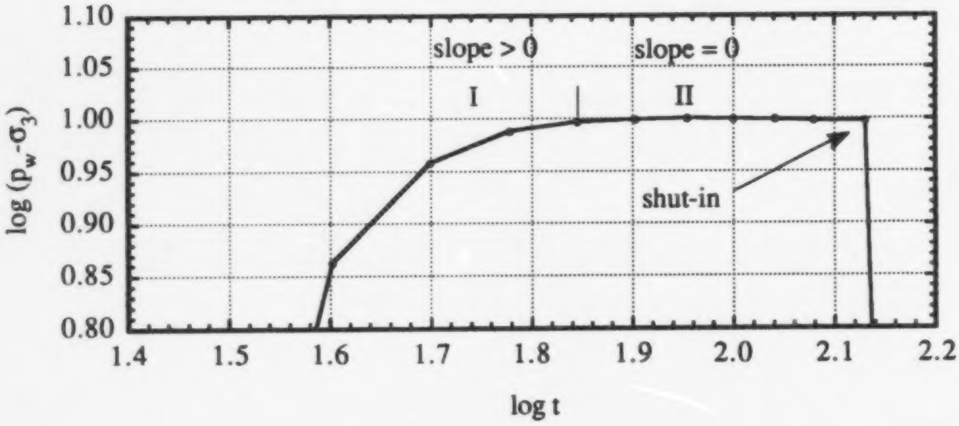

h. Hydraulic Fracture Test 16 Cycle-8

Figure 5.16 Continued

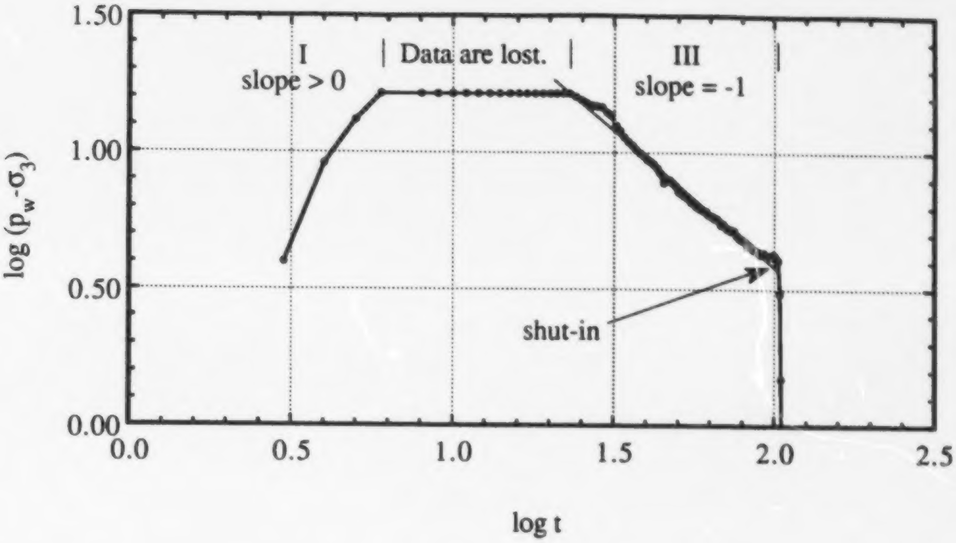

a. Hydraulic Fracture Test 19 Cycle-1

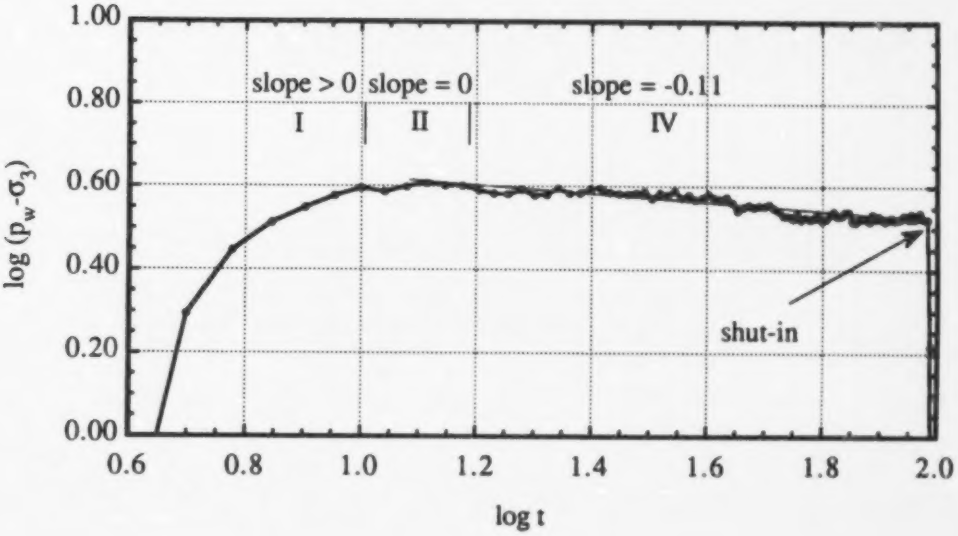

b. Hydraulic Fracture Test 19 Cycle-2

Figure 5.17 Fracture Pressure Analysis: Test 19

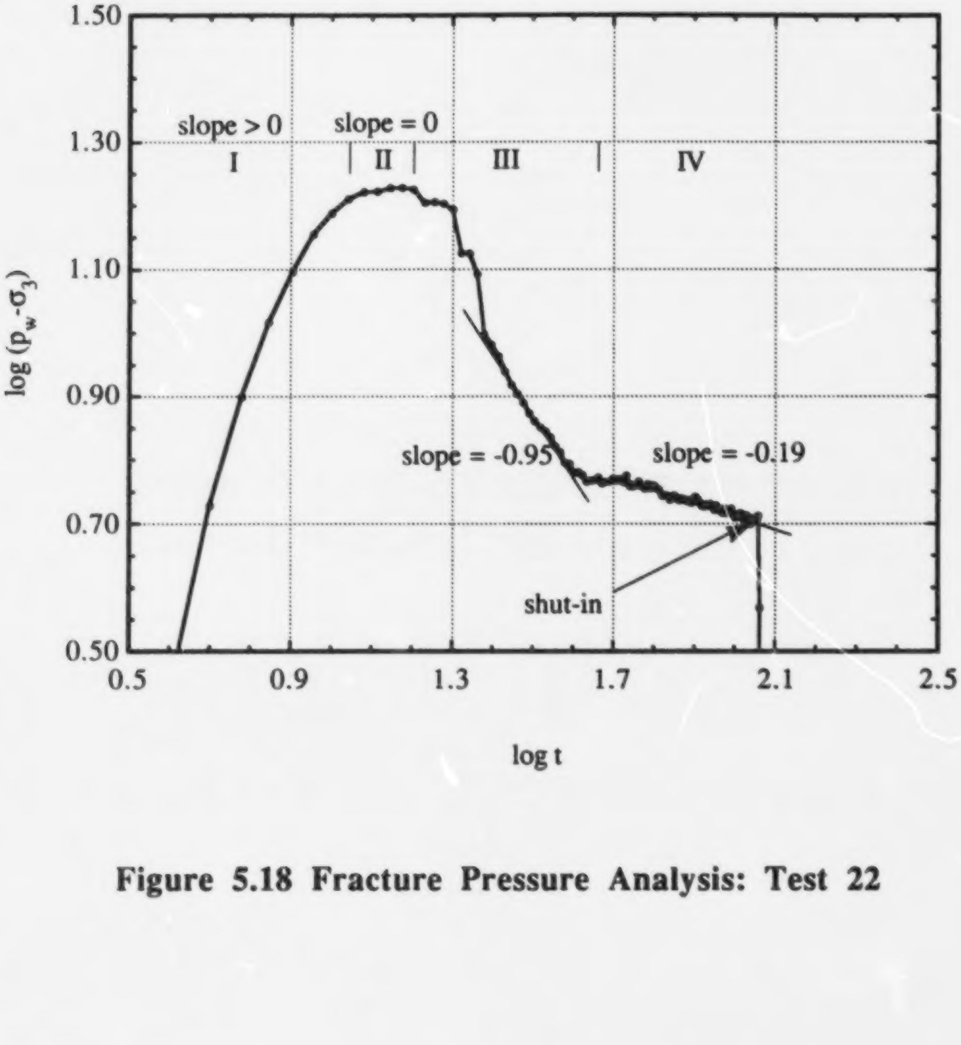

Figure 5.18 Fracture Pressure Analysis: Test 22

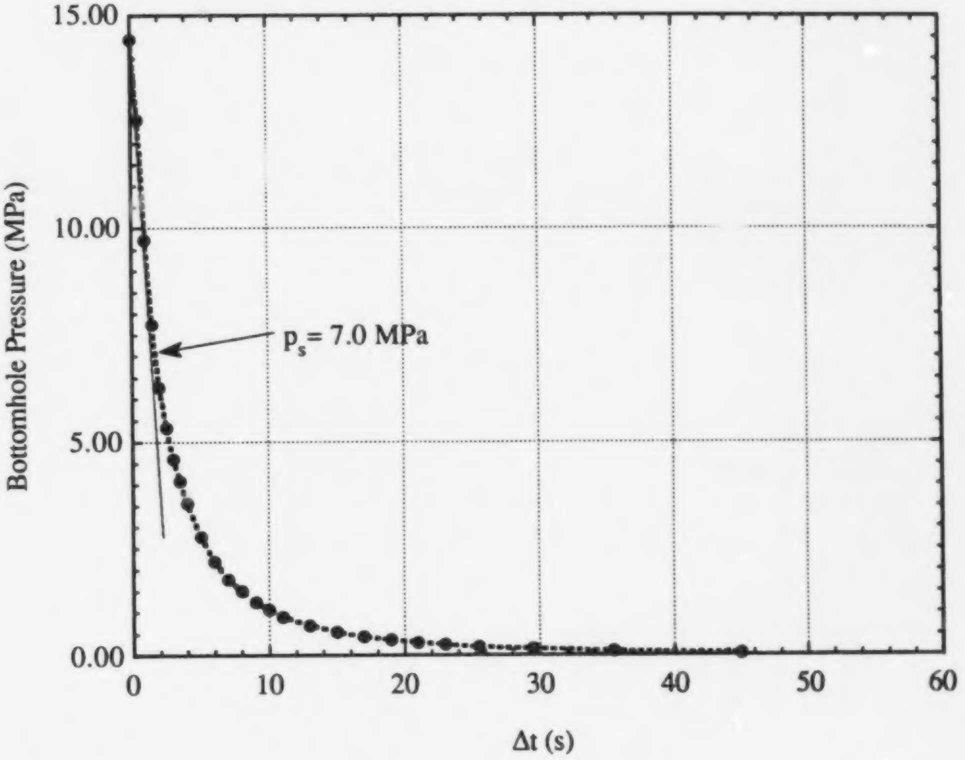

Hydraulic Fracture Test 3 Shut-in in Cycle-1

Figure 5.19 Inflection Point Method

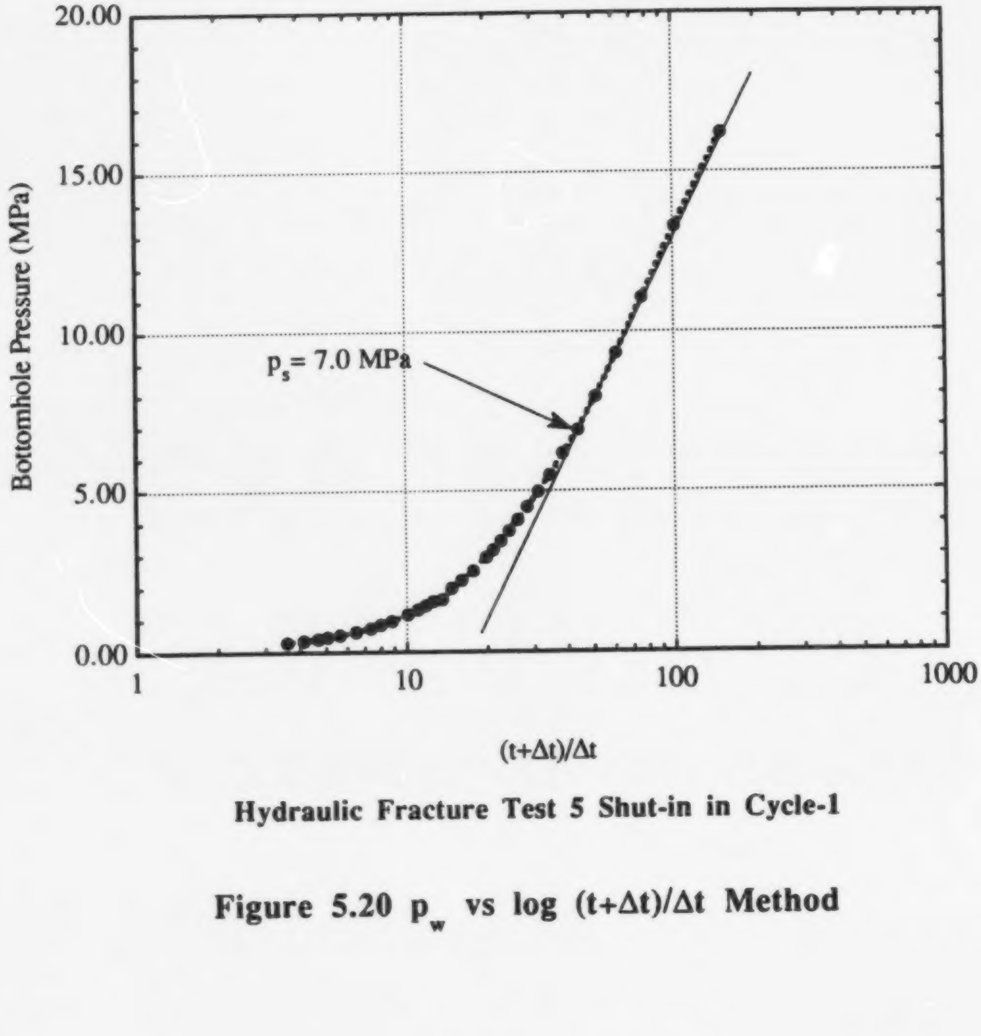

Hydraulic Fracture Test 5 Shut-in in Cycle-1

Figure 5.20 p_w vs log (t+Δt)/Δt Method

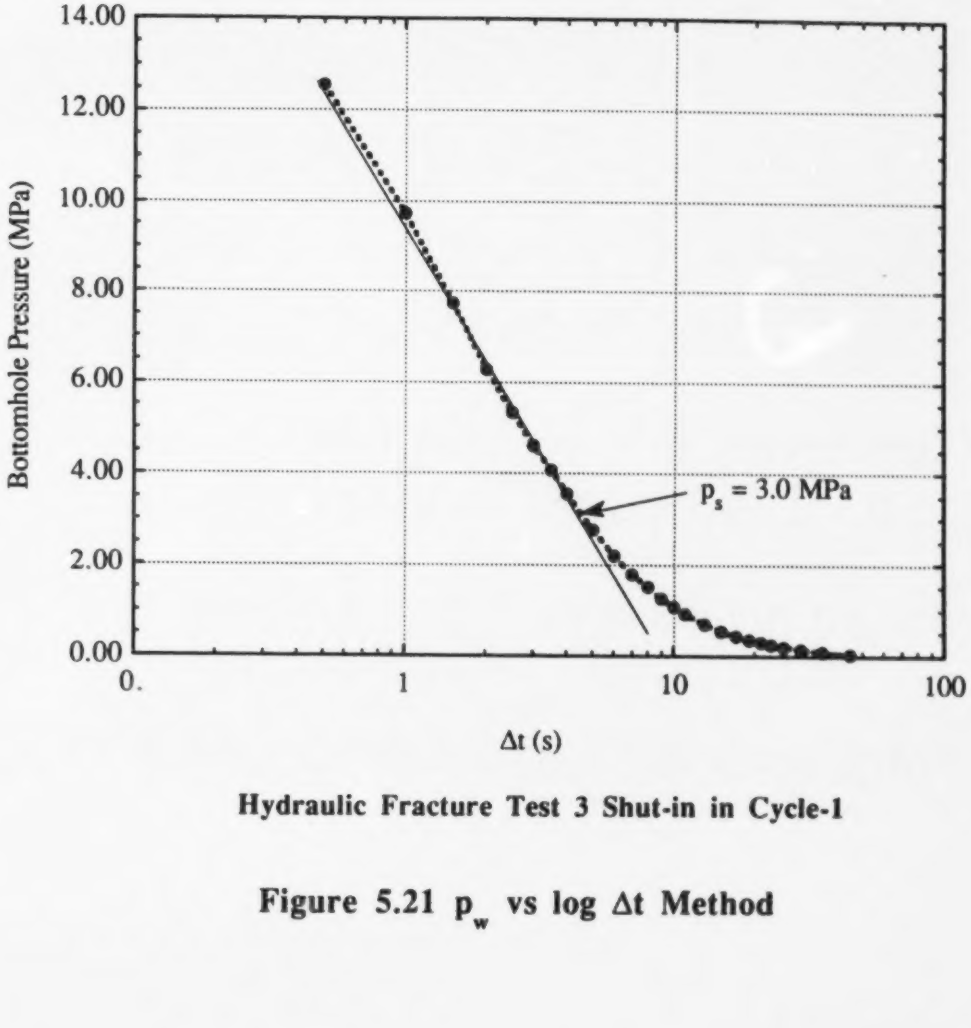

Hydraulic Fracture Test 3 Shut-in in Cycle-1

Figure 5.21 p_w vs log Δt Method

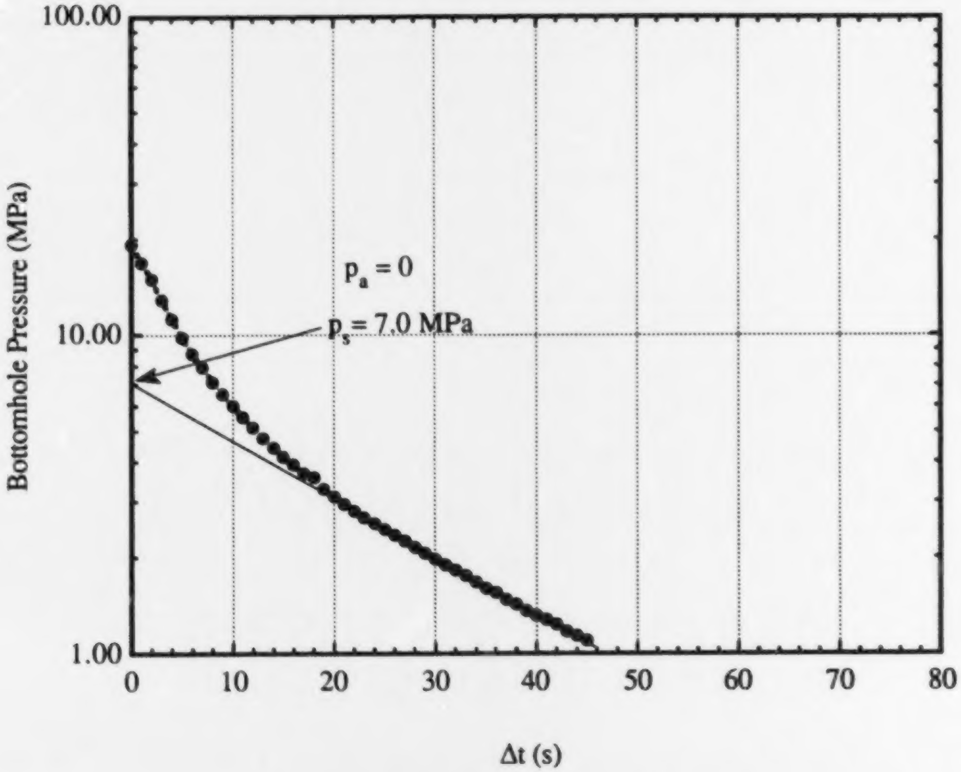

Hydraulic Fracture Test 5 Shut-in in Cycle-3

Figure 5.22 log (p_w-p_a) vs Δt Method (Muskat Method)

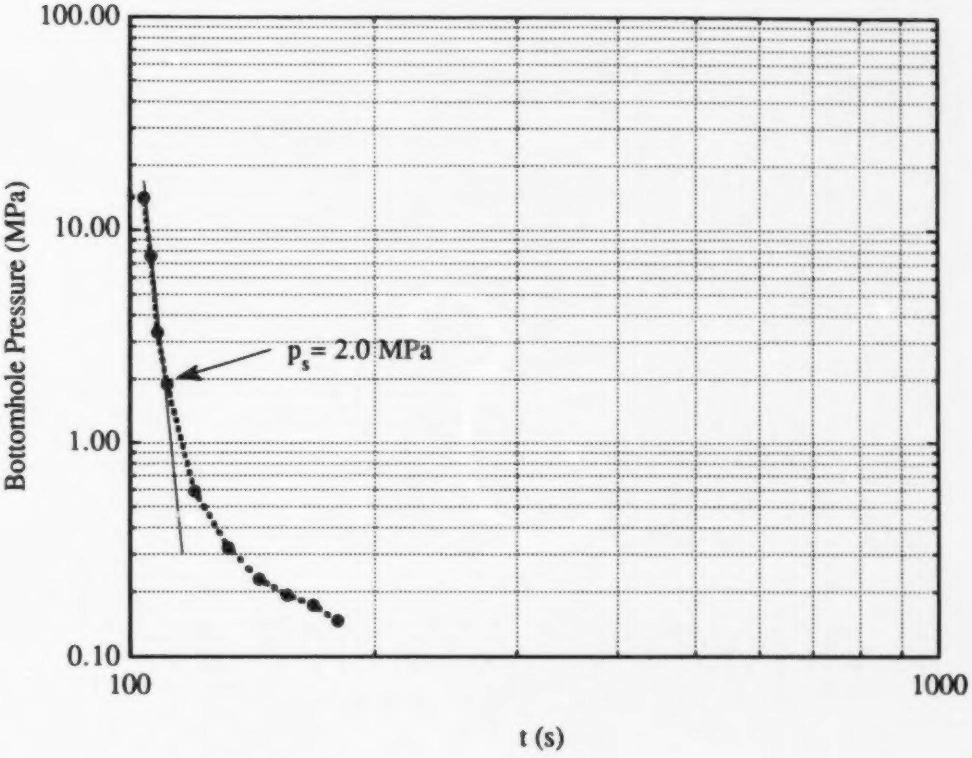

Hydraulic Fracture Test 3 Shut-in in Cycle-1

Figure 5.23 log p_w vs log t Method

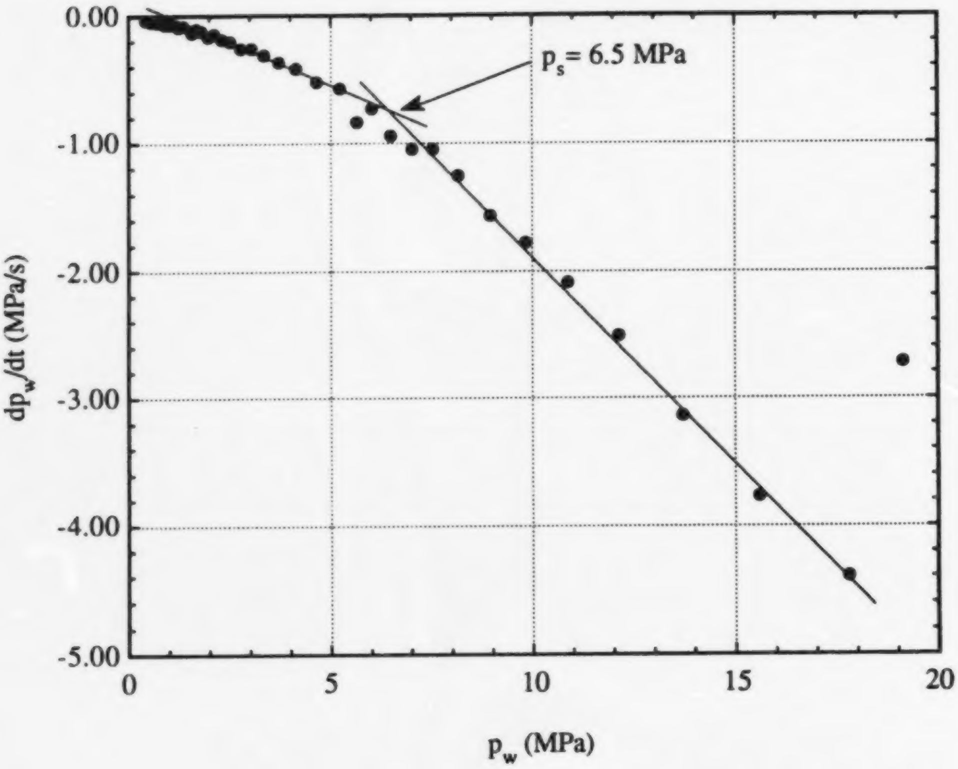

Hydraulic Fracture Test 5 Shut-in in Cycle-2

Figure 5.24 dp_w/dt vs p_w Method

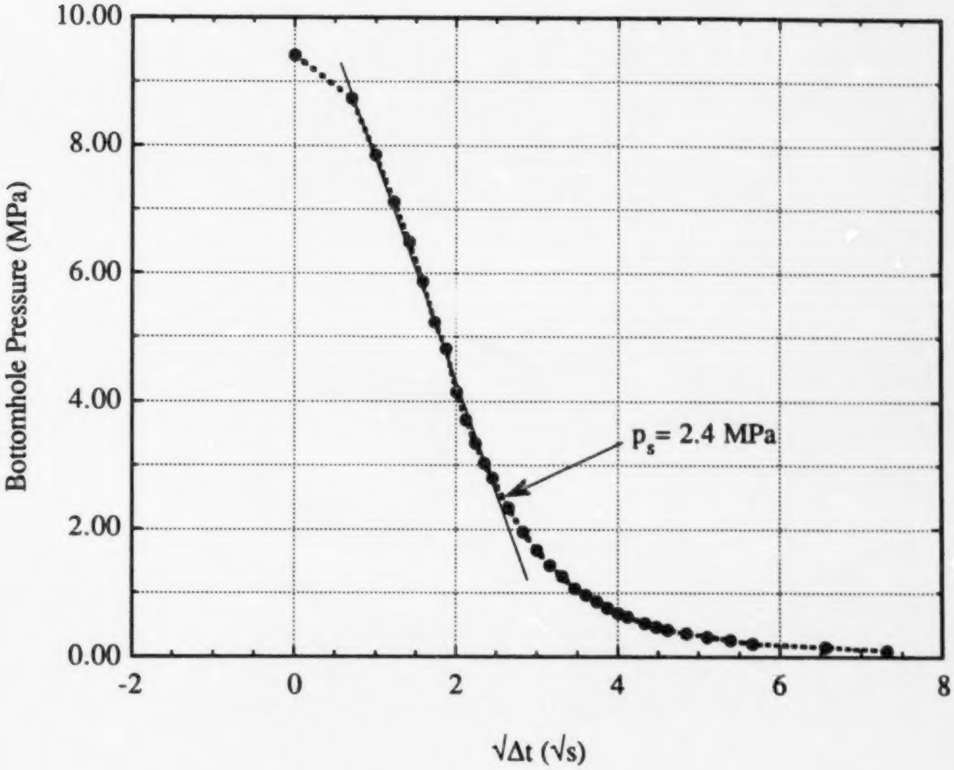

Hydraulic Fracture Test 3 Shut-in in Cycle-2

Figure 5.25 p_w vs $\sqrt{\Delta t}$ Method

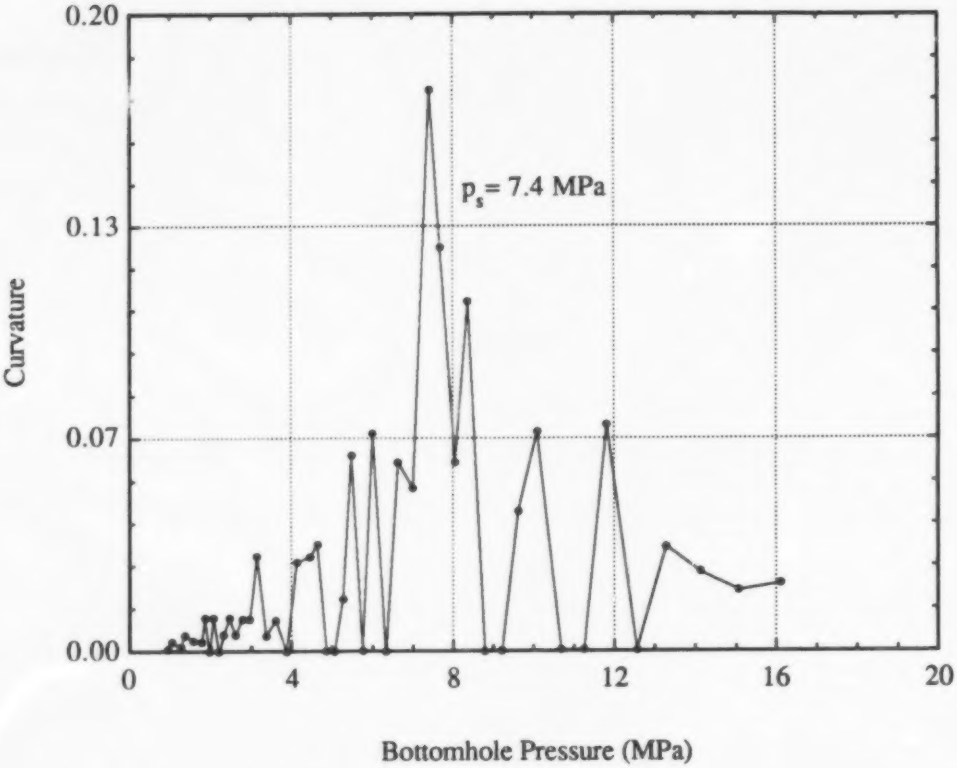

Hydraulic Fracture Test 9 shut-in in Cycle-3

Figure 5.26 Maximum Curvature Method

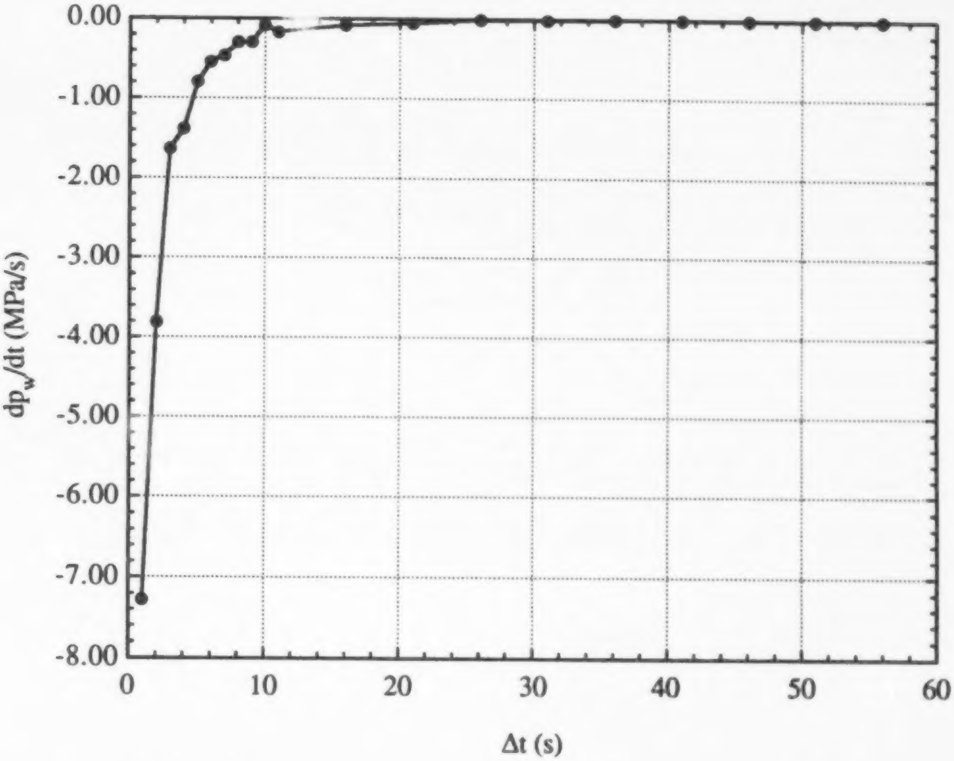

Figure 5.27 Hydraulic Fracture Test 16: Shut-in in Cycle-1

Chapter 6

Conclusions

Hydraulic fracturing is a process whereby a fluid is pumped into a well at a rate and pressure high enough to overcome the in situ confining stress and tensile strength of a formation so that a fracture or parting forms. This process, as a powerful technique, has widely been used to determine in situ stresses in rock engineering, and to enhance either injectivity or recovery in the petroleum and geothermal energy industries. To understand and improve this technique, more than 2000 publications have appeared in the technical literature. Despite its wide applications and numerous efforts contributed to it, several aspects of hydraulic fracturing are not well developed such as inadequate data for verification of the numerical models, lack in understanding of the breakdown mechanism, and little knowledge of well communication by hydraulic fracturing. Two sets of controlled hydraulic fracturing experiments have been undertaken to make such a contribution. The main conclusions drawn from this experimental study are summarized below.

6.1 Single Well Hydraulic Fracturing and Fracture Propagation

Twenty-three hydraulic fracture tests have been conducted in a large test frame which is capable of taking a block specimen of 610 x 584 x 305 mm (24" x 23" x 12") and applying true triaxial stresses up to 10 MPa (1,450 psi). Leak-off was incorporated. Boundary displacement was instrumented. Effects of the least principal stress and the injection rate on fracture propagation were studied. The bottomhole pressure monitored was analyzed by the radial flow model and the fracture pressure analysis technique based on 2D hydraulic fracture models. The breakdown pressure was compared with various breakdown models. The methods to determine the least principal stress were evaluated. From these tests, the following conclusions were drawn.

Before Breakdown

The fracture has been initiated in this region. A sudden change in the slope of the bottomhole pressure versus time curve illustrates the existence of the fracture. Although the fracture has been initiated in this region, the radial flow dominates the leak-off of the fracture fluid. Consequently, a circular oil penetration area is left in the specimen. This also indicates that the fracture is narrow. As a result of the radial flow, fracture propagation is stable, and the bottomhole pressure increases with fracture extension. Although radial flow prevails, the prediction of the build-up of the bottomhole pressure, as illustrated by the theoretical analysis, is still a complex process. This is because the wellbore storage, the skin effect, and the change in permeability caused by the change of effective stress have a strong influence on the build-up of the bottomhole pressure.

Breakdown

Abnormally high breakdown pressures were observed in all the tests. The statistical analysis revealed that the breakdown pressure is related to σ_3 rather than the $3\sigma_3 - \sigma_{hmax}$. To explain these phenomena, various breakdown models are evaluated. The classical breakdown equation and various methods to determine the tensile strength are first evaluated. Bredehoeft's fracture reopening pressure gives an extremely variable tensile strength (from 0.35 to 11.75 MPa). The tensile strength from Brazilian tests predicts too low a breakdown pressure. The apparent tensile strength seems to make sense. However, it depends on specimen size and cannot explain the latter phenomenon. The effect of fluid penetration complicated the explanation of fracturing process. The fluid penetration changes the pore pressure in the formation. This change in the pore pressure is equivalent to transferring a surface load acting on the wall of a well and the fracture into a distributing body force $\partial p/\partial r$. The effect of it on the breakdown pressure is illustrated by the breakdown equation based on the poroelastic theory. The breakdown pressure is decreased. Shear failure is possible when the injection rate and viscosity of fracture fluid are so low that the pore pressure increase in the formation is almost uniform. Shear failure also results in a low breakdown pressure. Ito's point stress model predicts the fracture initiation pressure, not breakdown pressure. All these models cannot explain the extremely high breakdown pressure.

The fracture mechanics model is a promising model. The bottomhole pressure increases before breakdown, which indicates that the fracture is not propagating or is propagating stably. The bottomhole pressure decreases after the breakdown, which indicates that the fracture is propagating unstably. Therefore, the breakdown pressure is the onset of the unstable fracture propagation. This is identical with the assumption in the fracture mechanics model. It should be stressed that fracture criterion for the unstable fracture propagation is $K_I - K_{Ic} = 0$ and $\partial(K_I - K_{Ic})/\partial L \geq 0$, not only $K_I - K_{Ic} = 0$. Introduction of $\partial(K_I - K_{Ic})/\partial L \geq 0$ makes it possible to explain the several phenomena such as rate-dependent, size-dependent, fracture fluid-dependent, and σ_3-dependent responses and the high breakdown pressure.

The flow of the fracture fluid also reveals insight to the breakdown pressure. The experimental results show that radial flow dominates leak-off before breakdown. The linear flow along the fracture dominates flow of the fracture fluid after breakdown, and leak-off from the fracture into the rock is the main leak-off mode after breakdown. The breakdown is a transient point between the two flow modes.

In brief, the analysis and experiments seem to show that the breakdown is a point in the process of fracture propagation. At this point, the flow of the fracture fluid transfers from the mode dominated by the radial flow into the mode dominated by the linear flow along the fracture, and fracture propagation transfers from stable into unstable fracture propagation.

Post-Breakdown

The experimental results show that the fracture pressure declines after breakdown. The fracture propagates in the manner similar to the GdK and the radial models. However, the models are able to predict quantitatively only part of the pressure-time curve. The other parts of the curve have such a rapid decline or such a slow decline that the models fail to predict. The occurrence of these unpredictable parts depends on the testing conditions. When a high injection rate or a low least principal stress is applied, a rapid decline usually follows the breakdown. If the injection rate is low, or the least principal stress is very high, a slow decline appears.

The analysis shows that this is due to the introduction of two simplifications in the 2D models to obtain closed-form solutions. The first assumption is the leak-off model used. The leak-off model assumes that leak-off velocity is equal to $C/\sqrt{t}$, where C is a constant called the leak-off coefficient. It is not related to the pressure or hydraulic gradient, the viscosity of the fracture fluid, or the permeability of the formation. This leak-off model underestimates the upper limit of the decline in fracture pressure so that the slow decline cannot be predicted. The other assumption is the mass conservation. The mass conservation equation in the hydraulic fracturing models assumes that the injection rate is equal to the rate of leak-off plus the rate of change in fracture volume. It implies that the fracture fluid fills all the fracture space. Actually, the fracture fluid does not always fill the whole fracture space, especially in the region just after breakdown for the high injection rate and the low least principal stress. As a result, the models is not able to predict the rapid decline in fracture pressure.

Shut-in Pressure

The existing methods are capable of estimating the least principal stress from the shut-in curve even though the leak-off is incorporated and the shut-in pressure is indistinct. Eight methods are compared with the experimental results. The comparison shows that p_w vs log $(t+\Delta t)/\Delta t$ method, p_w vs log Δt method, and log (p_w-p_a) vs Δt method are able to obtain the shut-in pressure close to σ_3 if the shut-in curve following the first injection cycle is used in the plot of p_w vs log $(t+\Delta t)/\Delta t$ and the plot of p_w vs log Δt, and the shut-in curves in the subsequent injection cycles are used in the plot of log (p_w-p_a) vs Δt. Inflection point method, log p_w vs log t method, dp_w/dt vs Δt method, p_w vs $\sqrt{\Delta t}$ method, and the maximum curvature method can sometimes obtain the shut-in pressure close to σ_3. However, the results are unstable.

6.2 Double well Hydraulic Fracturing and Well Communication

The possibility of well communication by hydraulic fracturing depends on the interaction of fractures driven hydraulically. The interaction of fractures is affected by many factors. Among the more important are the angle between the well line and the direction of the maximum horizontal stress, the state of stress (the ratio among three principal stresses, or stress difference), the well spacing, the injection procedure, and the injection rate. In this program, a new injection procedure–injecting simultaneously oil into two wells–was used. The effect of the angle between the well line and the direction of the maximum horizontal stress on well communication was studied systematically. The angle ranged from 0° to 60°. Two states of stress were applied. From the ten double well hydraulic fracture tests conducted on 610 x 584 x 305 mm (24" x 23" x 12") Gypstone blocks, the following conclusions are drawn.

For a low stress difference (σ_1/σ_3 is around 1.5), well communication by hydraulic fracturing is still possible for ß as high as 60°. The orientation of fracture initiation under this low stress difference is hard to predict by the state of stress on the wall of wells because other factors such as anisotropy of permeability and strength of rocks play a dominant role. The rotation of fractures was observed during fracture propagation.

For a high stress difference (σ_1/σ_3 is around 2), well communication by hydraulic fracturing is possible for ß up to 30°. A high stress difference makes well communication difficult. The orientation of fracture initiation is under control for this high stress difference. The orientation of fracture initiation is capable of being predicted by the state of stress on the wall of wells.

Appendix A

Measurements of Properties of Gypstone

A.1 Measurements of Physical Properties

See Table A.1.

A.2. Measurements of Tensile Strength

Two sets of the tensile tests were conducted. One incorporated eight Brazilian tests. The specimens for Brazilian tests were cored from a 305 x 305 x 305 mm (12" x 12" x 12") block specimen. The other was seven splitting tests. The specimens for splitting tests were cylindrical specimens fabricated according to the same procedure as the block specimens. The Brazilian tests were conducted without steel loading jaws. The testing procedures and interpration of experimental results follow "Suggested Methods for Determining Tensile Strength of Rock Materials" by International Society for Rock Mechanics [1-3]. The splitting tests were conducted and interpreted according to ASTM Standards, D3967-86–

"Standard Test Method for Splitting Tensile Strength of Intact Rock Core Specimens." [4].

The experimental results are listed in Tables A.2 and A.3. All the specimens failed in tensile failure mode. Fractures were perfect planes.

A.3 Measurement of Deformation and Shear Strength

Twenty-seven triaxial tests were conducted. The objective of them was to supply deformation and strength behavior of Gypstone. Fourteen of them were conducted under saturated and drained conditions. The other 13 were run under natural water content, and three strain rates were used. The deformation and strength parameters of Gypstone and the effects of water and strain rate were obtained.

The specimens for the triaxial compressive tests were cylinders with 75 mm (3") diameter and 150 mm (6") height. The specimens for the drained triaxial compressive tests came from two sources. Six of them were cored from a 305 x 305 x 305 mm (12" x 12" x 12") block specimen. They were counted in T#number or B#number, where T means specimens from the top of the block, and B means specimens from the bottom of the block. The others were directly fabricated in the same procedure as that of the block specimens. The specimens for the tests under natural water content were fabricated according to the same procedure as that of block specimens.

The tests were strain-controlled. The saturated and drained triaxial tests were run at a constant strain rate of 1×10^{-6} s^{-1}. The triaxial tests under natural water content were run at a strain rate of $8.4 \times 10^{-6}\ s^{-1}$, $8.4 \times 10^{-5}\ s^{-1}$, and $4.2 \times 10^{-4}\ s^{-1}$, respectively.

Failure for the saturated and drained tests were ductile. No failure planes were found. For the tests under natural water content, cracks were visible during testing. At failure, some parts of the specimens were crushed, or a failure plane developed. The experimental results are summarized in Tables A.4 and A.5, Figure 1, and Figure A.1.

A.4 Measurements of Hydraulic Conductivity

Hydraulic conductivity of Gypstone was measured in the saturated and drained triaxial tests. The layout of the tests is shown in Figure A.1. The top of a specimen was connected to a big water reservoir with constant air pressure. In the triaxial tests, this reservoir was used to apply and obtain constant pore pressure in specimens. In permeability tests, it is the source of water. The bottom of a specimen was connected to a pressure transducer and a valve that was used to control the flow rate.

The tests were run after the B test and before the triaxial test. The pore pressure at the top of the specimen was maintained constant, and the pore pressure at the bottom of the specimen was changed through leaking off water from the specimen at the bottom of the specimen. After the pressure at the bottom of the specimen stabilizes, the flow rate was measured. Then, the pressure at the bottom of the specimen was changed to a different value; consequently, a group of the flow rates was obtained. Through them, the hydraulic conductivity of Gypstone was obtained. The results of seven permeability tests are listed in Table A.6. Hydraulic conductivity of Gypstone ranges from 4.14 x 10^{-4} to 4.09 x 10^{-5} cm/s (0.43 to 0.4 μm^2).

A.5 References

1. Bieniawski Z. T. and Hawkes I. Suggested methods for determining tensile strength of rock materials. *Int. J. Rock Mech. Min. Sci. & Geomech. Abstr.* **15**, 99-103 (1978).

2. Anderson K. O. and Hahn W. P. Design and evaluation of asphalt concrete with respect to thermal cracking. proceedings Association of Asphalt Paving Technologists, Vol 37, pp 1-31 (1968).

3. Mellor M. and Hawkes I Measurement of tensile strength by diametral compression of discs and annuli. *Engng Geol.* **5**, 173-225 (1971).

4. ASTM Standards, D3967-86–Standard test method for splitting tensile strength of intact rock core specimens.

5. ASTM Standard, D854-83–Standard test method for specific gravity of soils.

Table A.1 Physical Properties of Gypstone

Specimen No.	T#1	T#2	B#2	B#3	Average
Diameter (cm)	7.513	7.547	7.644	7.583	
Height (cm)	15.600	14.961	15.232	14.719	
Volume (cm^3)	691.58	669.27	699.02	664.74	
Total weight (g)	1199.38	1211.80	1242.89	1180.75	
Weight of solid(g)	1172.14	1184.20	1214.62	1151.91	
Weight of water (g)	27.24	27.60	28.27	28.84	
Volume of solid (cm^3)	450.13	454.76	466.44	442.38	
Volume of void (cm^3)	241.45	214.51	232.58	222.38	
Bulk density (kg/m^3)	1730	1810	1780	1780	1780
Dry density (kg/m^3)	1690	1760	1740	1730	1730
Void ratio	0.536	0.472	0.499	0.503	0.503
Porosity %	34.9	32.1	33.3	33.5	33.45
Water content %	2.32	2.33	2.33	2.50	2.37
Degree of saturation[*]	11.3	12.9	12.2	13.0	12.3

---

[*] Specific gravity: 2.604. The specific gravity was measured according to ASTM Standard D854-83–Standard Test Method for Specific Gravity of Soils [5].

Table A.2. Brazilian Tests

Specimen No.	Height mm	Diameter mm	Maximum load N	Tensile strength kPa
M#1	35.74	76.47	666	156
M#2	35.10	75.20	666	161
M#3	33.15	75.81	635	165
M#4	34.59	74.47	958	237
M#5	34.01	74.16	921	233
M#6	33.81	74.35	1030	261
M#7	35.38	70.56	-	-
M#8	35.71	72.80	1400	343

Table A.3. Splitting Tests

Specimen No.	Height mm	Diameter mm	Maximum load N	Tensile strength kPa
1*	152.30	75.80		
3*	153.90	75.35		
5*	151.80	75.50		
14	142.30	75.50	2600	154
18	149.10	75.75	2300	130
21	151.40	75.30	2600	145
22	150.20	75.30	2000	113

---

* The dry density of specimens 1, 3, and 5 was measured. They were dried at 110°C for 24 hours. Their tensile strength was almost zero. In addition, the cement between sand grains losed when they were put into water.

Table A.4 Summary of the Saturated and Drained Triaxial Tests

Specimen No.	σ_3 kPa	σ_1-σ_3 kPa	u kPa	ε_f	B	Strain rate s^{-1}
10	2.7	157.0	1056.0	0.008	–	1×10^{-6}
12	34.3	235.8	1052.2	0.009	0.882	1×10^{-6}
29	86.9	411.1	1004.1	0.017	0.813	1×10^{-6}
15	97.9	471.0	1000.1	0.020	0.720	1×10^{-6}
27	141.0	632.7	960.3	0.019	0.771	1×10^{-6}
23	250.4	941.5	847.8	0.022	0.560	1×10^{-6}
7	269.7	1094.5	788.1	0.031	0.363	1×10^{-6}
11	272.8	1111.8	823.5	0.029	0.427	1×10^{-6}
T#3	0	498.3	1091.0	0.007	–	1×10^{-6}
T#4	0	674.0	885.0	0.007	0.719	1×10^{-6}
T#1	93.8	825.4	995.9	0.011	0.860	1×10^{-6}
T#2	96.0	821.7	982.7	0.011	0.972	1×10^{-6}
B#4	270.1	1611.6	782.6	0.011	0.473	1×10^{-6}
B#1	271.6	1604.6	733.7	0.016	0.492	1×10^{-6}

Table A.5 Summary of the Triaxial Tests Under Natural Water Content

Specimen No.	σ_3 kPa	σ_1-σ_3 kPa	u kPa	ε_f	E MPa	Strain rate s^{-1}
26	0	536.1	no	0.0110	58	8.4×10^{-6}
24	104.4	1109.5	no	0.0190	88	8.4×10^{-6}
25	202.7	1655.2	no	0.0150	199	8.4×10^{-6}
16	303.5	2122.8	no	0.0200	163	8.4×10^{-6}
30	0	1686.0	no	0.0144	129	8.4×10^{-5}
31	106.768	2348.0	no	0.0135	239	8.4×10^{-5}
32	205.776	2610.0	no	0.0150	282	8.4×10^{-5}
33	308.134	3300.0	no	0.0176	323	8.4×10^{-5}
34	316.635	3174.0	no			8.4×10^{-5}
35	0	1451.0	no	0.0130	229	4.2×10^{-4}
36	113.111	2474.0	no	0.0145	243	4.2×10^{-4}
37	216.155	2697.0	no	0.0155	226	4.2×10^{-4}
38	299.392	2866.0	no	0.0170	259	4.2×10^{-4}

Table A.6 Summary of Permeability Tests

Specimen No.	Diameter mm	Height mm	σ_3 kPa	p_1 kPa	p_2 kPa	k cm/s
T#1	74.40	150.50	1096.89	1003.70	1003.70 to 936.34	2.08×10^{-4}
T#2	74.82	149.65	1080.94	982.55	982.55 to 912.34	2.93×10^{-4}
12	75.44	153.50	1099.87	1064.01	1064.01 to 956.24	1.13×10^{-4}
27	75.63	152.20	1106.68	973.73	973.73 to 800.06	1.28×10^{-4}
15	75.40	145.00	1099.4	1005.3	1005.3 to 939.2	4.04×10^{-4}
23	75.47	148.50	1100.9	849.2	849.2 to 783.0	4.14×10^{-4}
28	75.67	143.35	1113.1	1065.9	1065.9 to 0	4.09×10^{-5}

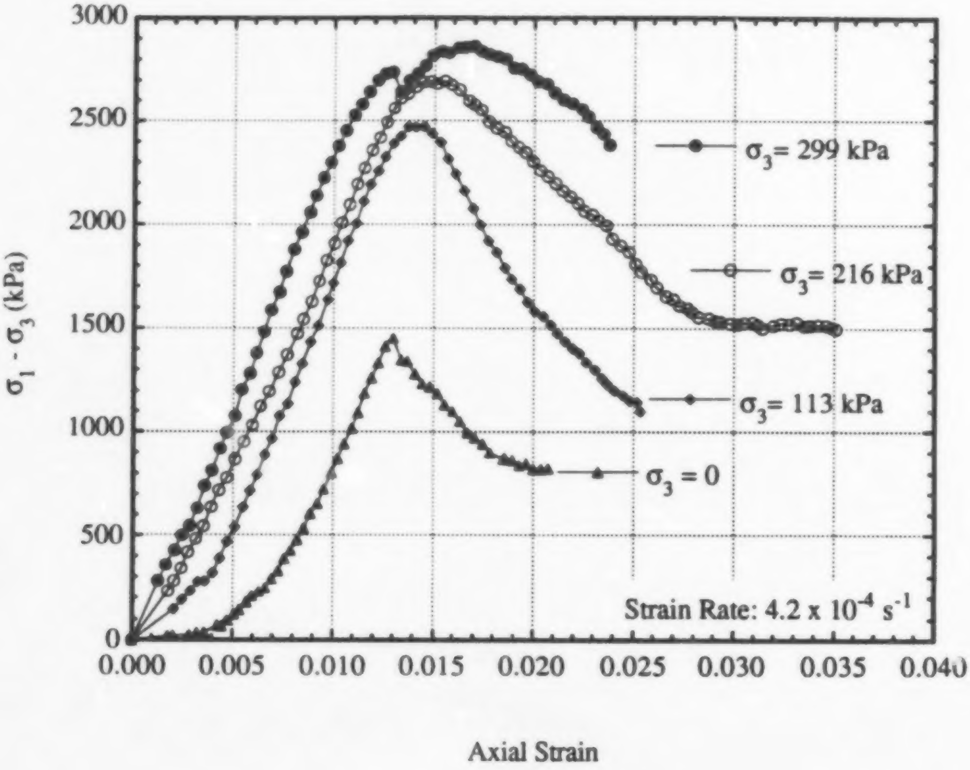

Figure A.1 Stress-Strain Curve of Gypstone under Natural Water Content

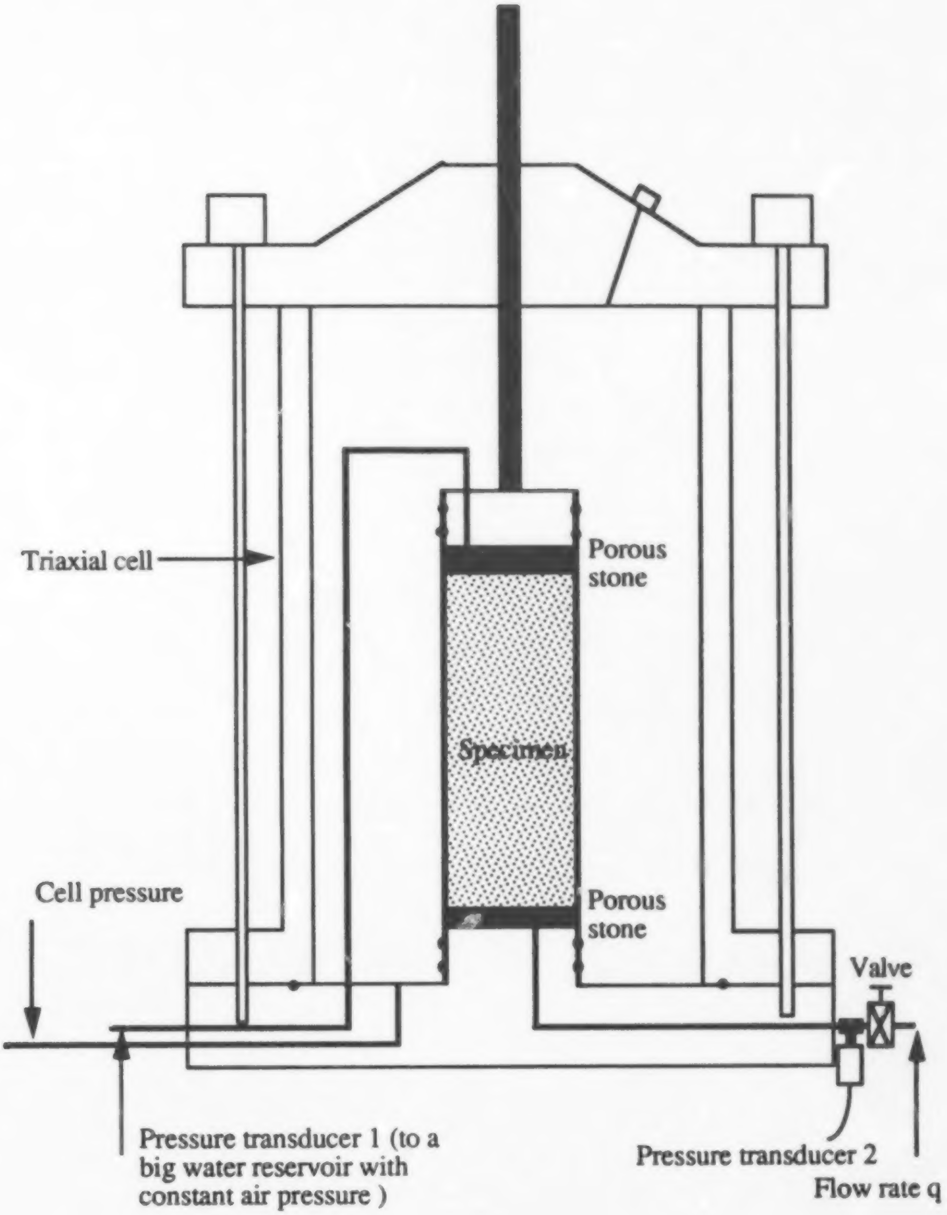
Triaxial cell
Porous stone
Specimen
Cell pressure
Porous stone
Valve
Pressure transducer 1 (to a big water reservoir with constant air pressure)
Pressure transducer 2
Flow rate q

Figure A.2 Layout of Permeability Tests

Appendix B

Injection Procedures, Bottomhole Pressure, Stresses, and Boundary Displacement Measured in Double Well Hydraulic Fracture Tests

The fractures induced in the double well hydraulic fracture tests have been described and discussed in Chapter 4. A representative instrumentation has also been shown in Chapter 4. This appendix presents the instrumentation (injection procedures, bottomhole pressure, stresses, and boundary displacement) for the rest double well hydraulic fracture tests.

a. Injection History

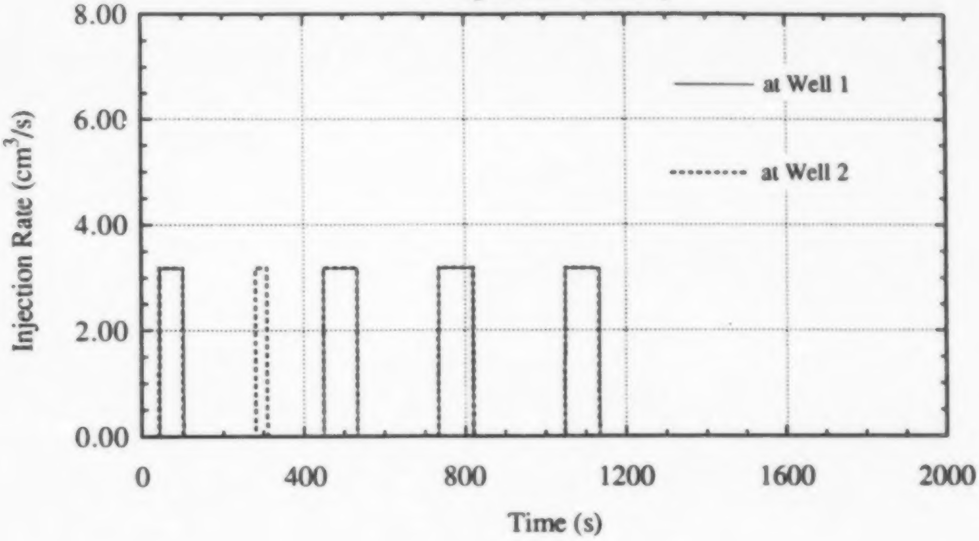

b. Bottomhole Pressure

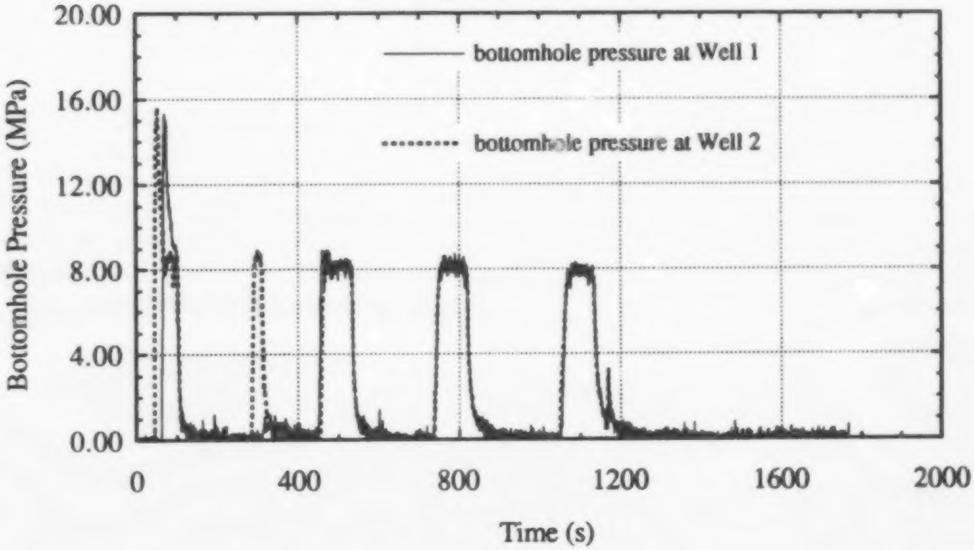

Figure B.1 Double Well Hydraulic Fracture Test 1

c. Principal Stresses

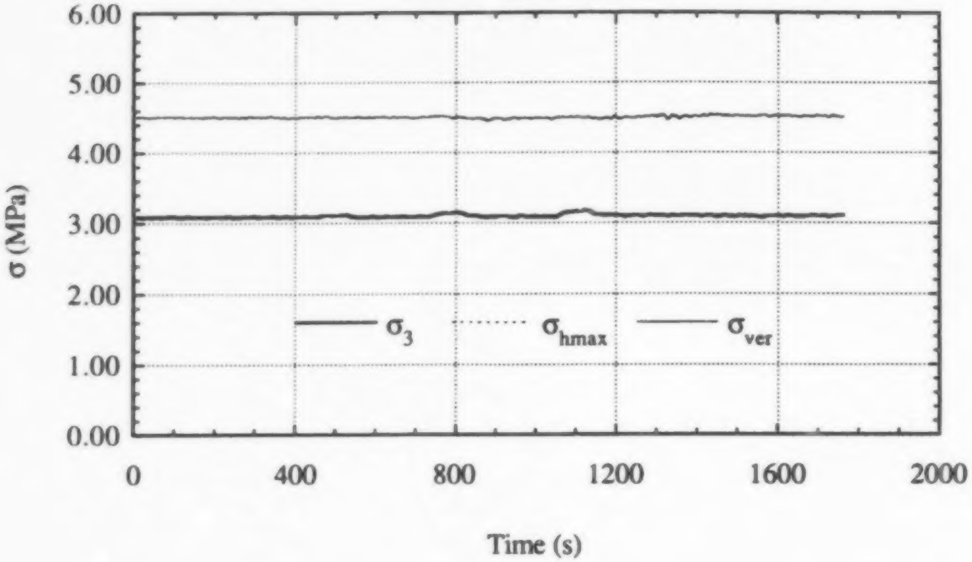

d. Boundary Displacements

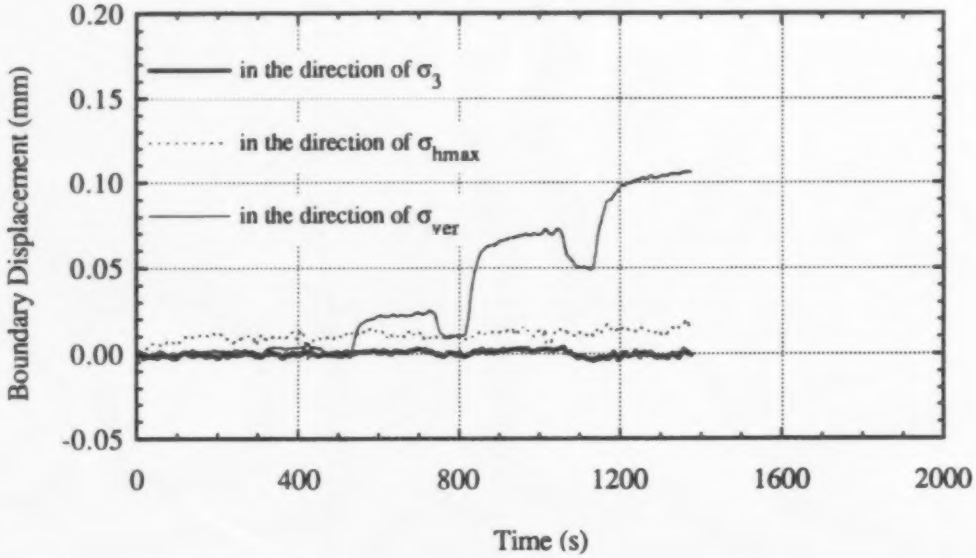

Figure B.1 Continued

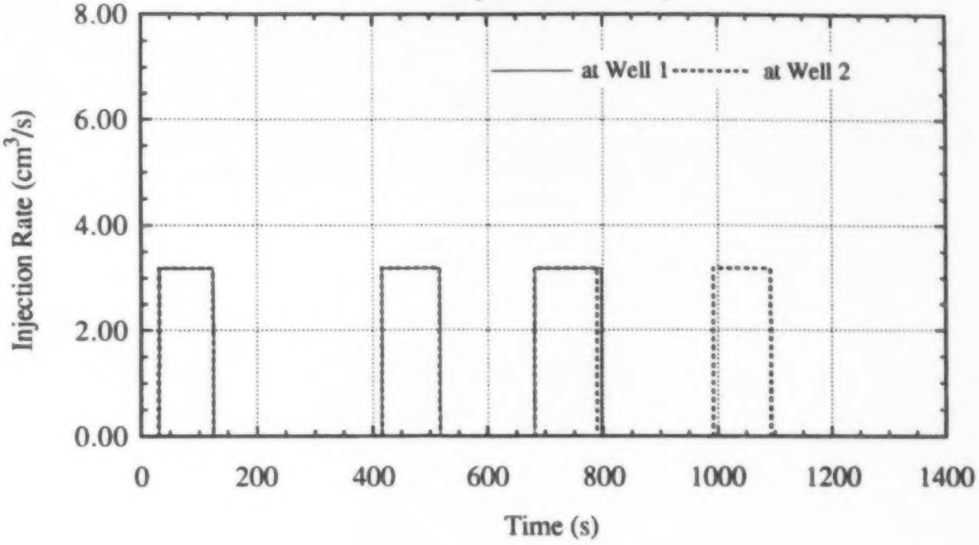
a. Injection History

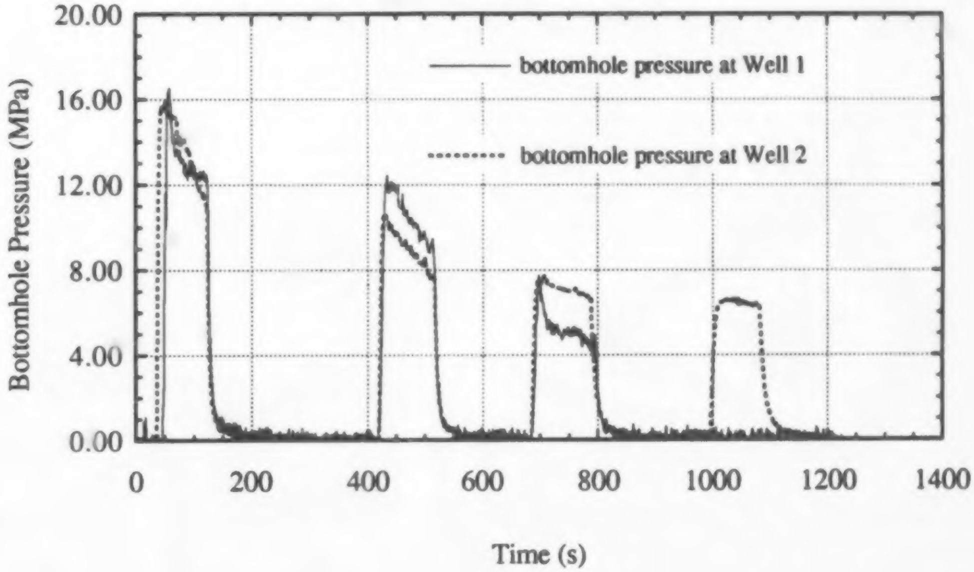
b. Bottomhole Pressure

Figure B.2 Double Well Hydraulic Fracture Test 2

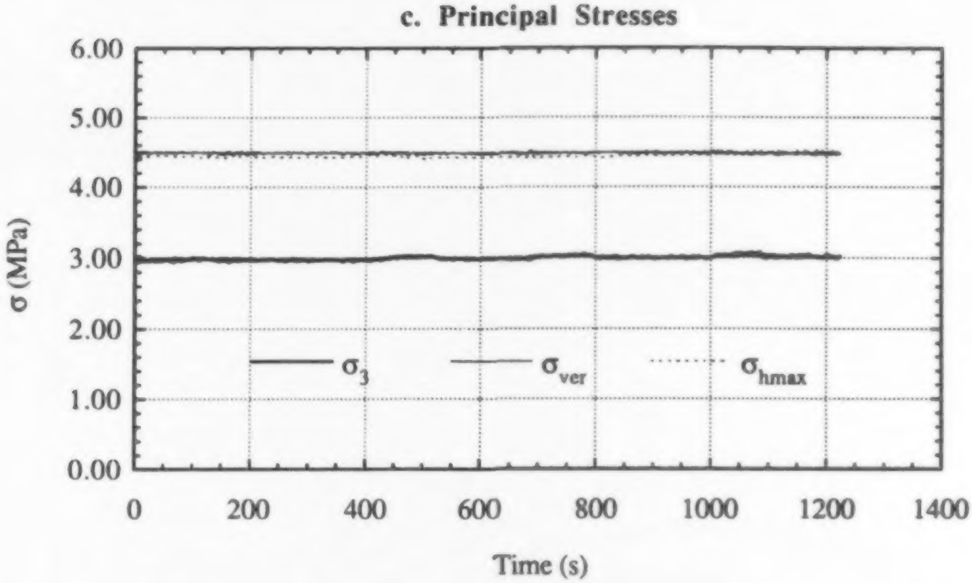

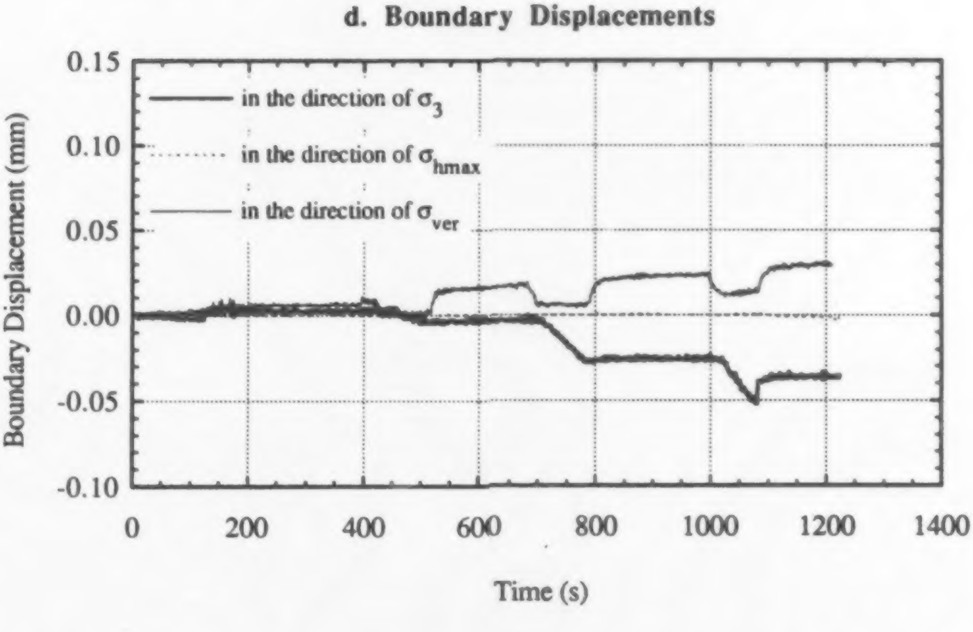

Figure B.2 Continued

a. Injection History

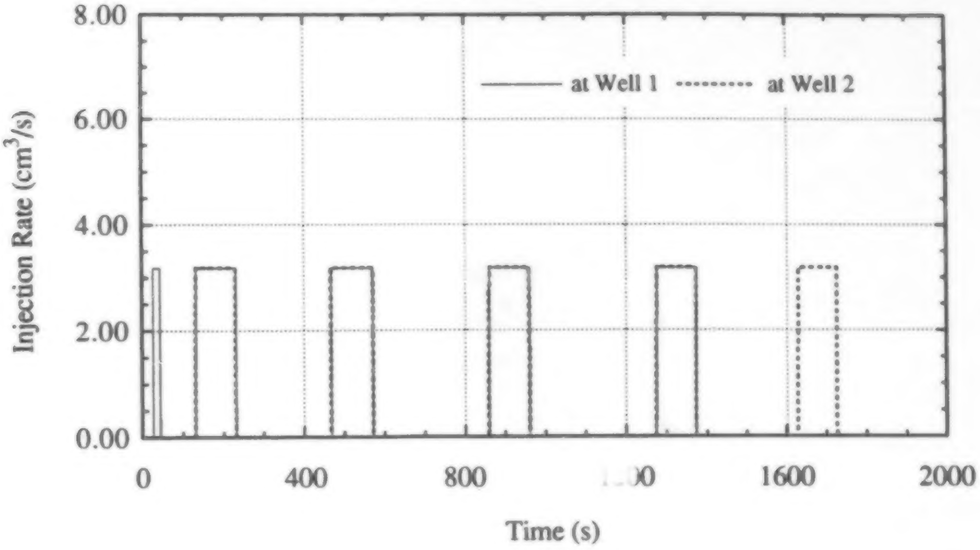

b. Bottomhole Pressure

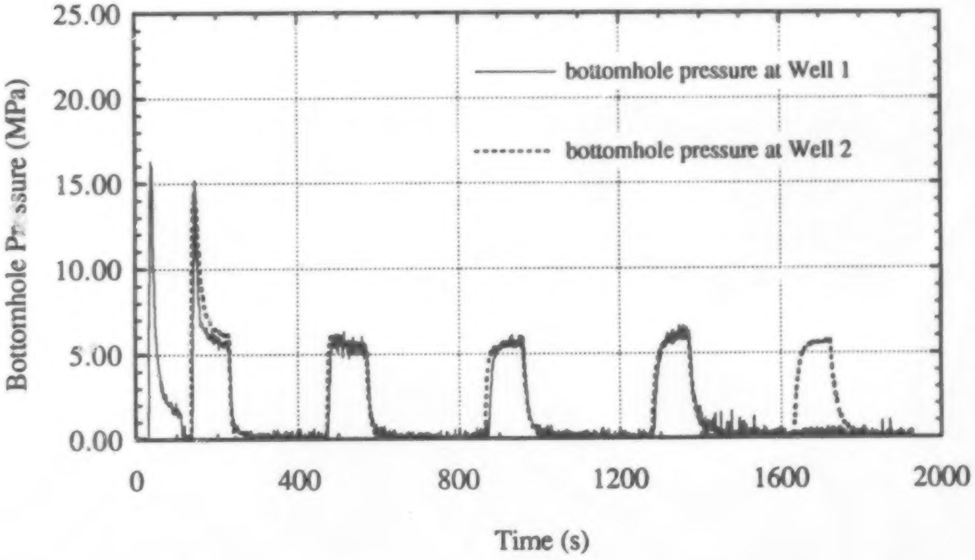

Figure B.3 Double Well Hydraulic Fracture Test 3

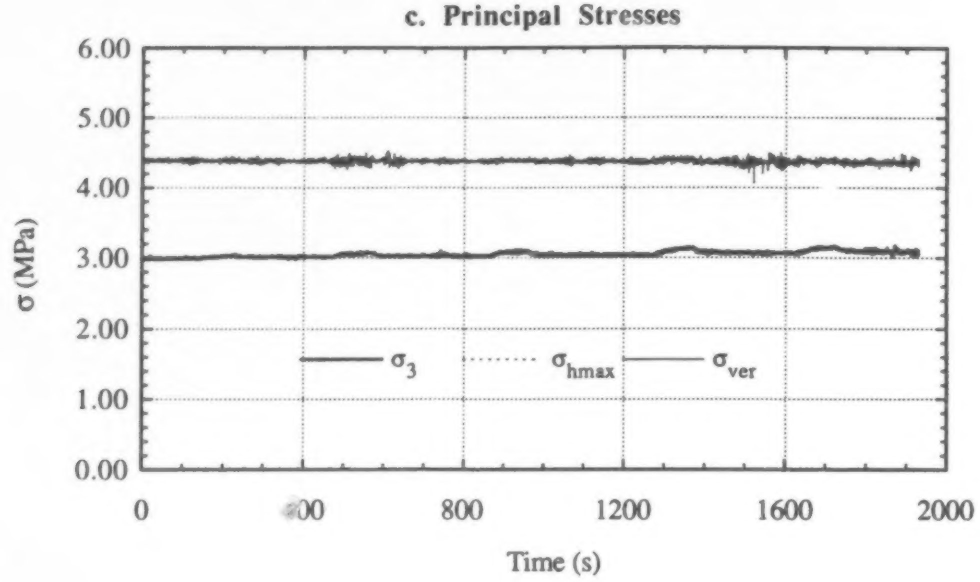

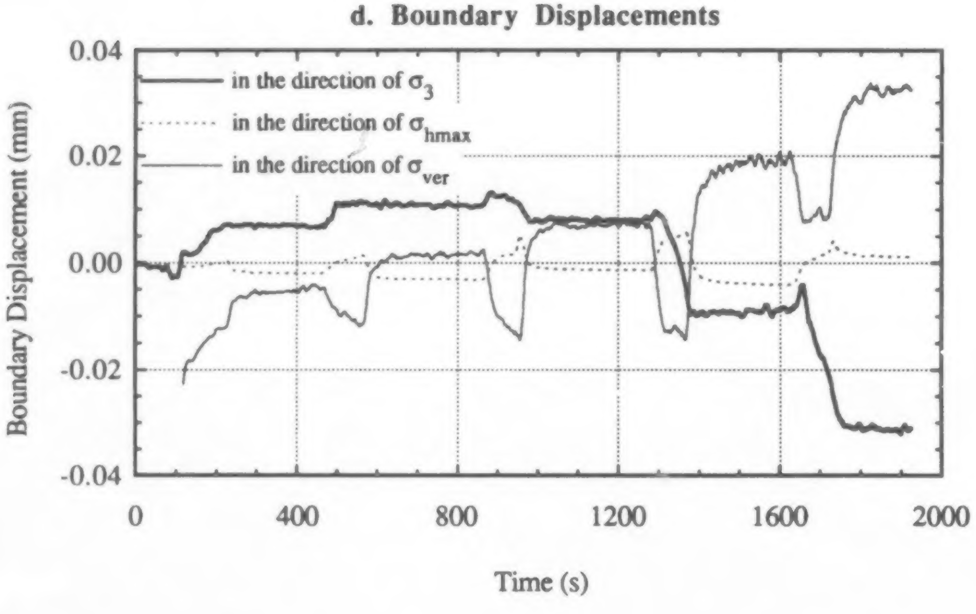

Figure B.3 Continued

a. Injection History

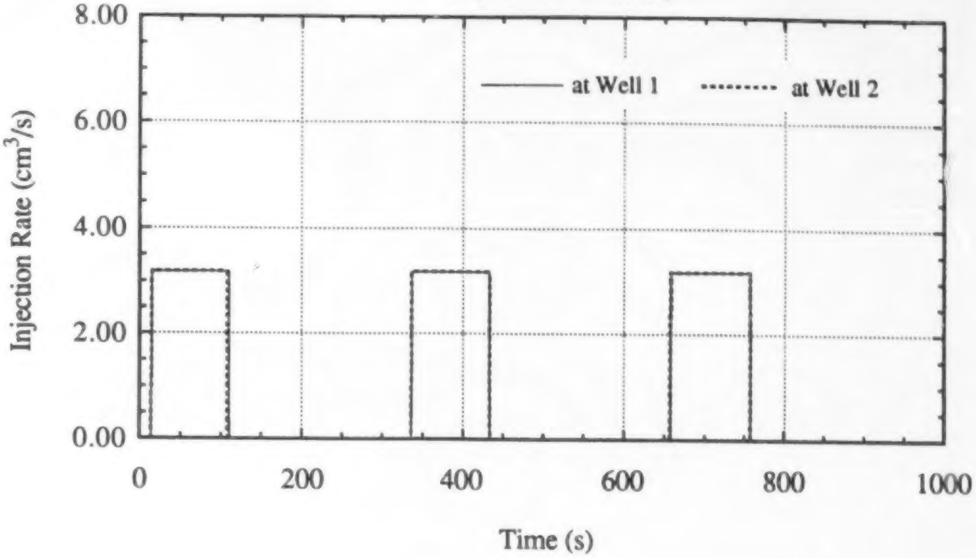

b. Bottomhole Pressure

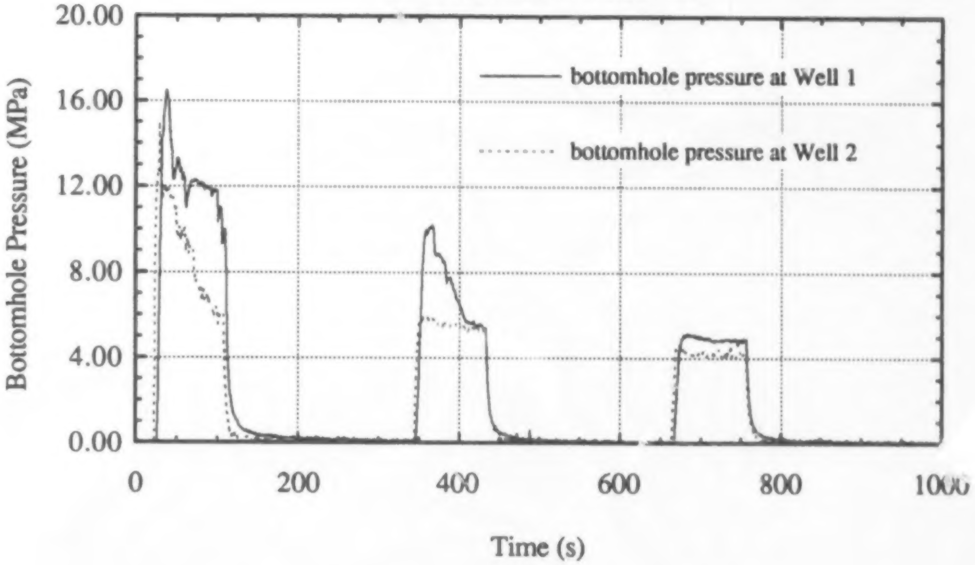

Figure B.4 Double Well Hydraulic Fracture Test 4

c. Principal Stresses

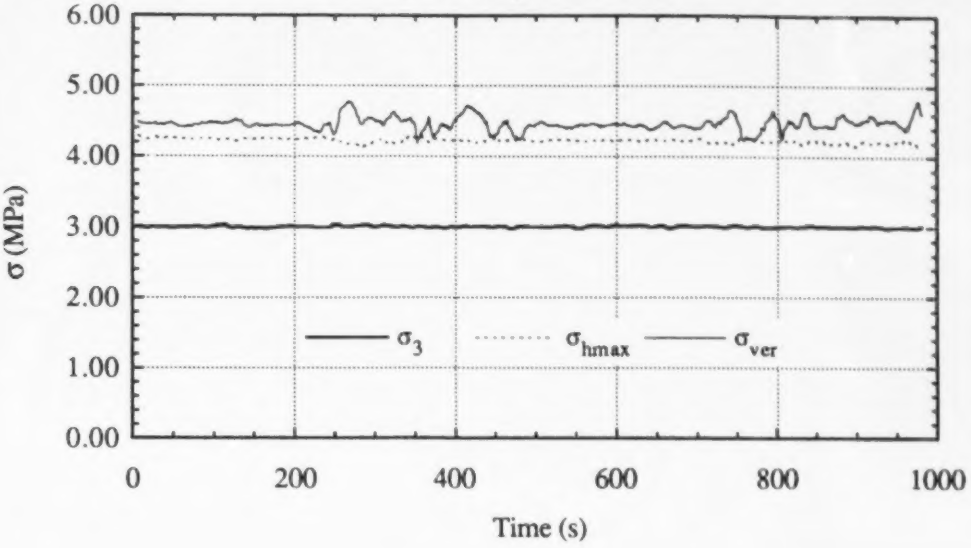

d. Boundary Displacements

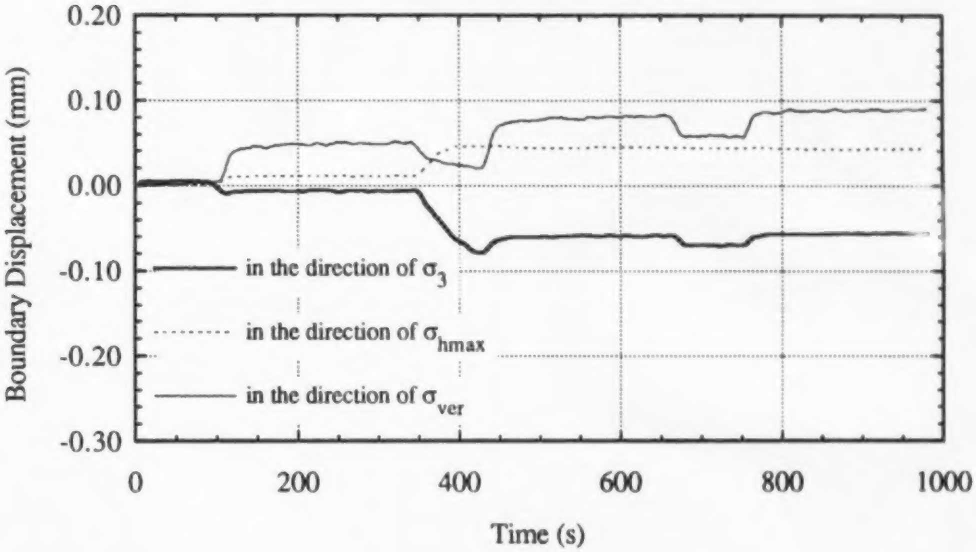

Figure B.4 Continued

a. Injection History

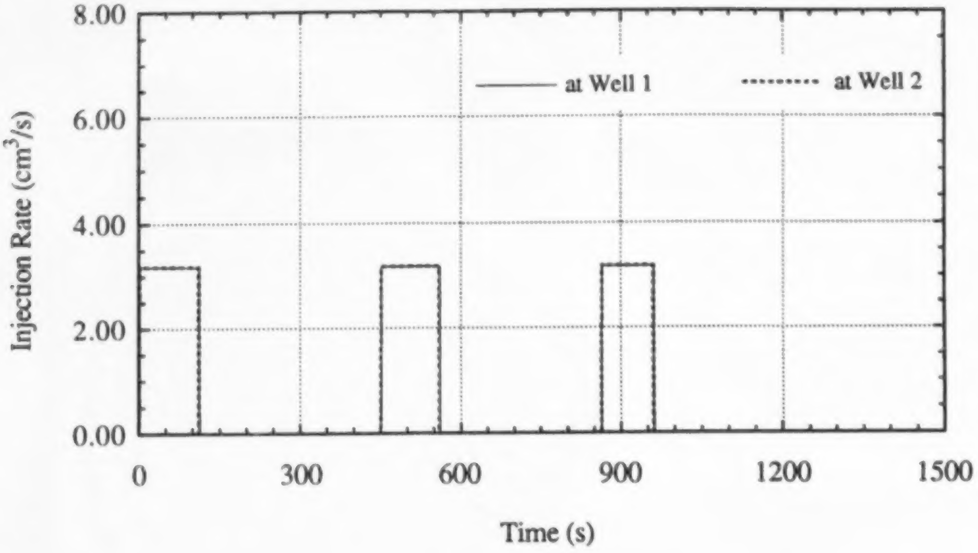

b. Bottomhole Pressure

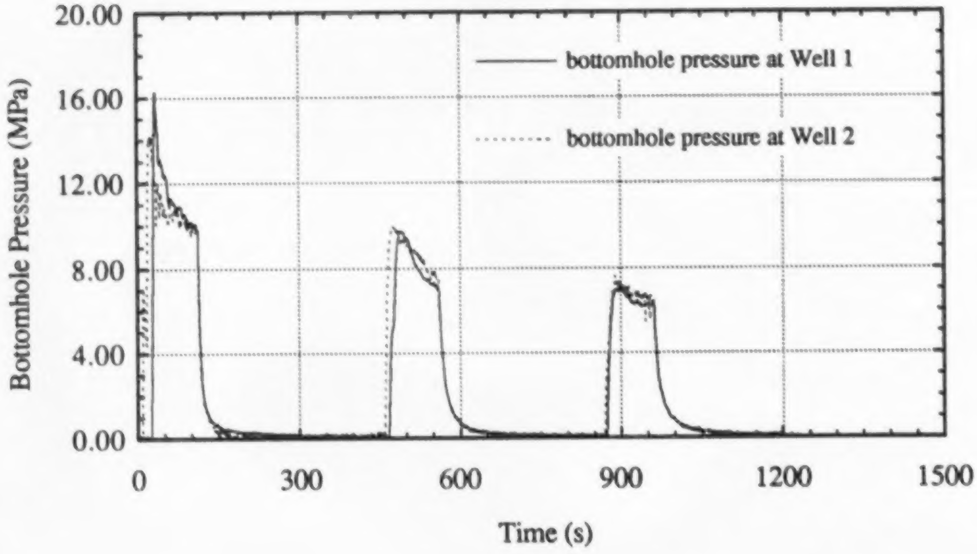

Figure B.5 Double Well Hydraulic Fracture Test 5

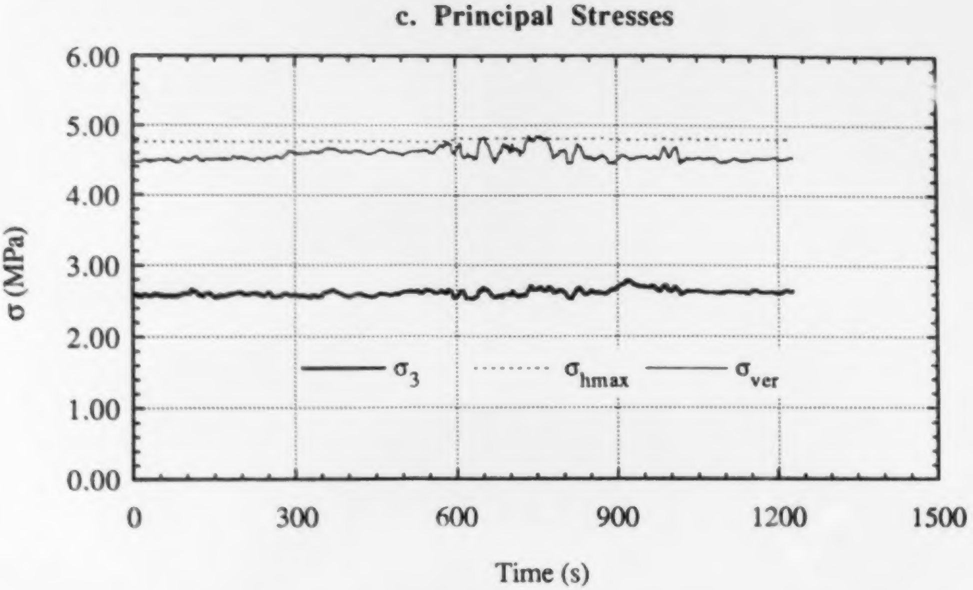

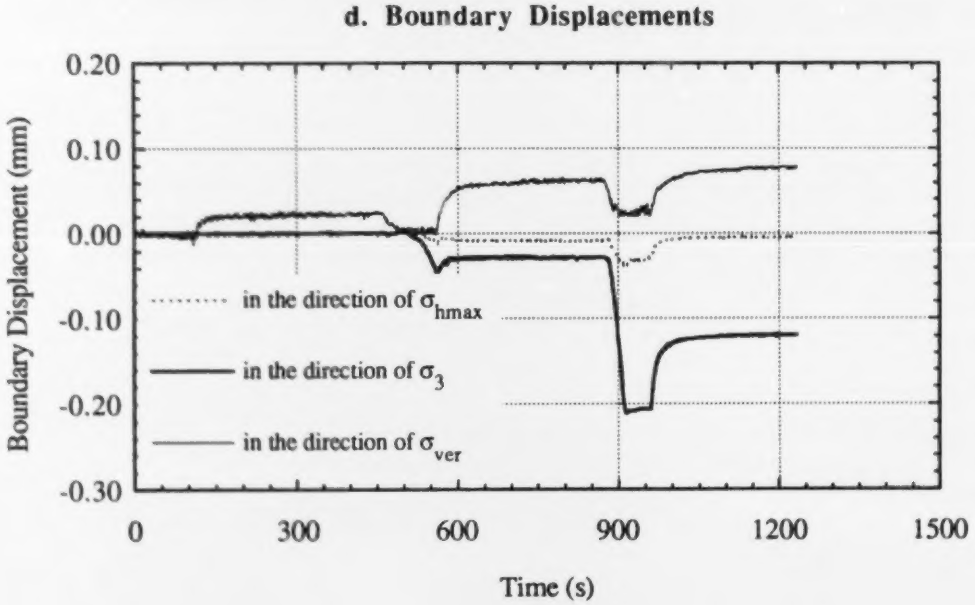

Figure B.5 Continued

a. Injection History

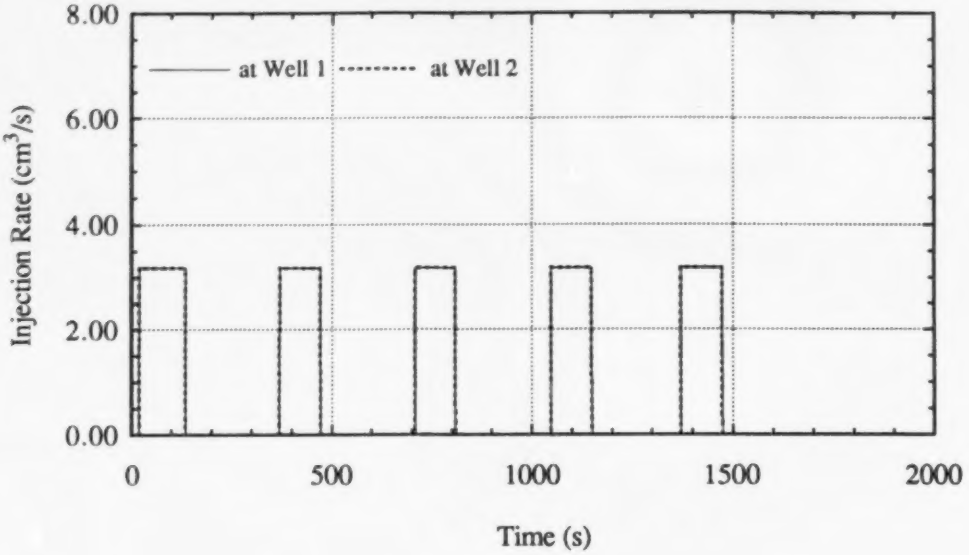

b. Bottomhole Pressure

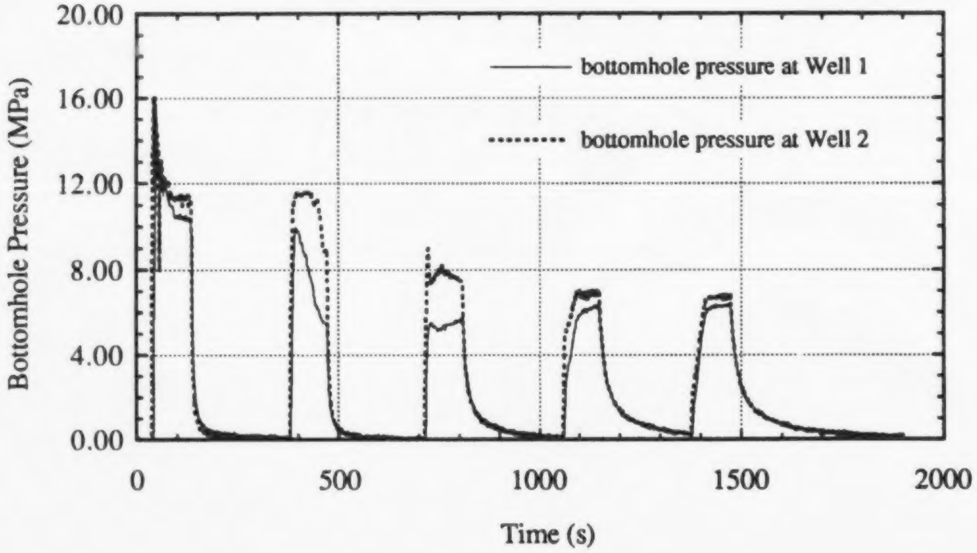

Figure B.6 Double Well Hydraulic Fracture Test 6

c. Principal Stresses

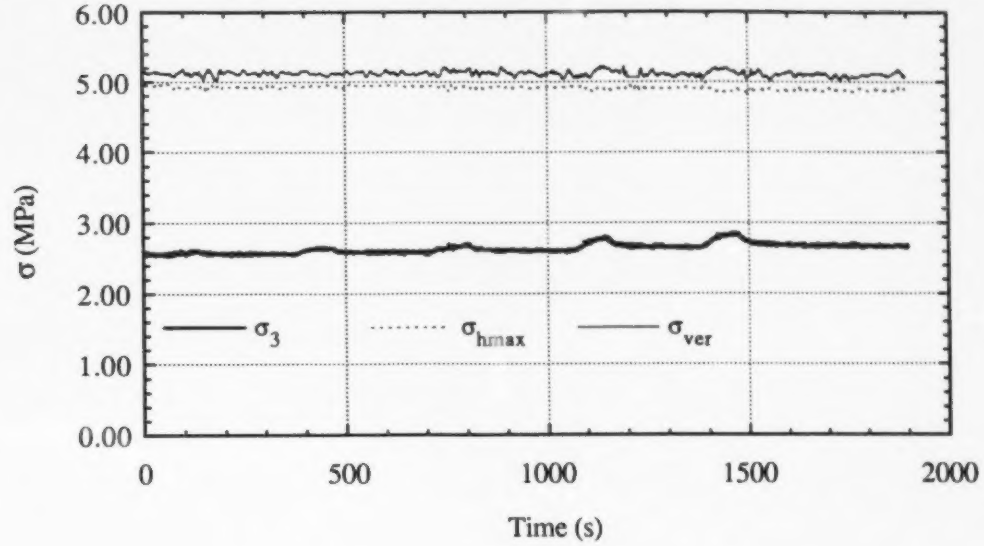

e. Boundary Displacements

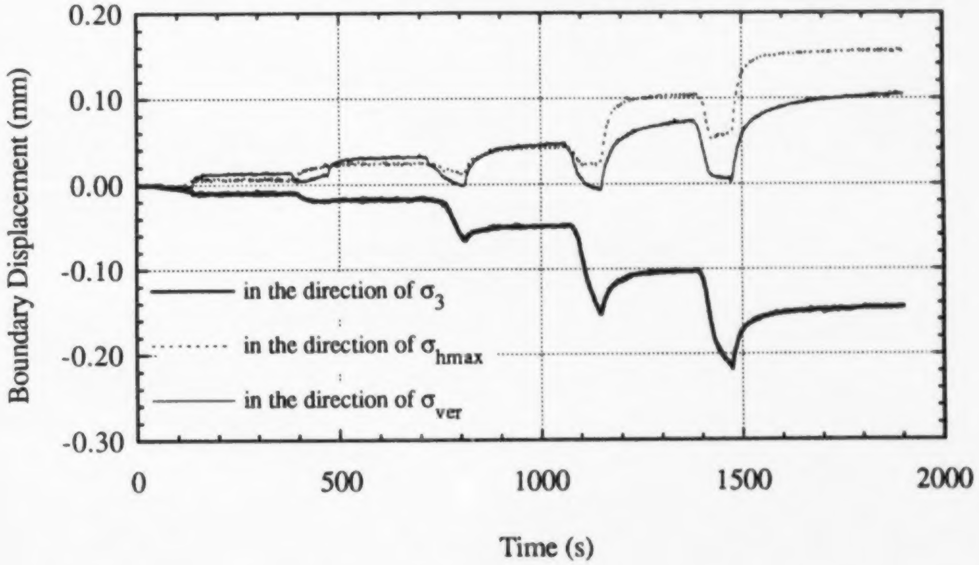

Figure B.6 Continued

a. Injection History

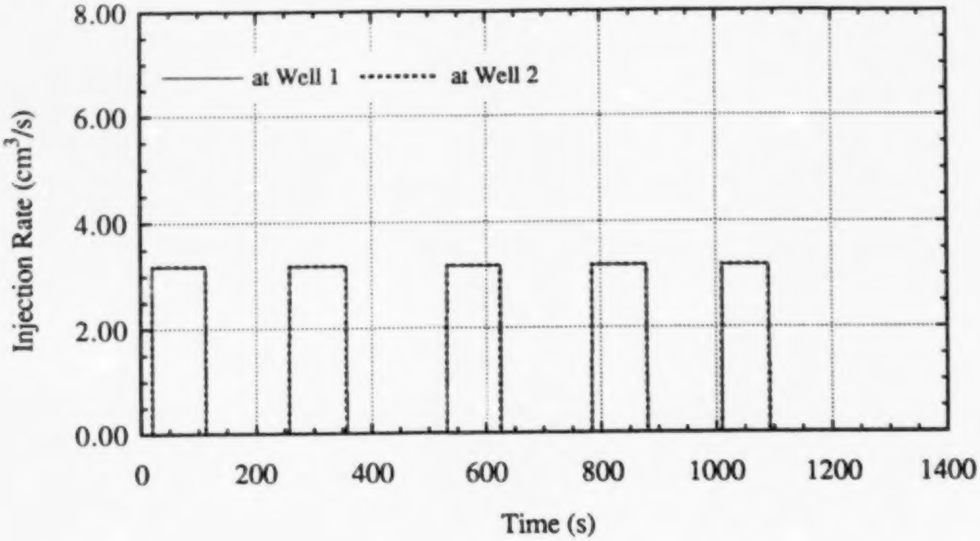

b. Bottomhole Pressure

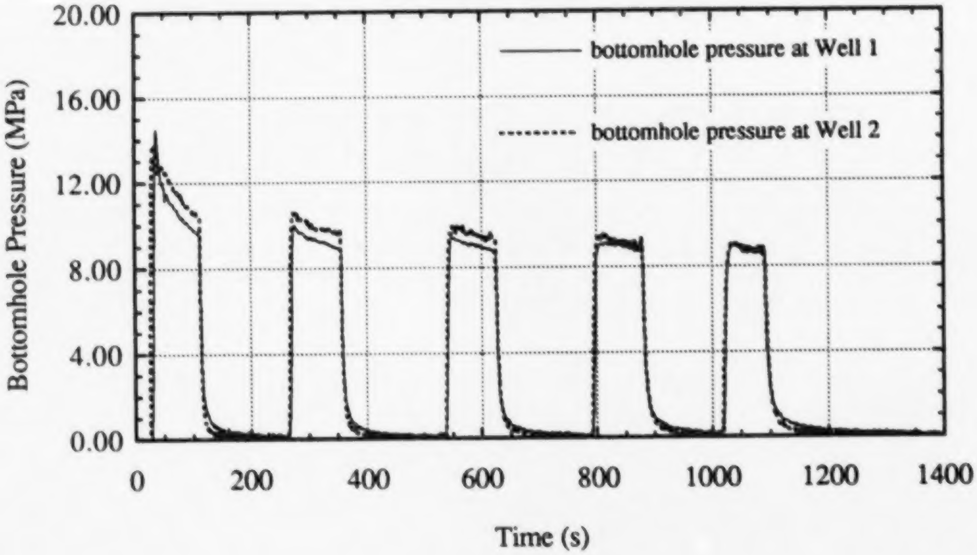

Figure B.7 Double Well Hydraulic Fracture Test 7

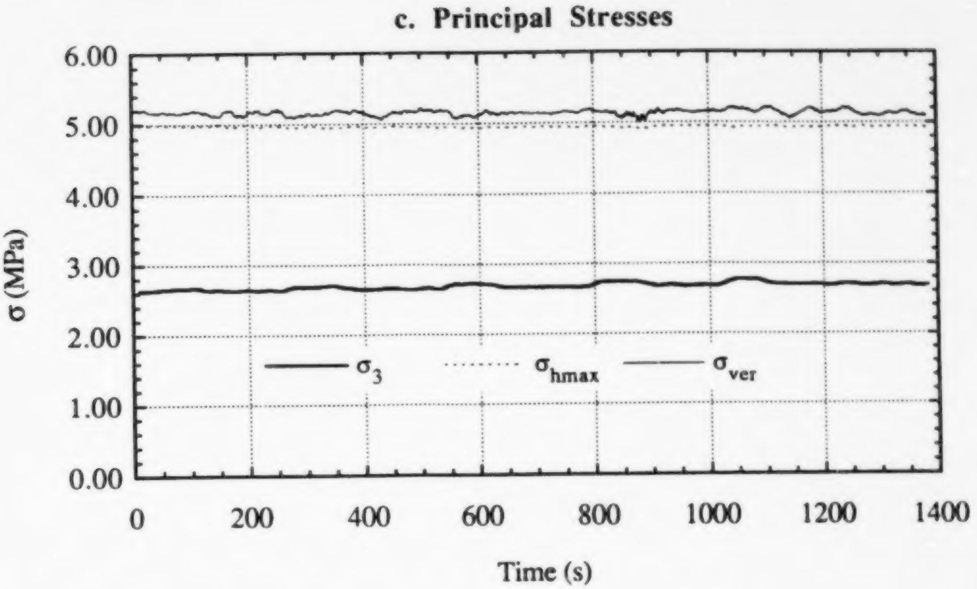

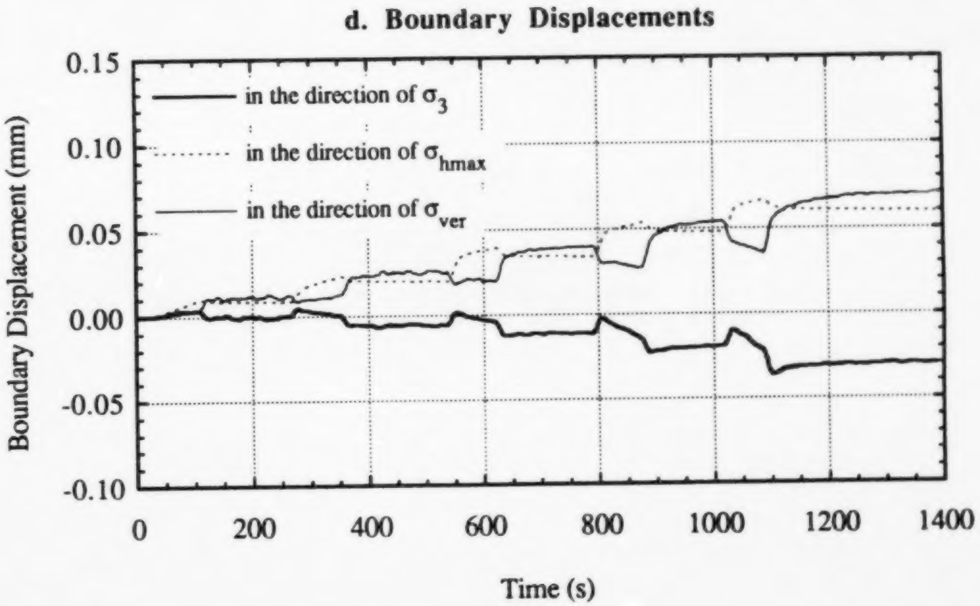

Figure B.7 Continued

a. Injection History

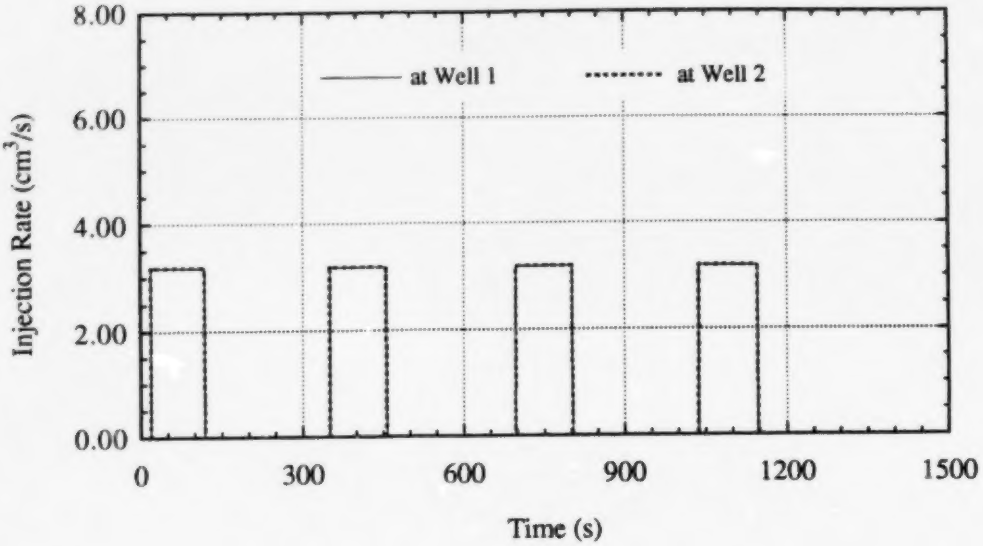

b. Bottomhole Pressure

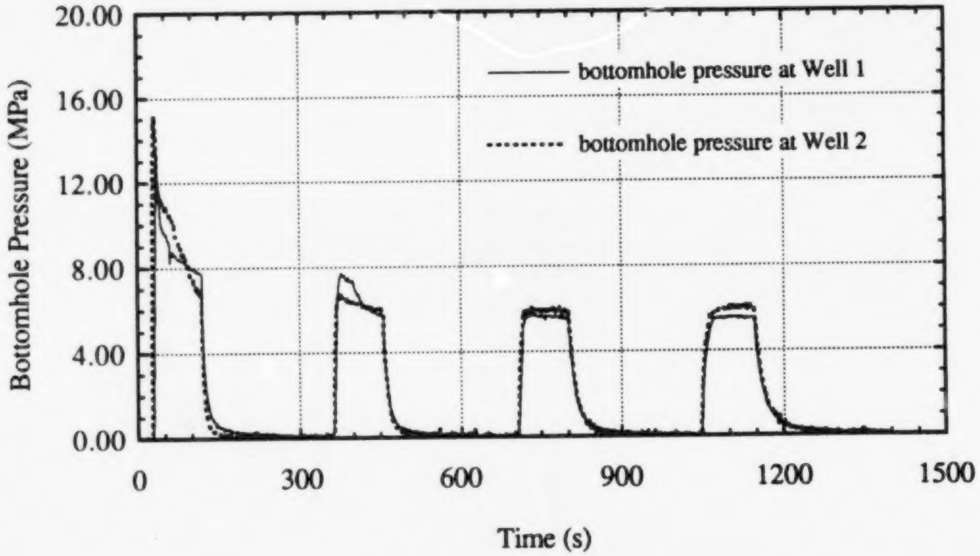

Figure B.8 Double Well Hydraulic Fracture Test 9

c. Principal Stresses

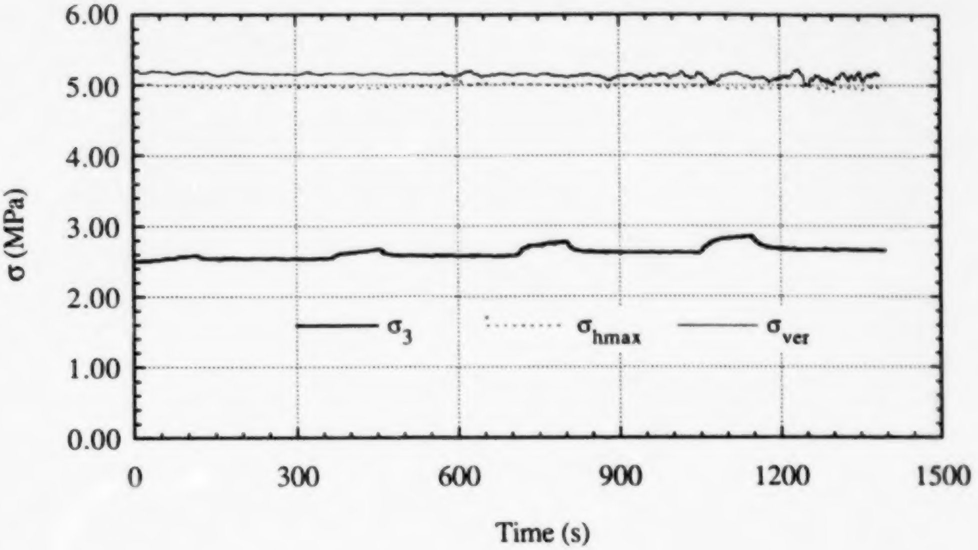

d. Boundary Displacements

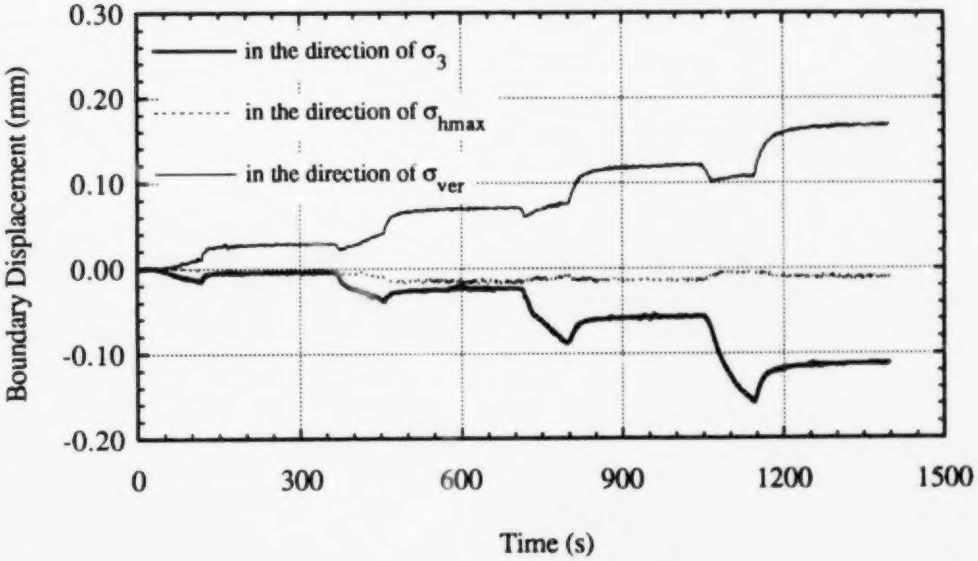

Figure B.8 Continued

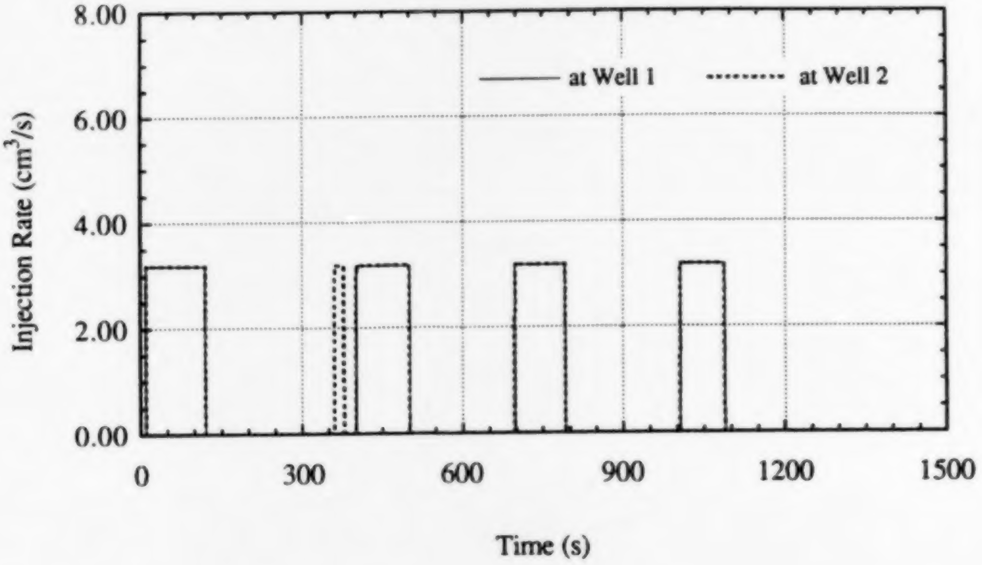
a. Injection History

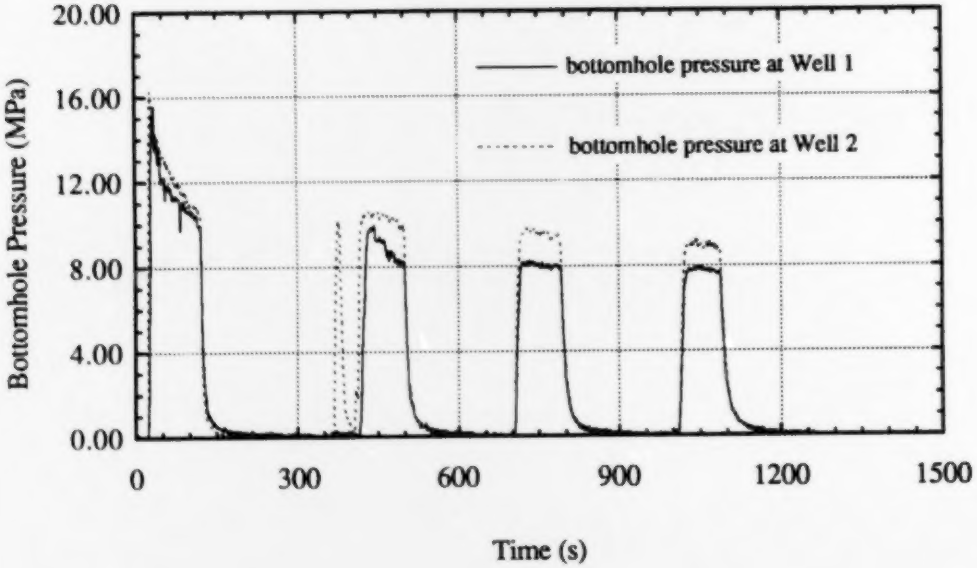
b. Bottomhole Pressure

Figure B.9 Double Well Hydraulic Fracture Test 10

c. Principal Stresses

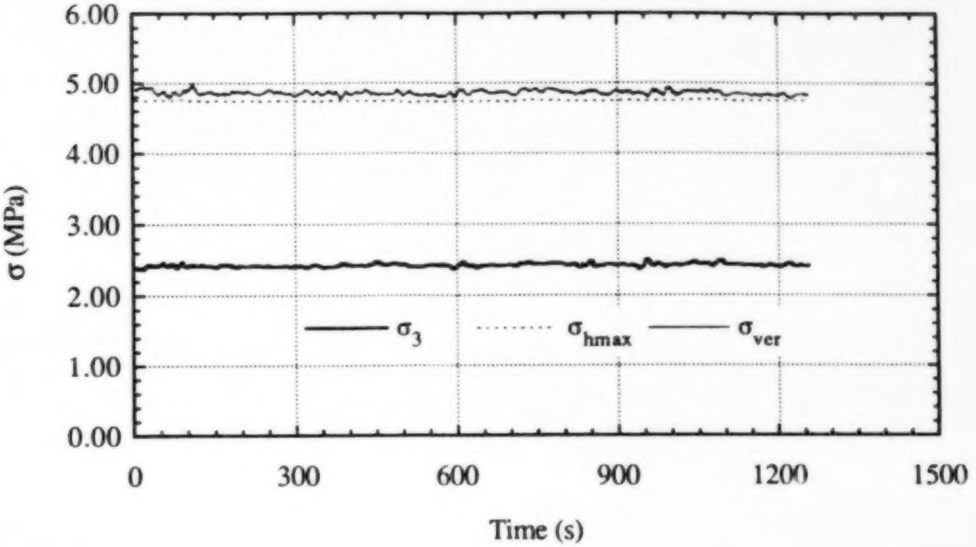

d. Boundary Displacements

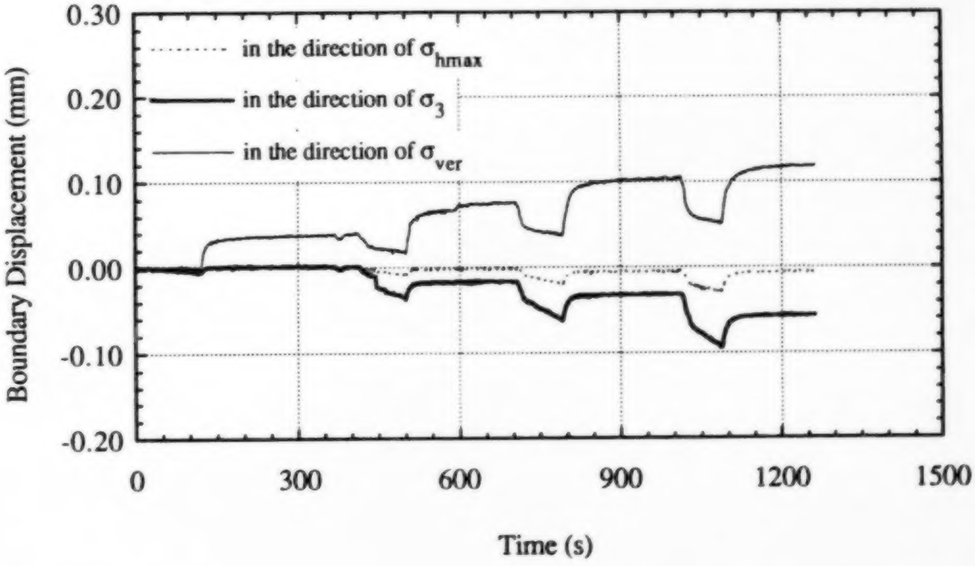

Figure B.9 Continued